University of Strathclyde

Department of Mechanical and Aerospace Engineering

The Orbital Dynamics of Advanced Planetary Observation Systems

by

Pamela Catherine Anderson

A thesis presented in fulfilment of the requirements for the degree of

Doctor of Philosophy

2013

Declaration of Author's Rights

This thesis is the result of the author's original research. It has been composed by the author and has not been previously submitted for examination, which has led to the award of a degree. The copyright of this thesis belongs to the author under the terms of the United Kingdom Copyright Acts as qualified by University of Strathclyde Regulation 3.50. Due acknowledgement must always be made of the use of any material contained, or derived from, this thesis.

Signed:  Date: 01/03/2013

Acknowledgements

I would like to thank everyone who has made it possible for me to complete this thesis.

I am extremely grateful to my PhD supervisor, Dr Malcolm Macdonald for his continuous guidance and patience and for providing so many ideas and opportunities throughout my PhD.

To Dr Chen-wan Yen, for hosting me at the Jet Propulsion Laboratory for three months in the latter stages of my PhD, thank you for looking after me so well whilst I was there. A big thank you also goes to my friends and staff at the University of Strathclyde.

For financial support I acknowledge and thank the scholarship awards received from the British Federation of Women Graduates, the Royal Society of Edinburgh, the University of Strathclyde, the University of Glasgow, the Institution of Mechanical Engineers (x2), the Royal Aeronautical Society (x2) and the Royal Academy of Engineering.

Special thanks go to my family, in particular my mum, dad and brother who have always encouraged and believed in me. To David, thank you for the support and laughter you have given me through the tough times.

Abstract

The increasing interest from the science community to obtain greater quality and quantity of data from Earth and other planets in the Solar System drives research towards developing new means of performing space-based observation. This thesis attempts to address some aspects of this issue by developing novel spacecraft orbits to enhance the opportunities for remote sensing of Earth and the inner planets.

Within this thesis, particular emphasis is placed on investigation of a system that can overcome the critical data deficit for the high-latitude regions of the Earth. These newly proposed highly-elliptical orbits are termed Taranis orbits (Celtic God of thunder) and can offer completion of the Global Observing System using fewer spacecraft and to higher resolution than any other proposed system. Various low-thrust propulsion technologies are considered to enable the Taranis orbits, with electric propulsion found to be the most beneficial following mission analysis. Design of constellations for high-latitude remote sensing is also conducted which highlights both 12 and 16 h orbits to meet the defined requirements of a polar orbiting mission.

Similar methods are also used to develop elliptical sun-synchronous orbits at Earth and novel orbits around Mars, Mercury and Venus to enable new and unique investigations.

Contents

List of Figures

List of Tables

List of Symbols

Symbols

Symbol	Description
a	Semi-major axis, km
A	Spacecraft area, m^2
a_{atmos}	Atmospheric drag acceleration, mm/s^2
a_p	Electric propulsion acceleration, mm/s^2
$\boldsymbol{a_s}, a_s$	Sail acceleration vector, Acceleration from perfectly reflecting solar sail, mm/s^2
a_{sc}	Solar sail characteristic acceleration, mm/s^2
a_{tot}	Total acceleration ($a_s + a_p$), mm/s^2
A_s	Solar sail surface area, m^2
C_D	Drag coefficient
$C_{n,m}$	Harmonic coefficients of body potential
e	Eccentricity
E	Eccentric Anomaly, degrees
f	Modified equinoctial element
f_s	Force, N
$\boldsymbol{f_i}$	Force exerted due to incident photons, N
$\boldsymbol{f_r}$	Force exerted due to reflected photons, N
F_n	Low-thrust normal perturbation scalar
F_r	Low-thrust radial perturbation scalar
F_t	Low-thrust transverse perturbation scalar
g	Modified equinoctial element
h	Modified equinoctial element
H	Altitude, km

H_a	Apogee altitude, km
i	Inclination, degrees
I_{sp}	Specific impulse, s
J_n	Gravitational perturbations
k	Modified equinoctial element
k_{SA}	Solar array specific performance, kg/W
k_{EP}	Electric propulsion specific performance, kg/W
L	True longitude, degrees
m	Mass, kg
m_f	Final spacecraft mass, kg
m_0	Initial spacecraft mass, kg
m_p	Mass of spacecraft minus solar sail, kg
m_{pay}	Payload mass, kg
m_{power}	Mass of power system, kg
m_{prop}	Propellant mass, kg
m_s	Mass of solar sail, kg
m_{EP}	Mass of electric propulsion system, kg
m_{sys}	System mass, kg
m_{tank}	Mass of propellant tanks, kg
$\dot{m}$	Mass flowrate, kg/s^2
$\boldsymbol{n}$	Unit vector normal to solar sail surface
N	Normal perturbation, mm/s^2
p	Semi-latus rectum, km
P	Pressure, W/m^2
P_{max}	Maximum power, W
$P_{n,m}$	Associated Legendre polynomials
r	Orbit radius, km
r_s	Radius of spacecraft from Sun, km

R	Radial perturbation, mm/s^2
R_B	Mean radius of body under consideration, km
R_s	Sun – Earth distance, km
s	Auxiliary variable
$S_{n,m}$	Harmonic coefficients of body potential
T	Transverse perturbation, mm/s^2
t	Time, s
t_f	Final time, s
T_h	Thrust, N
T_{max}	Maximum thrust, N
T_s	Orbit period, s
u	Argument of latitude, degrees
$\boldsymbol{u_i}$	Direction of incident photons impinging sail surface
$\boldsymbol{u_r}$	Direction of specularly reflected photons from sail surface
U	Potential
U_0	Point-mass gravitational potential
U_p	Perturbing component of potential body
V	Velocity, m/s^2
w	Auxiliary variable
W	Solar irradiance, W/m^2
α	Solar sail pitch angle, degrees
$\tilde{\alpha}$	Pitch angle for ideal force vector, degrees
β	Solar sail lightness number
β_s	Declination of spacecraft, degrees
δ	Sail clock angle, degrees
ε	Elevation, degrees
η	Nadir angle, degrees
η_s	Solar sail efficiency

η_{EP}	Electric propulsion efficiency
ϑ	Angle measured from the first point of Aries to the planet, within the ecliptic plane, degrees
θ	True anomaly, degrees
λ	Geographical longitude, degrees
λ_{rp}	Function of radius of periapsis
λ_0	Earth central angle, degrees
λ_ω	Function of argument of perigee
μ	Gravitational parameter of body under consideration, km^3/s^2
ν	Velocity, m/s
ρ	Angular radius of Earth, degrees
ρ_0	Density, kg/m^3
σ_s	Sail loading, g/m^2
ω	Argument of periapsis, degrees
Ω	Ascending node angle, degrees

Constants

Symbol	Value	Description
c	2.99792458×10^{8} m/s	Speed of light
G	6.6742×10^{-11} Nm^2/kg^2	Universal gravitational constant
g_0	9.80665 m/s^2	Gravity of Earth
L_s	3.827×10^{26} W	Solar luminosity
M_s	1.989×10^{30} kg	Solar mass
P	4.56×10^{-6} N/m^2	Solar radiation pressure
R_E	6,371 km	Mean radius of Earth
R_m	3,389.5 km	Mean radius of Mars
R_M	2,439.99 km	Mean radius of Mercury
R_V	6,051.8 km	Mean radius of Venus
W_e	1367.6 W/m^2	Mean solar irradiance measured at the Earth's distance from the Sun
ε_{obl}	23.45 degrees	Obliquity of the ecliptic of Earth
μ_E	3.986032×10^{14} m^3/s^2	Gravitational parameter of Earth
μ_m	4.283×10^{13} m^3/s^2	Gravitational parameter of Mars
μ_M	2.2032080×10^{13} m^3/s^2	Gravitational parameter of Mercury
μ_V	3.249×10^{14} m^3/s^2	Gravitational parameter of Venus
σ^*	1.53 g/m^2	Critical solar sail loading parameter

List of Acronyms

Acronyms

Acronym	Meaning
AD^2	Advanced Degree of Difficulty
CCD	Charge Coupled Device
COT	Commercial off the Shelf
ECSS	European Cooperation for Space Standardization
ECV	Essential Climate Variable
EO	Earth Observation
EoL	End-of-Life
EP	Electric Propulsion
ESA	European Space Agency
GEO	Geostationary Earth Orbit
GOCE	Gravity Field and Steady State Ocean Circulation Explorer
GOS	Global Observing System
HEO	Highly Elliptical Orbit
HiPEP	High Power Electric Propulsion
IKAROS	Interplanetary Kite-Craft Accelerated by Radiation of the Sun
JAXA	Japan Aerospace Exploration Agency
JPL	Jet Propulsion Laboratory
LED	Light Emitting Diode
LEO	Low Earth Orbit
MESSAGE	Mercury Solar Sailing Advanced Geoscience Exploration
MESSENGER	Mercury Surface Space Environment Geochemistry and Ranging Mission
MPD	Magnetoplasmadynamic

MRO	Mars Reconnaissance Orbiter
NASA	National Aeronautics and Space Administration
NEXIS	Nuclear Electric Xenon Ion Thruster System
NEXT	NASA's Evolutionary Xenon Thruster
NKO	Non-Keplerian Orbit
NLSA	Northern Lights Software Associates
NOAA	National Oceanic and Atmospheric Administration
NSTAR	NASA's Solar Electric Propulsion Technology Application Readiness
OZA	Observational Zenith Angle
PCW	Polar Communication and Weather
PPT	Pulsed Plasma Thruster
RTN	Radial, Transverse and Normal (axes)
SMOS	Soil Moisture Ocean Salinity
STEM	Science Technology Engineering and Mathematics
TRL	Technology Readiness Level
XIPS	Xenon Ion Propulsion System

Chapter 1

1 Introduction

Spacecraft have delivered vital information about the Earth, its nearest neighbours and lesser explored bodies in the Solar System since the beginning of the space-age, allowing an understanding of the history and evolution of Earth and other planetary bodies and providing detailed weather forecasting, surveillance, navigation and communication systems. However, as the demand grows to increase the quality and quantity of this data, conventional orbit slots employed by spacecraft to provide this information become more congested. New means of performing planetary observation, making use of the evolution of spacecraft technology, are therefore sought to enable new and unique investigations.

1.1 Earth Observation Systems

Platforms in orbit around the Earth provide fundamental services such as communication, navigation, surveillance, and observation. Earth Observation (EO) spacecraft image the Earth's surface and seas and monitor more than twenty of the fifty recognised Essential Climate Variables (ECVs) identified by the Committee on Earth Observation Satellites as being largely dependent on space-based observation [1, 2]. ECVs such as solar fluctuations, ocean surface temperature and volcanic activity are parameters defined by the Global Climate Observing System and are required for the validation of, and assimilation into, Earth system models to predict future climate trends [1, 2].

1.1.1 Current Systems

To date, EO missions have been conducted from two main types of orbit; Low-Earth orbit (LEO) and geostationary Earth orbit (GEO), which constitute the Global Observing System (GOS) detailed in Figure 1-1. LEOs are typically circular, polar orbits with altitudes ranging from below *1,000 km* to around *2,000 km*, with typical altitudes in the range of *500 – 800 km,* and offer high-resolution observations [3]. These orbits are often sun-synchronous: the orbit's nodal precession rate matches the Earth's mean orbital rate around the Sun such that the lighting along the ground-track remains approximately constant over the mission duration. This property is useful both in terms of the spacecraft design, due to the significant simplification of the thermal environment, and for comparison of images, to enable repeat observations of a target over an extended period under similar illumination conditions, making them particularly useful for EO missions including CryoSat, the Soil Moisture Ocean Salinity satellite (SMOS), and the Gravity field and steady-state Ocean Circulation Explorer mission (GOCE) [4-7]. These orbits are however, essentially a finite resource and new solutions are therefore being sought to enhance the opportunities for observation; discussed in greater detail in **Section 2.1.4** and **Chapter 6**.

Conversely, GEOs are circular orbits around the Earth's equator with altitudes in the region of *36,000 km* and orbital period equal to the rotational period of the Earth [8]. They provide the large scale contextual information that is lacking from LEOs and are most often used for communication and weather satellites, such as Meteosat and GOES-O[1] [9]. Nevertheless, GEO slots are becoming increasingly congested, thus new solutions are being investigated to ease this congestion; discussed further in **Chapter 2**. Despite the popularity of GEOs, observations are critically limited beyond approximately *55 degrees* latitude due

[1] GOES-O homepage at http://www.nasa.gov/mission_pages/GOES-O/main/index.html Accessed on October 4th 2012

to the rapidly decreasing horizontal resolution with increasing latitude [10]. This, combined with the poor temporal resolution of spacecraft in LEO results in a data-deficit over the critical polar regions of the Earth. This deficit can be partially addressed using composite images, however a 'ring' of missing observations still occurs between latitudes of approximately *50* and *70 degrees* [11]. Composite images include data from geostationary and polar orbiting spacecraft and are widely available for temporal resolutions of *3 hours* which, following recent developments, has been reduced to *1 hour* [11, 12]. However, deriving high-quality climate records, including monitoring of atmospheric motion vectors, requires a data refresh rate of at least *15 minutes* as is typically required for so-called continuous meteorological observations. It is noted that next generation GEO platforms are capable of providing data refresh rates of *5 minutes*. Composite images therefore do not fully overcome the data deficit at the high-latitude regions of the Earth, leaving critical climate and meteorological datasets lacking in vital polar regions.

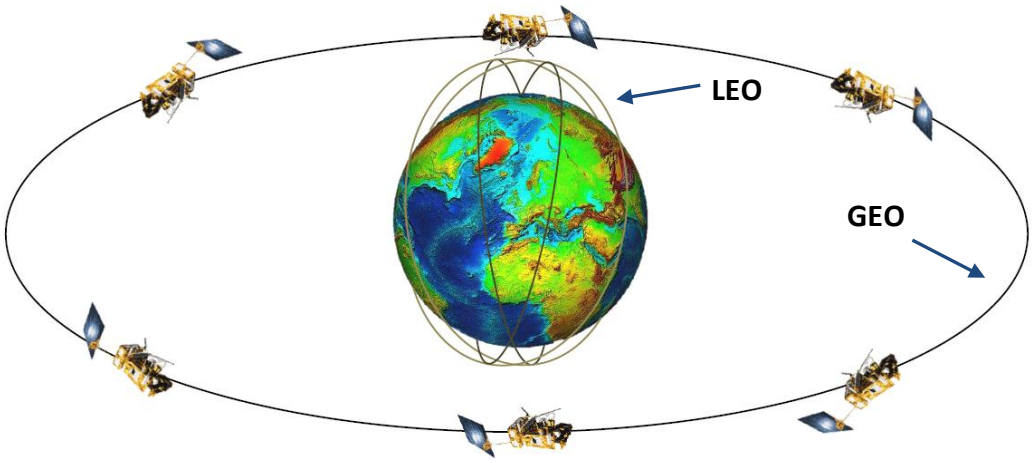

Figure 1-1 Global Observing System showing GEO and LEOs (image credit Malcolm Macdonald)

1.2 High-Latitude Observation

In recent years, there has been significant interest in building an observation system to accurately track environmental processes in the polar and frigid zones [13]. The rapidly changing environment of, in-particular, the Arctic is of great meteorological and climate significance as the climate in these regions has been shown to have a disproportionate impact on global weather and climate predictions [14-16]. Furthermore, the Arctic is a significant region for transportation of volcanic ash, air pollution, fog, and for sea-ice movement, and is thus a region of high priority science. Moreover, exploitation of oil and mineral resources in the Arctic regions is set to increase in the coming years as hidden energy reserves are revealed. There is also increasing demand for reliable communication and data relay in the remote polar regions, with ESA initiating the ArcticOM study to map future demand and identify communication gaps in the Arctic, with a view to using this region as a possible commercial shipping route [17].

It is clear from **Section 1.1.1** that no current EO system can provide the level of temporal or spatial resolution required at the high-latitudes and the current use of composite images to map these areas still results in a ring of missing observations between latitudes of approximately *50* and *70 degrees*, as detailed in Figure 1-2 [11]. Critical climate and meteorological datasets at the Earth's frigid and neighbouring temperate zones are therefore lacking.

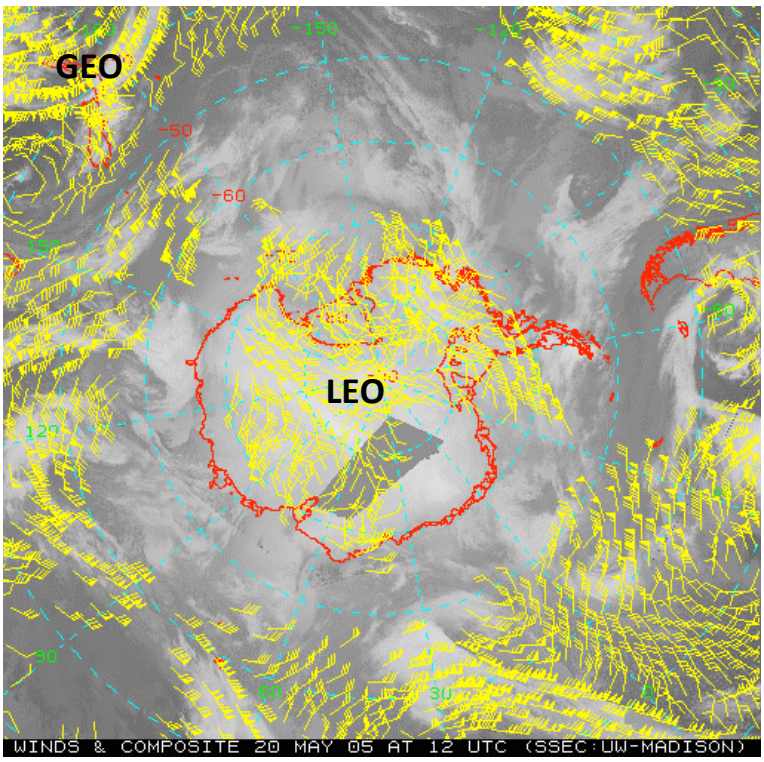

Figure 1-2 Ring of missing Atmospheric Motion Vectors from ~ *50* to ~*70 degrees* (image credit Lazzara et al. in [11])

The emerging commercial shipping activity in the North-East passage has caused various bodies to recognise the gaps in telecommunications at high-latitudes and express interest in the creation of an Arctic communication system for several applications. The Arctic Marine Shipping Assessment (ASMA, 2009) conducted by the Arctic Council stated that *"There are serious limitations to radio and satellite communications and few systems to monitor and control the movement of ships in ice-covered waters"* [18]. Similarly, the MarSafe North study identified the requirement for a comprehensive Arctic observing system for high-latitude maritime telecommunications [19].

In addition to telecommunications, the high-latitude data deficit is required to be filled for many EO applications. A comprehensive Arctic-observing system would allow improved monitoring of ECVs to enhance understanding of climate change modelling. Temperatures

in the polar regions are also increasing several times faster than the global average [20]; sea-ice coverage is also decreasing, creating a feedback effect on the climate [21, 22]. Enhanced polar observation, provided by a Taranis constellation of spacecraft for example, would enable:

- *Acquisition of cloud-motion wind vectors* – These form an important input to weather-forecasting systems. *90 degree* inclination Taranis orbits could fill the gap in information caused by the degradation of information from geostationary orbits above latitudes around *55 degrees* and the narrow swaths of data from LEO.

- *Monitoring of sea ice* – As this changes rapidly from day to day, continuous coverage from a Taranis orbit means that the probability of seeing through a gap in the clouds at any given location is much higher than from a LEO mission.

- *Observation of tropospheric chemistry in the polar regions* – Tropospheric chemistry is often driven by sporadic pollution events and/or has a strong diurnal cycle. Observing this from LEO misses much of the cycle due to the intermittent nature of the opportunities provided. Taranis orbits have the potential to make these observations with a high repeat rate.

- *Observation of stratospheric ozone* – The causes of ozone depletion are well understood but the dynamical context in which they take place is very variable in the Northern Hemisphere. Also, the way in which polar ozone responds to climate change is currently difficult to predict.

- *Volcanic Ash* – The distribution of smoke and ash is of particular interest for aviation and air quality, with volcanic ash posing a significant geohazard to the economy.

- *Telecommunications* – A reliable communications system is required in the remote polar regions for various applications such as commercial shipping.

In addition to these observations, improved polar observation would also allow enhanced surface observations due to the collection of all possible clear-sky pixels, whilst key polar observations would be radically improved through observation of parameters such as sea surface temperature, snow cover, vegetation properties and wild fires.

It is apparent that an observation system capable of continuously imaging the high-latitude regions of the Earth with sufficient resolution would offer significant benefits for a number of applications. Consequently, this thesis will investigate possible new orbit solutions to build a comprehensive Arctic observing system and fulfil the gap in data for high-latitude regions, allowing improved monitoring of ECVs to enhance understanding of climate change modelling. Comparison is firstly made in the subsequent sections between current Arctic observing system concepts, including conventional highly-elliptical Molniya orbits, the Polesitter concept and displaced eight-shaped orbits.

1.2.1 Highly-Elliptical Orbits

The World Meteorological Organization has recently identified highly-elliptical orbits (HEOs) as a possible solution to the lack of adequate observations of key high-latitude regions as part of the vision for the GOS in 2025, where, the concept of an HEO mission *'for quasi-permanent monitoring of high-latitudes and polar regions'* has been proposed [13]. HEOs, such as the Molniya (Russian: *lightnin*g) orbit, have been used extensively by the Russian Federation for high-latitude communication since 1965 [23], however they have never previously been employed for EO missions.

The mass distribution of the Earth is not uniform; there is a bulge at the equator, a slight pear shape and flattening of the poles, which causes periodic variations in all of the orbital

elements of a spacecraft. The most significant spherical harmonic term is the second-degree zonal harmonic, J_2, which accounts for the oblateness of the planet and causes secular variations in the right ascension of the ascending node and argument of perigee. However, the Molniya orbit has a fixed 'critical inclination' of either *63.43* or *116.6 degrees* which negates the drift in argument of perigee usually caused by the Earth's equatorial bulge (J_2 effect) [24]. The derivation of these critical inclination values is given in more detail in **Section 3.2.1**. These orbits have an orbital period approximately equal to one-half of a sidereal day, with apogee altitudes comparable to the altitude of GEO platforms.

Although Molniya orbits have only previously been used for high-latitude communication missions, their benefits for remote sensing have been considered for a number of years. In 1990, Kidder et al. discussed how Molniya orbits can function much like high-latitude geostationary orbits to improve the temporal frequency of polar observations [23]. In their 2000 paper, Draim et al. also state that constellations of spacecraft on highly-elliptical, Molniya-like, orbits may become the new paradigm for telecommunications space systems as well as offering benefits for many other applications [25]. Significantly, elliptical systems can be designed to give coverage of particular latitudes and continuous global coverage for telecommunication and imaging applications can be achieved at a lower cost than using existing orbit solutions, such as LEOs as a result of the fewer spacecraft required [25, 26].

In view of the direction of the GOS to include a constellation of spacecraft in HEOs to complement current EO systems, an HEO system is being proposed by Canada for launch by 2017 [27]. This Polar Communication and Weather (PCW) mission consists of two spacecraft in 16 h, Molniya-like, orbits in a single orbit plane which give Observational Zenith Angles (OZAs) not exceeding *70 degrees* to provide broadband services to regions of Canadian interest [27-29].

The Russian Federation is also proposing a more ambitious Arctic observation system known as 'Arktika' which consists of spacecraft in GEO, LEO and HEOs to obtain real-time information such as wind velocity and direction, precipitation and ice conditions for weather forecasting, flight safety and navigation in the high-latitude regions [30].

Although Molniya orbits can provide enhanced high-latitude observation, they cannot provide hemispheric observations to the latitudes required to fully overcome the identified data-deficit, from a single spacecraft. A spacecraft at apogee on a Molniya orbit observing to *55 degrees* latitude, where observations from GEO begin to breakdown [10], has a peak OZA around *10 degrees* higher than when the same location is observed from GEO, shown in Figure 1-3. The problem of viewing frigid and neighbouring temperate regions is therefore not fully resolved with the use of spacecraft on the Molniya orbit as no single platform can provide hemispheric observations that can be coupled with the observations obtained from GEO. Observations would therefore continue to be dependent on composite images that will be discontinuous in viewing geometry. It is noted that throughout this thesis, a composite image is defined as a single image consisting of perspectives from more than one spacecraft. The viewing geometry and number of spacecraft required using the Molniya orbit will be described in more detail in **Chapter 5**.

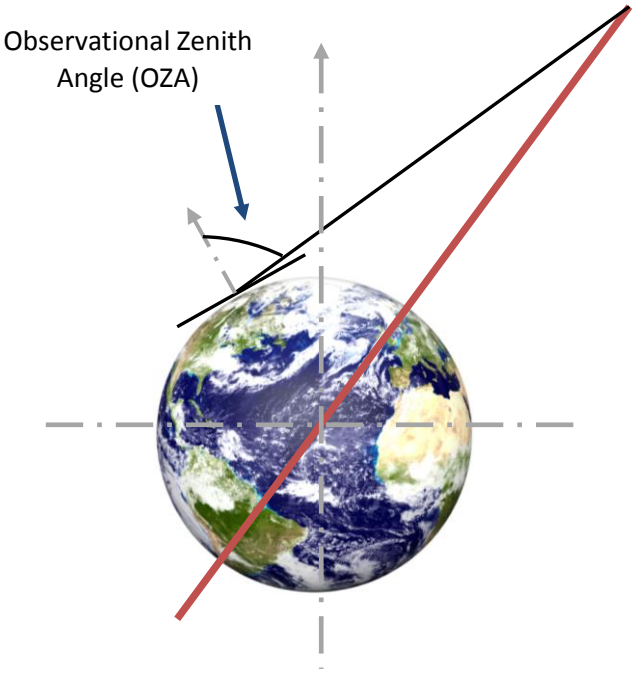

Figure 1-3 Observation over the pole from Molniya orbit at apogee with *63.43 degree* inclination

1.2.2 Non-Keplerian Orbits

Recent investigations have been conducted into the use of the Polesitter mission concept, first introduced in 1980, to allow continuous, high-latitude observation [31]. This concept will be discussed in greater detail in **Chapter 2**, but essentially involves placing a spacecraft above one of the Earth's poles at around *2 million km* altitude, by means of continuous acceleration, to allow hemispheric observations [32, 33].

A similar concept to the Polesitter mission is the solar sail displaced eight-shaped orbit, which will also be discussed in further detail in **Chapter 2**, has recently been considered by Ceriotti et al. [34]. Displaced eight-shaped orbits use the acceleration generated from solar sails to displace the Lagrangian points, L_1 and L_2, however as with the Polesitter concept, the spacecraft is around *1* and *2 million km* from Earth.

1.2.3 High – Latitude Observation Requirements

A list of requirements for a polar remote sensing constellation has been developed, based on the requirements outlined for other Arctic observation missions [27, 28]. Further detailed discussion of these requirements is also given in **Chapter 5**, these are as follows:

R1. *The constellation shall provide continuous coverage above 55 degrees latitude as a minimum.*

R2. *The rate of change of argument of perigee of the orbit shall be zero.*

R3. *The apogee altitude of the orbit shall be less than 45,000 km.*

R4. *The OZAs shall be less than or equal to the OZA from GEO.*

R5. *Above the target region, a single image shall be used to provide the required coverage.*

R6. *The mission shall comply with debris mitigation guidelines.*

1.2.4 Arctic Observation System Comparison

Comparisons can be made between the mission concepts described in **Sections 1.2.1** and **1.2.2** in relation to the requirements outlined in **Section 1.2.3**. A summary is given in Table 1-1 to show the mission concepts that are capable of meeting the given requirements.

Table 1-1 - Arctic observation mission concepts summary

Mission Concept	R1	R2	R3	R4	R5	R6
Molniya orbit	✔	✔	✔	X	X	✔
Polesitter	✔	✔	X	✔	✔	✔
Eight-shaped orbit	✔	✔	X	X	X	✔

It is clear from Table 1-1 that neither the Polesitter or displaced eight-shaped orbits can provide sufficient spatial resolution to meet the requirements defined in **Section 1.2.3**, these concepts therefore do not fully resolve the high-latitude data deficit. It is also clear from Table 1-1 that the OZAs of the conventional Molniya orbit do not match those from GEO platforms when viewing the same location, this will however be discussed in more detail in **Chapter 5**. The requirement for a new comprehensive Arctic observing system to fully resolve the high-latitude data deficit is therefore clear.

1.3 Planetary Observation Systems

In addition to EO, there is significant interest in the observation of other bodies in the Solar System. Since the first successful flyby of Venus by Mariner 2 in 1962, robotic interplanetary missions have returned a wealth of valuable information about other planetary bodies [35]. Planetary exploration is vital to gain an insight into the formulation and evolution of, not only Earth, but also other planets in the Solar System. It can aid the understanding of how life began on Earth, determine whether extra-terrestrial habitable environments exist in the Solar System, enhance quality of life through technology innovation and reinforce science, technology, engineering and mathematics (STEM) education.

1.3.1 Mars

Exploration of the Martian environment, in particular, sparked early interest with efforts made by both Russia and the US to flyby, orbit and land on the surface of Mars. The first successful artificial Martian satellite, Mars 2, was placed in orbit in 1971, closely followed by the Russian Mars 3 and US Mariner 9 later that year[2] [36]. The mid 1970s saw three further spacecraft placed in orbit around Mars: the Russian Mars 5 in 1973, and American

[2] The Mars Exploration Program Historical Log, found online at: http://mars.jpl.nasa.gov/programmissions/missions/log/ Accessed 27th November 2012

Viking 1 and Viking 2 in 1975 [37, 38]. The following two decades saw no successful missions to Mars, until the launch of Mars Global Surveyor (MGS) by the US in late 1996 [39]. This mission delivered a vast amount of valuable information about the Martian atmosphere, surface and subsurface including photographs from the Mars Orbiter Camera of gullies and debris flow, and also produced evidence of the presence of water ice on both polar caps [40]. In the early 2000s, both NASA's Mars Odyssey and ESA's Mars Express reached orbit, with the former returning evidence of large amounts of hydrogen: an indication of vast quantities of water ice near the Martian South Pole, a discovery later confirmed by Mars Express [41-44].

The most recent spacecraft to conduct exploration of Mars from orbit is the Mars Reconnaissance Orbiter (MRO) launched in 2006. Still in operation, as of February 2013, it is responsible for the daily monitoring of Martian weather, investigation of the surface and searching for possible future landing sites [45]. Exploration over the past three decades by such systems has allowed a comprehensive and multidisciplinary view of Mars to be obtained. Detailed information has been provided about the Martian surface geology and mineralogy, atmospheric composition and circulation, mineral composition, subsurface structure, radiation environment and weather. However, each discovery about the Martian environment poses further questions, thus extensive investigation is still necessary.

Natural orbits typically used for remote sensing applications at Earth, as described in **Section 1.1.1**, also exist at Mars. For example sun-synchronous orbits, which have in the past been employed by spacecraft such as Mars Odyssey [46], MRO [47] and Mars Global Surveyor (MGS) [39], and Molniya-like orbits with fixed values of the critical inclination, which can also offer benefits for remote sensing of Mars by allowing the spacecraft to spend a large amount of time over a region of interest as a result of apoareion dwell.

Additional significance has recently been placed upon the exploration of Mars with the reformulation of the Mars Exploration Program, which aims to assess both near-term mission concepts and longer-term foundations of program level architectures for future robotic exploration of Mars. The goals of the program are to discover whether life ever arose on Mars, characterise the climate and geology of the surface and ultimately prepare for human exploration, with the challenge of sending humans to orbit Mars in the decade of the 2030s. Thus, missions must be developed which are responsive to the scientific goals of both the National Research Council Planetary Decadal Survey [48] and the ESA Aurora Programme[3], and extensive investigation is required into the Martian surface, subsurface, lower atmosphere, winds and densities. Research has consequently been conducted into a variety of Mars orbits to allow the best possible opportunities for remote sensing and in support of future Mars exploration [49]. This thesis therefore employs similar methods used to derive new orbits at Earth to also develop novel orbits around Mars to enable new and unique investigations.

1.3.2 The Inner Planets

The NASA Vision and Voyages Decadal Survey for 2013 – 2022 has identified three themes for the future development of planetary science, within which the importance of investigating the evolution of the inner planets and their atmosphere's is highlighted [48]. Exploration of Venus is emphasised to determine whether the ancient aqueous environment was conducive to early life and investigate if life ever emerged. Furthermore, examination of the chemistry, geology and climates of the inner planets can lead to better understanding of climate change here on Earth. Accordingly, the importance of exploration of Mercury and Venus is clear.

[3] http://www.esa.int/esaMI/Aurora/ Accessed 27th August 2012.

To date, there have been only two missions to Mercury: Mariner 10, a Mercury and Venus flyby mission launched in 1973: and the Mercury Surface, Space Environment, Geochemistry and Ranging (MESSENGER) mission which was launched in 2004 and reached orbit in 2011 [50]. The prime objectives of the MESSENGER spacecraft are to characterise the chemical composition of Mercury's surface, determine the nature of the magnetic field, the geologic history and the structure and state of the core [51]. A joint ESA and JAXA mission to Mercury is also scheduled for launch in 2015 - the Mercury Planetary Orbiter (MPO), and the Mercury Magnetospheric Orbiter (MMO) are part of the BepiColombo mission to study the evolution, geology, structure, interior, composition, magnetic field, exosphere and magnetosphere of Mercury [52].

The better-explored Venus has missions dating back to 1962, with Mariner 2 the first space probe to encounter another planet [35]. Since this time, a number of flyby missions have returned scientific data including magnetic field fluctuations, temperature measurements, atmospheric data, detection of gamma ray bursts and composition and properties of Venusian rocks from Mariner 2 and 5 and Venera 11-14 [35, 53-55]. Early missions to Venus also included a number of orbiters such as Venera 9, 10, 15 and 16, the Pioneer Venus 1 orbiter and Magellan, which have provided data on the cloud layers of Venus, atmospheric parameters, mapping of the surface and gravity measurements [56-59]. More recently, the Venus Express spacecraft launched by ESA in 2005 is, for the first time, performing long-term comprehensive investigation of the Venusian atmosphere [60]. The Japanese solar sail mission IKAROS, (Interplanetary Kite-craft Accelerated by Radiation Of the Sun) launched in 2010, also performed a flyby of Venus [61].

Similar to Earth and Mars, orbits inclined at the critical inclination also exist at Mercury and Venus which, as previously detailed, can offer significant benefits for remote sensing of

other bodies in the Solar System. However, although these Molniya-like orbits exist, the reciprocal of flattening of these planets is so low that natural perturbations are of no use for generating sun-synchronous orbits. Investigation has therefore been conducted into the use of a solar sail to deliver a payload into a sun-synchronous orbit around Mercury [62]. The Mercury Solar Sailing Advanced Geoscience Exploration (MESSAGE) mission was proposed in the mid 1990s to enable a spacecraft to enter a sun-synchronous orbit to provide benefits for the spacecraft thermal environment and give complete coverage of the planet's surface within two years [63].

Within this thesis, novel orbits around Mercury and Venus are also presented to enhance the potential opportunities for observation.

1.4 Thesis Objectives

The objectives of this work are to:

- Develop new highly-elliptical orbit solutions, to provide possible resolutions to the data deficit at the high-latitude regions of the Earth and for application to other as yet unspecified applications, through consideration of advanced orbital dynamics.
- Examine the use of electric, chemical and hybrid solar sail / electric propulsion systems to enable new highly-elliptical mission concepts and determine the most beneficial.
- Perform a trade space analysis of possible mission concepts, and conduct mission analysis to characterise the mission lifetimes and mass budgets.
- Develop highly-elliptical sun-synchronous orbits around Earth, using low-thrust propulsion, through consideration of advanced orbital dynamics.

- Develop novel orbits around other bodies in the Solar System, including Mars, Mercury and Venus, by using techniques developed for Earth orbits, to enhance the opportunities for remote sensing.

To achieve these objectives this thesis considers the application of acceleration, using locally optimal control laws [64], to develop novel orbits around the Earth to provide improved EO and enhanced data collection, focussing specifically on the remote sensing of high-latitude regions. However it is noted that several new orbit concepts are developed which may be of benefit for other unspecified applications. Consideration is given to the use of continuous acceleration to allow free-selection of the critical inclination of HEOs, while maintaining the zero change in argument of perigee condition essential to Molniya-like orbits. The value of the inclination can therefore be selected to fulfil the specific mission objectives. Conventional chemical propulsion, electric propulsion (EP) and hybrid solar sail / EP are investigated to determine the most beneficial system to enable such missions. Trade space analysis is also conducted to present various mission architectures which satisfy a set of mission requirements.

The use of low-thrust propulsion to develop highly-elliptical, sun-synchronous orbits is also investigated. In this case, acceleration is used to force a change in the ascending node angle whilst maintaining zero average change in the argument of perigee over the orbit. Parameters are again selected to best satisfy the mission objectives. These newly developed orbits can potentially enhance the opportunities for EO and by maintaining a sun-synchronous condition can offer considerable simplification of the spacecraft thermal environment.

Comparable methods are also used to develop new families of orbits around Mars, Mercury and Venus, where low-thrust propulsion is used for the extension of the critical inclination

of HEOs, the extension of circular and elliptical sun-synchronous orbits and to enable sun-synchronous orbits around bodies where they are otherwise not feasible.

The key contribution to knowledge of this thesis is that;

> *Novel planetary observation systems are developed both at Earth and other planets, which at Earth allow completion of the GOS using fewer spacecraft and to higher resolution than any other proposed solution.*

1.5 Thesis Layout

An introduction to Earth and planetary observation systems was given in **Chapter 1**, where the limitations of current EO systems for remote sensing of high-latitude regions of the Earth were discussed. The necessity for new mission architectures to overcome this data deficit was also identified. Thesis objectives state that investigation will be conducted into new EO systems to fulfil this gap in data, through the use of low-thrust propulsion. **Chapter 2** therefore introduces various low-thrust propulsion systems, including EP, solar sailing and hybrid solar sail and EP systems, and their uses on previous missions.

Chapter 3 will introduce novel HEOs at Earth, termed Taranis orbits, and presents the derivation of the orbits using a general perturbations solution, that is to say an analytical solution, which uses locally optimal control laws to apply continuous acceleration for the extension of the critical inclination. The effect of the applied acceleration on the orbital elements is also considered. A special perturbations, or numerical method is also used to verify the general perturbations solution, and a fuel optimal solution is generated using Pseudospectral optimisation. Although this chapter develops several new orbit concepts for a variety of possible applications, a *90 degree* inclination orbit, to meet the

requirements specified in **Section 1.2.3**, is the main focus for the mission design conducted in subsequent chapters.

Various propulsion systems are considered to enable the *90 degree* Taranis orbit to determine the most beneficial. **Chapter 4** therefore examines the use of hybrid solar sail / EP and conventional chemical propulsion and compares these against a pure EP system by performing mission analysis to determine the available useful payload masses and possible mission lifetimes.

Trade space analysis is conducted in **Chapter 5** to allow the selection of a particular 90 degree inclination orbit dependent upon the mission objectives and mission cost. This chapter also presents validation of the visibility analysis using NOVA Satellite Tracking Software.

Chapters 6 and **7** employ the methods used to develop a Taranis orbit system capable of meeting the specified requirements in the previous chapters to develop orbits for other unspecified applications at Earth and other bodies in the Solar System.

Chapter 6 presents the addition of a further element of acceleration to force a change in the ascending node angle of the orbit, in addition to the zero average change in argument of perigee condition, to create sun-synchronous HEOs. Once again these orbits are derived using a general perturbation solution and validated using a special perturbations technique.

Chapter 7 will apply the methods used to derive novel orbits at Earth to develop new families of both highly-elliptical and sun-synchronous orbits at Mars, Mercury and Venus.

Finally, **Chapter 8** will review the thesis and outline the future work.

1.6 Publications List

The following section of the thesis details the papers published by the candidate in support of the application for the degree of Doctor of Philosophy.

1.6.1 Journal Publications

The following journal papers support the application for the degree of Doctor of Philosophy:

1. Anderson, P, and Macdonald, M. “Novel Orbits of Inner Solar System Planets Enabled using Low-Thrust Propulsion” Acta Astronautica. Submitted May 2013.
2. Anderson, P, and Macdonald, M. “Static Highly Elliptical Orbits using Hybrid Low-Thrust Propulsion” Journal of Guidance Control and Dynamics, Vol. 36, No.3, 2013, 870-880, May 2013. DOI: 10.2514/1.56636
3. Anderson, P, and Macdonald, M. “Extension of Highly Elliptical Earth Orbits using Continuous Low-Thrust Propulsion” Journal of Guidance Control and Dynamics. Vol. 36, No.1, 2013, 282-292, AIAA, January 2013. ISSN: 0731-5090.
4. Anderson, P, and Macdonald, M. “Sun-Synchronous Highly Elliptical Orbits using Low-Thrust Propulsion” Journal of Guidance Control and Dynamics. Accepted December 2012.

1.6.2 Supporting Conference Papers

The following conference papers support the application for the degree of Doctor of Philosophy:

1. Anderson, P., Macdonald, M., and Yen, C. W. "Novel orbits of Mercury and Venus enabled using Low-Thrust Propulsion," AAS 13-180. Proceedings of 22nd AAS/AIAA Spaceflight Mechanics Meeting, Kauai, HI, February 2013.

2. Anderson, P., Macdonald, M., and Yen, C. W. "Extension of Martian Orbits using Continuous Low-Thrust Propulsion," *23rd International Symposium on Spaceflight Dynamics*. Pasadena, CA, 2012, 29 October - 2 November 2012.
3. Macdonald, M, Anderson, P, and Warren, C. "A Novel Design Concept for Space-Based Polar Remote Sensing". Proceedings of SPIE Remote Sensing Conference 2012, Edinburgh, UK, September 2012.
4. Anderson, P, and Macdonald, M. "Static Highly Elliptical Orbits using Hybrid Low-Thrust Propulsion", AAS 12-257. Proceedings of 22nd AAS/AIAA Spaceflight Mechanics Meeting, Charleston, SC, January 2012.
5. Anderson, P, and Macdonald, M. "Extension of the Molniya Orbit using Low-Thrust Propulsion", AAS 11-236. Proceedings of 21st AAS/AIAA Spaceflight Mechanics Meeting, New Orleans, LA, February 2011.
6. Anderson, P, and Macdonald, M. "Extension of Earth Orbits using Low-Thrust Propulsion", IAC-10.B1.2.7. Proceedings of 61st International Astronautical Congress. Prague, Czech Republic, October 2010.

Chapter 2

2 Low-Thrust Propulsion Systems

Several newly proposed Earth and planetary observation systems rely on the application of continuous acceleration provided either by an EP system, solar sails or a hybrid solar sail and EP system: Each of these systems is subsequently presented, followed by a discussion of the possible applications

2.1 Electric Propulsion

First conceived over one-hundred years ago by Robert Goddard [65] electric propulsion has undergone significant development with the launch of the first experimental ion thrusters in the early 1960s [66]. EP has now become a mature technology with high Technology Readiness Level (TRL) and low Advancement Degree of Difficulty (AD^2) [67, 68].

These systems accelerate propellant to high exhaust velocities, produce thrust of typically around a fraction of a Newton per thruster [66], and can offer a reduction in the propellant consumption over conventional propulsion. This can, in turn, create increased capacity for useful payload or lower launch masses leading to reduced launch costs through the use of smaller launch vehicles. EP can be divided into three main categories; electrothermal, electromagnetic and electrostatic, where each is subsequently discussed in **Sections 2.1.1** through **2.1.3**.

2.1.1 Electrothermal Propulsion

Electrothermal propulsion systems, such as resistojets (Figure 2-1) and arcjets (Figure 2-2), electrically heat propellant causing it to expand through a nozzle to generate thrust [69]. The specific impulse of a resistojet, which transfers heat to the propellant using a solid surface such as the chamber wall, is typically < *500 seconds* [66]. For arcjets, which heat the propellant using an electric arc, the specific impulse is limited to around *700 seconds* [66]. Resistojets were first operational in the 1980s where they were used for stationkeeping of communication platforms [69]. More recently, resistojets have been employed for attitude control, orbit insertion and de-orbit of spacecraft in LEO, such as spacecraft in the Iridium constellation [69, 70]. The first use of arcjets was subsequent to that of resistojets, with their use for north-south stationkeeping on geosynchronous platforms, such as the Telstar-4 series in the 1990s [69].

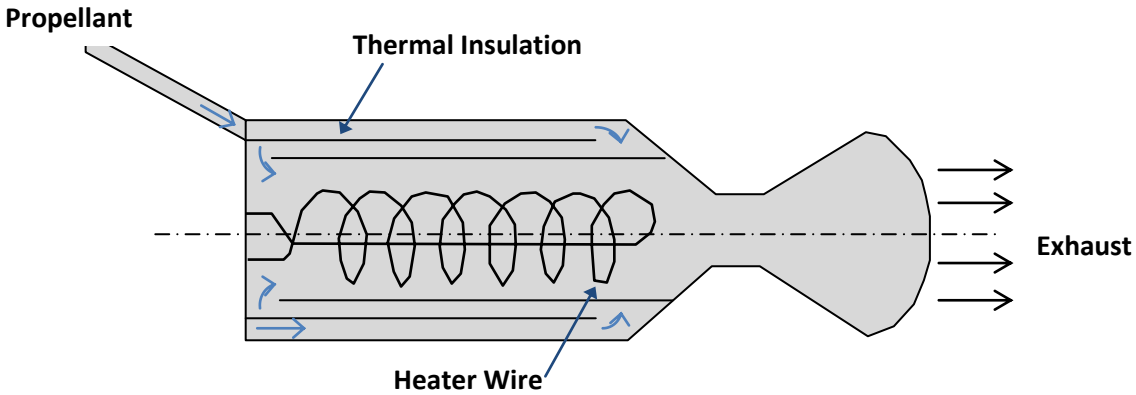

Figure 2-1 Resistojet schematic

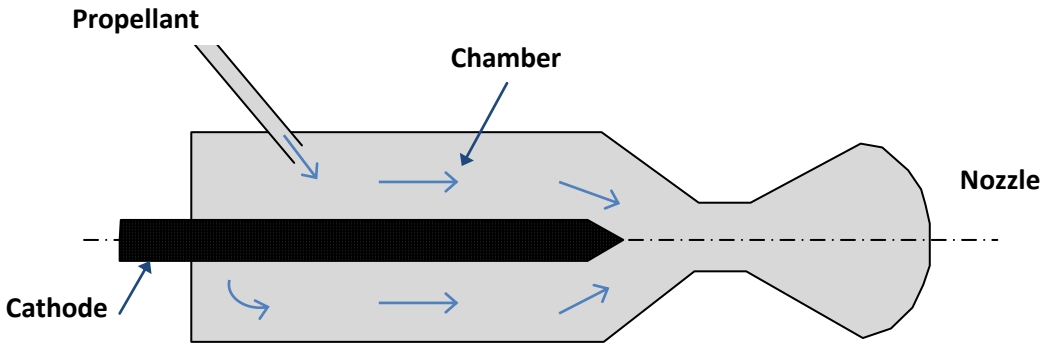

Figure 2-2 Arcjet schematic

2.1.2 Electromagnetic Propulsion

Electromagnetic propulsion systems accelerate propellant through a combination of electric and magnetic fields to produce thrust [69]. These systems can be categorised as either Magnetoplasmadynamic (MPD) thrusters (Figure 2-3) or Pulsed Plasma Thrusters (PPTs) (Figure 2-4). MPD thrusters use a very high current arc to ionise the propellant, which is then accelerated using electromagnetic forces in the plasma [66]. They typically operate at very high power levels and have demonstrated specific impulses between *1500* and *8000 seconds* [69], however at the time of submission of this dissertation, these have not yet gained any flight experience [71]. PPTs use a pulsed discharge to ionise a fraction of solid propellant ablated to a plasma arc and electromagnetic effects in the pulse to accelerate the ions to high exit velocities [66]. Ablative Pulsed Plasma Thrusters have an early history with their use on the Soviet Zond-2 spacecraft in 1964 and the United States LES-6 spacecraft in 1968 for Sun pointing control and east-west stationkeeping respectively [72, 73]. PPTs have also been used more recently on board NASA's Earth Observing 1 (EO-1) to provide spacecraft attitude control [74].

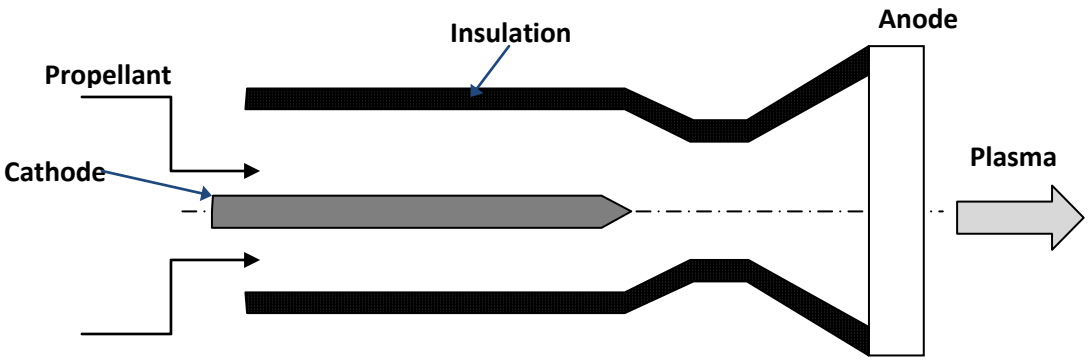

Figure 2-3 Magnetoplasmadynamic thruster schematic

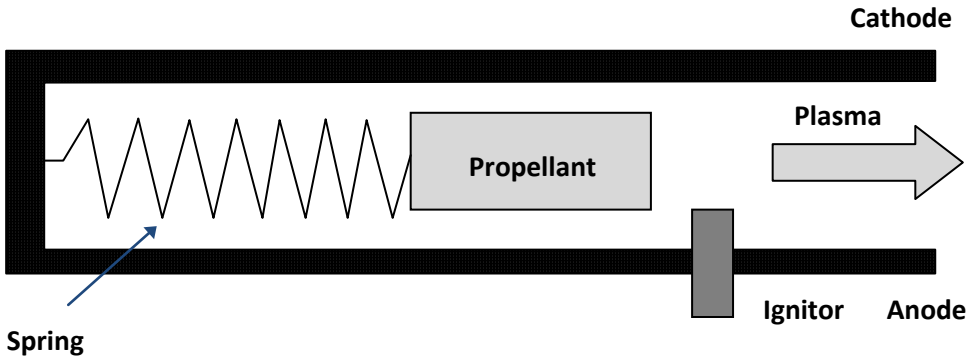

Figure 2-4 Pulsed Plasma Thruster

2.1.3 Electrostatic Propulsion

Gridded-ion (Figure 2-5) and Hall thrusters (Figure 2-6) are the two primary electrostatic propulsion devices, which accelerate the propellant through application of electrostatic forces to ionised particles [69]. Ion-thrusters ionise a large fraction of the propellant and use grids to electrostatically extract ions from the plasma and accelerate them to extremely high exhaust velocities [69]. Such systems have specific impulse ranges between 2*000 seconds* and *10,000 seconds* [66]. Although technically complex, ion engines are the most developed and well tested EP devices and have been operational since their use on the Japanese ETS-6 in 1994 [66]. Since then the L-3 25 cm Xenon Ion Propulsion System (XIPS) have been used on the Boeing 702 communications satellite for near-Earth applications

including attitude control, North-South and East-West stationkeeping, de-orbit and momentum dumping [71]. The XIPS can operate at a low power of *2.7 kW* producing *79 mN* of thrust or at high power level of *4.2 kW* giving a thrust of *165 mN* [75].

Low-thrust, high specific impulse ion engines are particularly useful for deep-space missions where longer thrusting times are more acceptable. Such as the 1998 Deep Space 1 (DS-1) technology demonstration mission, with a duration of over two years, it employed NASA's Solar electric propulsion Technology Application Readiness (NSTAR) thruster, capable of providing between *20* and *94 mN* of thrust at *2.3 kW* of power [76-78]. Following successful demonstration, EP was the enabling technology for the Dawn mission to Ceres and Vesta, which employed NSTAR thrusters [71, 79].

In 2003, JAXA employed four units of the microwave discharge ion engine, μ10, as the main method of propulsion onboard the HAYABUSA asteroid sample return mission. The μ10 ion engine is capable of producing *8 mN* of thrust at *350 W* of electric power and during the two-year flight of Hayabusa each thruster was operational for around *25,800 hours* consuming *22 kg* of xenon propellant [80].

Current developments in ion thrusters include NASA's Evolutionary Xenon Thruster (NEXT), which is designed to improve on the performance of the NSTAR thruster by achieving lower specific mass, higher specific impulse, greater propellant throughput, and increased power handling capability, thrust, and throttle range [71]. Testing has revealed this to be the case with NEXT shown to be capable of providing *236 mN* of thrust at around *7 kW* of power. Long duration life testing of an engineering model NEXT thruster has accumulated more than *9990 hours* of operation at full power [81].

NASA have also led the development of both the *20 kW* Nuclear Electric Xenon Ion thruster System (NEXIS) for outer planet robotic missions, which has been shown to produce a

maximum thrust of *476 mN* [82], and the High Power Electric Propulsion (HiPEP) thruster which has undergone ground testing and is capable of providing a maximum thrust of *670 mN* at a power level of *40 kW* [83].

In the UK, QinetiQ have developed the T5 ion thruster to provide a thrust range of *1 – 20 mN* at between *55* and *585 W* of power across the thrust range, with a nominal thrust range between *15* and *25 mN* [84]. The T5 thrusters have been used to provide drag compensation for the ESA GOCE mission [84]. GOCE was originally intended to last around 20 months and was due to end when the *40 kg* of Xenon propellant was consumed. However, unusually low solar activity has reduced the propellant usage and the mission has been extended until the end of 2013 [85]. The larger *4.5 kW* T6 thruster developed by QinetiQ has also been shown to be capable of providing *230 mN* of thrust [86].

Hall thrusters, which are essentially grid-less ion engines, have fewer parts and lower complexity than gridded ion thrusters [71] and have become a common method of EP since their first use by Russia in the 1970s, where two SPT-60 were employed on the Meteor satellite [87]. In recent times, ESA's Small Missions for Advanced Research in Technology (SMART-1) mission travelled to the moon to search for water using EP provided by Snecma's PPS-1350-G Hall thruster, which set a World record for Hall effect thrusters operating for more than *1700 hours* in flight [88]. The nominal operating conditions of the thruster are *90 mN* of thrust and *1.5 kW* of power [89].

The Advanced Extremely High Frequency (AEHF) satellites have also employed the *4.5 kW* Aerojet BPT-4000 Hall thrusters, capable of providing a thrust of *295 mN* [90], with projected design life of at least *7,000 hours* at *4.5 kW*, for orbit raising and stationkeeping in GEO [91].

The High Voltage Hall Accelerator has also been developed and tested by NASA to advance the Hall thruster technology readiness for science mission applications, with a view to providing a lower-cost EP alternative for future missions [92]. Testing has revealed the maximum power as *3.5 kW* and a thrust range of *24 – 150 mN* with a predicted lifetime exceeding *15,000 hours* [92].

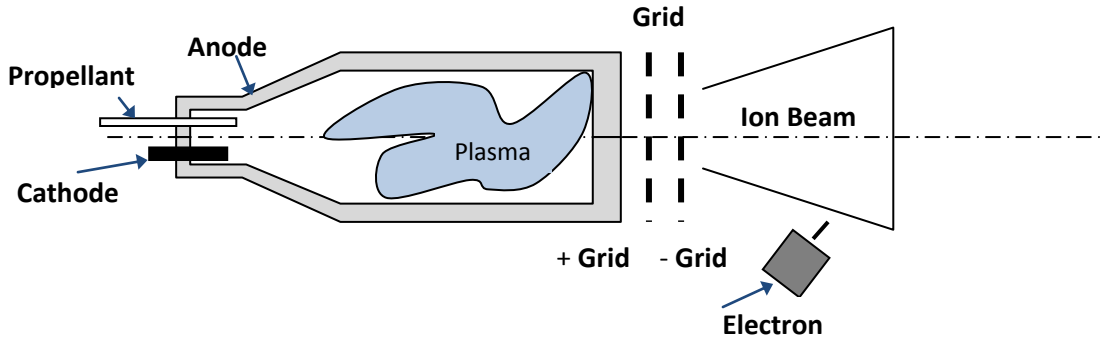

Figure 2-5 Gridded-Ion thruster schematic

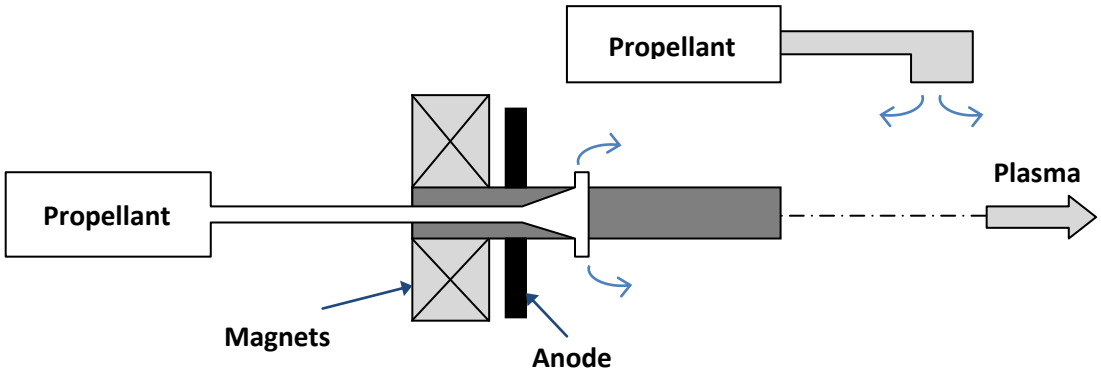

Figure 2-6 Hall thruster schematic

2.1.4 Applications

The use of EP can offer many advantages. Foremost being the possible reduction in the required propellant mass [69], which can either lower the launch mass of the spacecraft, leading to reduced launch costs, or increase the capacity for payload, offering additional

opportunities for remote sensing. Further benefits of EP include the variability of thrust levels [69], control of arrival conditions and reduction in the number of mission critical events [93].

The recent developments in the performance of EP systems, particularly the electrostatic thrusters described in **Section 2.1.3** and their ability to process large amounts of on board solar power, means they can enable a new range of missions which are otherwise not possible using conventional, high-thrust, chemical propulsion [69]. EP systems could enable multiple target missions, travelling to multiple targets using a single spacecraft, there are significant savings in spacecraft development and launch costs, considerable science return can also be achieved for a single spacecraft [71]. Such missions include the Dawn mission to Ceres and Vesta [94] and possible future sample return missions to Phobos and Deimos [95]. EP may also be used for heavy cargo and piloted missions to Mars [96, 97], the outer planets and beyond [69].

EP has also been considered for EO applications for a number of years, for example to enable non-Keplerian orbits (NKOs), which can offer additional opportunities for remote sensing. NKOs are herein defined as those which take into account perturbations such as solar radiation pressure and artificial propulsion methods [98].

In the late 1970's/early 1980's it was proposed by Driver to use the continuous low-thrust provided by an EP system to allow a spacecraft to be placed above one of the Earth's poles, to give hemispheric views, a concept termed "Polesitter" [31]. This involved positioning a spacecraft between *1* and *3 million kilometres* above the surface of the Earth where the minimum required acceleration occurred at an altitude range of *2.29 – 2.74 million kilometres* depending on the time of year, where within this range the acceleration varies between *0.155* and *0.166 mm/s*^{2} [99]. Driver also considered a spacecraft positioned closer

to Earth. For example at *1.1 million kilometres* altitude where the acceleration necessary to achieve such an orbit is shown to be relatively high at *0.35 mm/s^2*, which in turn limits the mission lifetimes to around two years [31]. The considerable distance of the spacecraft from the Earth also constrains the resolution and thus the potential applications of the Polesitter concept. In the visible range, resolutions around *20 km* are said to be achievable, with resolutions less than *1 km* expected to be extremely unlikely for these systems [31]. In the infrared range, resolutions are limited to between *12* and *70 km* for a spacecraft positioned at *2 million kilometres* range depending on the instrument size [31]. In the microwave band significant issues arise, with an instrument of at least *7 m* required to achieve a resolution less than *100 km* with a spacecraft at an altitude of *2 million kilometres* [31]. A further drawback of this concept is that twice a year the thrusters point back to Earth and the exhaust plume from the thruster may therefore interfere with the observations.

A recent investigation has also considered the extension of Earth-centred sun-synchronous orbits using continuous acceleration, likely provided by an EP system, to enable free-selection of the orbit inclination and altitude [100]. Within this work, the thrust magnitude is not defined as a function of the local gravity field but instead by the magnitude of the perturbations within that field, augmenting the Earth oblateness perturbation to modify the sun-synchronous orbit. As the sun-synchronous orbit is essentially a finite resource, these newly developed orbits can increase the number of vantage points and enhance the potential opportunities for EO. This study considered the extension of circular sun-synchronous orbits with altitudes varying from *250* to *3000 km* using accelerations from *-1* to *1 mm/s^2* in step sizes of *0.1 mm/s^2* to achieve the displacements. It is noted however, that in order to achieve significant displacements a relatively large thrust is required.

2.2 Solar Sailing

Highly reflective solar sails are another means of low-thrust propulsion. Although first discussed in 1921 by Tsiolkovsky [101] and again in the first practical paper on the subject by Tsander in 1924 [102], they have only recently undergone testing, owing to the necessary advances in materials to make solar sailing a viable means of spacecraft propulsion. Recently elements of this technology were successfully demonstrated in space on board both the Japanese IKAROS spacecraft (Figure 2-7) [61, 103] and NASA's NanoSail-D mission (Figure 2-7) [104].

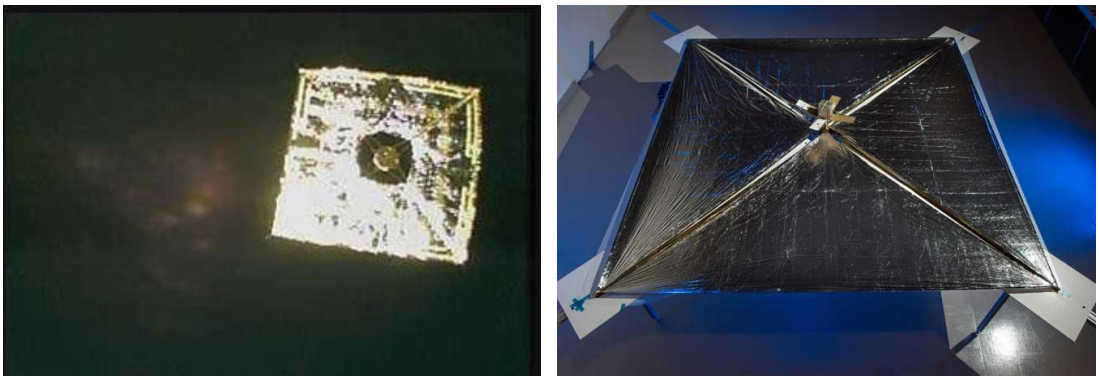

Figure 2-7 IKAROS flying in deep space (left, image credit JAXA), NanoSail-D (right, image credit NASA)

Solar sails exploit Solar Radiation Pressure and the subsequent momentum transfer generated by photons reflecting off a large sail to produce continuous propellant-less thrust. The force supplied by a single photon is extremely small and so large, light sails are used to maximise the number and impact of incident photons and supply a useful level of thrust. The main benefit of solar sailing is the lack of reaction mass required to propel the spacecraft.

2.2.1 Solar Sail Technology Development

The early 20th century saw the first ideas emerge on the use of solar radiation pressure as a means of space propulsion by Konstantin Tsiolkovsky and Fridrikh Tsander [101, 102]. The initial concept was then revisited in the 1950s by the American engineer Carl Wiley, writing under the pseudonym Russell Sanders, who discussed the use of solar sails for orbit raising [105]. In the late 1950s Richard Garwin coined the term 'solar sailing' [106].

Development of the concept was on going throughout the late 1950s/early 1960s and in 1973 NASA launched Mariner 10, which flew by Mercury and Venus and made use of solar radiation pressure to control the attitude of the spacecraft [107].

The first demonstrations of in orbit deployment of sail-like structures were in 1993 and 1996 by the Russian Space Regatta Consortium with Znamya 2 [108] and NASA Goddard with the Inflatable Antenna Experiment (IAE) on board the Spartan mission 207 [109]. Again in 1999, the successful deployment of a *20 m* square sail was carried out by the German space agency DLR in association with ESA and INVENT GmbH [110].

In the early to mid 2000s NASA made significant advancements in solar sail development. In conjunction with L'Garde, they embarked on a project which aimed to raise the TRL of a solar sail from 3 to 6, which involved the design, development and vacuum testing of a *10 m* square solar sail [111]. This effort subsequently led to the development of a *20 m* square sail which was successfully deployed and tested inside NASA's Plum Brook vacuum chamber in Ohio [112].

IKAROS, first introduced in **Section 1.3.2**, became the first spacecraft to successfully use a solar sail as the main method of propulsion in interplanetary space in 2010, where a *14 x 14 m* polyimide sail was employed to perform a flyby of Venus [61]. The IKAROS mission was successful in a number of criteria, namely: demonstrating the deployment of a large

membrane sail; generating electricity by thin film solar cells; demonstrating photon propulsion and guidance and navigation and control skills for solar sail propulsion. It will thus be used as the precursor to future Japanese solar sail concepts [113].

The late 2000s also saw NASA resources directed towards the development of solar sails for small satellite propulsion with the use of NanoSail-D, a subscale solar sail system on board a three-unit (3U) CubeSat measuring *30 x 10 x 10 cm* and a mass of *4 kg*. NanoSail-D first launched in 2008 but due to failure of the rocket, never achieved orbit [114]. However on the second attempt in 2011 the sail was successfully deployed [104].

Similar to NanoSail-D, CubeSail (Figure 2-8) is a nano-solar sail mission based on the 3U CubeSat standard which is being designed and built at the Surrey Space Centre, University of Surrey [115]. The CubeSail mission will deploy a *3 kg*, *5 x 5 m* sail to demonstrate the concept of solar sailing and end-of-life de-orbiting using the sail membrane as a drag sail [115]. The 3U CubeSat configuration is also being used to house LightSail-1, a project being developed by the Planetary Society which aims to demonstrate the viability of solar sailing as well as develop key technologies, such as sail deployment, sail management during flight and gossamer structure dynamics [116].

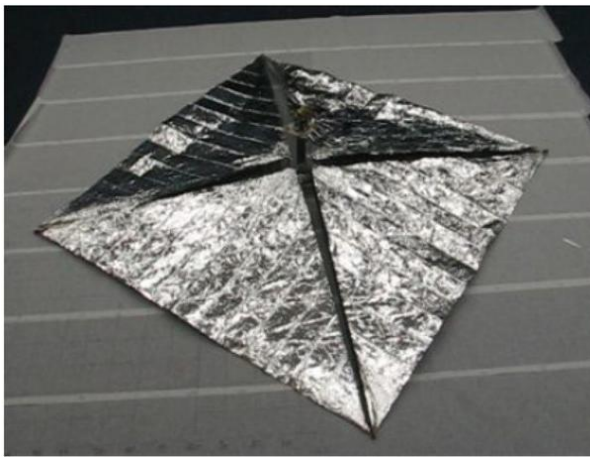

Figure 2-8 CubeSail engineering model ground deployment (image credit Surrey Space Centre, University of Surrey)

Previous missions demonstrating the use of solar sails for various purposes have been pioneering and will be used as a foundation for the future development of sail technology. In late 2011, NASA announced three proposals for flight demonstration. These included the "In-Space Demonstration of a Mission-Capable Solar Sail", a mission which builds on the previous tests by L'Garde and seeks to fly a *1200* m^2 sail - the largest ever flown in space - to prove the viability of the technology. This Solar Sail Demonstration could launch as early as 2014[4]. Missions such as these will provide the necessary advances in technology to further develop the solar sailing concept to enable more advanced future solar sail missions.

2.2.2 Design Parameters

The acceleration produced by the solar sail is derived and in doing so the design parameters, which characterise the performance of the sail, are introduced. These metrics determine the transfer time of the spacecraft to a particular target or whether a class of orbits is possible [108].

[4] http://www.nasa.gov/mission_pages/tdm/solarsail/solarsail_overview.html. Accessed November 20th 2012

From [108], the force exerted by photons on a solar sail of area A_s, with unit vector $\boldsymbol{n}$ directed normal to the surface of the sail, is given by

$$f_i = PA_s\left(\mathbf{u_i}\cdot\mathbf{n}\right)\mathbf{u_i} \tag{2.1}$$

where P is the pressure exerted on the surface due to the momentum transport by photons and $\boldsymbol{u_i}$ is the direction of incident photons, shown in Figure 2-9. The reflected photons will exert a force of equal magnitude on the surface, but in the specular reflected direction, $\boldsymbol{-u_r}$, given by

$$f_r = -PA_s\left(\mathbf{u_i}\cdot\mathbf{n}\right)\mathbf{u}_r \tag{2.2}$$

Using the vector identity $\mathbf{u_i}-\mathbf{u_r}=2\left(\mathbf{u_i}\cdot\mathbf{n}\right)\mathbf{n}$, the total force exerted on the sail is

$$f = 2PA_s\left(\mathbf{u_i}\cdot\mathbf{n}\right)^2\mathbf{n} \tag{2.3}$$

The total force on the sail can also be given using the expressions for the pressure exerted on the surface P (Eq. (2.4)), and the energy flux of photons (Eq. (2.5)) which is given in terms of the solar luminosity, L_s, the distance from the Sun, r_s, and is scaled by the Sun-Earth distance, R_s.

$$P = \frac{W}{c} \tag{2.4}$$

where, c is the speed of light

$$W = \frac{L_s}{4\pi {R_s}^2}\left[\frac{R_s}{r_s}\right]^2 = W_e\left[\frac{R_s}{r_s}\right]^2 \tag{2.5}$$

$$f_s = \frac{2A_sW_e}{c}\left[\frac{R_s}{r_s}\right]^2\left(\mathbf{u_i}\cdot\mathbf{n}\right)^2\mathbf{n} \tag{2.6}$$

where W_e is the mean solar irradiance measured at Earth's distance from the Sun, which has a value of *1366.1 W/m²* [117].

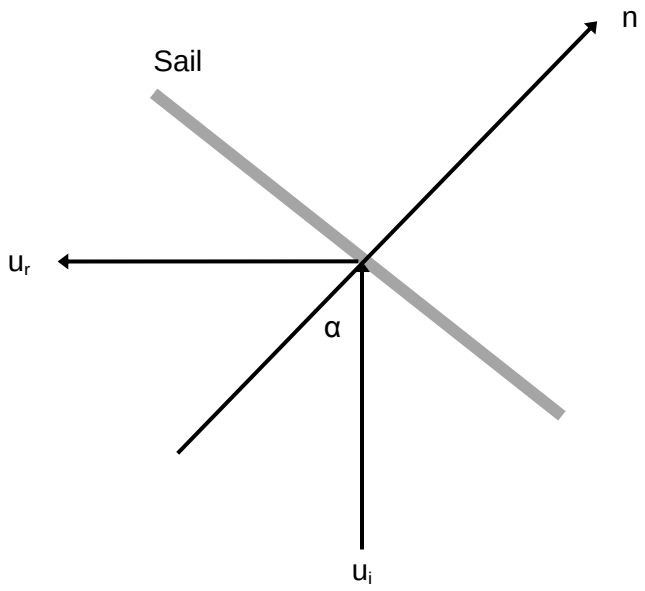

Figure 2-9 Perfectly reflecting solar sail

The acceleration experienced by the solar sail can be given in terms of the sail loading, σ_s, a performance parameter defined as the sail mass per unit area (m_s / A_s), and the sail pitch angle, α, which is the angle between the sail normal and the incident radiation, shown in Figure 2-9.

$$\mathbf{a}_s = \frac{2W_e}{c}\frac{1}{\sigma_s}\left[\frac{R_s}{r_s}\right]^2 \cos^2(\alpha)\ \mathbf{n} \tag{2.7}$$

An analogous parameter to the sail loading is the solar sail characteristic acceleration, defined as the actual acceleration experienced by a solar sail facing the Sun ($\alpha=0$) at a distance of one astronomical unit (AU), the mean distance of the Earth from the Sun. At this distance the magnitude of the solar radiation pressure, *P,* is 4.56×10^{-6} *N/m²*. The sail characteristic acceleration is then given by

$$a_{sc} = \frac{9.12\eta_s}{\sigma_s\left[gm^{-2}\right]}\left[mms^{-2}\right] \tag{2.8}$$

or

$$a_{sc} = \frac{2\eta_s P}{\sigma_s} \tag{2.9}$$

where η_s is the overall efficiency of the solar sail used to account for the reflectivity of the sail film which is typically of the order *0.85 – 0.9* [108]. The mass of the solar sail in the sail loading expression consists of two components, the sail film and structure and the mass of the spacecraft. The characteristic acceleration may now be written as

$$a_{sc} = \frac{2\eta_s P}{\sigma_s + \left(m_p / A_s\right)} \tag{2.10}$$

Where m_p is the spacecraft mass. The acceleration generated by a perfectly reflecting solar sail may also be written in terms of the solar gravitational acceleration as

$$\mathbf{a_s} = \beta \frac{GM_s}{r_s^2}(\hat{\mathbf{r}} \cdot \mathbf{n})^2 \mathbf{n} \tag{2.11}$$

where G is the universal gravitational constant, M_s is the solar mass and β is defined as the sail lightness number, given by the ratio of the solar radiation pressure acceleration to the solar gravitational acceleration. Using Eqs. (2.5), (2.7) and (2.11) the solar sail lightness number is given by

$$\beta = \frac{\sigma^*}{\sigma_s} \tag{2.12}$$

where

$$\sigma^* = \frac{L_s}{2\pi G M_s c} \tag{2.13}$$

The critical sail loading, σ^*, has a constant value of $1.53\ g/m^2$ for our Solar System for the values of solar mass and solar luminosity. The sail lightness number is equal to one when the mass per unit area is equal to the critical loading parameter; this however is an extremely challenging requirement to achieve.

The design space for various solar sail missions, including those first introduced in Section 2.2.1 and those which will be discussed in Section 2.2.3, are shown in Figure 2-10 and Figure 2-11. The design space plots show the required sail loading and solar sail areas, with missions split into lower, upper and mean application bounds to show the nearest term and most advanced proposed solar sail missions. The sail loading and area values and the corresponding characteristic accelerations for selected missions are also shown in Table 2-1.

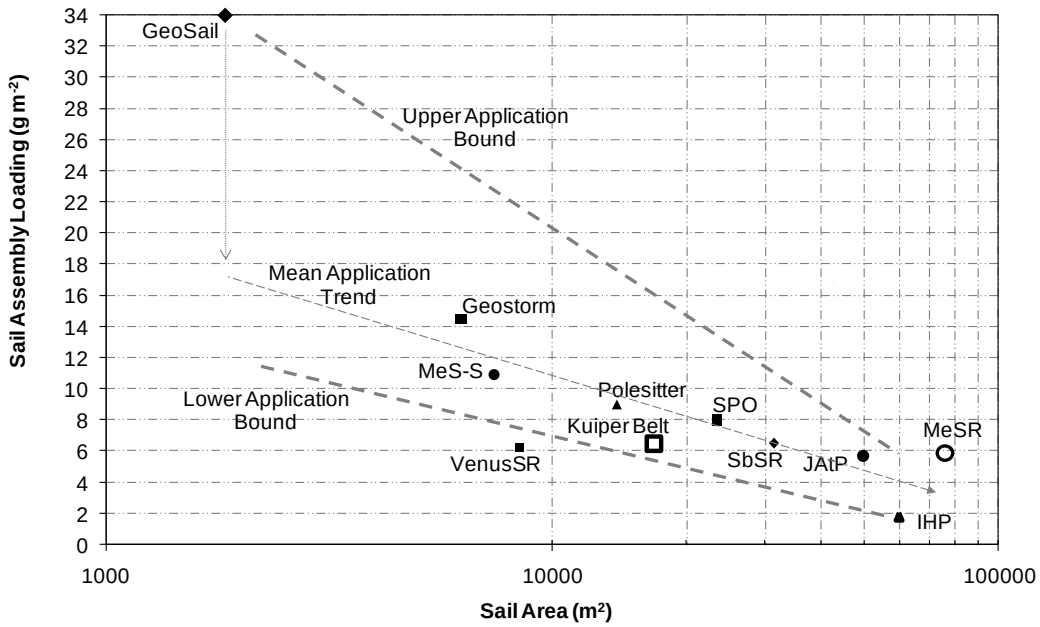

Figure 2-10 Solar sail mission catalogue application technology requirements (image credit Macdonald et al. in [67]). *IHP = Interstellar Heliopause Probe; JAtP = Jupiter Fly-by with Atmospheric Probe release; MeSR = Mercury Sample Return; MeS-S = Mercury Sun-Synchronous; SbSR = High-Energy Small-Body Sample Return; SPO = Solar Polar Orbiter; VenusSR = Venus Sample Return*

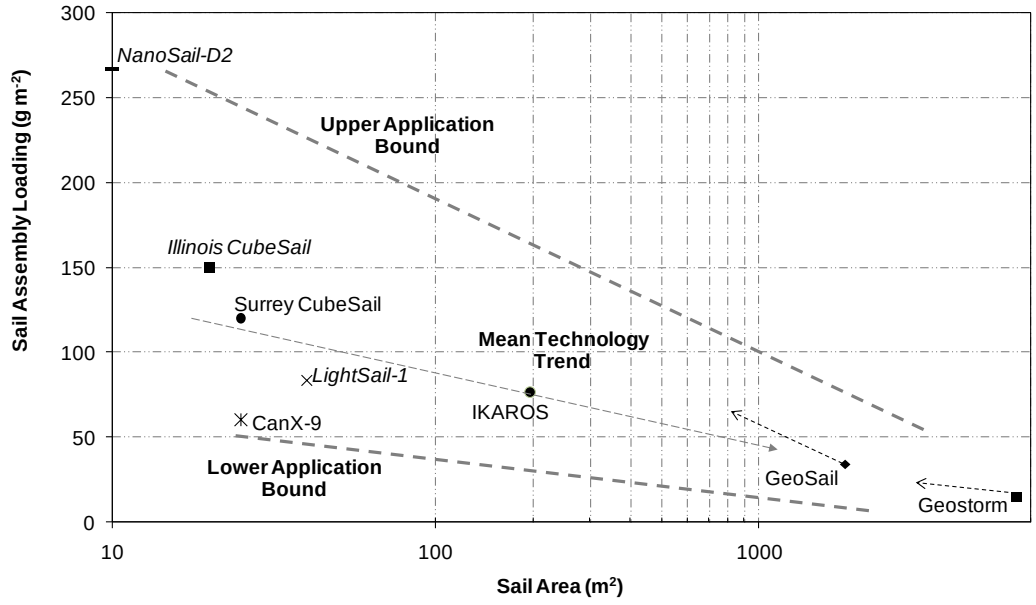

Figure 2-11 CubeSat solar sail design space (image credit Macdonald et al. in [67])

Table 2-1 Solar sail mission applications and summaries; sorted from near to far term [118]

Mission	a_{sc} [mm/s^2]	σ_s [g/m^2]	A_s [m^2]
GeoSail	0.10	35	1850
Geostorm	0.31	15	6200
Solar Polar Observer	0.42	8	23400
Kuiper Belt	0.50	6	16900
High-Energy Small Body Sample Return	0.50	6.5	31000
Interstellar Heliopause Probe	1.50	< 2	60000

2.2.3 Applications

Developments in solar sail technology and recent successes in initial solar sail demonstration missions makes the prospect of using solar sails as a viable means of spacecraft propulsion in the near future more probable. New mission concepts can be enabled using solar sails, while others may be significantly enhanced – for example high-energy missions requiring very close solar passes or for missions which spend the majority of time within the inner solar system. The use of solar sails for applications at Earth has also previously been considered.

As early as 1981, Forward presented the concept of using a solar sail to displace a body north or south of the geostationary ring around the Earth [119, 120]. This initial idea was advanced by Baig and McInnes in 2010, where it was shown that solar sails could be placed around *25 km* above the nominal geostationary ring whilst maintaining the 24 h orbit period [121]. These orbits were proposed as a possible solution to the increasing problem of the congestion of the conventional geostationary orbit and to reduce the propellant demands from EP systems [122].

In the early 1990s Forward also recommended the use of a solar sail to provide the required thrust for the so-called 'statite' mission concept [123], previously described in **Section 2.1.4** using EP. In this case the spacecraft is positioned high above one of the Earth's poles, using a solar sail to enable polar communications. Notably, this work considered an ideal solar sail model; however, subsequent investigation of this concept using a partially reflecting solar sail has shown that the reflectivity of the solar sail has a significant effect on the volume of space where equilibrium solutions are possible [124]. Extensive investigation has been conducted into this concept using other propulsion systems, which will be described further in **Section 2.3**.

The GeoStorm mission concept arose in the late 1990s as a result of an enquiry from the National Oceanic and Atmospheric Administration (NOAA) to the Jet Propulsion Laboratory (JPL) for a possible solution to improve the warning time of impending space weather events, such as geomagnetic storms [125]. These events can pose a risk to electronics and telecommunication systems both on Earth and in LEO. The proposed mission involved positioning a solar sail inside the L_1 point at $\sim 0.98\ au$ to provide real-time monitoring of solar activity and enhance the warning time of space weather events by a factor of three [125]. Investigation by McKay et al. into the use of EP to enable a similar mission shows that in this case the mission lifetime would be limited to around 3 years [98]. Thus, subsequent missions would be required after this time, making solar sails a more viable option for this type of mission. Although the 1999 St-5 GeoStorm mission was not selected by NASA for flight demonstration, it was useful to highlight the potential performance [125].

The GeoSail mission, proposed in 2000 [126], aimed to achieve long residence times in the Earth's magnetotail to allow high-resolution data of the plasma in a region subjected to a

variety of external solar wind conditions. A solar sail is used to precess an elliptical, Earth-centred orbit at a rate designed to match the rotation of the geomagnetic tail. Previous research has shown that conventional, inertially fixed orbits with apogee inside the geomagnetic tail are limited to provide less than three months of science due to the rotation of the geomagnetic tail with the Sun-Earth line in an inertial reference frame [127]. Solar sails have been shown to be the optimal propulsion systems to enable such a mission with mission lifetimes for chemical propulsion being restrictively low and the high propellant mass requirements of an EP system in this case [118-120]. However, issues may arise due to the interference of the solar sail with the science suite during mission operation [127].

A similar concept to the Polesitter mission is the solar-sail displaced eight-shaped orbit which has recently been considered by Ceriotti et al. [34]. The use of such orbits for high-latitude observation was first proposed by Folta et al. in 2001 [128] and more recently displaced eight-shaped orbits have been investigated to provide similar applications [99]. These orbits use continuous acceleration produced by a solar sail to displace the Lagrangian points, L_1 and L_2. However, due to the oscillation above and below the ecliptic plane, continuous coverage of the Earth's polar regions cannot be provided using a single spacecraft. Two spacecraft are therefore required to provide continuous coverage of a single pole, with three necessary to view both poles continuously. The significant distance of these orbits from the surface of the Earth, between *1* and *2 million km,* means resolutions less than *500 m* are highly unlikely in the visible region [99].

2.3 Hybrid Solar Sail / Electric Propulsion

As explained previously, EP is a mature technology with high TRL and low AD^2 [67, 68]. However mission lifetimes are limited by the amount of propellant that can be carried.

Solar sailing, on the other hand, is essentially a propellant-less propulsion system and so can in theory maintain low-thrust indefinitely. However, it has a high AD^2 and cannot produce any thrust in the direction of the Sun. Consequently, consideration has been given to hybrid EP and solar sail propulsion, first proposed by Leipold and Götz [129]. Such systems can reduce the propellant requirements of the EP system and use the EP to compensate for the limitations of the sail thrusting direction. The use of a small solar sail on the spacecraft also contributes towards lowering the AD^2 of solar sailing [67].

The complementary nature of the two propulsion systems enables a new range of missions which require continuous low-thrust. These hybrid solar sail / EP systems have been proposed for various applications including modifying the well-known Polesitter concept previously detailed in **Sections 2.1.4** and **2.2.3**. The use of so-called hybrid propulsion to allow a spacecraft to be positioned above the L_1 point to provide low-resolution polar imaging was first suggested in 2008 by Baig et al. [130] and was further developed by Ceriotti et al. from 2010 onwards [32, 33]. Such a system allows the spacecraft to be statically stationed above one of the Earth's poles at around *2 million kilometres* range, giving continuous observation of one of the Earth's poles using a single spacecraft. Hybrid solar sail / EP Polesitter orbits can offer reductions in the propellant requirements over conventional Polesitter concepts and therefore allow increased mission durations or additional capacity for useful payload. However, the limitations of possible applications discussed in **Sections 2.1.4** and **2.2.3** remain valid.

Similarly, the concept of the displaced geostationary orbit above or below the conventional geostationary ring, as first outlined in **Section 2.2.3**, has also been considered using hybrid EP / solar sail propulsion [131, 132]. This allows displaced geostationary missions to be enabled where the use of a pure solar sail system is not feasible due to the obliquity of the

ecliptic. The hybrid propulsion also offers a solution for the problem of the inability of the sail to thrust in the direction of the sun and again offers a reduction in the propellant requirements over an EP-only case.

Hybrid solar sail / EP systems have also been suggested to create artificial equilibrium points in the circular restricted three body problem [130].

Chapter 3

3 Taranis Orbits

This chapter introduces the development of novel HEOs at Earth, termed Taranis orbits. **Section 3.2** derives the orbits using a general perturbations technique, which uses locally optimal control laws to apply the acceleration required to enable such orbits. This section also considers the effect of the applied acceleration on the orbital elements. **Section 3.3** then presents an extended general perturbations solution to reduce the required acceleration magnitude. **Section 3.4** presents validation of the general perturbations solution using a special perturbations method. Finally fuel optimal solutions are generated in **Section 3.5** using Pseudospectral optimisation.

3.1 Introduction

Taranis, the Celtic God of thunder, is the name given to a novel family of orbits developed using continuous low-thrust propulsion. These newly proposed orbits are essentially an extension of the conventional Molniya orbit (meaning lightning), and use applied acceleration to modify the critical inclination while maintaining the zero change in argument of perigee condition essential to HEOs. Continuous acceleration is applied to allow the value of the inclination to be varied from the fixed values of *63.43* or *166.6 degrees* to any inclination required to optimally fulfil the mission objectives, while still maintaining the zero change in argument of perigee condition essential to these HEOs. Thus increasing the potential opportunities for remote sensing of Earth, in particular of the high-latitude regions.

The extension of HEOs using general and special perturbation techniques is presented. Optimisation of these results using pseudo-spectral optimisation methods is also conducted; this process removes the assumptions which are used to generate the initial analytical expressions and allows fuel optimal solutions to be generated.

3.2 General Perturbations Solution

3.2.1 Spacecraft Motion about an Oblate Body

Taranis orbits employ acceleration to compensate for the drift in argument of perigee caused by the Earth's gravitational field. Thus, to investigate the effects of low-thrust propulsion applied to HEOs, the gravitational potential of a body is considered in Eq. (3.1) [133].

$$U\left(r,\beta_s,\lambda\right)=\frac{\mu}{r}\sum_{n=0}^{\infty}\sum_{m=0}^{\infty}\left(\frac{R_E}{r}\right)^n\left(C_{n,m}\cos\left(m\lambda\right)+S_{n,m}\sin\left(m\lambda\right)\right)P_{n,m}\sin\left(\beta_s\right) \tag{3.1}$$

For a body possessing axial symmetry, the influence of periodic effects (tesseral and sectorial harmonics) can be neglected for most orbits and, with the notable exception of GEO this holds true for Earth. The gravitational potential can therefore be written as

$$U\left(r,\beta_s\right)=\frac{\mu}{r}\left[1-\sum_{n=0}^{\infty}J_n\left(\frac{R_E}{r}\right)^n P_{n,m}\sin\left(\beta_s\right)\right] \tag{3.2}$$

Expanding Eq. (3.2), the gravitational potential becomes

$$
\begin{aligned}
U(r,\beta_s) = \frac{\mu}{r}[1 - J_2 \frac{1}{2}\left(\frac{R_E}{r}\right)^2 \left(3\sin^2(\beta_s) - 1\right) \\
- J_3 \frac{1}{2}\left(\frac{R_E}{r}\right)^3 \left(5\sin^2(\beta_s) - 3\right)\sin(\beta_s) \\
- J_4 \frac{1}{8}\left(\frac{R_E}{r}\right)^4 \left(3 - 30\sin^2(\beta_s) + 35\sin^4(\beta_s)\right) \\
- J_5 \frac{1}{8}\left(\frac{R_E}{r}\right)^5 \left(63\sin^5(\beta_s) - 70\sin^3(\beta_s) + 15\sin(\beta_s)\right) \\
- \ldots]
\end{aligned}
\tag{3.3}
$$

Where

$$
\sin(\beta_s) = \sin(i)\sin(u) \tag{3.4}
$$

From Eq. (3.4), u is the argument of latitude $(\theta + \omega)$. At Earth the values of J_2 to J_5 are 1.082627×10^{-3}, -2.53266×10^{-6}, -1.61962×10^{-6} and -0.227296×10^{-6} respectively. Considering only first order perturbations, a reasonable assumption at Earth, and using spherical triangle laws, Eq. (3.3) simplifies to

$$
U(r,\beta_s) = U_o + U_p = \frac{\mu}{r} - J_2 \frac{\mu R_E^2}{2r^3}\left(3\sin^2(i)\sin^2(\theta+\omega) - 1\right) \tag{3.5}
$$

The net impact of the perturbations caused by the oblate nature of the Earth must be zero to ensure the argument of perigee and thus the position of apogee remains unchanged. Using the Gauss form of the Lagrange Planetary Equation, in terms of a spacecraft centred Radial, Transverse and Normal (RTN) coordinate system the rate of change of argument of periapsis is written as [70]

$$
\frac{d\omega}{d\theta} = \frac{r^2}{\mu e}\left[-R\cos(\theta) + T\left(1 + \frac{r}{p}\right)\sin(\theta)\right] - \frac{r^3}{\mu p \tan(i)}\sin(\theta+\omega)N \tag{3.6}
$$

where the orbital radius is defined as

$$r = \frac{p}{1 + e\cos(\theta)} \tag{3.7}$$

The disturbing force components in the radial, transverse and normal directions due to J_2 are found by taking the partial derivatives of Eq. (3.5) with respect to *r*, *u* and *i* respectively as follows

$$R_{J_2} = \frac{\partial U_p}{\partial r} \tag{3.8}$$

$$T_{J_2} = \frac{\partial U_p}{r\partial u} \tag{3.9}$$

$$N_{J_2} = \frac{\partial U_p}{r\sin(u)\partial i} \tag{3.10}$$

This results in the following expressions for the R,T and N perturbations due to J_2 in Eqs. (3.11) - (3.13) [8]

$$R_{J_2} = \frac{3}{2}\frac{J_2 \mu R_E^2}{r^4}\left(3\sin^2(i)\sin^2(\theta+\omega) - 1\right) \tag{3.11}$$

$$T_{J_2} = -\frac{3}{2}\frac{J_2 \mu R_E^2}{r^4}\sin^2(i)\sin 2(\theta+\omega) \tag{3.12}$$

$$N_{J_2} = -\frac{3}{2}\frac{J_2 \mu R_E^2}{r^4}\sin(2i)\sin(\theta+\omega) \tag{3.13}$$

Substituting Eqs. (3.11) - (3.13) into Eq. (3.6) and integrating over one orbital revolution results in the well-known expression for the change in argument of perigee

$$(\Delta\omega)_0^{2\pi} = \frac{3J_2\pi R_E^2\left(3+5\cos(2i)\right)}{4a^2\left(-1+e^2\right)^2} \tag{3.14}$$

To determine the critical inclination, Eq. (3.14) is set equal to zero and solved, resulting in inclinations of *63.43* and *116.6 degrees*. Consequently, all Earth orbits inclined at these

values show no rotation of the apsidal line, irrespective of the values of semi-major axis or eccentricity. It is evident from Eq. (3.14) that altering the inclination from these critical values will result in a drift in the argument of periapsis due to the effect of J_2 perturbations. Therefore, for each value of inclination there exists an acceleration magnitude that will negate this drift and allow free-selection of the inclination.

3.2.2 Spacecraft Motion about an Oblate Body with Low-Thrust Propulsion

Taranis orbits are developed through the addition of low-thrust terms to the disturbing force components in Eqs. (3.11) - (3.13). This is achieved using the argument of periapsis locally optimal control, derived from the variational equation given in Eq. (3.6), by considering the sine and cosine terms in this equation. Locally optimal control laws maximise the instantaneous rate of change of the particular orbital element, provide the thrust orientation in analytical form and give the distinct position of the orbit where the sign of the thrust is required to switch direction [64].

The rate of change of argument of perigee, Eq.(3.6), can be written as

$$\frac{d\omega}{d\theta} = f_s \lambda_\omega \tag{3.15}$$

Which is in turn given by Eq. (3.16)

$$\frac{d\omega}{d\theta} = \frac{1}{\mu}\begin{bmatrix} F_r & F_t & F_n \end{bmatrix}\begin{bmatrix} -\frac{r^2}{e}\cos(\theta) \\ r^2\left(1+\frac{r}{p}\right)\sin(\theta) \\ -\frac{r^3}{p\tan(i)}\sin(\theta+\omega) \end{bmatrix} \tag{3.16}$$

Maximising the thrust vector along λ_ω maximises the right-hand side of Eqs. (3.15) and (3.16), thus the instantaneous rate of change of argument of perigee will be maximised.

From Eq. (3.16), it is clear that a switching relationship is required to maintain the desired rate of change of the argument of perigee. The radial component of acceleration switches direction with *cos(θ)*, the transverse acceleration switches direction with *sin(θ)*, and the normal acceleration switches direction with *sin(θ + ω)*. The combined J_2 and low-thrust perturbations in each of the radial, transverse and out-of-plane directions are thus given by

$$R_{J_2+F_r} = \frac{3}{2}\frac{J_2\mu R_E^2}{r^4}\left(3\sin^2(i)\sin^2(\theta+\omega)-1\right)+F_r\,\mathrm{sgn}\left[\cos(\theta)\right] \tag{3.17}$$

$$T_{J_2+F_t} = -\frac{3}{2}\frac{J_2\mu R_E^2}{r^4}\sin^2(i)\sin 2(\theta+\omega)+F_t\,\mathrm{sgn}\left[\sin(\theta)\right] \tag{3.18}$$

$$N_{J_2+F_n} = -\frac{3}{2}\frac{J_2\mu R_E^2}{r^4}\sin(2i)\sin(\theta+\omega)+F_n\,\mathrm{sgn}\left[\sin(\theta+\omega)\right] \tag{3.19}$$

The expression for the rate of change of the argument of periapsis with the application of low-thrust propulsion is determined by inserting Eqs. (3.17) - (3.19) into Eq. (3.6) to give

$$\begin{aligned}\frac{d\omega}{d\theta} = &-\frac{a^2\left(1-e^2\right)^2\cot(i)\sin(\theta+\omega)}{\mu\left(1+e\cos(\theta)\right)^3}\\ &\left(F_n\,\mathrm{sgn}\left[\sin(\theta+\omega)\right]-\frac{3J_2R_E^2\mu\left(1+e\cos(\theta)\right)^4\sin(2i)\sin(\theta+\omega)}{2a^4\left(1-e^2\right)^4}\right)\\ &+\frac{1}{e\mu\left(1+e\cos(\theta)\right)^2}a^2\left(1-e^2\right)^2\\ &\left(\cos\theta\left(-F_r\,\mathrm{sgn}\left[\cos(\theta)\right]-\frac{3J_2R_E^2\mu\left(1+e\cos(\theta)\right)^4\left(-1+3\sin^2(i)\sin^2(\theta+\omega)\right)}{2a^4\left(1-e^2\right)^4}\right)\right)\\ &+\left(1+\frac{1}{1+e\cos(\theta)}\right)\sin(\theta)\\ &\left(F_t\,\mathrm{sgn}\left[\sin(\theta)\right]-\frac{3J_2R_E^2\mu\left(1+e\cos(\theta)\right)^4\sin^2(i)\sin 2(\theta+\omega)}{2a^4\left(1-e^2\right)^4}\right)\end{aligned} \tag{3.20}$$

The change in argument of periapsis is found by integrating Eq. (3.20) over one orbital revolution, employing the assumption that the eccentricity is not equal to zero or one and

recognising the positions on the orbit where the low-thrust terms change sign. The total change in argument of perigee is made up of four terms, consisting of the change in argument of perigee due to J_2 effects and the effects of each of the *R*, *T* and *N* accelerations. The total variation in argument of perigee is given by

$$\left(\Delta\omega\right)_0^{2\pi} = \left(\Delta\omega\right)_{J_2} + \left(\Delta\omega\right)_{F_r} + \left(\Delta\omega\right)_{F_t} + \left(\Delta\omega\right)_{F_n} \tag{3.21}$$

where the gravitational component has previously been given in Eq. (3.14) and the radial and transverse acceleration components are given respectively as

$$\begin{aligned}\left(\Delta\omega\right)_{F_r} = \frac{1}{e\mu} 2a^2 F_r (&-2 + 2e^2 - 4e\sqrt{-1+e^2}\,\text{Arctanh}\left[\frac{-1+e}{\sqrt{-1+e^2}}\right] \\ &-e\sqrt{-1+e^2}\,\ln\left[\frac{1-e}{\sqrt{-1+e^2}}\right] + e\sqrt{-1+e^2}\,\ln\left[\frac{-1+e}{\sqrt{-1+e^2}}\right])\end{aligned} \tag{3.22}$$

$$\left(\Delta\omega\right)_{F_t} = -\frac{4a^2\left(-2+e^2\right)F_t}{e\mu} \tag{3.23}$$

It is also noted from Eq. (3.19) that the out of plane acceleration component, unlike the radial and transverse terms, switches sign as a function of argument of latitude. Consequently, the value assigned to the argument of perigee becomes important in this case. Considering an argument of perigee equal to both *0* and *270 degrees* therefore results in two normal acceleration components, given as

$$\left(\Delta\omega\right)_{F_n}^{\omega=0} = -\frac{4a^2 F_n \cot\left(i\right)}{\mu} \tag{3.24}$$

$$\begin{aligned}\left(\Delta\omega\right)_{F_n}^{\omega=\frac{\pi}{2}} = -\frac{1}{\sqrt{-1+e^2}\,\mu} a^2 F_n \cot\left(i\right)(&4\sqrt{-1+e^2} + 2e^2\sqrt{-1+e^2} - 12e\,\text{Arctanh}\left[\frac{-1+e}{\sqrt{-1+e^2}}\right] \\ &-3e\ln\left[\frac{1-e}{\sqrt{-1+e^2}}\right] + 3e\ln\left[\frac{-1+e}{\sqrt{-1+e^2}}\right]\end{aligned} \tag{3.25}$$

Substituting Eq. (3.14) and Eq. (3.22) - (3.25) into Eq. (3.21) results in two solutions for the change in argument of periapsis due to the applied acceleration. It is noted that if no additional out-of-plane acceleration is considered, the change in argument of perigee is the same irrespective of the value of argument of perigee. Initially, consideration is given to the application of continuous low-thrust in each of the RTN directions individually before multiple acceleration directions are studied. Considering each direction in turn, the analytical expressions from Eq. (3.21) are solved using the values of orbital parameters in Table 3-1 to give the constant acceleration magnitude required to compensate for the effects of the J_2 perturbation for a range of inclinations, out with the equatorial plane, between *5* and *175 degrees.* The results of which are shown in Figure 3-1.

Table 3-1 Orbital parameters – 12 h Earth orbit

Orbital Element	**Value**
Perigee Altitude	813 (km)
Apogee Altitude	39540 (km)
Ascending Node	330 (degrees)

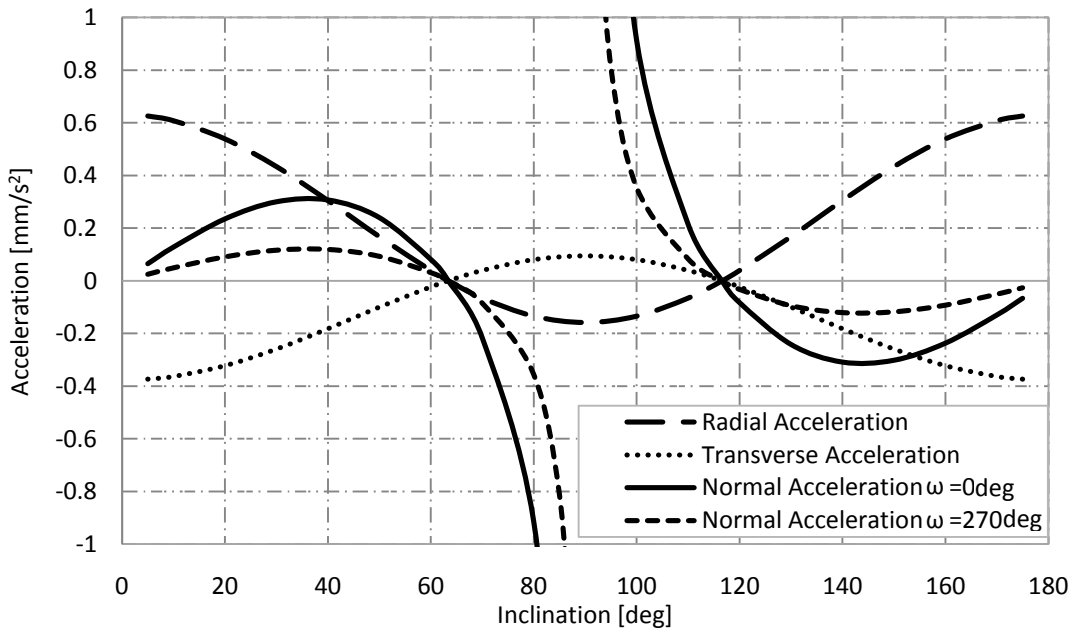

Figure 3-1 Required acceleration along a single axis to maintain zero change in argument of perigee over the orbit for various inclination values of the given 12 h Taranis orbit

The curves of minimum acceleration in any single axis required to alter the critical inclination of the orbit to a wide range of possible values for the orbit detailed in Table 3-1 are shown in Figure 3-1. It is noted that a singularity occurs at an inclination of *90 degrees* when thrusting in the normal direction. This can be explained by examining Eqs. (3.24) - (3.25), where it is shown that normal low-thrust terms in these expressions contain the term *cot(i)*, which at an inclination of *90 degrees* becomes undefined, causing the singularity. It is also shown that to allow an inclination of *90 degrees* by thrusting in any single direction a transverse acceleration of *0.094 mm/s²* is the lowest acceleration magnitude required. Nevertheless, Figure 3-3 illustrates that this total magnitude can be reduced to *0.0834 mm/s²* by combining equal magnitudes of radial and transverse accelerations. It is of note, however that the same cannot be said for combining the out-of-plane acceleration with either the radial or transverse accelerations, as shown in Figure 3-4 - Figure 3-7. The cause of this is once again the occurrence of *cot(i)* in the low-thrust

expression in the normal direction in Eqs. (3.24) - (3.25), As a result of the *cot(i)* term, the magnitude of this term is dependent on the value of inclination selected thus increasing the total thrust magnitude in certain instances. The combined multiple direction, equal magnitude thrust is sometimes greater than individual direction thrust magnitude, depending on the value of inclination. Therefore this is a clear indication that the choice of the proportion of the total acceleration in each direction is not optimal. The *90 degree* inclination orbit detailed in Table 3-1, is illustrated in Figure 3-2.

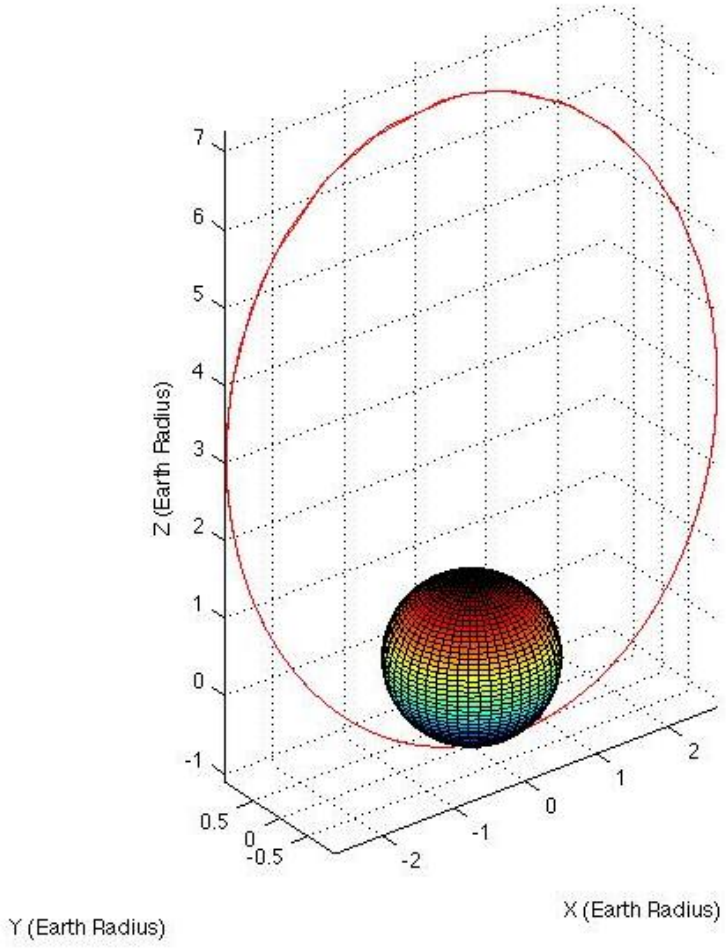

Figure 3-2 - *90 degree* inclination Taranis orbit

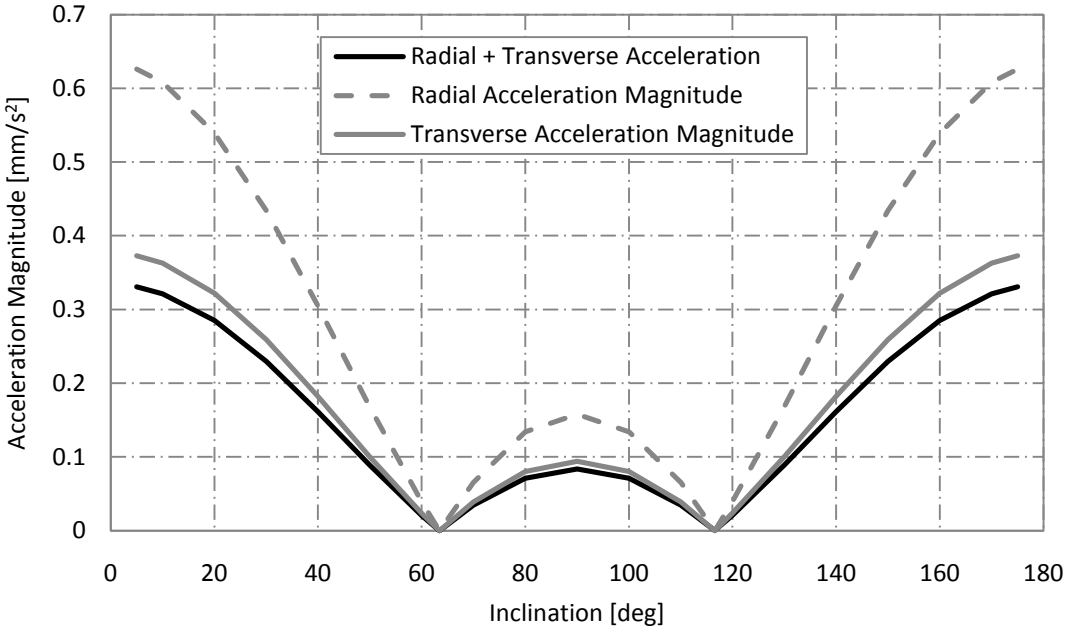

Figure 3-3 Comparison of combined Radial and Transverse acceleration with individual direction magnitudes for a 12 h Taranis orbit, from Table 3-1

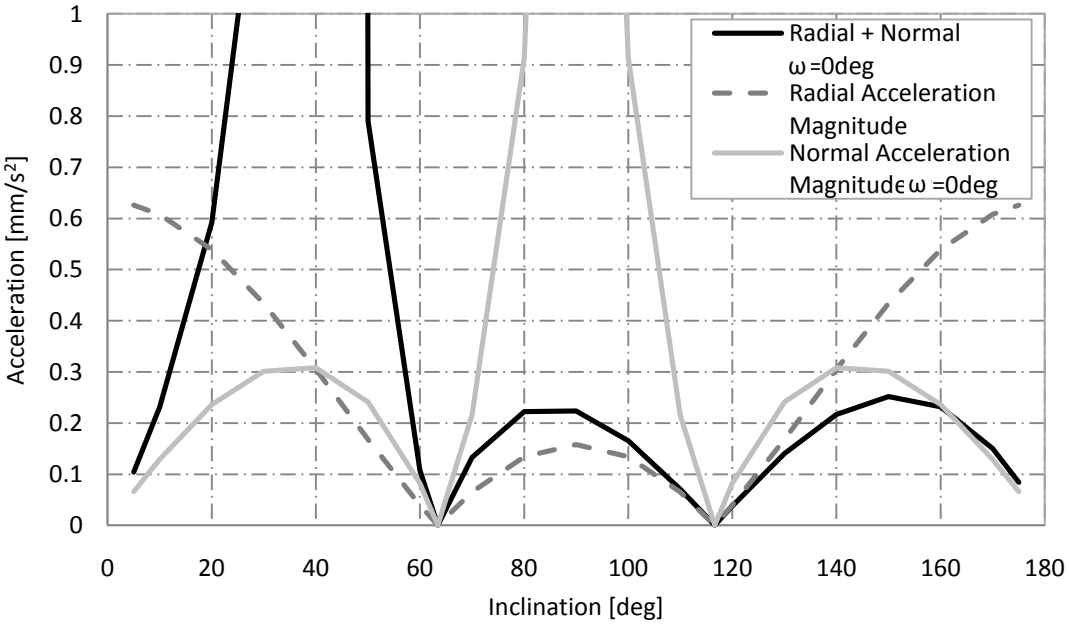

Figure 3-4 Comparison of combined Radial and Normal acceleration with individual direction magnitudes for a 12 h orbit with argument of perigee equal to *0 degrees*

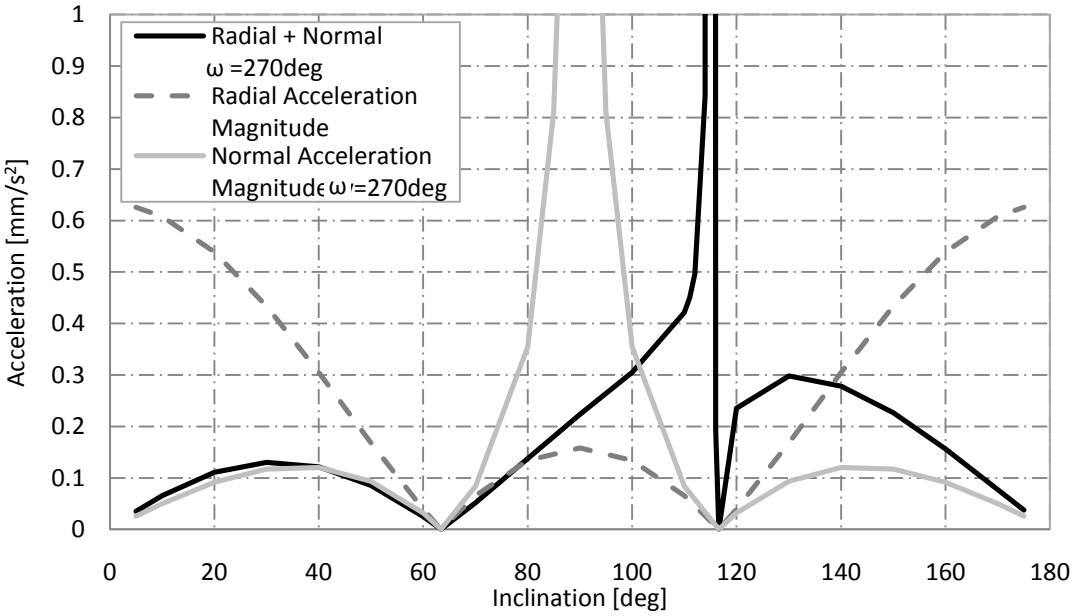

Figure 3-5 Comparison of combined Radial and Normal acceleration with individual direction magnitudes for a 12 h orbit with argument of perigee equal to *270 degrees*

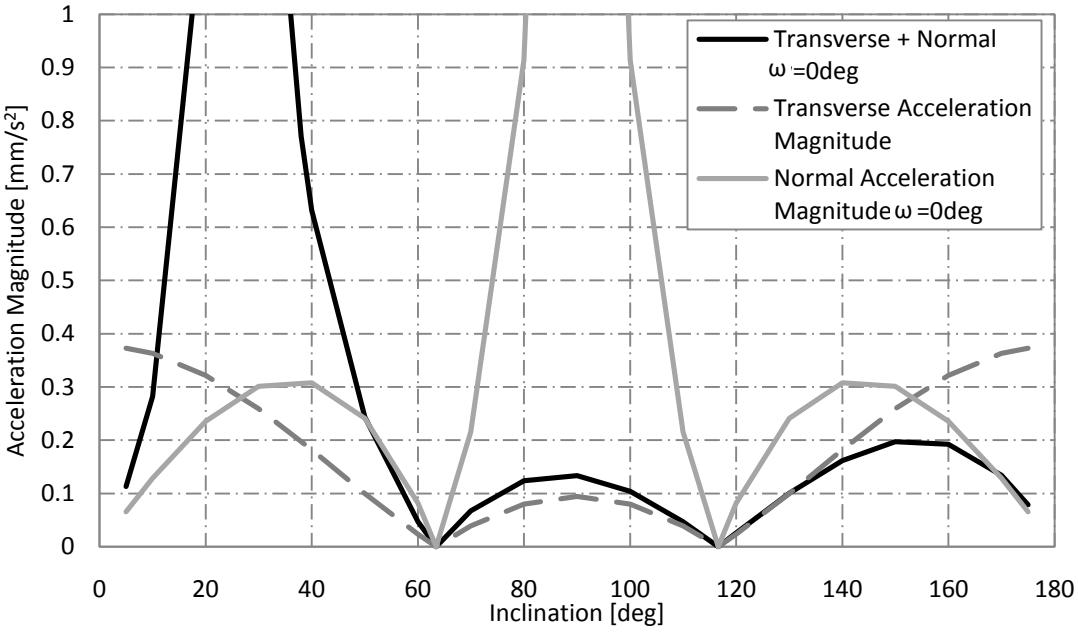

Figure 3-6 Comparison of combined Transverse and Normal acceleration with individual direction magnitudes for a 12 h orbit with argument of perigee equal to *0 degrees*

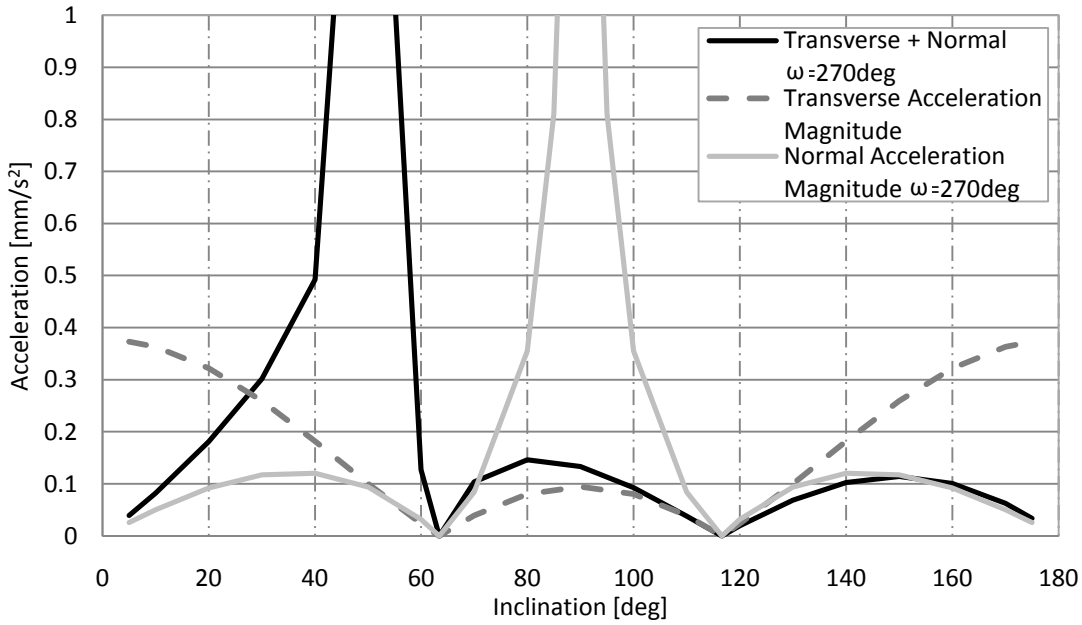

Figure 3-7 Comparison of combined Transverse and Normal acceleration with individual direction magnitudes for a 12 h orbit with argument of perigee equal to *270 degrees*

Figure 3-1 - Figure 3-7 show the acceleration magnitude required for a 12 h Taranis orbit in each direction individually compared with the acceleration combined in two directions. Although the results so far have detailed a 12 h orbit, this method can also be used to apply low-thrust to alter the critical inclination of an orbit with any period. A 16 h orbit is therefore also considered to examine the effect of changing the orbital period on the required acceleration. The orbital parameters for the 16 h orbit are given in Table 3-2.

Table 3-2 Orbital parameters – 16 h Earth orbit

Orbital Element	**Value**
Perigee Altitude	813 (km)
Apogee Altitude	50897 (km)
Ascending Node	330 (degrees)

As in the previous 12 h orbit case, acceleration is first applied in each direction individually. The acceleration required along each individual axis to alter the inclination is given in Figure 3-8.

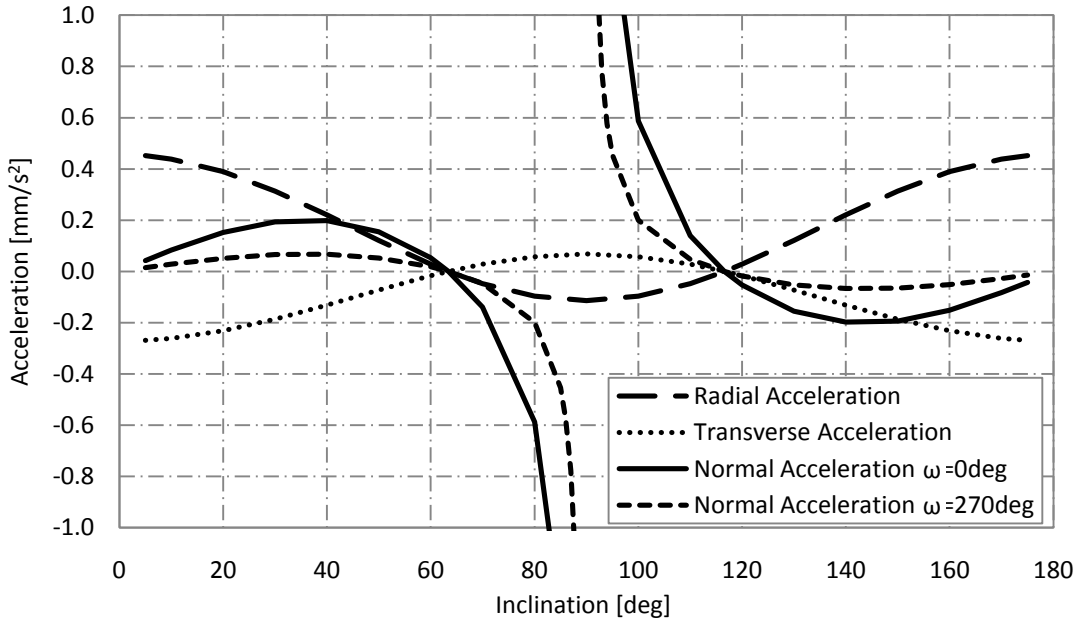

Figure 3-8 Required acceleration for acceleration along a single axis to vary the critical inclination of the given 16 h Taranis orbit

It can be seen from Figure 3-8 that applying the acceleration in each individual direction to orbits of various periods presents the same trends as shown in Figure 3-1. The acceleration magnitude required to alter the critical inclination is seen to decrease as the orbital period increases. This is further emphasised by considering the acceleration combined in multiple directions, as in Figure 3-9 - Figure 3-13 combining radial and transverse acceleration, radial and normal acceleration with argument of perigee values of both *0* and *270 degrees* and transverse and normal acceleration again for two values of argument of perigee.

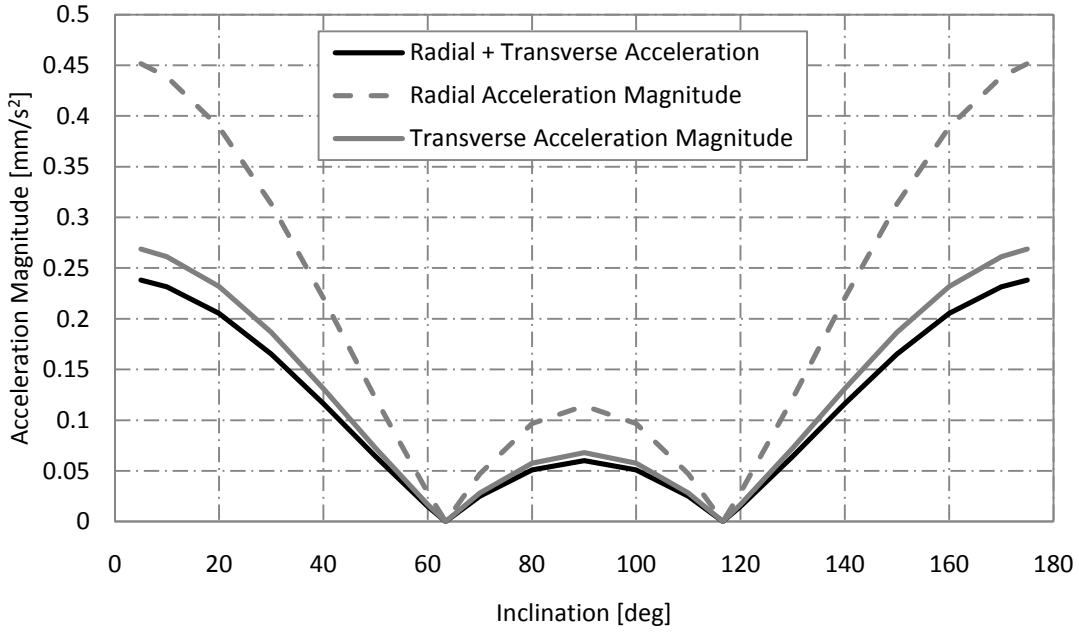

Figure 3-9 Comparison of combined Radial and Transverse acceleration with individual direction magnitudes for a 16 h orbit, from Table 3-2

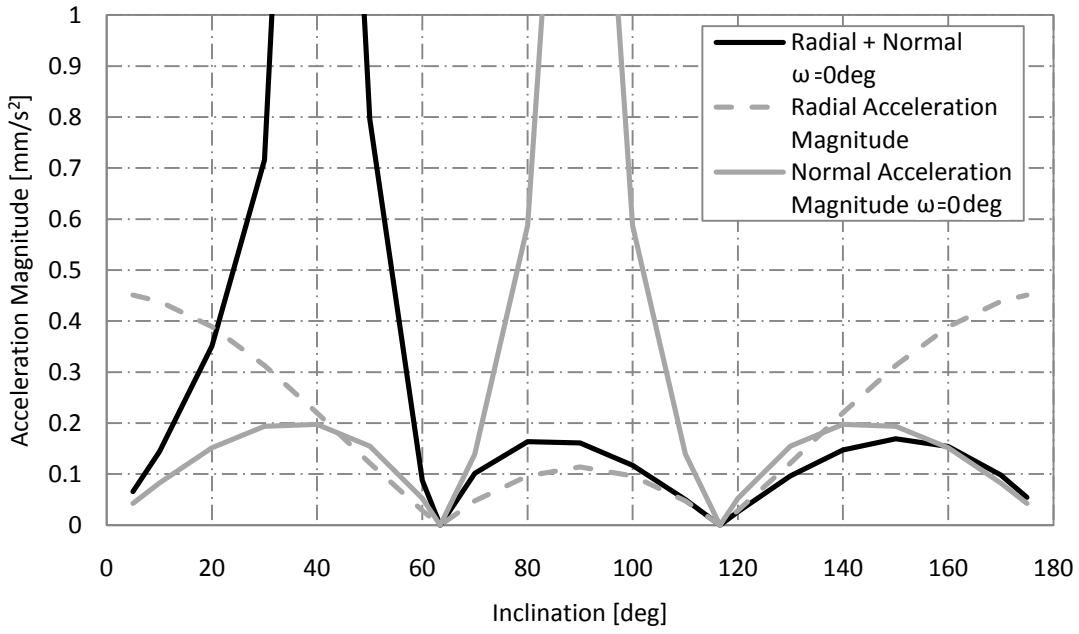

Figure 3-10 Comparison of combined Radial and Normal acceleration with individual direction magnitudes for a 16 h orbit with argument of perigee equal to *0 degrees*

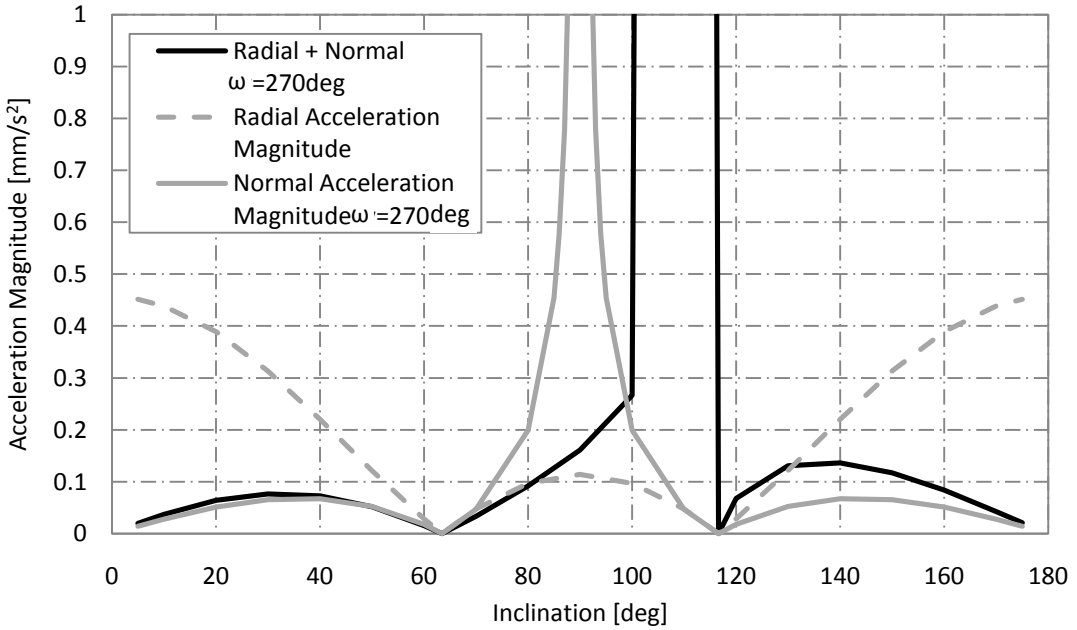

Figure 3-11 Comparison of combined Radial and Normal acceleration with individual direction magnitudes for a 16 h orbit with argument of perigee equal to *270 degrees*

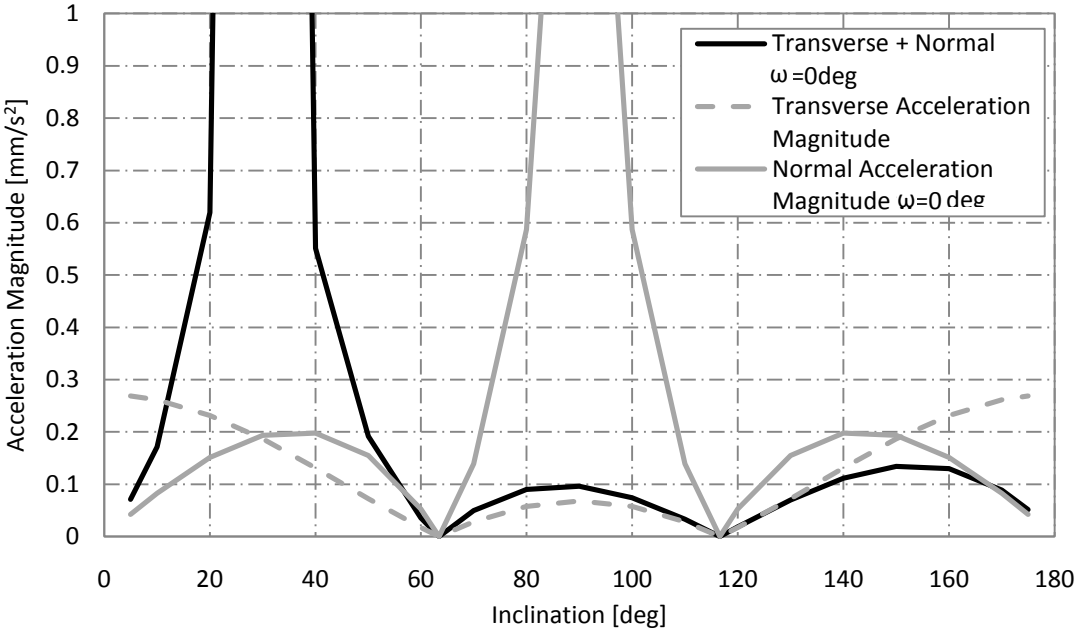

Figure 3-12 Comparison of combined Transverse and Normal acceleration with individual direction magnitudes for a 16 h orbit with argument of perigee equal to *0 degrees*

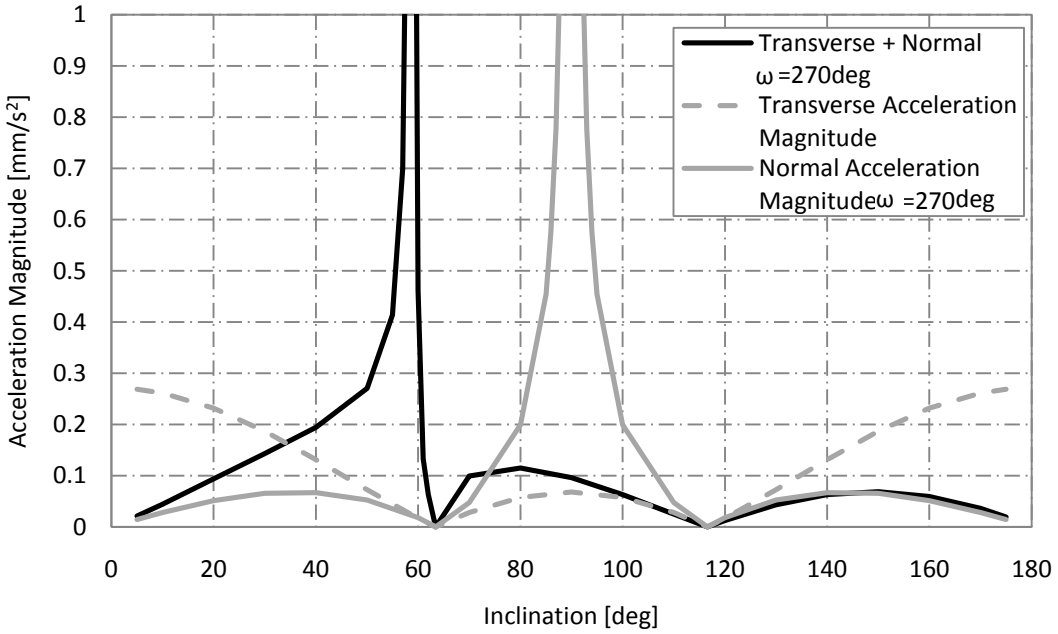

Figure 3-13 Comparison of combined Transverse and Normal acceleration with individual direction magnitudes for a 16 h orbit with argument of perigee equal to *270 degrees*

Consideration of both the 12 h and 16 h orbit examples reveals that the minimum acceleration magnitude occurs when combining acceleration in the radial and transverse directions, for an orbit with an inclination of *90 degrees*. This is therefore the combination of acceleration considered herein.

Figure 3-14 gives the total acceleration magnitude required to negate the effect of the J_2 perturbation when varying the inclination of orbits with periods between 6 and 24 hours. The acceleration magnitude consists of equal components in both the radial and transverse directions, the perigee altitude defined in Table 3-1 and Table 3-2 is maintained.

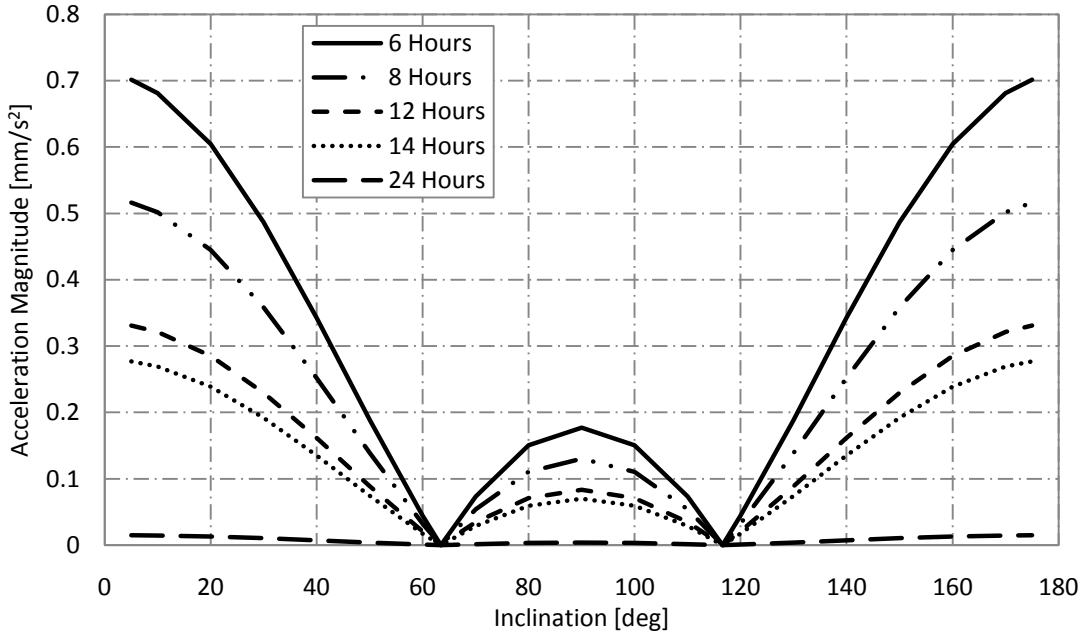

Figure 3-14 Combined radial and transverse acceleration

It is seen from Figure 3-14 that orbits with lower orbital periods require larger total accelerations than higher period orbits. For example, to reach an inclination of *90 degrees* an orbit with a 24 h period requires *0.00378 mm/s²* of acceleration whereas an orbit with a period of 6 hrs requires a total acceleration of *0.177 mm/s²*.

It is clear from the analysis presented that any inclination of HEO can be achieved using this method, with the value of the inclination selected such that the mission objectives are best satisfied. However, it appears that significant benefit could be gained from an orbit inclined at *90 degrees* to fulfil the gap in data at the high-latitude regions of the Earth. The conventional Molniya orbit also has an orbital period of 12 hrs, thus a 12 h, *90 degree* inclination Taranis orbit is considered for analysis in subsequent chapters until the trade space analysis is conducted in **Chapter 5** where the most beneficial orbits are selected.

3.2.3 Change in Orbital Elements

Analytical expressions are also developed for the remaining orbital elements, semi-major axis, eccentricity, inclination and ascending node angle using the Gauss form of the Lagrange Planetary Equations, in terms of a spacecraft centred RTN coordinate system [70]. This process is carried out to ensure the desired zero secular rate of change of orbital elements is maintained in the presence of continuous low-thrust.

Semi-major Axis

$$\frac{da}{d\theta} = \frac{2pr^2}{\mu\left(1-e^2\right)^2}\left(R_{J_2+F_r} e\sin\left(\theta\right) + T_{J_2+F_t}\frac{p}{r}\right) \tag{3.26}$$

Substituting appropriate expressions for perturbing forces from Eq. (3.17) - (3.18) gives

$$\begin{aligned}\frac{da}{d\theta} = \frac{1}{\mu\left(1+e\cos\left(\theta\right)\right)^2} 2a^2\left(1-e^2\right)\Bigg(& e\sin\left(\theta\right)\left(F_r \operatorname{sgn}\left[\cos\left(\theta\right)\right] + \frac{3J_2R_E^2\mu\left(1+e\cos\left(\theta\right)\right)^4\left(-1+3\sin^2\left(i\right)\sin^2\left(\theta+\omega\right)\right)}{2a^4\left(1-e^2\right)^4}\right)\\ &+\left(1+e\cos\left(\theta\right)\right)\left(F_t \operatorname{sgn}\left[\sin\left(\theta\right)\right] - \frac{3J_2R_E^2\mu\left(1+e\cos\left(\theta\right)\right)^4\sin^2\left(i\right)\sin 2\left(\theta+\omega\right)}{2a^4\left(1-e^2\right)^4}\right)\end{aligned} \tag{3.27}$$

Eq. (3.27) is then integrated over one orbital revolution to find the change in semi-major axis to give

$$\left(\Delta a\right)_0^{2\pi} = 0 \tag{3.28}$$

Eccentricity

$$\frac{de}{d\theta} = \frac{r^2}{\mu p}\left(R_{J_2+F_r}\sin\left(\theta\right) + T_{J_2+F_r}\left(\left(1+\frac{r}{p}\right)\cos\left(\theta\right) + \frac{re}{p}\right)\right) \tag{3.29}$$

Inserting radial and transverse perturbations into Eq. (3.29) gives

$$\frac{de}{d\theta}=\frac{1}{\mu\left(1+e\cos\left(\theta\right)\right)^{2}}a\left(1-e^{2}\right)\left(\sin\left(\theta\right)\left(F_{r}\,\mathrm{sgn}\left[\cos\left(\theta\right)\right]+\frac{3J_{2}R_{E}^{2}\mu\left(1+e\cos\left(\theta\right)\right)^{4}\left(-1+3\sin^{2}\left(i\right)\sin^{2}\left(\theta+\omega\right)\right)}{2a^{4}\left(1-e^{2}\right)^{4}}\right)\right)$$
$$+\left(\frac{e}{1+e\cos\left(\theta\right)}+\cos\left(\theta\right)\left(1+\frac{1}{1+e\cos\left(\theta\right)}\right)\right)\left(F_{t}\,\mathrm{sgn}\left[\sin\left(\theta\right)\right]-\frac{3J_{2}R_{E}^{2}\mu\left(1+e\cos\left(\theta\right)\right)^{4}\sin^{2}\left(i\right)\sin 2\left(\theta+\omega\right)}{2a^{4}\left(1-e^{2}\right)^{4}}\right) \tag{3.30}$$

Integrating over one orbit, the change in eccentricity is written as

$$\left(\Delta e\right)_{0}^{2\pi}=0 \tag{3.31}$$

Inclination

$$\frac{di}{d\theta}=\frac{r^{3}}{\mu p}\cos\left(\theta+\omega\right)N_{J_{2}+F_{n}} \tag{3.32}$$

Substituting the out-of-plane acceleration, Eq. (3.32) becomes

$$\frac{di}{d\theta}=\frac{a^{2}\left(1-e^{2}\right)^{2}\cos\left(\theta+\omega\right)}{\mu\left(1+e\cos\left(\theta\right)\right)^{3}}\left(F_{n}\,\mathrm{sgn}\left[\sin\left(\theta+\omega\right)\right]-\frac{3J_{2}R_{E}^{2}\mu\left(1+e\cos\left(\theta\right)\right)^{4}\sin\left(2i\right)\sin\left(\theta+\omega\right)}{2a^{4}\left(1-e^{2}\right)^{4}}\right) \tag{3.33}$$

Once more, the locally optimal control law state that normal thrust switches sign depending on the argument of latitude; consequently Eq. (3.33) integrated over one revolution using both argument of perigee equal to *0* and *270 degrees* gives the changes in inclination respectively as

$$\left[\left(\Delta i\right)_{0}^{2\pi}\right]_{\omega=0}=-\frac{4a^{2}F_{n}\sin\left(\omega\right)}{\mu} \tag{3.34}$$

$$\left[\left(\Delta i\right)_{0}^{2\pi}\right]_{\omega=\frac{3\pi}{2}}=-\frac{a^{2}F_{n}\cos\left(\omega\right)}{\sqrt{-1+e^{2}}\,\mu}(4\sqrt{-1+e^{2}}+2e^{2}\sqrt{-1+e^{2}}$$
$$-12e\,\mathrm{Arctanh}\left[\frac{-1+e}{\sqrt{-1+e^{2}}}\right]-3e\ln\left[\frac{1-e}{\sqrt{-1+e^{2}}}\right]+3e\ln\left[\frac{-1+e}{\sqrt{-1+e^{2}}}\right] \tag{3.35}$$

Inserting values of orbital elements from Table 3-1 gives the change in inclination for both cases as

$$\left(\Delta i\right)_0^{2\pi} = 0 \tag{3.36}$$

Ascending Node Angle

$$\frac{d\Omega}{d\theta} = \frac{r^3}{\mu p \sin\left(i\right)} \sin\left(\theta+\omega\right) N_{J_2+F_n} \tag{3.37}$$

Inserting the expression for the normal perturbation results

$$\frac{d\Omega}{d\theta} = \frac{a^2\left(1-e^2\right)^2 \sin\left(\theta+\omega\right)}{\sin\left(i\right)\left(1+e\cos\left(\theta\right)\right)^3}\left(F_n \operatorname{sgn}\left[\sin\left(\theta+\omega\right)\right] - \frac{3J_2R_E^2\mu\left(1+e\cos\left(\theta\right)\right)^4 \sin\left(2i\right)\sin\left(\theta+\omega\right)}{2a^4\left(1-e^2\right)^4}\right) \tag{3.38}$$

Similar to the inclination, the change in ascending node must be considered using both *ω = 0 degrees* and *ω = 270 degrees* giving the change in ascending node angle for each case respectively as

$$\left[\left(\Delta\Omega\right)_0^{2\pi}\right]_{\omega=0} = \frac{4a^2F_n\cos\left(\omega\right)}{\mu\sin\left(i\right)} - \frac{3J_2\pi R_E^2\cos\left(i\right)}{a^2\left(-1+e^2\right)^2} \tag{3.39}$$

$$\begin{aligned}\left[\left(\Delta\Omega\right)_0^{2\pi}\right]_{\omega=\frac{3\pi}{2}} = \Bigg(-\frac{a^2F_n}{\sin\left(i\right)\sqrt{-1+e^2}\,\mu}\Bigg(4\sqrt{-1+e^2} + 2e^2\sqrt{-1+e^2} - 12e\,\operatorname{Arctanh}\left[\frac{-1+e}{\sqrt{-1+e^2}}\right] \\ -3e\ln\left[\frac{1-e}{\sqrt{-1+e^2}}\right] + 3e\ln\left[\frac{-1+e}{\sqrt{-1+e^2}}\right]\Bigg)\sin\left(\omega\right)\Bigg) + \left(-\frac{3J_2\pi R_E^2\cos\left(i\right)}{a^2\left(-1+e^2\right)^2}\right)\end{aligned} \tag{3.40}$$

Note that if no out-of-plane acceleration is considered, the change in ascending node due only to J_2 effects is given by

$$\left(\Delta\Omega\right)_0^{2\pi} = -\frac{3J_2\pi R_E^2\cos\left(i\right)}{a^2\left(-1+e^2\right)^2} \tag{3.41}$$

Orbital element values are substituted into Eqs. (3.39) - (3.40) to quantify the drift in ascending node for HEOs, of varying inclinations, over the orbit due to applied normal acceleration. It is of note that when the appropriate orbital elements are substituted into Eqs. (3.39) - (3.40), the change in ascending node is equal for both of these expressions. Taranis orbits enabled using continuous normal acceleration are compared with orbits of various inclinations under the influence of J_2 effects only (from Eq. (3.41)), the results of which are shown in Figure 3-15.

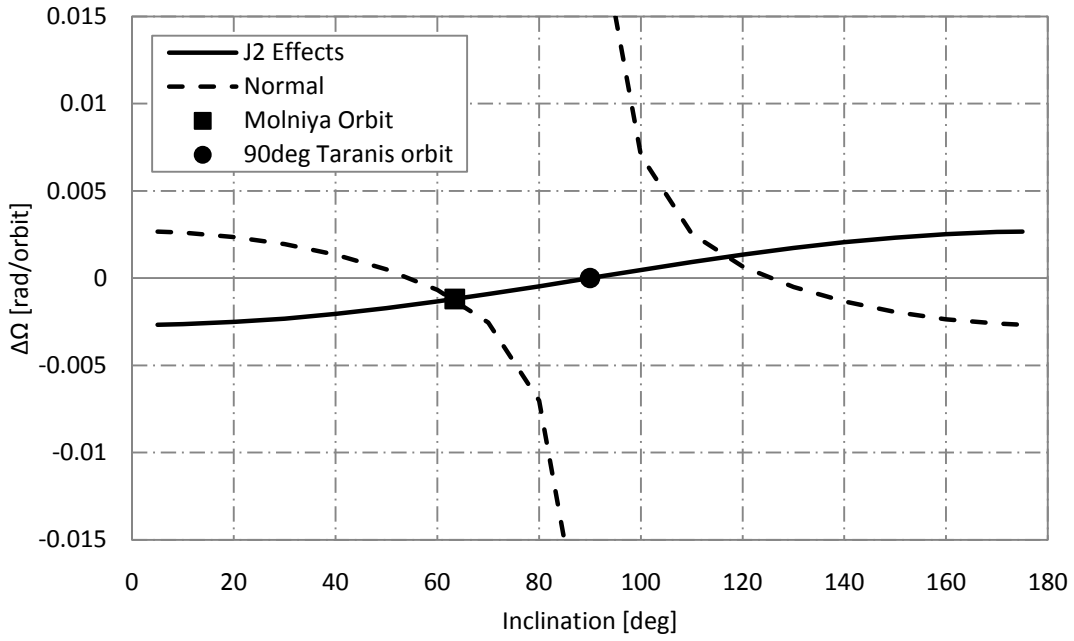

Figure 3-15 Ascending node drift per orbit for extended HEOs and a Molniya orbit

Most significantly, Figure 3-15 shows that the 12 h, *90 degree* inclination Taranis orbit experiences no drift in ascending node under the influence of J_2 perturbations. It is also shown that between the inclination ranges of *5 – 70 degrees* and *120 – 175 degrees,* Taranis orbits enabled using continuous normal acceleration have the same order of

magnitude change in ascending node as a conventional Molniya orbit. However, as the inclination approaches *90 degrees*, the change in ascending node increases rapidly and the singularity described in Figure 3-1 for the normal acceleration cases is also observed in Figure 3-15.

3.3 Extended General Perturbations Solution

Although the analysis presented in **Section 3.2** considers the total acceleration magnitude from the general perturbations method assuming equal magnitudes of radial and transverse accelerations, the general perturbations solution can be extended to consider solutions where this assumption is no longer made. This allows the minimum acceleration magnitude to be determined and an improvement on the previous solution to be made.

Substituting the orbital element values from Table 3-1 into Eq. (3.21) and setting the change in argument of perigee equal to zero results in the following expression for the radial acceleration as a function of transverse acceleration

$$F_r = -1.58\times10^{-4} + 1.676F_t \tag{3.42}$$

The transverse acceleration is assigned a range of values between *0* and *0.1 mm/s^2* and the corresponding radial acceleration is found using Eq. (3.42). The results shown in Figure 3-21 give a range of possible solutions for the *90 degree* Taranis orbit, while maintaining a constant argument of perigee over the orbit.

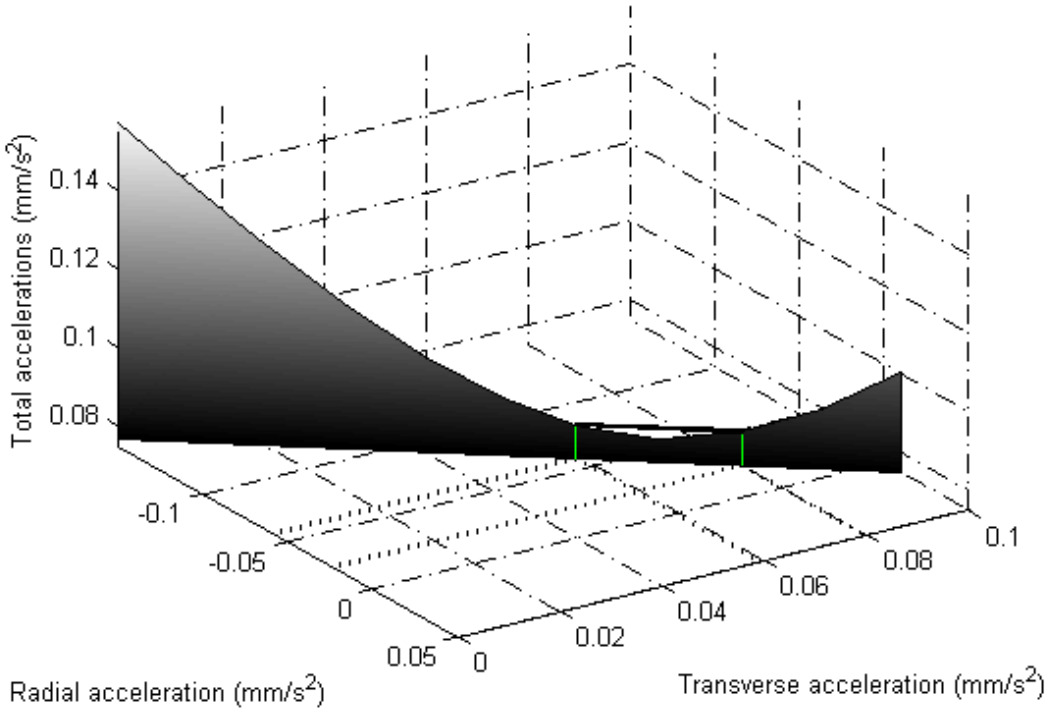

Figure 3-16 Radial and transverse accelerations, total acceleration magnitude for zero change in argument of perigee

Figure 3-16 shows the possible solutions for the Taranis orbit for a range of transverse accelerations between *0* and *0.1 mm/s²*. Between $F_t = 0.059$ *mm/s²* and $F_t = 0.08$ *mm/s²* the total acceleration magnitude of the solution is less than the previous general perturbations solution, i.e. using the assumption that the acceleration magnitudes are equal in both the radial and transverse directions. The previous equal magnitude general perturbations solution can also be seen in Figure 3-16 whilst it is also shown that the minimum acceleration magnitude occurs when the transverse acceleration is equal to *0.07 mm/s²* and the corresponding radial acceleration is *-0.0406 mm/s²* (from Eq. (3.42)). The radial and transverse control profiles for this orbit are shown in Figure 3-17 and Figure 3-18 respectively. This results in a total acceleration magnitude of *0.0809 mm/s²*, around a *3 %* reduction from the previous general perturbations solution.

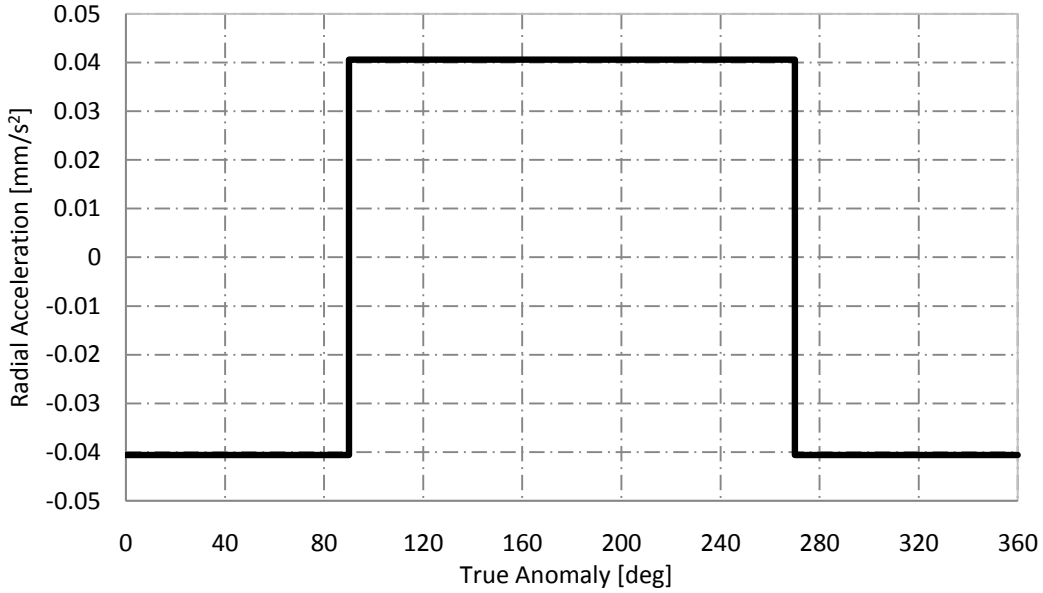

Figure 3-17 Radial control profile

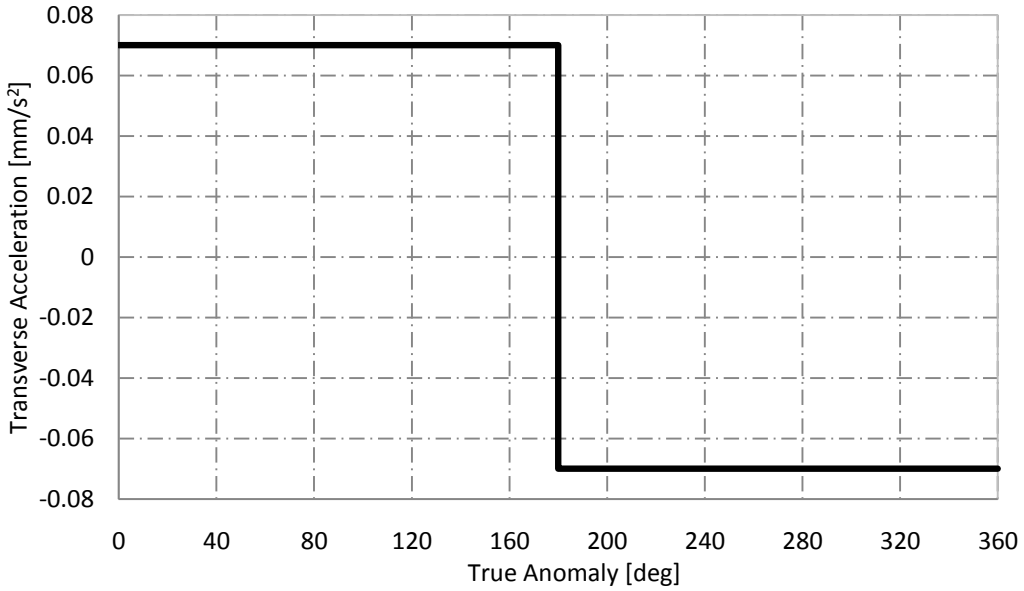

Figure 3-18 Transverse control profile

3.4 Special Perturbations Solution

To verify the general perturbations solution, a special perturbations solution is generated. This numerical model propagates the spacecraft position by integrating a set of Modified Equinoctial Elements [134] using an explicit variable step size Runge Kutta (4,5) formula, the Dormand-Price pair (a single step method) [135]. Modified equinoctial elements (Eqs. (3.43) - (3.48)) have been developed to avoid the singularities that occur when using classical orbital elements when the inclination and eccentricity tend towards zero [134]. Numerical simulations include only perturbations due to Earth oblateness to the order of J_2 and relative and absolute error tolerances are set to 10^{-8}.

$$\frac{dp}{dt} = \frac{2p}{w}\sqrt{\frac{p}{\mu}}\,T \tag{3.43}$$

$$\frac{df}{dt} = \sqrt{\frac{p}{\mu}}\left[R\,\sin(L) + \left[(w+1)\cos(L) + f\right]\frac{T}{w} - \left(h\sin(L) - k\cos(L)\right)\frac{g\,N}{w}\right] \tag{3.44}$$

$$\frac{dg}{dt} = \sqrt{\frac{p}{\mu}}\left[-R\,\cos(L) + \left[(w+1)\sin(L) + g\right]\frac{T}{w} + \left(h\sin(L) - k\cos(L)\right)\frac{f\,N}{w}\right] \tag{3.45}$$

$$\frac{dh}{dt} = \sqrt{\frac{p}{\mu}}\,\frac{s^2 N}{2w}\cos(L) \tag{3.46}$$

$$\frac{dk}{dt} = \sqrt{\frac{p}{\mu}}\,\frac{s^2 N}{2w}\sin(L) \tag{3.47}$$

$$\frac{dL}{dt} = \sqrt{\mu p}\left(\frac{w}{p}\right)^2 + \frac{1}{w}\sqrt{\frac{p}{\mu}}\left(h\sin(L) - k\cos(L)\right)N \tag{3.48}$$

Where the modified equinoctial elements are given in terms of the classical elements as

$$p = a\left(1 - e^2\right) \tag{3.49}$$

$$f = e\cos(\omega + \Omega) \tag{3.50}$$

$$g = e\sin\left(\omega+\Omega\right) \tag{3.51}$$

$$h = \tan\left(\frac{i}{2}\right)\cos\left(\Omega\right) \tag{3.52}$$

$$k = \tan\left(\frac{i}{2}\right)\sin\left(\Omega\right) \tag{3.53}$$

$$L = \Omega+\omega+\theta \tag{3.54}$$

The numerical model proves that not only is the change in argument of perigee negligible due to the applied low-thrust, but the change in all other orbital elements also matches the analytical results. Figure 3-19 shows the variation of semi-major axis, eccentricity and argument of perigee over five orbital revolutions of the 12 h Taranis orbit, inclined at *90 degrees* to the equator, enabled by combined radial and transverse accelerations with a total magnitude of *0.0809 mm/s²* i.e. the extended general perturbations solution.

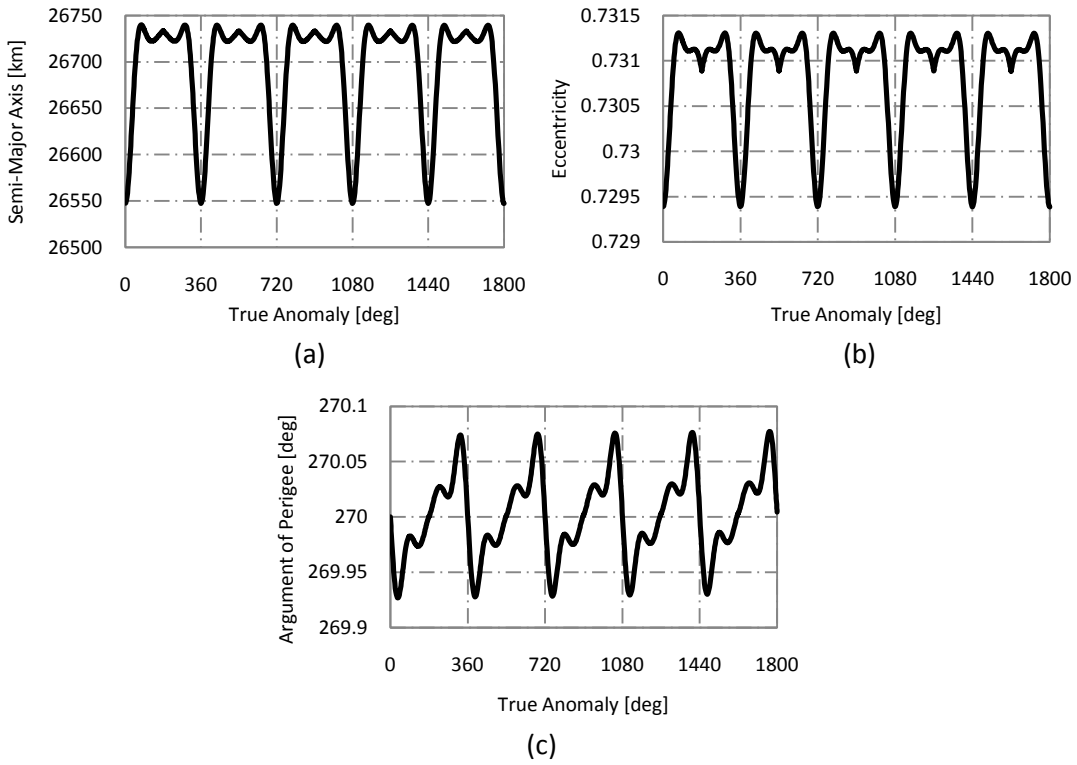

Figure 3-19 Oscillation of orbital elements over five orbital revolutions of a 12 h, *90 degree* inclination Taranis orbit (a) Semi-major axis (b) Eccentricity (c) Argument of perigee

Figure 3-19 shows that although the semi-major axis, argument of perigee and eccentricity oscillate during one orbital period, all elements return to the same initial value after each orbit. As expected, as no out-of-plane acceleration is included, no oscillation in the inclination or ascending node angle is observed, as shown in Figure 3-20.

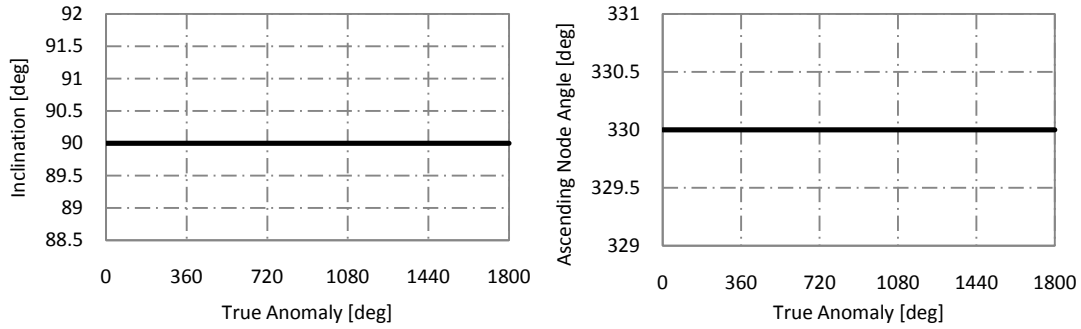

(a) (b)

Figure 3-20 Zero change in orbital elements over five orbital revolutions of a 12 h, *90 degree* inclination Taranis orbit (a) Inclination (b) Ascending node angle

3.5 Optimisation

As discussed previously, the problem becomes more complex when low-thrust normal to the orbit plane is included, meaning it is no longer possible to obtain a general perturbations solution. A Pseudospectral Optimal Control Solver (PSOPT) [136] is used to determine a numerically optimal solution combining low-thrust in all three axial directions in-order to quantify the optimality of the general perturbations solution. PSOPT uses a direct collocation method including pseudo-spectral and local discretisation to solve the optimal control problem by approximating the time-dependent variables using polynomials. The previous assumption that the fraction of the total acceleration is equal in each direction is no longer made. This, coupled with an objective function to maximise the final spacecraft mass, generates a fuel optimal solution.

The results of the special perturbations solution are used as the initial guess for the optimiser, which once again propagates the spacecraft trajectory using a set of modified equinoctial elements (Eqs. (3.43) - (3.48)) [134]. The spacecraft initial mass is set to *1000 kg* corresponding to the mass of GOCE [7], with a specific impulse of *4600 seconds*, representative of the specific impulse of the QinetiQ T6 thruster [86], and a total continuous acceleration of *0.0809 mm/s*^{2}. The analysis is initially conducted including perturbations due to the oblateness of the Earth to the order of J_2. This was subsequently extended to include J_3 and J_4, with no divergence found between the results. The optimised control profiles in the radial, transverse and out-of-plane directions along with the initial guess provided to PSOPT are shown in Figure 3-21.

Each optimised solution was obtained using 44 nodes. It should be noted that due to the use of a variable step integrator within the special perturbations solution, the initial guess does not simply contain equally spaced nodes. Furthermore, as an adaptive mesh is used within the PSOPT tool, the optimised nodes are not constrained by the initial guess.

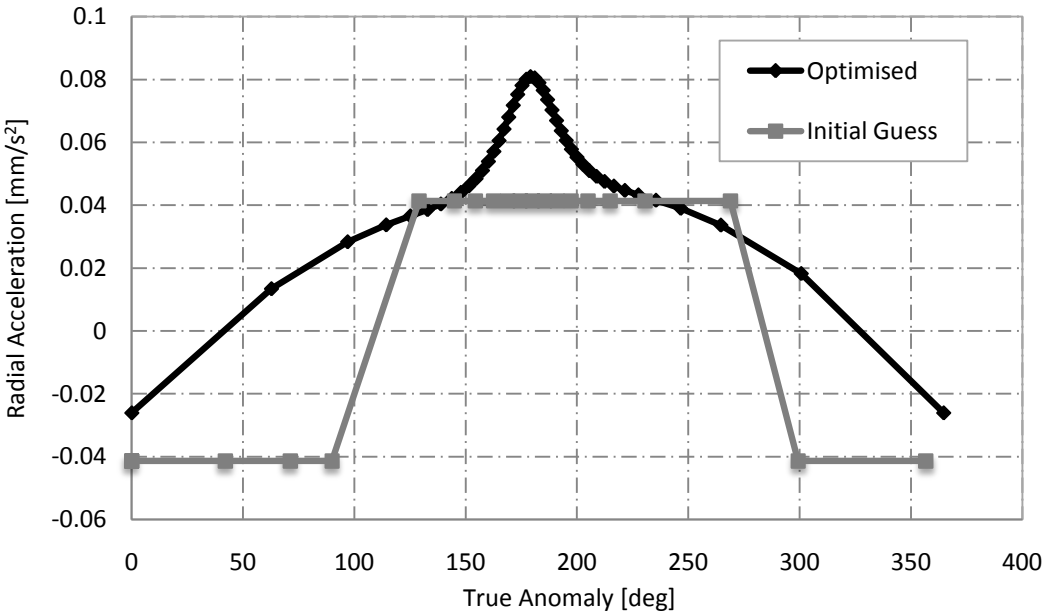

(a)

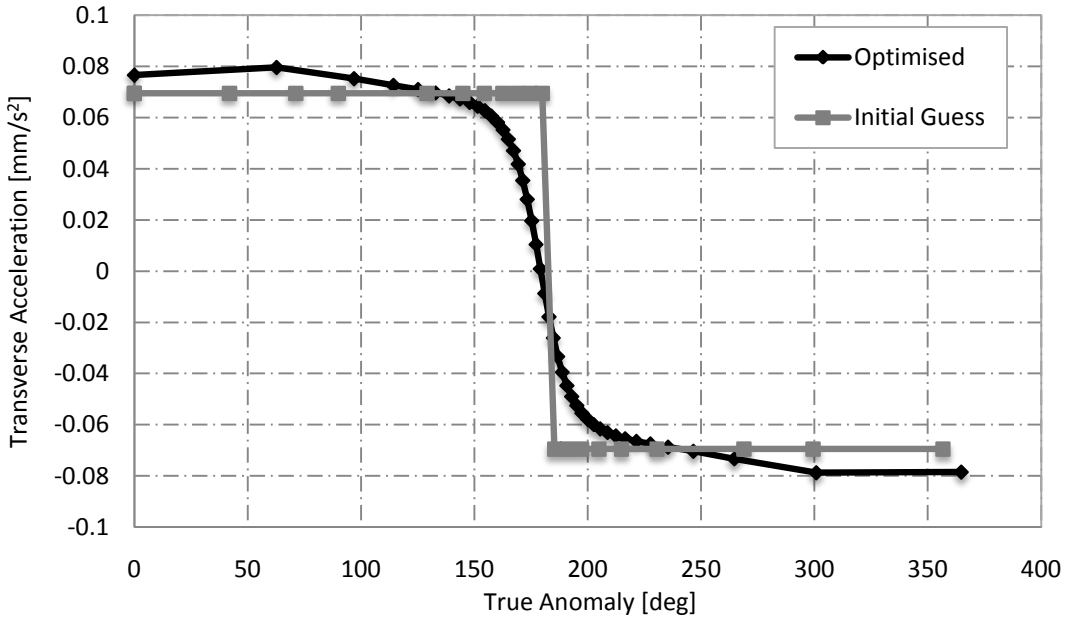

(b)

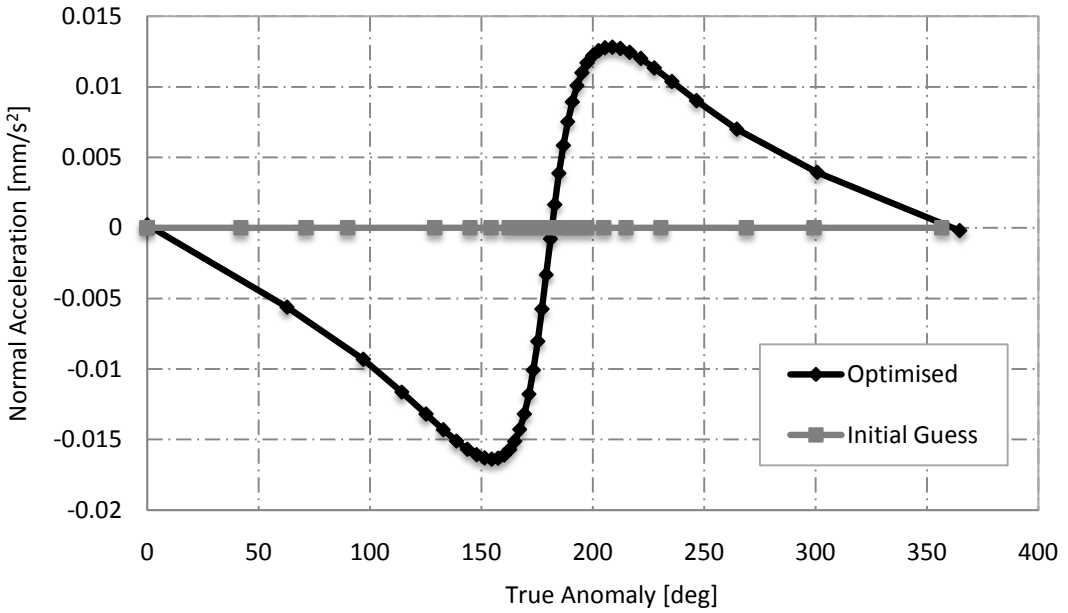

(c)

Figure 3-21 Analytical and optimised control profiles for the 12 h, *90 degree* Taranis orbit, defined in Table 3-1. (a) Radial control profile (b) Transverse control profile (c) Normal control profile

The control profiles show that as the assumption of equal acceleration magnitude is no longer made, the total acceleration is now composed of radial, transverse and out-of-plane components, with the fraction of the total acceleration in each direction varying with true anomaly. To complete one revolution of the Taranis orbit, the previous special perturbations technique required *75 g* of fuel, while the fuel optimal solution consumes *65 g* of fuel, resulting in a reduction in fuel consumption of *13.3 %.* Given that the analytical solution is suboptimal by *13.3 %* it is likely to be considered an acceptable cost due to the significantly reduced complexity of flying a spacecraft using the general perturbations control profile over the optimised profile. This also highlights the level of accuracy obtained using a relatively simple method of employing locally optimal control laws to apply continuous acceleration to enable Taranis orbits.

3.6 Summary

This chapter has introduced new HEOs, termed Taranis orbits, which use continuous low-thrust propulsion to offer free selection of the critical inclination to best satisfy the mission objectives. These orbits are derived using locally optimal control laws within a general perturbations solution, firstly considering acceleration applied in each of the radial, transverse and normal directions individually before combining the acceleration in multiple directions. Initial analytical results show that to alter the critical inclination, combining equal magnitudes of acceleration in the radial and transverse directions produces the smallest acceleration magnitude. An extended general perturbations solution no longer used the assumption that the acceleration magnitudes were equal and therefore allowed the total acceleration magnitude to be reduced. A special perturbations solution was also shown to verify the analytical results.

Finally, pseudospectral optimisation was conducted to produce fuel optimal solutions, which was shown to offer a reduction of *13.3* % in the propellant required over one orbital revolution. However, the small increase in propellant consumption of the analytical solution over the optimised solution is thought to be an acceptable cost due to the significant reduction in complexity of the control profiles.

Although Taranis orbits allow free selection of the critical inclination independent of the orbital period, perigee or apogee altitudes, the most significant benefit has been identified as an orbit with a *90 degree* inclination to provide a potential solution to the data deficit at high-latitude regions of the Earth. This particular example is therefore considered in the subsequent chapters

Chapter 4

4 Propulsion System Analysis for a 12 hour Taranis Orbit

Having derived the acceleration required to enable Taranis orbits with varying orbit periods and inclinations in **Chapter 3**, this chapter considers the use of different propulsion systems to provide the required acceleration and so determine the most feasible solution. **Section 4.2** investigates the use of a hybrid solar sail / EP system to reduce the propellant requirements from an EP only system. Mission analysis is conducted in **Section 4.3** to quantify the mission lifetime and mass budgets for various configurations. Subsequently the technology requirements for spacecraft are outlined in **Section 4.4**. Finally, **Section 4.5** considers the use of a conventional chemical propulsion system to deliver the thrust and compares this to a pure EP system.

4.1 Introduction

EP has been successfully demonstrated on board a number of missions and as such is a mature technology; however mission lifetimes are limited by the amount of propellant that can be carried. Consequently, consideration is given to the addition of a solar sail to the system to reduce the propellant requirements of the EP thruster when enabling Taranis orbits. Hybrid solar sail / EP systems, discussed in **Chapter 2**, offer advantages which include the capability of the EP system to thrust in any direction to overcome the issues associated with the inability of the solar sail to thrust in the direction of the Sun, and the

use of a small solar sail on the spacecraft to lower the AD^2 of solar sailing. EP, hybrid solar sail / EP and chemical propulsion systems are considered to provide the acceleration required to enable a 12 h, *90 degree* inclination Taranis orbit to determine the most beneficial means of propulsion.

Two hybrid solar sail / EP cases are presented considering different constraining parameters. Firstly, it is assumed that the launch mass of the spacecraft is fixed. The mass of the solar sail added to the system is limited to be no more than the mass of propellant saved through the addition of the sail. Consideration is also given to a system limited by the maximum thrust of the EP system, and so allowing the initial mass of the spacecraft to vary. The additional mass gained from the addition of the solar sail is allocated in two ways. In the first instance it is assigned solely to the solar sail. Thus there will be no allocation for additional propellant on board and this example is given to show the baseline solar sail technology required. In the second instance it is used in part for the solar sail and in part to increase the useful payload capacity. The impact of the added solar sail on mission lifetime is considered along with the development of Strawman mass budgets to quantify the benefit, if any, of a hybrid EP / solar sail system over a pure EP system to enable a 12 h, *90 degree* inclination Taranis orbit. The technology requirements are also presented for the spacecraft and solar sail.

The use of a chemical propulsion system to enable the 12 h Taranis orbit is also investigated, where in this case the acceleration is not continuous and the required Δv is provided by two impulses per orbit.

4.2 Hybrid EP / Solar Sail Propulsion

To lower the demands placed upon the EP system, by lowering its required thrust, the use of hybrid EP / solar sail propulsion to maintain the Taranis orbit is considered. The total acceleration needed to maintain a 12 h, *90 degree* inclination Taranis orbit has been shown in **Chapter 3** as *0.0809 mm/s*^{2}; using hybrid propulsion a fraction of this acceleration is now generated by the solar sail with the EP system supplying the remainder of the necessary acceleration. The total required acceleration is given by

$$a_{tot} = a_s + a_p \tag{4.1}$$

Where the acceleration, a_s, generated by a perfectly reflecting solar sail is given in Eq. (2.11) in **Section 2.2.2** and a_p is the continuous acceleration provided by the EP system.

4.2.1 Locally Optimal Control Laws

Locally optimal control laws are used by the solar sail component of the force, and the EP system uses the simple switching law previously derived in **Chapter 3**. In the absence of any low-thrust propulsion to maintain the 12 h Taranis orbit, the natural drift in argument of perigee due to the gravitational perturbation is *-0.15 degrees per day* (towards the ascending node). Thus, it is required that the sail attempt to impart positive rate of change of argument of perigee to compensate for this drift. The argument of perigee locally optimal control law is derived from the argument of perigee variational equation, given in terms of classical orbital elements

$$\frac{d\omega}{d\theta} = \begin{bmatrix} R & T & N \end{bmatrix} \lambda_\omega \tag{4.2}$$

where

$$\lambda_\omega = \begin{bmatrix} -\frac{\sqrt{p}}{e}\cos(\theta) \\ \left(1+\frac{r}{p}\right)\frac{\sqrt{p}}{e}\sin(\theta) \\ -\frac{r}{\sqrt{p}}\cot(i)\sin(\theta+\omega) \end{bmatrix} \tag{4.3}$$

The locally optimal control law therefore requires the solar sail thrust to be maximised along λ_ω, [64]. The solar sail trajectory is planet-centred and so λ_ω must be transposed into the Sun-sail line reference frame, shown in Figure 4-1, using standard transformation matrices. The transformation is performed in two stages; first, transformation from planet-centred RTN to Earth-centred inertial using the inverse of the transformation matrix [137]

$$\begin{aligned} O_{RTN} &= [T_m] O_{ECI} \\ &= \begin{bmatrix} \cos(\omega+\theta)\cos\Omega - \sin(\omega+\theta)\cos i\sin\Omega & \cos(\omega+\theta)\sin\Omega + \sin(\omega+\theta)\cos i\cos\Omega & \sin(\omega+\theta)\sin i \\ -\sin(\omega+\theta)\cos\Omega - \cos(\omega+\theta)\cos i\sin\Omega & -\sin(\omega+\theta)\sin\Omega + \cos(\omega+\theta)\cos i\cos\Omega & \cos(\omega+\theta)\sin i \\ \sin i\sin\Omega & -\sin i\cos\Omega & \cos i \end{bmatrix} O_{ECI} \end{aligned} \tag{4.4}$$

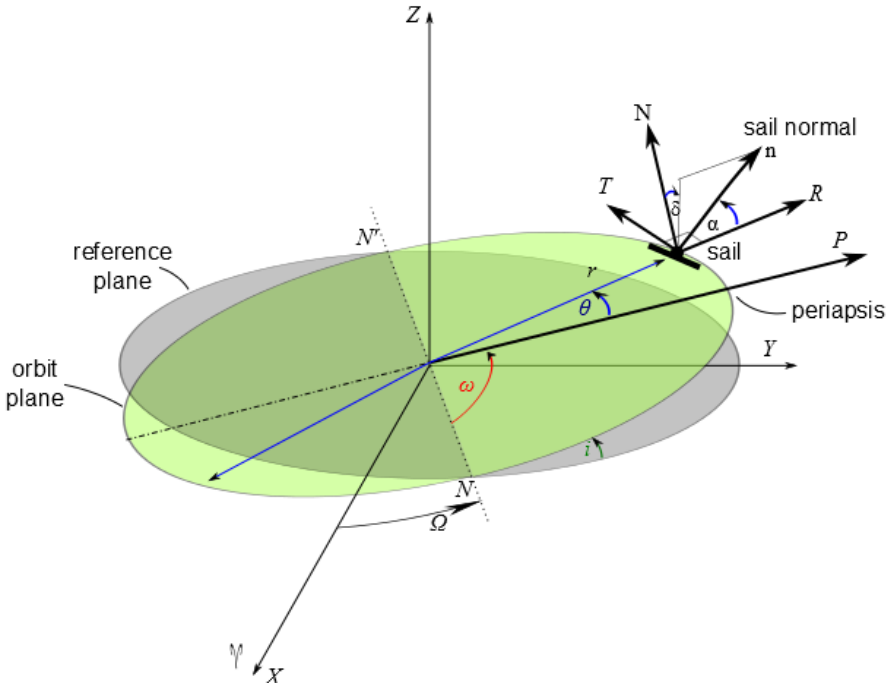

Figure 4-1 Orientation of solar sail pitch and clock angles

The second stage is to transform from Earth-centred inertial to Sun-line coordinates, using the transformation matrix given in Eq. (4.5) [138]. Where, ε_{obl}, is the obliquity of the ecliptic and ϑ is an angle measured from the first point of Aries to the planet, shown in Figure 4-2.

$$O_{SUN} = [T_m] O_{ECI} = \begin{bmatrix} \cos(\vartheta) & \sin(\vartheta)\cos(\varepsilon_{obl}) & \sin(\vartheta)\sin(\varepsilon_{obl}) \\ -\sin(\vartheta) & \cos(\vartheta)\cos(\varepsilon_{obl}) & \cos(\vartheta)\sin(\varepsilon_{obl}) \\ 0 & -\sin(\varepsilon_{obl}) & \cos(\varepsilon_{obl}) \end{bmatrix} O_{ECI} \tag{4.5}$$

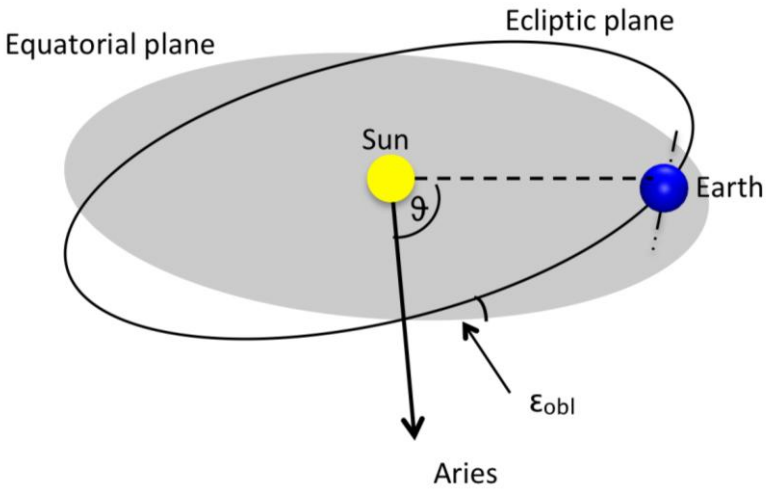

Figure 4-2 - Diagram representing the obliquity of ecliptic and angle measured from first point of Aries

With conversion of λ_ω into the Sun-sail line coordinate system, the pitch angle of the ideal force vector is found using Figure 4-1, and is given as

$$\tilde{\alpha} = \arccos\left(\lambda_{\hat{x}}^{ss}\right) \tag{4.6}$$

where $\hat{\boldsymbol{\lambda}}_\omega = \left[\lambda_{\omega x}^{ss} / |\boldsymbol{\lambda}_\omega| \quad \lambda_{\omega y}^{ss} / |\boldsymbol{\lambda}_\omega| \quad \lambda_{\omega z}^{ss} / |\boldsymbol{\lambda}_\omega|\right] = \left[\hat{\lambda}_{\omega x}^{ss} \quad \hat{\lambda}_{\omega y}^{ss} \quad \hat{\lambda}_{\omega z}^{ss}\right]$, the unit argument of perigee vector taken from the RTN co-ordinate system to the Sun-sail line coordinate system. Hence superscripts ss refer to the Sun-sail co-ordinate system and subscripts x, y, and z

refer to the x, y, and z components of the argument of perigee vector. The sail orientation to maximize the sail thrust vector is found, with the locally optimal sail pitch angle, shown in Figure 4-3, and given from [139]

$$\tan(\alpha) = \frac{-3\cos(\tilde{\alpha}) + \sqrt{9\cos^2(\tilde{\alpha}) + 8\sin^2(\tilde{\alpha})}}{4\sin(\tilde{\alpha})} \tag{4.7}$$

The locally optimal sail clock angle, which is the angle measured within a plane normal to the Sun line from the projection of the orbit normal vector in that plane, is also shown in Figure 4-3 and is given as

$$\delta = \arccos\left(\frac{\lambda_{\hat{z}}}{\sqrt{\lambda_{\hat{y}}^2 + \lambda_{\hat{z}}^2}}\right) \tag{4.8}$$

The solar sail thrust vector in Eq. (2.11) is found using [108]

$$\mathbf{n} = \begin{bmatrix} \cos(\alpha) \\ \sin(\alpha)\sin(\delta) \\ \sin(\alpha)\cos(\delta) \end{bmatrix} \tag{4.9}$$

As the sail is in an Earth-centred trajectory the normal vector orientation given in Eq. (4.9) must be transformed into planet-centred RTN coordinates. This is again performed in two stages, transforming from Sun-line coordinates to Earth-centred inertial using the inverse of the transformation matrix given in Eq. (4.5) and from Earth-centred inertial to Earth-centred RTN using the matrix in Eq. (4.4).

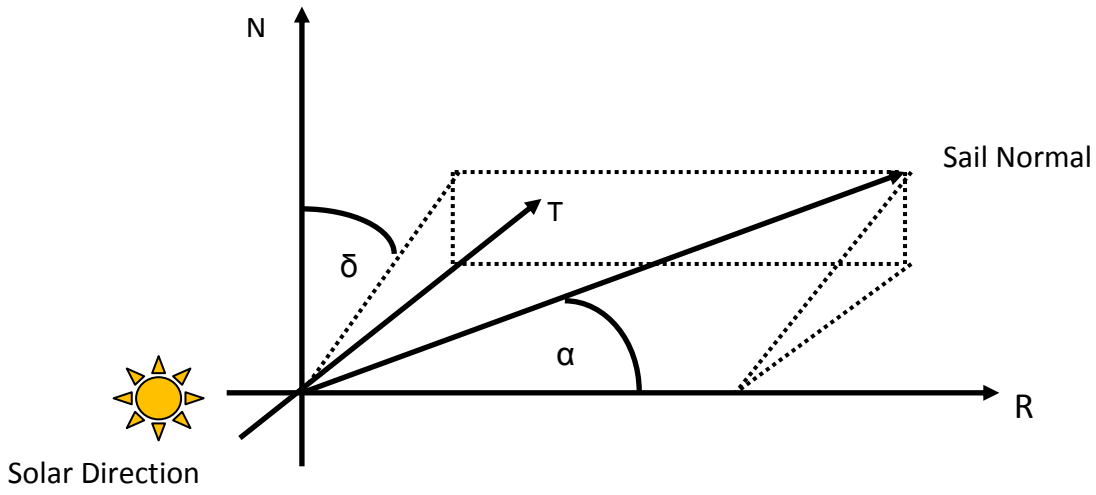

Figure 4-3 Sail pitch and clock angles in a Sun-sail line reference frame

Chapter 3 presented the derivation of a general perturbations solution to determine the total acceleration required to enable the Taranis orbits. Special perturbations techniques were also shown to validate analytical solutions. The analysis presented in this chapter uses the previously derived acceleration values and numerically integrate the Lagrange planetary equations including the motion of the solar sail. Various solar sail characteristic accelerations are considered to determine the sail that offers the most benefit in terms of the lowest acceleration demand on the EP system. As the characteristic acceleration of the sail is increased, at some point the acceleration provided by the solar sail will be so high that the EP system will be required to counteract the sail acceleration, rather than supplement it. Using a spacecraft with an initial mass of *1000 kg*, I_{sp} of *3000s* corresponding to the launch mass of GOCE [7] and specific impulse of the T5 thruster [140] and considering four values of solar sail characteristic accelerations of *0.03, 0.05, 0.07*, and *0.1 mm/s*^{2}, the mass of the spacecraft is shown in Figure 4-4 over the first year of operation. The remaining mass is also shown in Figure 4-5 as a function of the solar sail characteristic acceleration over various time intervals.

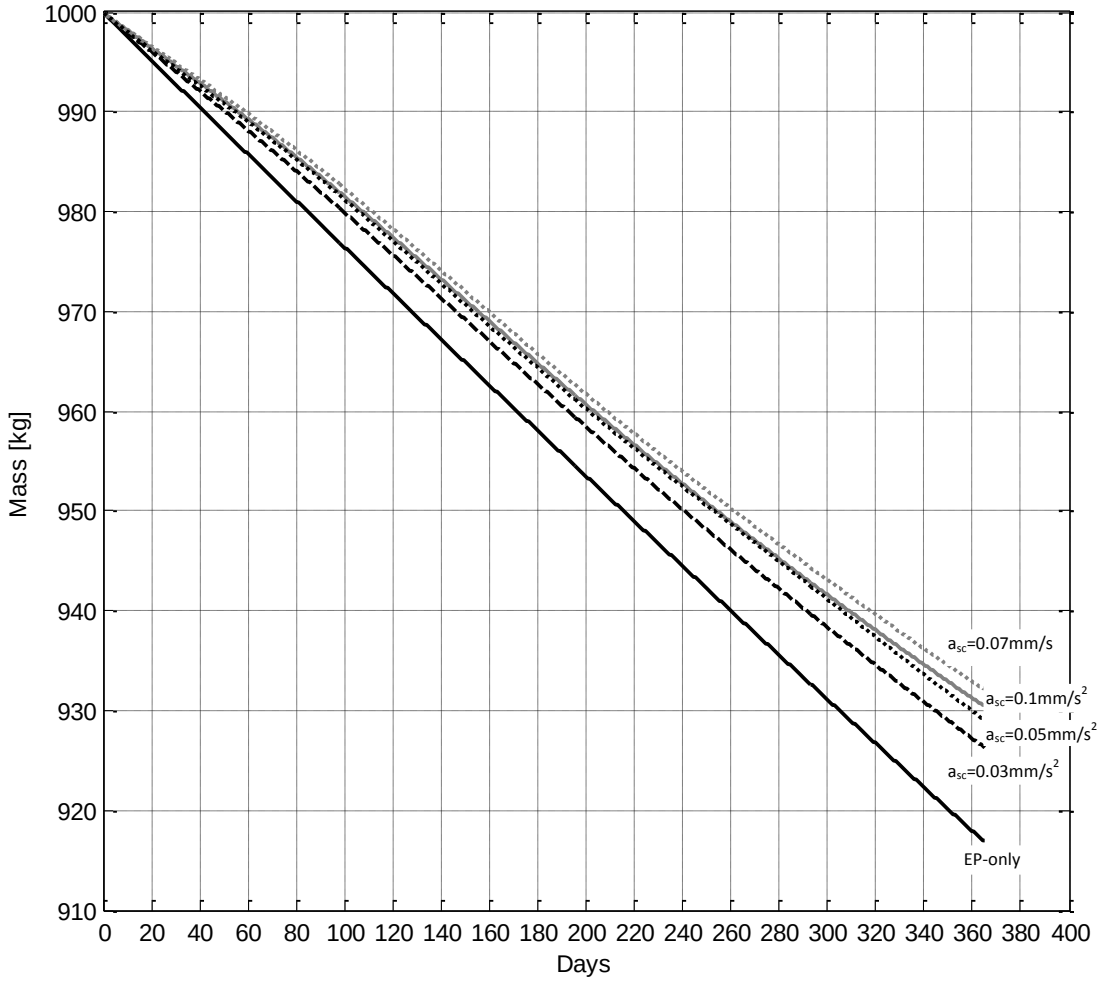

Figure 4-4 Fuel consumption of a spacecraft on a 12 h, *90 degree* inclination over the first operational year using various solar sail characteristic accelerations

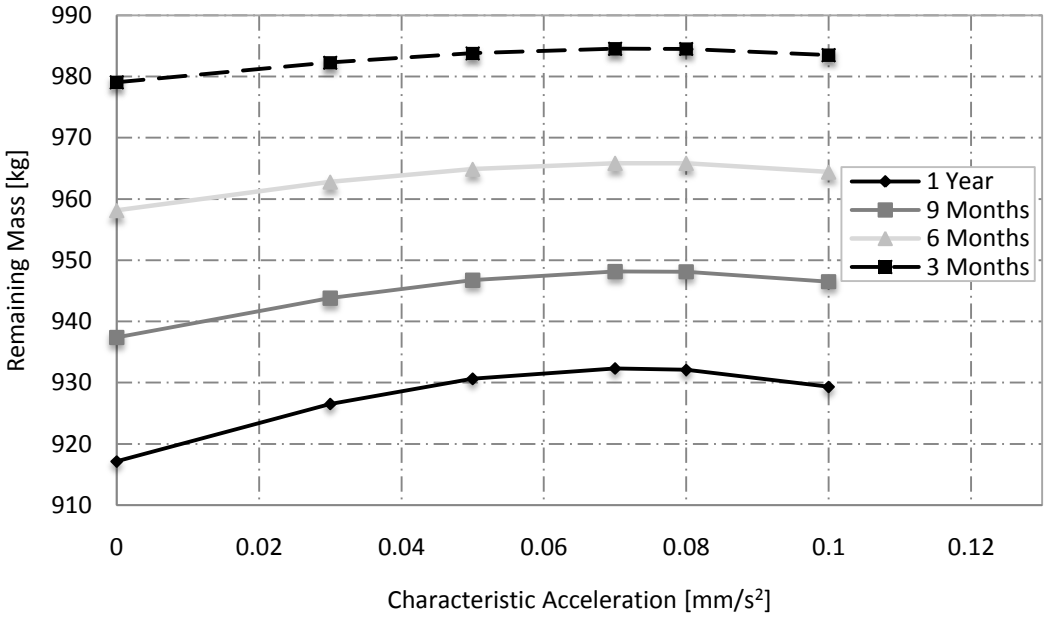

Figure 4-5 Remaining spacecraft mass as a function of the solar sail characteristic acceleration – 12 h, *90 degree* inclination Taranis orbit

It is seen from Figure 4-4 and Figure 4-5 that, as expected, each solar sail considered offers some benefit over the EP-only case by decreasing the amount of propellant consumed and increasing the final spacecraft mass. It is noted that a solar sail with a characteristic acceleration of *0.07 mm/s²* offers the highest reduction in fuel consumption. This turning point was determined by a process of trial and error, increasing the characteristic acceleration in increments of *0.001 mm/s²*. Increasing the characteristic acceleration above this value causes the EP system to counteract the acceleration generated by the solar sail, thereby increasing the fuel consumption of the EP system. This turning point will, however, move as the EP system uses up propellant and the solar sail acceleration increases, as in Eq. (2.10). The maximum propellant mass saving over the first year, given by a sail characteristic acceleration of *0.07 mm/s²*, is just over *15 kg*. Characteristic accelerations of *0.03* and *0.05 mm/s²* offer reductions in propellant consumption of around *9* and *13.5 kg,* respectively.

The acceleration provided by the solar sail varies throughout the year due to the tilt of the Earth's rotational axis with respect to the orbit plane. As a result the acceleration required by the EP system varies throughout the year as shown in Figure 4-6.

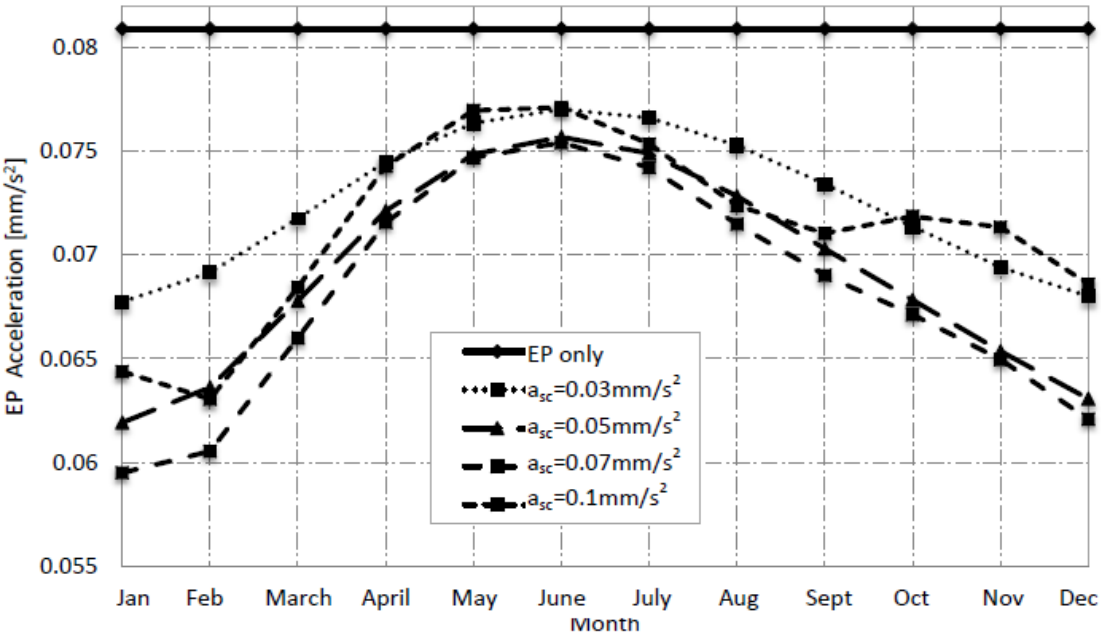

Figure 4-6 EP acceleration required over one year – 12 h, *90 degree* inclination Taranis orbit

It can be seen that from April to August the acceleration from the sail decreases, the maximum demand on the EP system occurs during this time. A significant decrease in the required EP acceleration is shown throughout the Northern Hemisphere winter. The turning point described in Figure 4-4 is again explained in Figure 4-6, where it is shown that the acceleration generated by the solar sail with a characteristic acceleration of *0.1 mm/s²* is so high that the EP thruster is required to counteract this.

The solar sail control angles required to achieve the *90 degree* inclination Taranis orbits and accomplish the stated reduction in total EP accelerations are shown in Figure 4-7 and Figure 4-8 respectively.

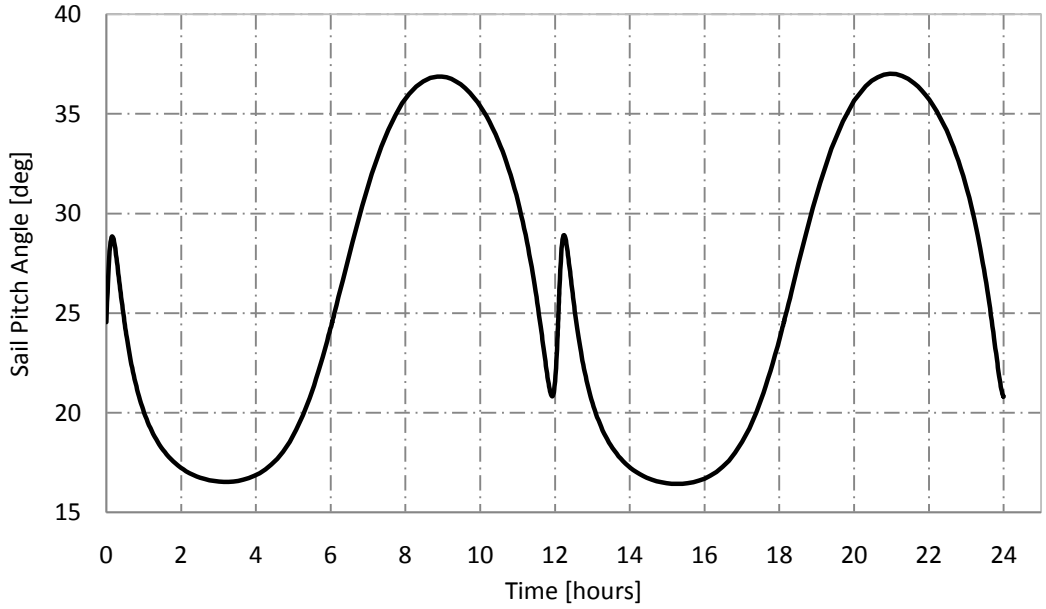

Figure 4-7 Solar sail pitch angle required to enable 12 h*, 90 degree* inclination Taranis orbit

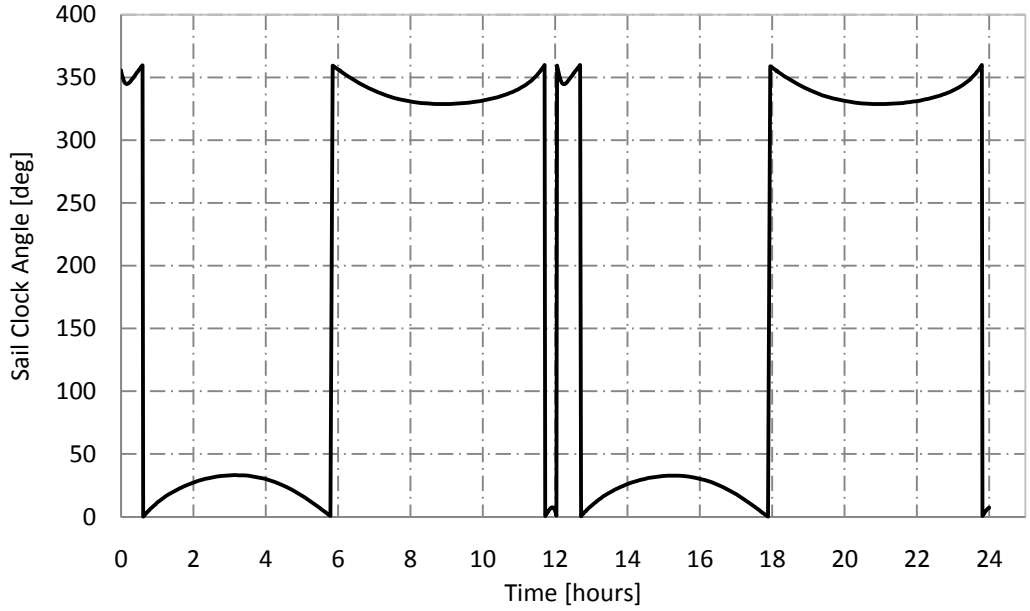

Figure 4-8 Solar sail clock angle required to enable 12 h*, 90 degree* inclination Taranis orbit

It is clear from Figure 4-7 that the sail pitch angle must rotate by around *20 degrees* per orbit, while from Figure 4-8 the sail clock angle completes two *50 degree* revolutions within 12 hrs. The relatively short orbit period of the Taranis orbits means that fast slew

manoeuvres are required by the solar sail, although there is very little detail in the literature about the slew rate capabilities of solar sails, it is expected that the rates required for the Taranis orbit are beyond the current capabilities of solar sail technology. For reference, the Solar Polar Orbiter is required to deliver *10 degrees per day* [141] which is clearly significantly lower than the rates required by the Taranis orbit.

4.3 Mission Analysis

Having derived the acceleration produced by various solar sails for the 12 h, *90 degree* Taranis orbit, mission analysis is conducted to characterise the possible mission lifetimes, payload capacity and technology requirements to determine the propulsion system which offers the most benefit.

4.3.1 Mission Lifetime

By evaluating the performance of the 12 h Taranis orbit in terms of propellant consumption, possible mission lifetimes of the orbit facilitated by means of EP-only and hybrid EP / solar sail systems are determined. Defining the differential equation for the mass of the spacecraft as

$$\dot{m} = -\frac{T_h}{I_{sp} g_0} \tag{4.10}$$

where T_h is the thrust magnitude of the EP system by

$$T_h = a_p m \tag{4.11}$$

In the hybrid EP / solar sail systems the continuous acceleration, a_p, is found by taking the average acceleration required by the EP system over the first year, given in Table 4-1. Then making the appropriate substitution of Eq. (4.11) into Eq. (4.10) results in the following integral

$$\int_{m_0}^{m_f} \frac{dm}{m} = -\int_{t_0}^{t_f} \frac{a_p}{I_{sp} g_0} dt \tag{4.12}$$

Evaluating the integrals and applying the condition that $t_0 = 0$ gives the following expression for the mission lifetime

$$t_f = -\ln\left(\frac{m_f}{m_0}\right)\frac{I_{sp} g_0}{a_p} \tag{4.13}$$

where, the mass fraction m_f/m_0 is defined as

$$\frac{m_f}{m_0} = \frac{\left(m_0 - m_{prop}\right)}{m_0} \tag{4.14}$$

Table 4-1 Average EP acceleration over a 12 month period

Characteristic Acceleration [mm/s^2]	**Average EP Acceleration [mm/s^2]**
EP-only	0.0809
0.03	0.0726
0.05	0.0692
0.07	0.0681
0.10	0.0712

It is noted from Table 4-1 that the acceleration required from the EP system decreases by less than the sail characteristic acceleration. This is due to the useful sail acceleration magnitude being set by the square of the cosine of the pitch angle (from Eq. (2.7)). The lifetime of the *90 degrees*, 12 h Taranis orbit, detailed previously in Table 3-1 in **Chapter 3**, is thus determinable for a particular mass fraction and specific impulse. The resulting possible mission lifetimes are shown in Figure 4-9 for the EP-only system and for each of the hybrid propulsion systems considered.

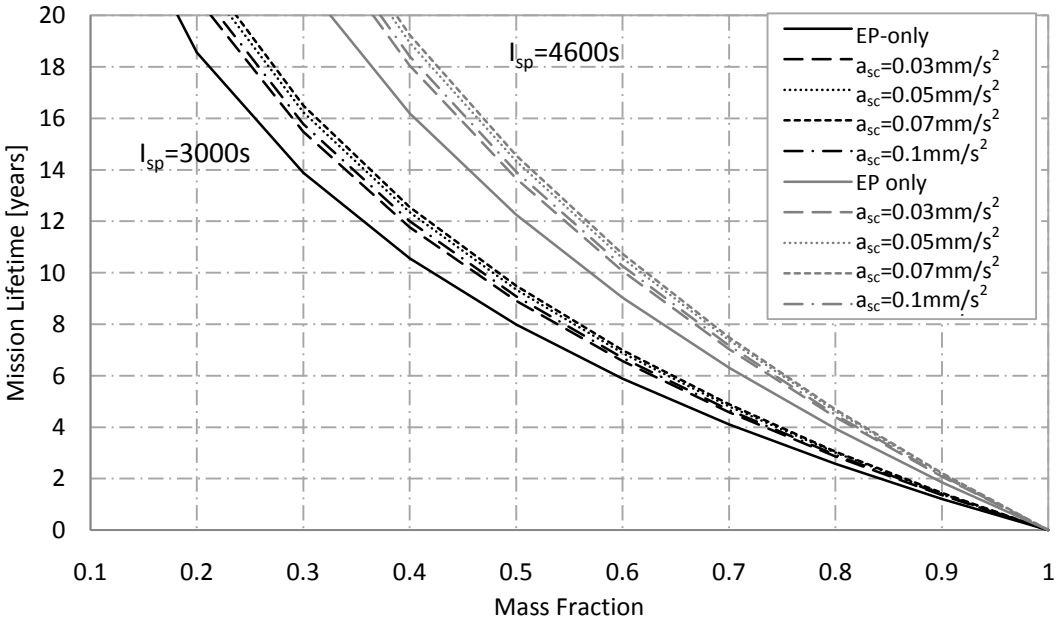

Figure 4-9 Taranis mission lifetime as a function of mass fraction for EP-only and various solar sail characteristic accelerations

Figure 4-9 shows the possible mission lifetimes for the Taranis orbit as a function of mass fraction for specific impulses of *3000* and *4600 seconds* representing the specific impulses of the QinetiQ T5 and T6 thrusters respectively [86, 140], using EP / sail systems with various solar sail characteristic accelerations. For example, using a mass fraction of 0.5 the resulting mission lifetime for each system and both specific impulses is given in Table 4-2.

Table 4-2 Mission Lifetime for a 12 h, *90 degree* inclination Taranis orbit for EP only and hybrid solar sail / EP systems for a mass fraction of 0.5

Characteristic Acceleration [mm/s^2]	I_{sp} = 3000s **Lifetime [years]**	I_{sp} = 4600s **Lifetime [years]**
EP-only	8.0	12.3
0.03	9.0	13.7
0.05	9.3	14.3
0.07	9.5	14.6
0.10	9.1	13.9

It can be seen that employing a solar sail with a characteristic acceleration of *0.07 mm/s^2* can enable a mission of around a year and a half longer than a Taranis orbit enabled using a pure EP system, with a specific impulse of *3000 seconds*. An increase in lifetime of over two years is also shown to be possible by increasing the specific impulse to *4600 seconds*. This highlights the benefit of the hybrid solar sail / EP system due to the reduced propellant consumption in comparison to the EP-only system. It is noted that as the propellant is depleted the acceleration generated by the solar sail will increase, however as noted previously from Figure 4-3, an increase in the solar sail acceleration above *0.07 mm/s^2* causes an increase in the propellant consumption, thus the mission lifetimes will in fact be shorter than detailed here. As the increases in mission lifetimes for the hybrid solar sail / EP systems are shown in Figure 4-9 to be little over the EP only case, this is an initial indicator that hybrid solar sail / EP systems may not be the most beneficial means of enabling the *90 degree* Taranis orbit.

4.3.2 Initial Spacecraft Mass

The maximum allowable initial mass of the spacecraft is determined for the given level of thrust using the constant EP accelerations given in Table 4-1; with the maximum allowable mass shown in Figure 4-10, determined using the following expression

$$T_{\max} = m_0 a_p \tag{4.15}$$

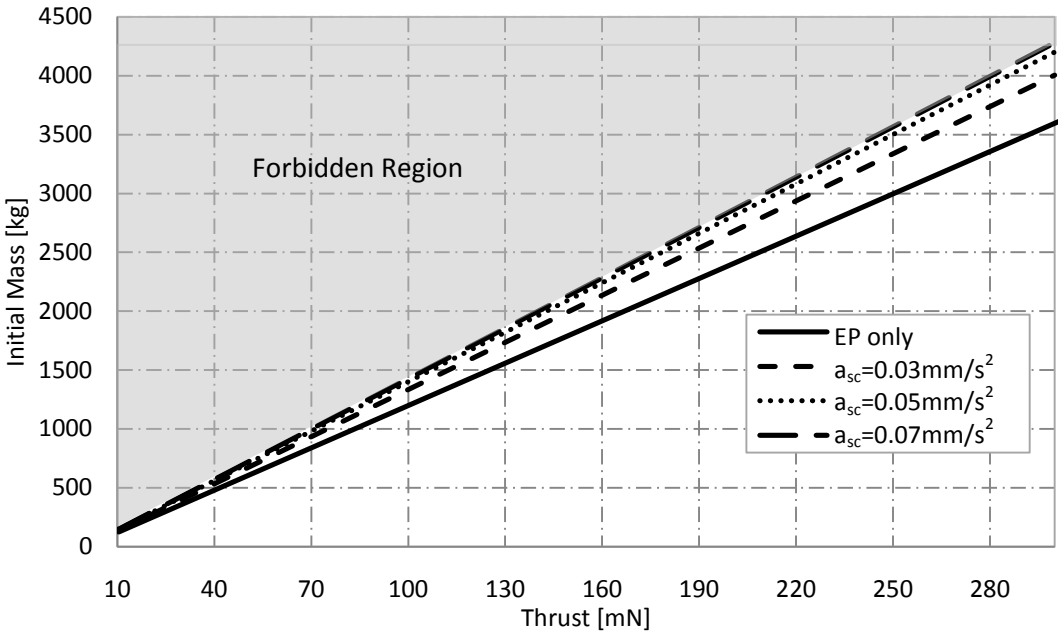

Figure 4-10 Maximum allowable initial mass for the 12 h Taranis orbit in Table 3-1 for an EP only system and hybrid solar sail / EP systems with various sail characteristic accelerations

Figure 4-10 shows the valid region for the initial mass of the spacecraft, where the forbidden region is the area where the thrust / mass ratio is less than that required to maintain the orbit. Two separate factors can clearly constrain the system; firstly, where the launch mass of the spacecraft is fixed and secondly where the maximum thrust of the EP system is used to constrain the mission. Each case is considered in subsequent sections (**4.3.2.1** and **4.3.2.2**) to examine the possible benefits of each. It is noted that although higher maximum thrust systems will allow a higher launch mass and thus more capacity for

payload, larger thrust results in higher power requirements and therefore larger solar arrays and larger electric propulsion mass, this is considered further in Sections 4.3.3 and 4.4.

4.3.2.1 Fixed Launch Mass

Firstly, the case where the launch mass of the spacecraft is fixed is considered. By selecting three initial masses of spacecraft of *1000*, *1500* and *2500 kg* corresponding to the initial masses of GOCE [7], the PCW mission[5], and ERS-1[6], the corresponding required initial thrust values are given in Table 4-3.

Table 4-3 Maximum initial thrust values

Characteristic Acceleration [mm/s^2]	1000 kg **Initial Thrust [mN]**	1500 kg **Initial Thrust [mN]**	2500 kg **Initial Thrust [mN]**
EP-only	80.9	121.4	202.3
0.03	72.6	108.9	181.5
0.05	69.2	103.8	173.0
0.07	68.1	102.2	170.3
0.10	71.2	106.8	178.0

It is shown that for a particular initial mass of spacecraft, the addition of a solar sail reduces the thrust required by the EP thruster, with the maximum reduction in thrust of *32 mN* occurring for the *2500 kg* spacecraft using a solar sail with a characteristic acceleration of *0.07 mm/s^2*. Note that the additional mass incurred by adding a solar sail remains constrained by the fixed launch mass. As such, the solar sail mass is constrained to be no more than the saving in propellant mass for a given mission lifetime.

[5] Presentation by the Canadian Space Agency at http://bprc.osu.edu/rsl/GIIPSY/documents/P7%20-%20PCW_Space%20and%20Arctic.pdf Accessed on May 24th 2013

[6] ESA Operations page at http://www.esa.int/Our_Activities/Operations/ERS-2 Accessed on May 24th 2013

4.3.2.2 Fixed Maximum Thrust

The second case considers the maximum thrust of the EP system as the constraining parameter. The maximum allowable initial mass of the spacecraft for a particular thrust value is found using Figure 4-10, with the allowable mass shown to increase for each of the hybrid systems considered. For example, fixing the available EP thrust at three particular values of *94*, *150*, and *210 mN* (corresponding to the thrust available from the NSTAR thruster [76], the qualified thrust of the QinetiQ T6 thruster and the maximum thrust of the QinetiQ T6 thruster [86] respectively) results in the maximum allowable mass values given in Table 4-4.

Table 4-4 Maximum allowable mass values

Characteristic Acceleration [mm/s^2]	94mN **Initial Mass [kg]**	150mN **Initial Mass [kg]**	210mN **Initial Mass [kg]**
EP-only	1162	1854	2596
0.03	1295	2066	2893
0.05	1358	2167	3035
0.07	1380	2203	3084
0.10	1320	2107	2949

The addition of solar sails to create a hybrid solar sail / EP system is shown to be capable of offering a significant increase in the allowable mass of the spacecraft. The maximum initial mass is determined using a solar sail of *0.07 mm/s^2* with considerable increases in mass of around *218, 349* and *488 kg* respectively for each available thrust. Consideration must now be given to how this additional mass is assigned. In the first instance this additional mass is considered to be the total mass of the solar sail added to the system. It is noted that this case will produce no increase in mission lifetime over the EP-only case as there is no additional propellant on board. However, the relevance of including this case is that it

provides the base line solar sail technology. To produce any addition in mission lifetime, solar sail performance will have to be improved beyond this. In the second instance, the additional mass is used to add an advanced light-weight solar sail to the system, providing the same characteristic acceleration allowing additional EP propellant or useful payload to be carried.

4.3.3 Mass Budget Analysis

Although the mission lifetime analysis characterises possible mission lifetimes of the Taranis mission in terms of propellant consumption, it should also be investigated whether these conditions allow a useful payload to be carried using a realistic solar sail. The initial mass of the spacecraft is composed of many elements [142].

$$m_0 = m_{\text{sys}} + m_{\text{prop}} + m_{\text{tank}} + m_{\text{EP}} + m_{\text{power}} + m_{\text{pay}} + m_{\text{s}} \tag{4.16}$$

From Eq. (4.16), the total mass of the onboard systems, m_{sys}, including data processing, telecommunications, guidance, navigation and control, structural mass, and any power system requirements beyond the EP system requirements is assumed to total *500 kg*. From Eq. (4.12), m_{prop}, is the mass of the available propellant and is given as a function of the mission duration, Δt

$$m_{prop} = \frac{T_{\max}}{I_{SP} g_0} \Delta t \tag{4.17}$$

The mass of the propellant tanks, m_{tank}, is a function of the propellant mass, $m_{tank} = 0.1\ m_{prop}$ [143]. The mass of the EP thruster, m_{EP}, is found as a function of the maximum power provided by the system, P_{max}

$$m_{\text{EP}} = k_{\text{EP}} P_{\max} \tag{4.18}$$

with the specific performance of the thruster given as $k_{EP} = 0.02\ kg/W$ [144], and the maximum power

$$P_{\max} = \frac{T_{\max} I_{SP} g_0}{2\eta_{EP}} \tag{4.19}$$

The thruster efficiency, η_{EP}, is assumed to be equal to 0.7 [145]. In Eq. (4.16), m_{power}, is the mass of the spacecraft power system required to provide electrical energy to the EP system. Thus, using a solar array the mass is given by

$$m_{\text{power}} = k_{SA} P_{\max} \tag{4.20}$$

A conservative estimate of the specific performance of the solar array, from [24], of $k_{SA} = {}^{1}/_{45}\ kg/W$ was used. Inserting the appropriate values into Eq. (4.12) to find the mass of the sub-systems, the remaining mass is the useful payload mass, m_{pay}, for a range of mission lifetimes. The process is again conducted for both the fixed launch mass and fixed maximum thrust cases.

4.3.3.1 Fixed Launch Mass

The maximum solar sail masses that can be added to the spacecraft, for the fixed launch mass case, are determined from the amount of propellant saved through the use of a hybrid low-thrust propulsion system (Figure 4-4). The propellant mass saving per year in orbit for the four solar sail characteristic accelerations considered are given in Table 4-5.

Table 4-5 Propellant mass saving per year for each solar sail characteristic acceleration

Characteristic Acceleration [mm/s^2]	**Mass Saving [kg]**
0.03	9.44
0.05	13.56
0.07	15.25
0.10	12.22

In order to obtain an estimate of the solar sail masses, in this instance, the sail mass is given by multiplying the mass saving during the first year multiplied by the EP only mission lifetimes, of *4.49*, *6.24*, and *7.63* years for *1000*, *1500*, and *2500 kg* spacecraft respectively. Using Eqs. (4.16) - (4.20), the payload mass is plotted as a function of the mission lifetime.

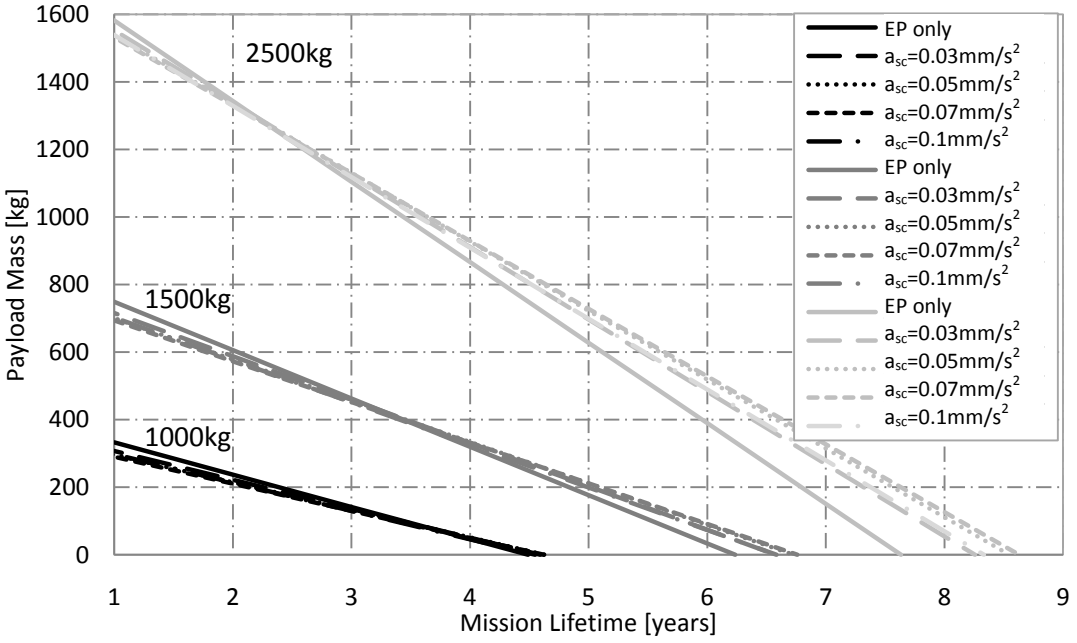

Figure 4-11 Payload mass as a function of mission lifetime for EP only and hybrid systems with varying sail performance – fixed launch mass

Figure 4-11 allows the maximum mission lifetime to be determined; that is, where there is no longer any capacity of useful payload. The maximum mission lifetimes for each initial spacecraft mass, for each of the solar sail characteristic accelerations considered, are given in Table 4-6. The mission lifetimes detailed in Table 4-6 are the maximum possible lifetimes for missions with no payload, thus to carry any payload, mission lifetimes will be shorter than shown here.

Table 4-6 Maximum mission lifetimes, given in years, for fixed launch masses for EP and hybrid propulsion systems

Characteristic Acceleration [mm/s^2]	1000 kg	1500 kg	2500 kg
EP only	4.5	6.2	7.6
0.03	4.6	6.6	8.3
0.05	4.6	6.7	8.5
0.07	4.6	6.8	8.6
0.10	4.5	6.6	8.3

A modest increase in the Taranis mission lifetimes are shown in Table 4-6 with the addition of various solar sails to the system. The maximum increase in mission lifetime is shown to be one year for the *2500 kg* spacecraft with a solar sail characteristic acceleration of *0.07 mm/s^2*. Table 4-6 shows that for the *1000* and *1500 kg* spacecraft the increases in mission lifetime produced by the addition of the solar sail are negligible, with all increases less than half a year for all solar sails. Thus it is shown from Table 4-6 that in order to obtain any significant increase in the mission lifetime using a hybrid system, the initial mass must be increased significantly.

4.3.3.2 Fixed Maximum Thrust

As constraining the mass of the spacecraft allows very little increase in the lifetime of the Taranis missions without significant development of the solar sails, the scenario where the maximum thrust of the EP system is the constraining parameter is now considered. As discussed previously, two cases are considered: firstly, where the mass of the solar sail is assumed to be equal to the entire additional mass gained through the use of the sail for the given thrust value (from Figure 4-10); and secondly, where the solar sails are assumed to equal half of the additional mass.

Case 1

Again, the additional mass gained from employing a hybrid solar sail / EP system is entirely dedicated to the solar sail in this case. The payload mass as a function of mission lifetime is given in Figure 4-12 for each of the thrust values considered. In this case the mission lifetime for each initial thrust is equal to the EP-only lifetime regardless of the sail characteristic acceleration as all of the additional mass is used to add the sail and not for any additional propellant.

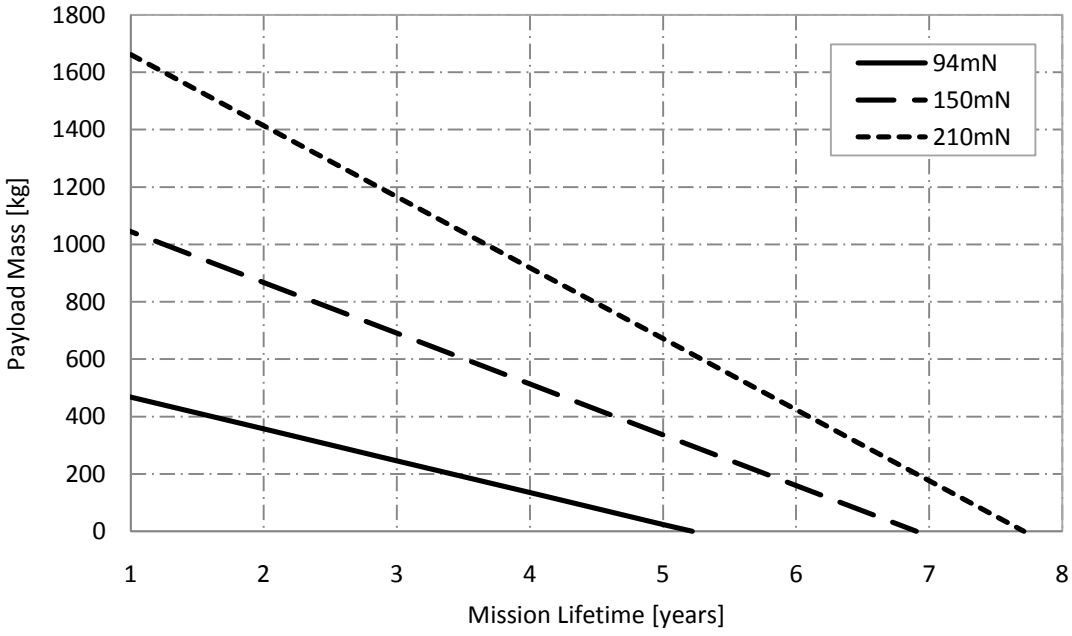

Figure 4-12 Payload mass a function of mission lifetime – fixed maximum thrust, case 1

Figure 4-12 shows maximum mission lifetimes of around 5.2, 6.9, and 7.7 years respectively for each of the maximum thrust values. Once again, Figure 4-12 shows there is no increase in mission lifetime from the EP-only case when a solar sail is added as the additional mass created by the lower acceleration is consumed fully by the solar sail and not for additional propellant. Thus, the solar sail technology required in this case is the base line, and to offer

any increase in the mission lifetime an improvement in solar sail technology will be required.

Case 2

In this instance, half of the additional mass gained by lowering the required acceleration from the EP system is assigned to the solar sail with the remaining half being used to increase the capacity for useful payload. The resulting payload masses for each system are given in Figure 4-13.

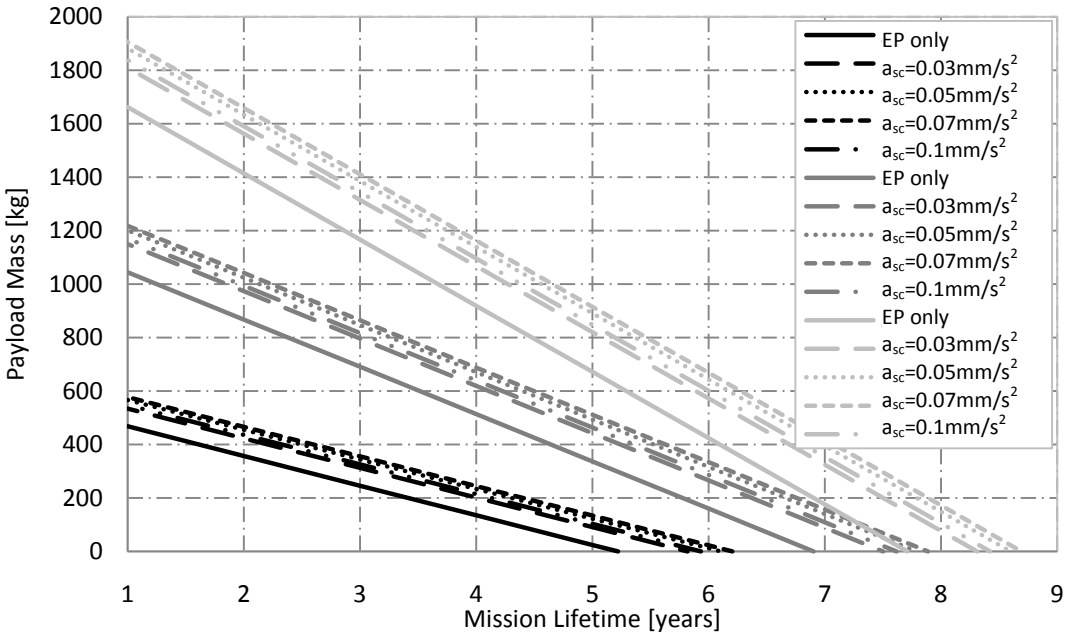

Figure 4-13 Payload mass as a function of mission lifetime for EP only and various solar sail characteristic accelerations – fixed maximum thrust, case 2

The increase in the mission lifetime for each of the hybrid solar sail / EP systems considered are shown in Figure 4-13 for each of the initial thrust values, with the maximum mission lifetimes given in Table 4-7.

Table 4-7 Maximum mission lifetimes, given in years – fixed maximum thrust, case 2

Characteristic Acceleration [mm/s^2]	94 mN	150 mN	210 mN
EP only	5.2	6.9	7.7
0.03	5.8	7.5	8.3
0.05	6.1	7.8	8.6
0.07	6.2	7.9	8.7
0.10	5.9	7.6	8.4

It can be seen from Table 4-7 that although the maximum increase in mission lifetime is the same as the fixed launch mass case, more significant increases are shown for the smaller initial thrusts and for solar sails with smaller characteristic accelerations. In addition to the greater increase in mission lifetime, the solar sails required to achieve this increase are considerably heavier and are thus more feasible solutions. Where solar sails in the fixed launch mass case range between around *42* and *116 kg*, the fixed thrust cases 1 and 2 require launch masses between *135 - 488 kg* and *67 - 244 kg* respectively.

4.3.4 Thrust Range Analysis

Although the Taranis orbit requires a constant acceleration, in reality as the propellant is consumed, the mass of the spacecraft decreases, causing an increase in the acceleration from the EP system. A variable thrust EP system is therefore required. The thrust range necessary from the EP system can be determined by finding the thrust at the beginning of the mission with all the propellant, and the thrust at the end of the mission with zero propellant. These thrust ranges are shown for a range of mission lifetimes for each of the hybrid systems considered and the EP-only case for both the fixed launch mass case in Figure 4-14 and the fixed maximum thrust case in Figure 4-15.

As shown by Eqs. (4.17) - (4.20), the mass budget analysis in **Section 4.3.3** is based on the value of the maximum thrust, thus as the thrust level is variable there is an over estimation of the power requirements, and in turn of the mass of the EP system, solar arrays, propellant and tank mass. Calculations show that the maximum over estimation of the power requirements ranges from *37* to *78 %*.

4.3.4.1 Fixed Launch Mass

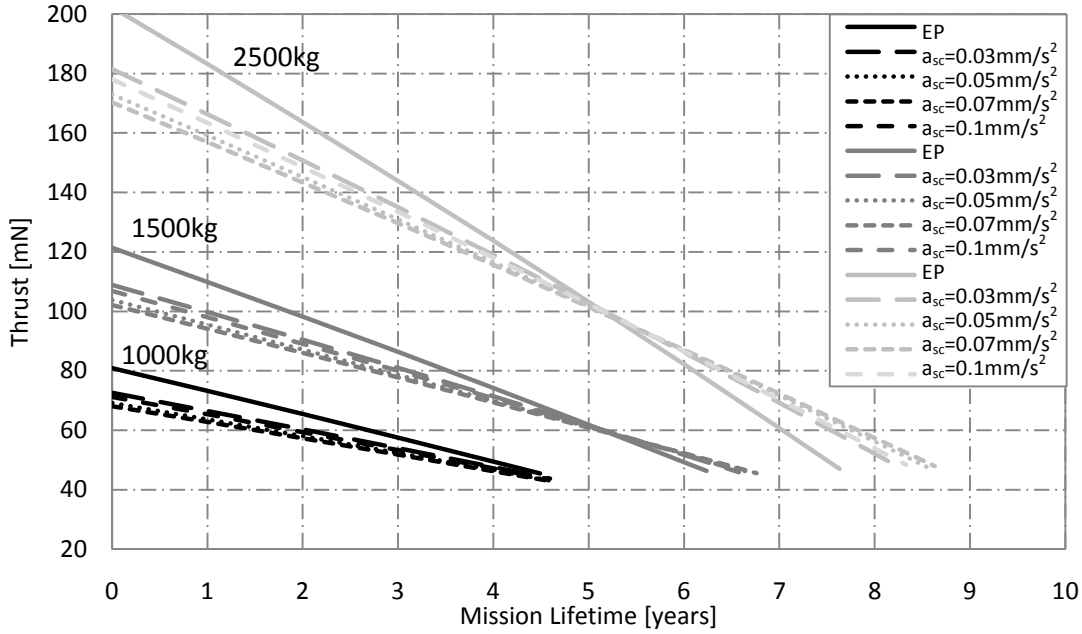

Figure 4-14 Thrust ranges required by the EP system – fixed launch mass

In Figure 4-14 it is shown that the addition of a solar sail to the EP system decreases the thrust range required by the EP system. For example, considering the *1500 kg* initial mass, a 4 year mission the EP-only system requires *121.3 mN* at the beginning of the mission and *74.2 mN* at the end of the mission. This is compared with *102.2 mN* at the beginning of the mission and *69.4 mN* at the end of the four years for the solar sail of characteristic acceleration *0.07 mm/s²*.

4.3.4.2 Fixed Maximum Thrust

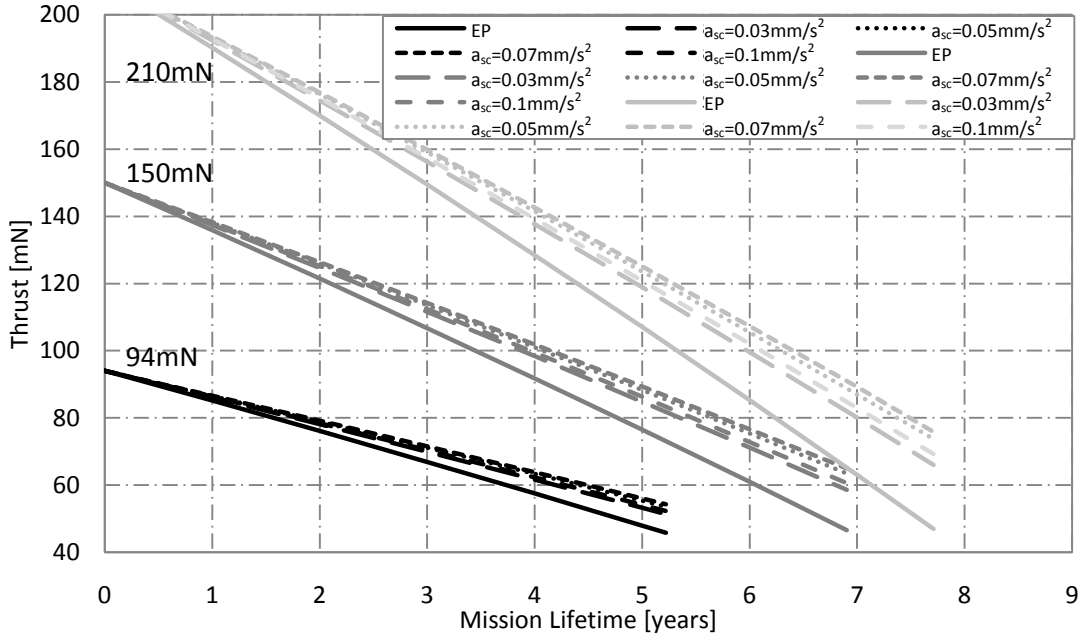

Figure 4-15 Thrust ranges required by EP system – fixed maximum thrust

Figure 4-15 shows that, similar to the fixed launch mass case, as larger solar sails are added to the system the required EP thrust range decreases. Considering the spacecraft with an initial thrust of *210 mN* and mission duration of 5 years, the EP-only case has a final thrust of *107.1 mN*. This is compared with final thrusts of *118.9*, *123.6*, *125.1*, and *120.8 mN* respectively for each of the given solar sail characteristic accelerations.

4.4 Technology Requirements

Given that the parameters of the Taranis platform are defined for the mass and power required the systems and technology requirements of the platform can be investigated. Firstly, the requirements of the spacecraft including EP thrusters, solar arrays and propellant tanks are ascertained, followed by investigation of the possible solar sail design for each case discussed.

4.4.1 EP Thrusters

Assuming the total acceleration is constituted by two thrusters at any given time, one for each of the radial and transverse directions, the approximate required range per thruster for various mission durations, for the EP-only case and the hybrid solar sail / EP systems, are stated in Table 4-8.

Fixed Launch Mass

The reduction in thrust range required by the EP thrusters which occurs for all hybrid systems proposed is made clear from Table 4-8, where it is shown that the thrust range decreasing as the solar sail characteristic acceleration increases. Notably, all of the thrust ranges shown in Table 4-8 are achievable using current technology. The NSTAR thruster, which has undergone significant ground testing in addition to a flight test on the Deep Space 1 (DS1) spacecraft [76], is capable of providing between *20* and *94 mN* of thrust. Thus, four NSTAR thrusters, one per required direction, are capable of providing the necessary thrust range for both the *1000* and *1500 kg* initial masses, for all mission durations considered, and for the *2500 kg* spacecraft for all hybrid systems proposed. Furthermore, the QinetiQ T6 thruster, is throttleable between *30* and *210 mN* [86] and so is capable of providing the required thrust range for all of the mission durations for an initial mass of *2500 kg* and all systems for a 4 year mission for the *1500 kg* spacecraft.

Table 4-8 Maximum and minimum thrust per thruster

Initial Mass [kg]	Duration [years]	EP		0.03mm/s^2		0.05mm/s^2		0.07mm/s^2		0.1mm/s^2	
		Max [mN]	Min [mN]	Max [mN]	Min [mN]	Max [mN]	Min [mN]	Max [mN]	Min [mN]	Max [mN]	Min [mN]
1000	**3**	40	29	36	27	35	26	34	26	36	27
1000	**4**	40	25	36	24	35	23	34	23	36	24
1500	**4**	61	37	54	36	52	35	51	35	53	35
1500	**6**	61	25	54	26	52	26	51	26	53	26
2500	**4**	101	62	91	60	87	58	85	58	89	59
2500	**6**	101	41	91	43	87	43	85	44	89	43
2500	**7**	101	30	91	35	87	36	85	36	89	35

Fixed Maximum Thrust

Again, assuming the total acceleration is constituted by two thrusters at any given time, one for each of the radial and transverse directions, the approximate required range per thruster are stated in Table 4-9.

Table 4-9 Maximum and minimum thrust per thruster

Initial Thrust [mN]	Duration [years]	Max Thrust [mN]	EP-only Min [mN]	0.03mm/s^2 Min [mN]	0.05mm/s^2 Min [mN]	0.07mm/s^2 Min [mN]	0.1mm/s^2 Min [mN]
94	**3**	47	33	35	36	36	35
94	**4**	47	29	31	32	32	31
150	**4**	75	46	49	51	51	50
150	**6**	75	30	36	38	38	36
210	**4**	105	64	69	71	71	70
210	**6**	105	43	50	53	54	51
210	**7**	105	32	40	44	45	42

The reduction in thrust range required by the EP thrusters for all of the hybrid systems proposed is again evident from Table 4-9. It is shown that four NSTAR thrusters, one per required direction, are capable of providing the thrust range required for both the *94 mN*

and *150 mN* initial thrust systems, for all durations of mission considered, and for both EP-only and hybrid systems. The QinetiQ T6 thruster is also capable of providing the required thrust range for all of the systems for all mission lifetimes with the exception of a 4 year mission using the EP-only system with an initial thrust of *94 mN*.

4.4.2 Solar Arrays

To enable the *90 degree* Taranis orbit, the power requirements of the spacecraft must be considered. The sizing of the required solar arrays is based on an end-of-life (EOL) solar array efficiency of *0.25* at *1 au* [146]. The power required by each spacecraft of different initial thrust values, the mass of the solar arrays (from Eq. (4.20)) and the required solar array area, found using the solar flux of *1370 W/m^2* at *1 au*, are given in Table 4-10 - Table 4-14 for the fixed launch mass and Table 4-15 for fixed maximum thrust.

Fixed Launch Mass

The maximum thrust used to determine the power requirements are also given in Table 4-10 - Table 4-14. A modest reduction in both mass and required area of the solar arrays by the use of hybrid solar sail / EP system is shown in Table 4-10 - Table 4-14 with the required area decreasing as the solar sail characteristic acceleration is increased. Results show that the required sizes of the solar arrays, for all cases, are modest and feasible using current solar array technology. The solar arrays in this case are significantly smaller than those of Rosetta, totalling *61.5 m^2* for a *3000 kg* spacecraft [147], and are comparable to the *10 m^2* arrays of SMART-1 for a *370 kg* spacecraft [148].

Table 4-10 Solar array sizing – EP only

Initial Mass [kg]	Max. Thrust [mN]	Max. Power [kW]	Solar Array Mass [kg]	Solar Array Area [m^2]
1000	80.9	1.7	38	5
1500	121.4	2.6	57	8
2500	202.3	4.3	94	13

Table 4-11 Solar array sizing – $a_{sc} = 0.03\ mm/s^2$

Initial Mass [kg]	Max. Thrust [mN]	Max. Power [kW]	Solar Array Mass [kg]	Solar Array Area [m^2]
1000	72.6	1.5	34	5
1500	108.9	2.3	51	7
2500	181.5	3.8	85	11

Table 4-12 Solar array sizing – $a_{sc} = 0.05\ mm/s^2$

Initial Mass [kg]	Max. Thrust [mN]	Max. Power [kW]	Solar Array Mass [kg]	Solar Array Area [m^2]
1000	69.2	1.5	32	4
1500	103.8	2.2	48	6
2500	173.0	3.6	81	11

Table 4-13 Solar array sizing – $a_{sc} = 0.07\ mm/s^2$

Initial Mass [kg]	Max. Thrust [mN]	Max. Power [kW]	Solar Array Mass [kg]	Solar Array Area [m^2]
1000	68.1	1.4	32	4
1500	102.2	2.1	48	6
2500	170.3	3.6	80	11

Table 4-14 Solar array sizing – $a_{sc} = 0.1\ mm/s^2$

Initial Mass [kg]	Max. Thrust [mN]	Max. Power [kW]	Solar Array Mass [kg]	Solar Array Area [m^2]
1000	71.2	1.5	33	4
1500	106.8	2.2	50	6
2500	178.0	3.7	83	11

Fixed Maximum Thrust

Table 4-15 shows that, as with the fixed launch mass case, the required sizes of the solar arrays, for all cases, are feasible using current solar array technology.

Table 4-15 Solar array sizing – fixed maximum thrust

Initial Thrust [mN]	Maximum Power [kW]	Solar Array Mass [kg]	Solar Array Area [m^2]
94	2.0	44	6
150	3.2	70	9
210	4.4	98	13

4.4.3 Propellant Tanks

Finally, the storage requirements for the requisite propellant mass for given mission durations are examined. The propellant mass for each initial thrust value considered are determined using Eq. (4.17) and are shown in Table 4-16 and Table 4-17.

Fixed Launch Mass

The reduced propellant mass for the hybrid solar sail / EP systems, over pure EP systems, are detailed in Table 4-16. The NASA Dawn mission Xenon tanks have a capacity of *425 kg* of propellant, the Taranis spacecrafts (both EP-only and hybrid systems) propellant mass

requirements can be accommodated using a single propellant tank for a four year mission. For a six year mission this is increased to two tanks for all proposed systems. Finally, four tanks are required for all seven year missions. As the single tank volume is *0.27 m^3*, the equivalent tank radius for a spherical tank is *0.4 m* and so the total propellant mass requirements for the possible Taranis platforms can be accommodated in a modest volume. Note that results are included for the *0.1 mm/s^2* solar sail to show the increase in propellant mass from the *0.07 mm/s^2* sail.

Table 4-16 Propellant mass – fixed launch mass

Initial Mass [kg]	**Mission Duration [years]**	EP-only **Propellant Mass [kg]**	0.03mm/s^2 **Propellant Mass [kg]**	0.05mm/s^2 **Propellant Mass [kg]**	0.07mm/s^2 **Propellant Mass [kg]**	0.1mm/s^2 **Propellant Mass [kg]**
1000	4	347	311	297	292	305
1500	6	780	700	668	657	687
2500	7	1578	1362	1298	1277	1335

Fixed Maximum Thrust

Table 4-17 shows that the propellant mass requirements can be accommodated using a single propellant tank for four year missions and three propellant tanks for the six year mission and finally four tanks for the seven year missions.

Table 4-17 Propellant mass – fixed maximum thrust

Initial Thrust [mN]	**Mission Duration [years]**	**Propellant Mass [kg]**
94	4	403
150	6	965
210	7	1576

4.4.4 Solar Sail

Following design of the spacecraft components, possible design of the solar sails is considered. Sizing of the solar sail is conducted to determine the technology development, if any, needed to allow the proposed hybrid low-thrust propulsion missions to become feasible.

Fixed Launch Mass

The design space for each of the solar sails for all initial masses considered are shown in Figure 4-16 - Figure 4-18. Eq. (2.10) is used to determine the sail area for each characteristic acceleration considered, assuming a sail efficiency of *0.85* [108], solar radiation pressure equal to $4.56 \times 10^{-6}\ N/m^2$ and varying the sail loading.

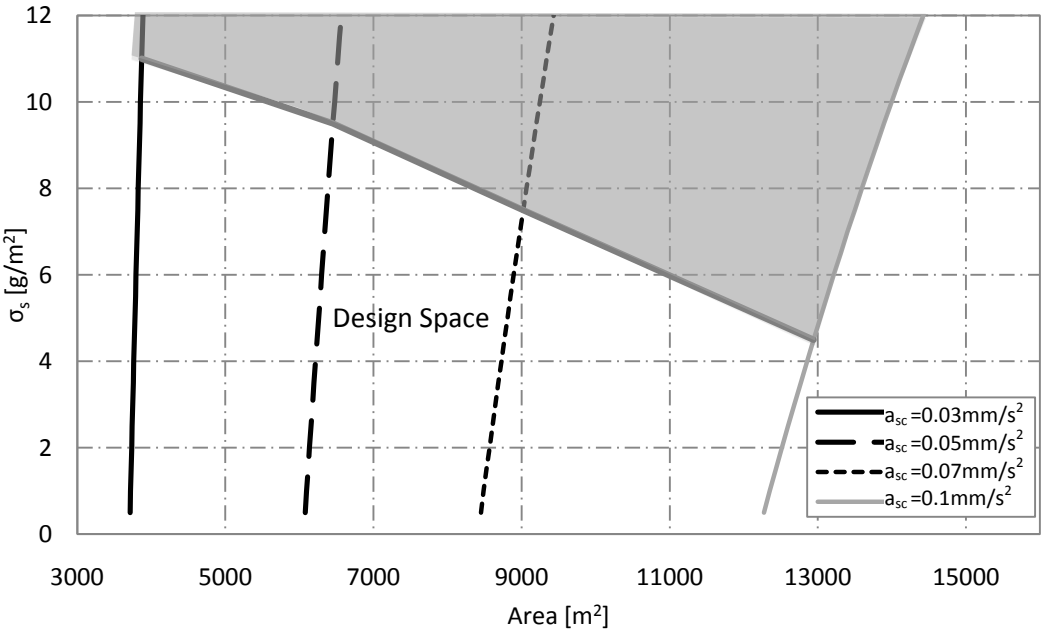

Figure 4-16 Design space for various characteristic accelerations – *1000 kg* initial mass

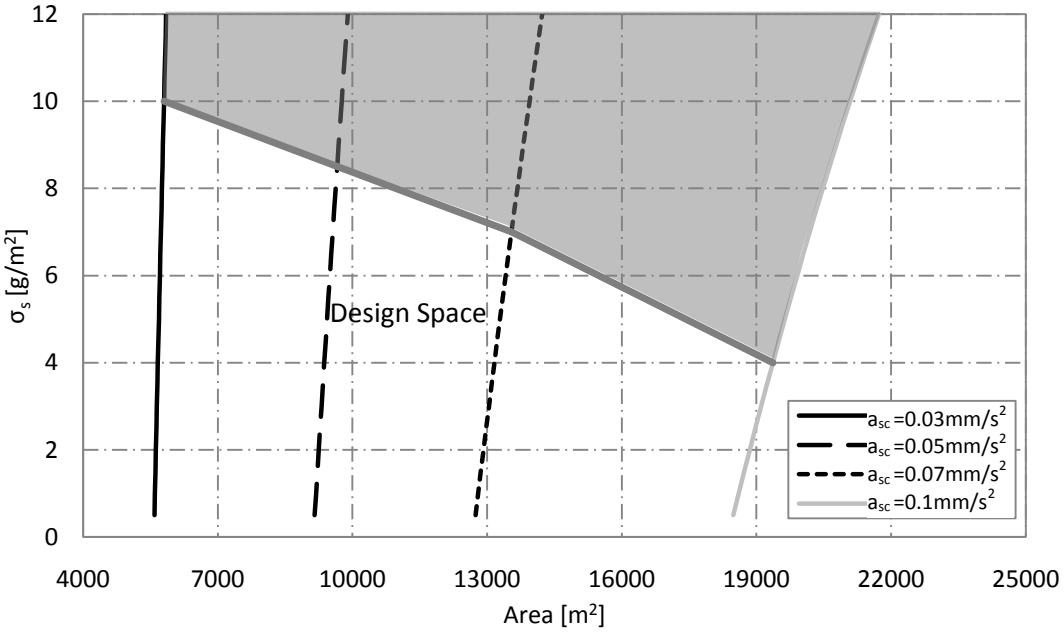

Figure 4-17 Design space for various characteristic accelerations – *1500 k*g initial mass

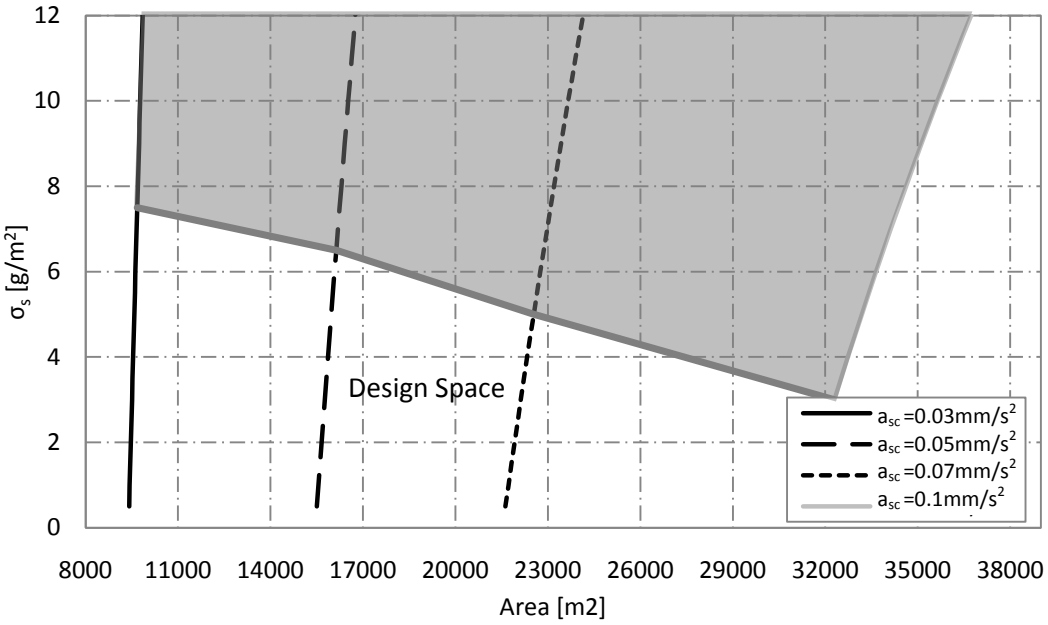

Figure 4-18 Design space for various characteristic accelerations – *2500 kg* initial mass

Below the shaded area in Figure 4-16 - Figure 4-18 the total spacecraft mass is below the initial mass value, thus the shaded area bounds the design limit of the sail. Comparison of

these plots reveals an increase in the solar sail area and a significant decrease in the sail loading as the initial spacecraft mass increases. Comparison of Figure 4-16 - Figure 4-18 with Figure 2-10 clearly shows the solar sails required to enable the Taranis orbit lie within the mid to far term technology region and thus require significant technology development before becoming feasible.

Fixed Maximum Thrust

Case 1

The design space for each of the solar sails for each initial thrust case is shown in Figure 4-19 - Figure 4-21. These figures give the required solar sail area, again assuming a sail efficiency of 0.85 [108].

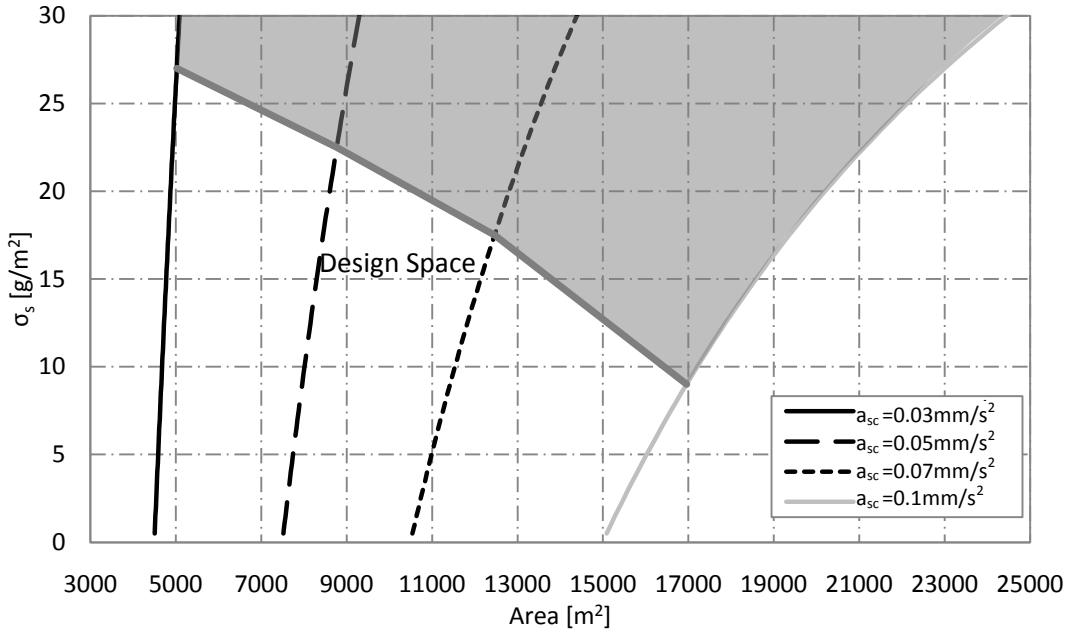

Figure 4-19 Design space for various characteristic accelerations – case 1, *94 mN* initial thrust

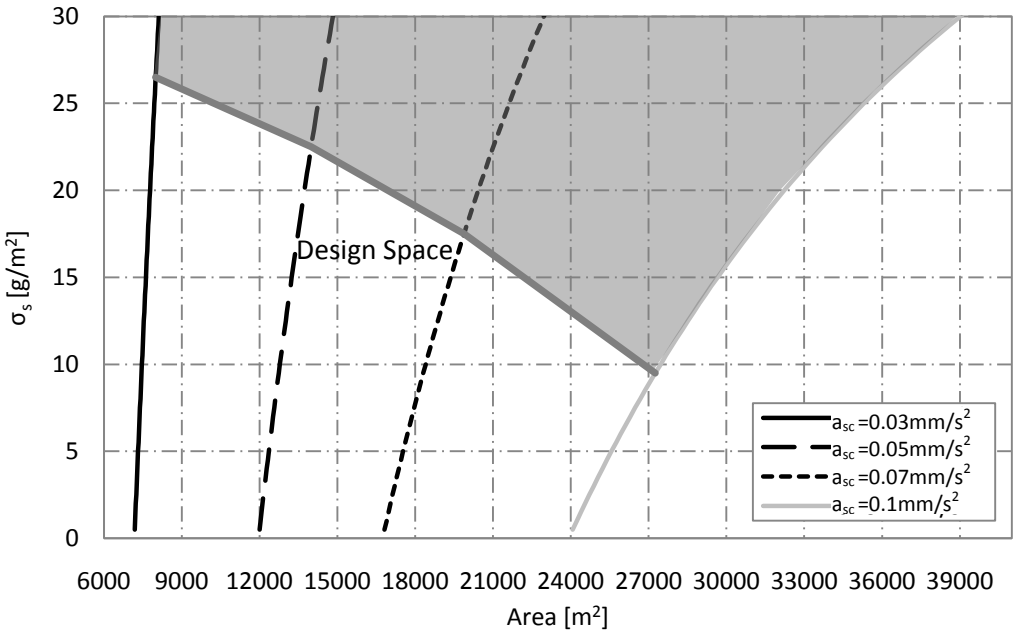

Figure 4-20 Design space for various characteristic accelerations – case 1, *150 mN* initial thrust

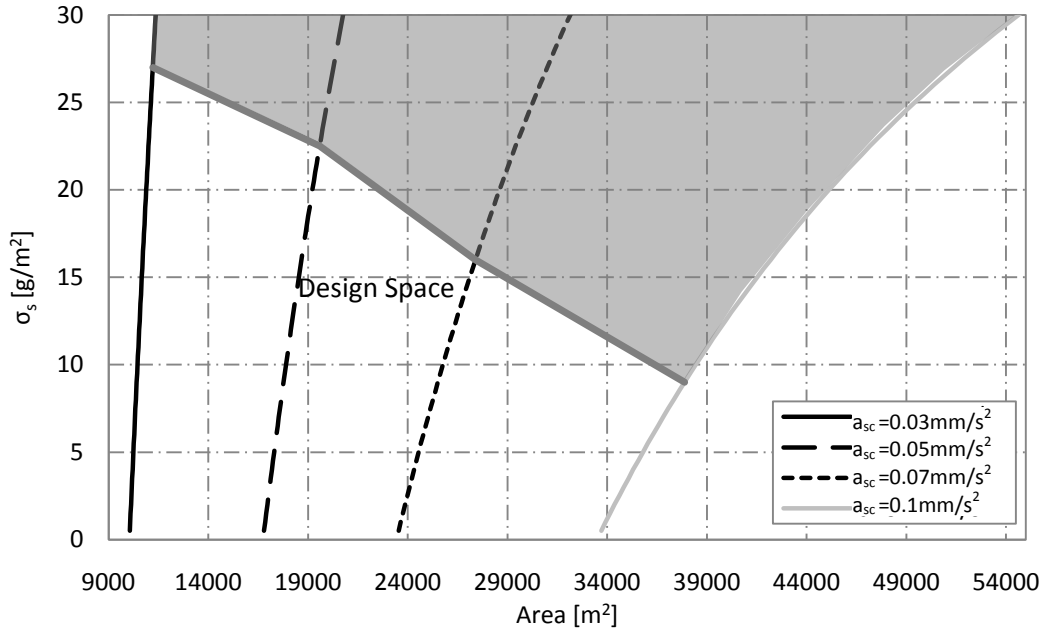

Figure 4-21 Design space for various characteristic accelerations – case 1, *210 mN* initial thrust

The design space for each of the solar sails considered for initial thrusts of *94*, *150* and *210 mN* is given in Figure 4-19 - Figure 4-21 respectively, where once again the shaded area bounds the design limit. It is shown that although the sail area is of the same order of magnitude as those required for the fixed mass case, the sail loading is significantly higher. Thus, from comparison with Figure 2-10 the solar sails in this case (Figure 4-19 - Figure 4-21) are within near or midterm technology. Comparison of the design space for each initial thrust value again reveals that as the initial thrust increases the required solar sail area also increases. Once again, the solar sails in Figure 4-19 - Figure 4-21 show the baseline solar sail technology required as all additional mass is assigned to the solar sail. The sails in case 2 will therefore have to demonstrate an advance in technology.

Case 2

In this instance, lighter solar sails constituting half of the additional mass are considered for each of the given characteristic accelerations, again assuming an efficiency of *0.85* [108] and varying the sail loading to determine the requisite area, the results for all initial thrust values investigated are shown in Figure 4-22 - Figure 4-24.

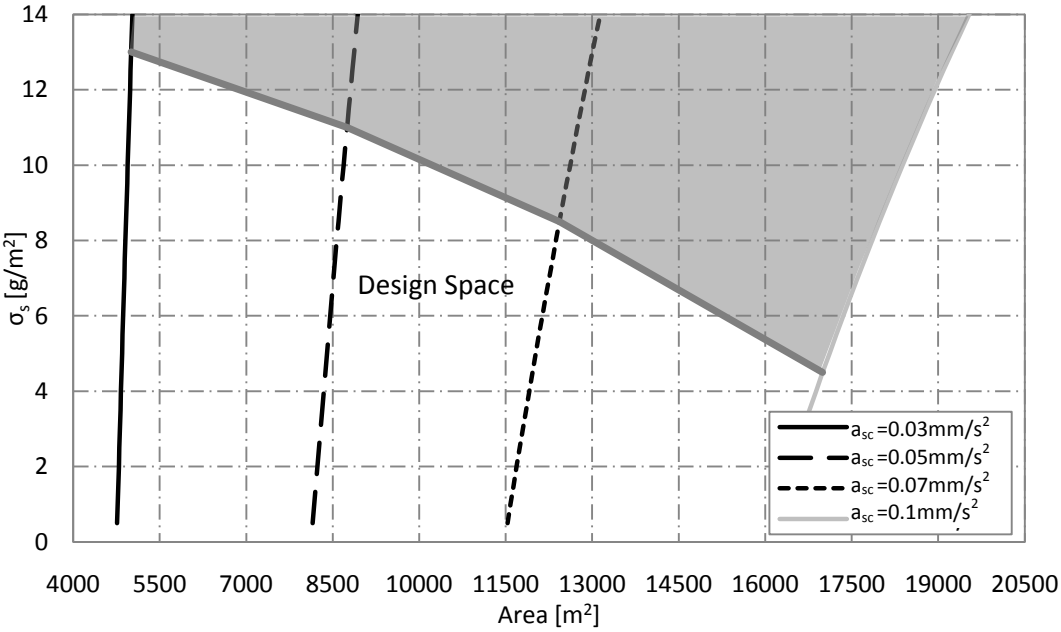

Figure 4-22 Design space for various characteristic accelerations – case 2, *94 mN* initial thrust

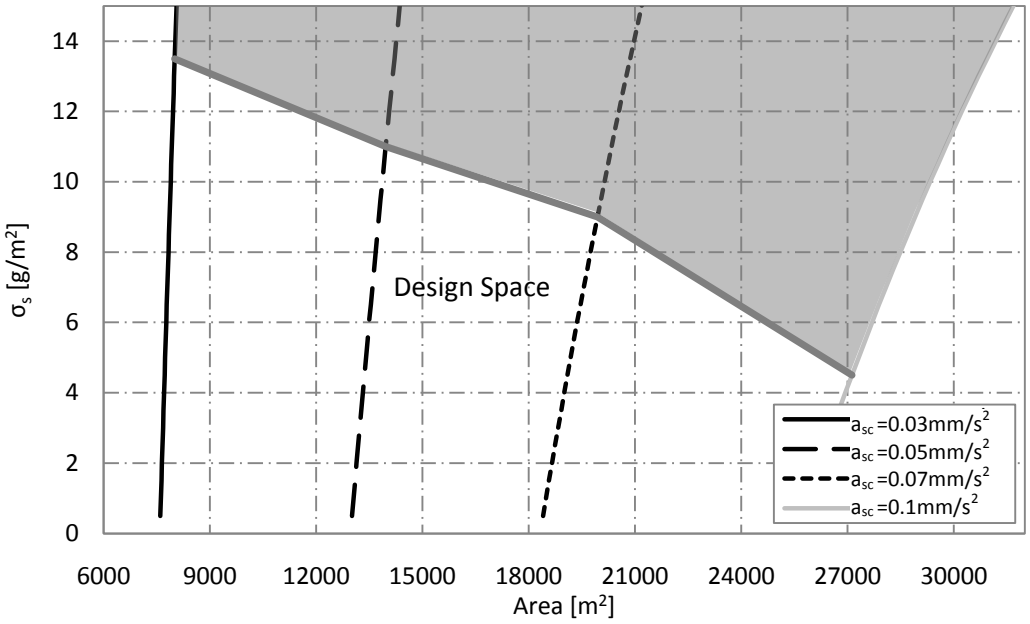

Figure 4-23 Design space for various characteristic accelerations – case 2, *150 mN* initial thrust

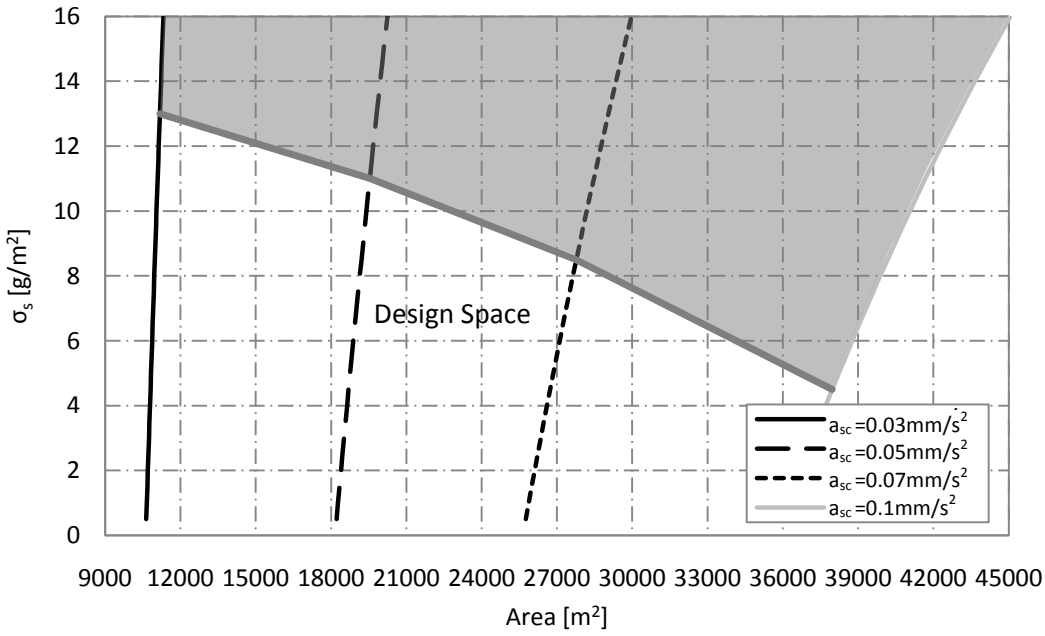

Figure 4-24 Design space for various characteristic accelerations – case 2, *210 mN* initial thrust

Comparison of design space charts from case 1 and case 2 shows that although the required areas of the sails are of the same order of magnitude, the solar sails in case 2 are significantly lighter. From comparison between Figure 4-22 - Figure 4-24 and Figure 2-10 it is clear that to enhance the lifetime of the Taranis mission, developments in sail technology are required to produce these relatively large lights sails, as these lie within the mid to far term technology region. Again, comparison of Figure 4-22 - Figure 4-24 shows that the solar sail area is significantly increased as the initial thrust increases.

4.5 Chemical Propulsion

Comparison can also be made between the use of conventional chemical propulsion and low-thrust EP to maintain the artificial critical inclination of the 12 h Taranis orbit. The effective Δv to enable the Taranis orbits using continuous low-thrust propulsion can be found from the product of the required acceleration and mission duration, given by

$$\Delta v = a_p \Delta t \tag{4.21}$$

As previously stated in **Section 4.2.1**, at an inclination of *90 degrees* the natural drift in argument of perigee is - *0.15 degrees per day*. To compensate for this change in argument of perigee chemical thrusters would be required to provide two equal impulses per orbit. The total Δv through the application of the two impulses is given by [149]

$$\Delta v = \frac{\Delta \omega}{(2/e)\sqrt{a\left(1-e^2\right)/\mu}} \tag{4.22}$$

The respective Δv and propellant mass fraction, $\Delta m/m_0$, calculated using the rocket equation, for one year of operation are shown in Table 4-18, with results extended over various mission durations shown in Figure 4-25.

Table 4-18 Δv requirements for one year of operation

Propulsion System	**Δv [km/s]**	**Propellant Mass Fraction**
Electric (I_{sp} = 3000 – 4600s)	2.55	0.083 – 0.055
Chemical (I_{sp} = 200 –340s)	1.96	0.632 – 0.444

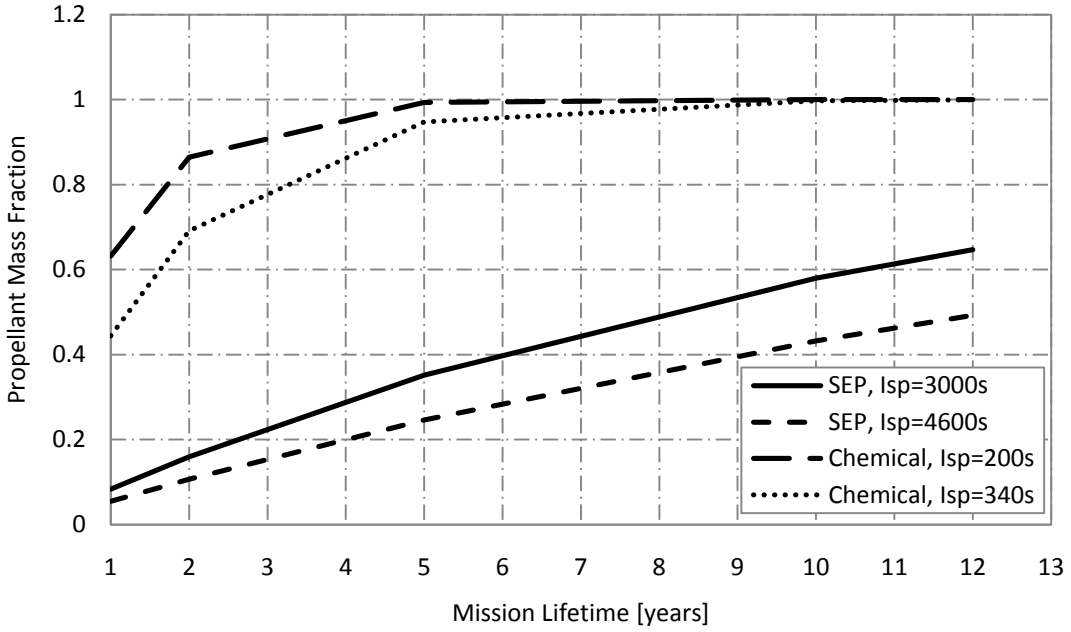

Figure 4-25 Electric and chemical Δv comparison

The benefit of using EP to enable Taranis orbits as opposed to conventional chemical propulsion is highlighted in Figure 4-25, where it is shown that although chemical propulsion is feasible for low mission durations, it becomes impractical for longer duration missions. Above 5 years, the chemical propellant mass fraction begins to tend to one, with low-thrust propulsion enabling much greater mission lifetimes.

4.6 Summary

Hybrid solar sail / electric propulsion and high-thrust chemical propulsion systems have been considered to maintain the novel 12 h Taranis orbit, inclined at *90 degrees* to the equator, and comparison made with the use of a pure electric propulsion system.

Hybrid solar sail and electric propulsion systems, in theory, lower the demand on the electric propulsion system by reducing the propellant consumption, thus increasing the possible lifetime of the mission or the capacity for useful payload. The addition of the solar sail to the system could lower the advancement degree of difficulty of the solar sail, while

the electric thruster compensates for the solar sail's inability to thrust in the direction of the Sun. Two constraining parameters were considered, firstly the case where the launch mass of the spacecraft is fixed; and secondly where the maximum thrust of the electric propulsion thruster constrains the system. When the launch mass of the spacecraft is fixed, the increase in the mission lifetime from the pure electric propulsion system is negligible and there is no tangible benefit from the addition of a solar sail. The solar sails required to achieve these increases in lifetime are extremely large, light sails. Thus considerable developments in solar sail technology are necessary to make these missions feasible. In the case of the fixed maximum thrust, the increase in mission lifetime is greater than that achieved using a fixed launch mass. In addition to this, the physical size of the solar sails required are of the same order of magnitude as the fixed launch mass sails, however, these are much heavier sails making them more feasible solutions. It has therefore been shown that the gain from the addition of a solar sail to the system is negligible to enable the 12 h, *90 degree* inclination Taranis orbit. It is also noted that whilst the analysis considers constant sail acceleration, the sail will in fact generate excess acceleration as propellant is consumed, requiring an equivalent increase in the acceleration from the EP system. Therefore the mission lifetimes calculated in this chapter are in fact biased towards the use of the solar sail, this further substantiates the original conclusion that hybrid solar sail / EP systems are of no benefit to enable the Taranis orbit.

A chemical propulsion system was also considered to maintain the zero change in argument of perigee condition of a *90 degree*, 12 h Taranis orbit. The chemical thruster provides two impulses per orbit to maintain the zero rate of change of argument of periapsis over the orbit and is shown to be feasible to enable mission durations less than five years. However, this becomes impractical for longer duration missions.

Electric propulsion is therefore considered the most viable means of propulsion to enable a 12 h, *90 degree* inclination Taranis orbit for high-latitude observation.

Chapter 5

5 Trade Space Analysis for a Polar Remote Sensing Constellation

The requirements for a polar monitoring platform have previously been derived in **Chapter 1**, these are outlined again in **Section 5.2** for clarity, and a more detailed requirements analysis is conducted in **Section 5.3**. **Section 5.4** is divided into two sub-sections considering continuous observation of constellations of spacecraft on various Taranis orbits to both *55* and *50 degrees* latitude respectively. **Section 5.5** displays the view of Earth as seen by a spacecraft on a 12 h, *90 degree* Taranis orbit, to illustrate the rotation of the Earth below the spacecraft at apogee. Finally, validation of the visibility analysis is conducted in **Section 5.6** using NOVA Satellite Tracking Software.

5.1 Introduction

The importance of building an observation system capable of providing high resolution imaging of high-latitude regions of the Earth has previously been detailed in **Chapter 1**. This chapter therefore considers the design of a *90 degree* inclination Taranis orbit constellation for high-latitude sensing by considering spatial resolution, possible launch options, the radiation environment, EoL debris mitigation measures and the required number of spacecraft to give continuous coverage of defined high-latitude regions.

As explained in **Chapter 1**, in order to complete the GOS, the minimum requirement of the constellation is continuous observation to *55 degrees* latitude to compensate for the

limitations of GEO platforms beyond this point [10]. Consideration is also given to a constellation capable of continuously observing to *50 degrees* latitude to increase the overlap in data from GEO-based instruments. This chapter considers the design of a constellation capable of continuously sensing one of the Earth's polar regions, in this case the North Pole. Thus in order to complete the GOS, a duplication of this constellation is required for the South Pole.

5.2 Requirements for Selecting Polar Remote Sensing Constellation

The key requirements for selecting the most beneficial Taranis orbit for spacecraft in the constellation, as defined in **Chapter 1**, are as follows:

R1. *The constellation shall provide continuous coverage above 55 degrees latitude as a minimum.*

R2. *The rate of change of argument of perigee of the orbit shall be zero.*

R3. *The apogee altitude of the orbit shall be less than 45,000 km.*

R4. *The OZAs shall be less than or equal to the OZA from GEO.*

R5. *Above the target region, a single image shall be used to provide the required coverage.*

R6. *The mission shall comply with debris mitigation guidelines.*

Although the following is not a strict requirement, it is a condition that should be considered when designing the constellation:

- *To avoid the highest density region of high-energy protons the altitude of the semi-latus rectum should be > 15,000 km.*

5.3 Requirement Analysis

R1. *The constellation shall provide continuous coverage above 55 degrees latitude as a minimum.*

In order to complete the GOS and allow continuous coverage of the Earth at any time, the Taranis constellation is required to provide continuous observation of the regions above *55 degrees* latitude. This is the minimum level of coverage required by the constellation, as at around *55 degrees* latitude observations from geostationary platforms are considered to be of unacceptable quality [10]. However, to provide a significant overlap with data from GEO, the design of a constellation capable of imaging continuously to *50 degrees* latitude is also considered.

R2. *The rate of change of argument of perigee of the orbit shall be zero.*

This is a condition which is satisfied by both the conventional Molniya orbit and a Taranis orbit. However, whilst the inclination of the Molniya orbit is fixed at either *63.43* or *116.6 degrees* the Taranis orbit, through the use of continuous low-thrust propulsion, can be given any inclination. A Taranis orbit with an inclination of *90 degrees* and argument of perigee of *270 degrees* places the apogee of the orbit directly above the Earth's North Pole. Thus, the spacecraft will spend the longest period of time above this region, giving enhanced observation of the polar regions. This analysis therefore considers *90 degree* inclination Taranis orbits.

R3. *The apogee altitude of the orbit shall be less than 45,000 km.*

In order to ensure adequate spatial resolution with current imaging platforms, the limit placed on the apogee altitude is selected as *25 %* higher than GEO altitude. This matches the limit currently being used by other HEO mission concepts, including the PCW mission [27, 28].

The requirement on the apogee altitude to be below *45,000 km* can be converted into a valid region of values for the semi-major axis using

$$H_a = a(1+e) - R_E < 45,000km \tag{5.1}$$

where, H_a, is the apogee altitude of the spacecraft. The corresponding orbital period, T_s, is then determined using

$$T_s = 2\pi\sqrt{\frac{a^3}{\mu}} \tag{5.2}$$

R4. *The OZAs shall be less than or equal to the OZA from GEO.*

In order to ensure data product quality the OZA of the defined latitude limit, when viewed from GEO, is calculated and is then used as the OZA for the Taranis orbit. This is achieved by calculating the minimum elevation angle, using Eqs. (5.3) - (5.5), where the parameters used are introduced in Figure 5-1.

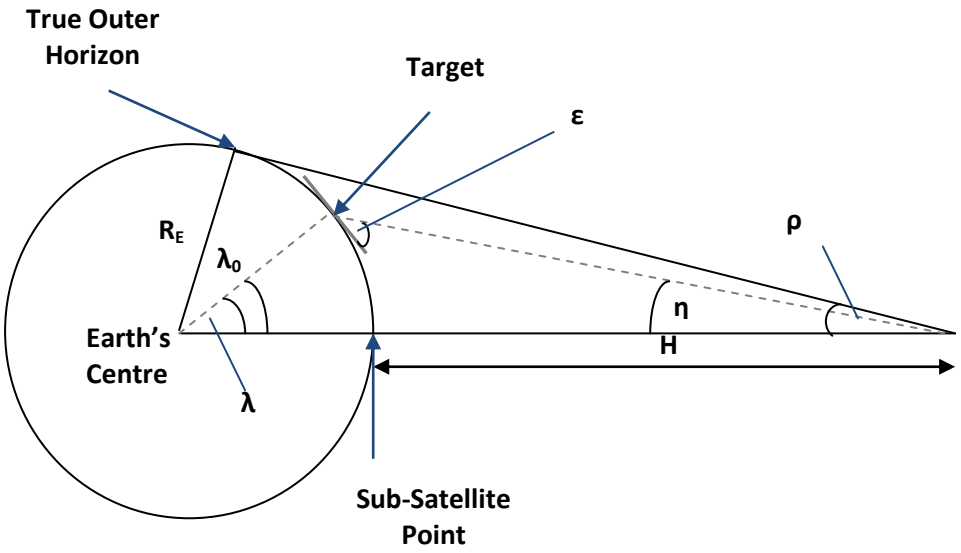

Figure 5-1 Angular relationships between spacecraft, target and Earth centre

Firstly, the angular radius of the Earth, ρ, is calculated using

$$\sin(\rho) = \cos(\lambda_0) = \frac{R_E}{R_E + H} \tag{5.3}$$

where, λ_0, is the Earth central angle and H is the altitude of the spacecraft. The nadir angle, η, is determined as

$$\tan\eta = \frac{\sin(\rho)\sin(\lambda)}{1-\sin(\rho)\cos(\lambda)} \tag{5.4}$$

The angular radius of the Earth and the nadir angle are used to obtain the minimum elevation ε, as

$$\cos\varepsilon = \frac{\sin(\eta)}{\sin(\rho)} \tag{5.5}$$

Considering a GEO at an altitude of approximately *36,000 km* results in minimum elevation angles of *27* and *33 degrees*, or corresponding OZAs of *63* and *57 degrees* viewing to latitudes of *55* and *50 degrees* respectively. Employing these minimum OZAs for the Taranis orbits ensures that these provide at the very least data of equal quality to that

produced by geostationary systems viewing the same location. It is important to note that spacecraft on a Molniya orbit are incapable of providing data of equal quality to those produced by geostationary systems to latitudes of *55* and *50 degrees.* For example, a platform on Molniya orbit observing to *55 degrees* has a peak OZA observing 'over' the pole approximately *10 degrees* higher than when the same location is observed from GEO. This is further explained in **Section 5.4.1**. Thus, Taranis orbits are required to complete the GOS. Similarly, viewing to *50 degrees* latitude a Molniya orbit has an OZA of *75 degrees*, i.e. *42 degrees* higher than when viewed from GEO. This highlights the benefit of using a Taranis orbit constellation to enhance the observations of the poorly observed high-latitude regions of the Earth to complete the GOS and further emphasises the contribution of this thesis.

R5. *Above the target region, a single image shall be used to provide the required coverage.*

Observation of the polar regions is currently approximated using composite images. Therefore to offer an improvement from current systems composite images are not considered to be acceptable.

R6. *The mission shall comply with debris mitigation guidelines.*

Development of a debris mitigation plan is required by the European Cooperation for Space Standardization (ECSS) for all spacecraft from Phase 0 studies onwards [150].

Guidelines identify protected regions for LEO up to altitudes of *2,000 km* and around geostationary altitude in bands extending *200 km* above and below *35,678 km* as well as plus and minus *15 degrees* in latitude [151]. Thus, at the EoL, spacecraft should be removed from these regions.

Post mission disposal options include maneuvering to an orbit in which atmospheric drag will limit the orbital lifetime to less than 25 years after completion of operations. Re-orbiting the spacecraft to an orbit out with these protected regions or direct retrieval of the spacecraft may also be considered as a disposal option. Debris mitigation measures are considered when quantifying the design space for a HEO constellation.

It is worth noting that as the Taranis platform will only have a low-thrust propulsion system, the spacecraft is unable to target a specific point at which to re-enter. As a result uncontrolled re-entry must be assumed from the outset and the spacecraft designed to burn up completely in the Earth's atmosphere.

To determine the time taken for a spacecraft to re-enter the Earth's atmosphere due to atmospheric drag, these effects are included within the numerical simulation using the expression for the acceleration due to atmospheric drag given in Eq.(5.6), expressed in an RTN coordinate system.

$$a_{atmos} = \frac{1}{2}\rho_0 C_D \frac{A}{m} V^2 \tag{5.6}$$

Where, ρ_0 is the density as a function of altitude, implemented into the numerical model using the U.S. Standard 1976 atmosphere model, C_D is the drag coefficient, which is assumed to equal *2* i.e. the drag of a flat plate [152] and *A* is the spacecraft area.

- *Radiation Environment*

To avoid the highest density region of high-energy protons the altitude of the semi-latus rectum should be > 15,000 km.

One downside to HEOs is the potentially hazardous radiation environment, caused by solar flares, cosmic particles, and the spacecraft crossing the Van Allen radiation belts twice per orbit. These sources can have various effects on the spacecraft, for example on materials, coatings, and epoxies [153]: However, the two elements of platforms most susceptible to

damage are microelectronics, degraded by the ionizing effects of colliding particles [154], and solar cells. Solar cells are constructed from materials that are susceptible to both ionizing and non-ionizing radiation and can thus be degraded due to displacement or bulk damage of atoms within their crystal structure by the non-ionizing component of particle radiation [154]. Solar cells are also shown to suffer higher degradation due to lower energy protons, which can stop within the solar cell and cause a large amount of damage concentrated at the end of the proton track[7].

Collision with highly energetic particles can cause radioactive radiation, or activation, which leads to increased background noise in sensitive measuring equipment [154]. Gamma ray observers and x-ray detectors are particularly susceptible to this background noise [155]. Displacement damage is also responsible for reduced sensitivity of highly sensitive Charge Coupled Devices (CCDs) used in image sensors, resolution degradation in solid state detectors, and greater inefficiencies in Light Emitting Diodes (LEDs) [155]. Ionisation and atomic displacement processes in extreme cases can lead to complete loss of optoelectronic components such as optocouplers used in modern space-borne scientific instruments. These are also prone to damage by energetic solar-protons[7]. Single event effects can cause a change in state of memory cells and could trigger certain devices into a state of high current drain which may lead to burn-out and hardware failure [155]. The trend in recent years towards smaller, faster electronics and more sensitive detectors means these components are more susceptible to damage from single particles than with previous larger systems. The use of larger spacecraft means single particles could only affect a limited volume, thus only cumulative damage resulting from multiple interactions could cause loss of the spacecraft.

[7] SPENVIS Documentation http://www.spenvis.oma.be/

Although the spacecraft experiences effects from both electrons and protons, the main threat to microelectronics comes from high-energy protons [156]. It follows that in order to minimise the effects of radiation, the spacecraft should avoid the region containing protons with energy *E > 10 MeV.* The altitude distribution of proton flux in the equatorial plane is given in Figure 5-2, and shows the regions in space where the peak density of high-energy protons occur.

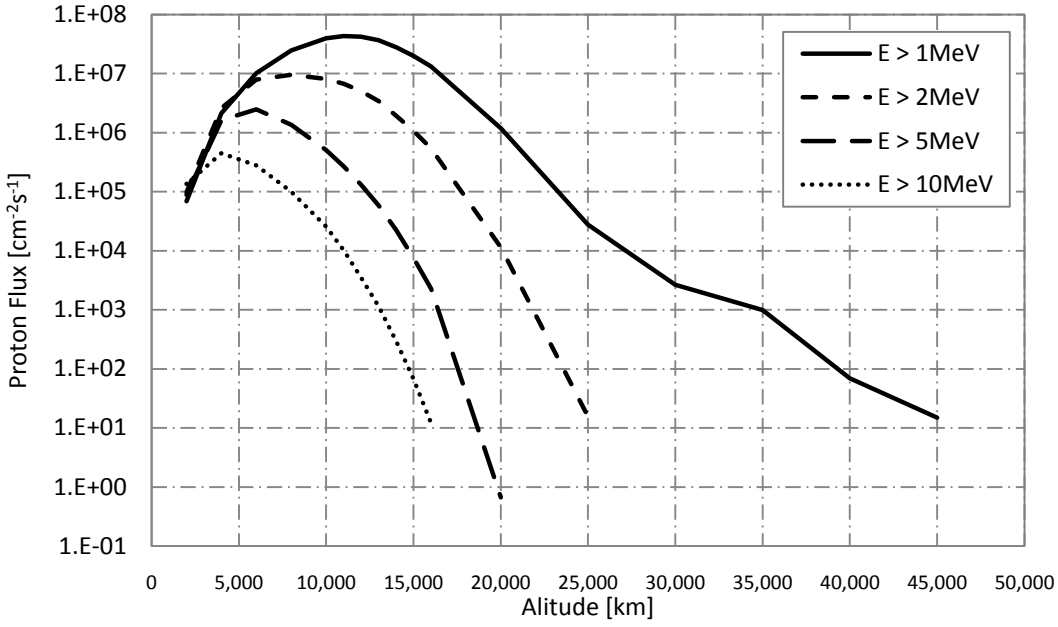

Figure 5-2 Example of vertical profile of trapped proton spectrum in the equatorial plane found using SPENVIS

The radiation environment encountered by spacecraft on each of the Taranis orbits considered in this paper has been determined using ESA's online Space Environment Information System (SPENVIS). Trapped proton and electron environments presented in this thesis are modelled using NASA models *AP-8* [157] and *AE-8* [158] respectively. To give the most conservative analysis of the radiation environment, and to follow ESA guidelines

[159], the trapped proton environment is modelled at solar minimum conditions while the trapped electron environment uses solar maximum conditions.

Figure 5-2 shows that the proton flux for high-energy protons (> *10 MeV*) falls to below *100 particles per cm^2 per second*, a standard used by other HEO missions [27, 28], at an altitude of *15,000 km*. Therefore, to avoid a high density of highly energetic protons and reduce the risk of damage to the spacecraft, therefore for an argument of perigee of *90* or *270 degrees*, the semi-latus rectum altitude should be above *15,000 km.*

The requirement on the semi-latus rectum altitude, *p*, can be stated as

$$p = a(1-e^2) > 15,000km + R_E \tag{5.7}$$

As with Eq. (5.1), the semi-latus rectum limit can be expressed in terms of the orbital period and eccentricity. This is then plotted alongside the apogee altitude limit, from Eq. (5.1), in Figure 5-3, to illustrate the valid region for orbit solution. The possible eccentricities for the low-radiation orbits are shown to be limited to between *0* and around *0.55*.

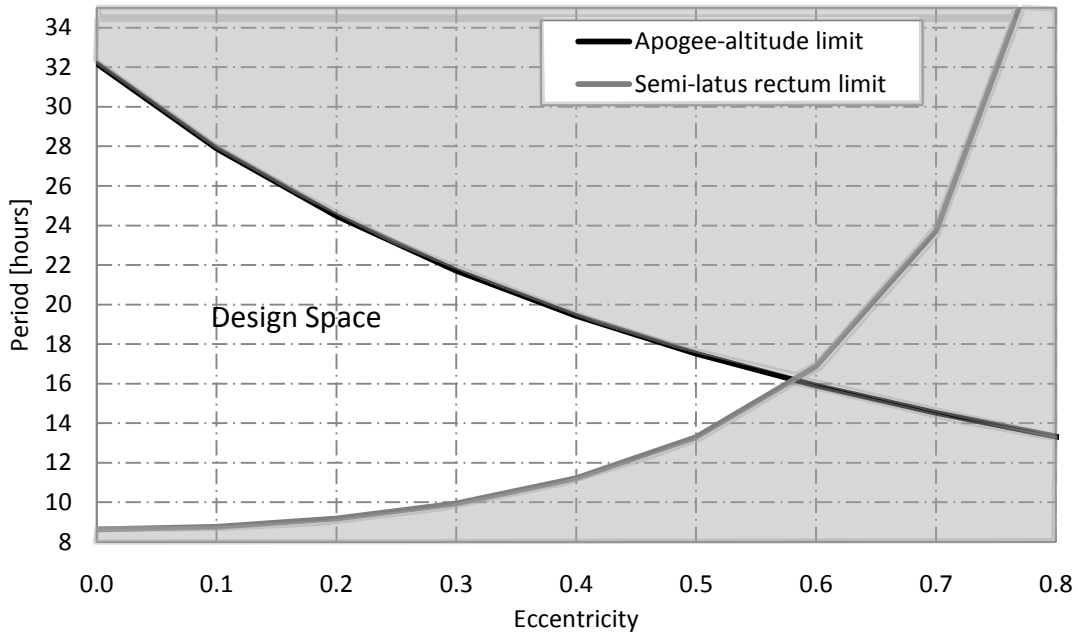

Figure 5-3 Valid region, displaying apogee altitude and semi-latus rectum limit

5.4 Visibility Analysis

The number of spacecraft required to provide continuous observation of the frigid and neighbouring temperate zones, to latitudes of *55* and *50 degrees*, from a Taranis orbit inclined at *90 degrees* to the equator, is determined.

The continuous visibility analysis is achieved using numerical analysis to determine the time spacecraft on Taranis orbits, of varying orbit periods, can view ground stations located at longitude intervals of *10 degrees,* at latitudes of *55* and *50 degrees.* This is done by numerically determining the spacecraft elevation with respect to each ground station, and if this value is greater than the minimum value specified the spacecraft is said to be in view of all ground stations and thus can provide coverage of the specified region. The number of spacecraft in the constellation is then varied, and if all ground stations are in view of at least one spacecraft, the observation of the given region is said to be continuous. This process is repeated to build up the trade space shown in Figure 5-13.

In this thesis a composite image is defined as a single image made up of images from two perspectives at the same time. If composite images are considered acceptable, the Molniya orbit can image polar regions using three spacecraft on three different orbit planes. This requires three separate launches. However, two spacecraft on a 12 h Taranis orbit can view continuously to *55 degrees* latitude using composite images; importantly this is possible using a single launch assuming orbit phasing is used to separate the spacecraft appropriately around the orbit. This is illustrated using outputs from the satellite visualisation tool SaVi[8]. Figure 5-4 - Figure 5-6 show the coverage from two spacecraft on a single plane of a 12 h, *90 degree* inclination Taranis orbit, at *4*, *8* and *12* hours into the orbit respectively using a minimum elevation of *27 degrees*. The key shown on these figures

[8] http://personal.ee.surrey.ac.uk/Personal/L.Wood/software/SaVi/ Accessed on 27th May 2013

illustrate the number of spacecraft that can view a given location. It is clear from these results that two spacecraft on a single plane of the 12 h Taranis orbit are capable of imaging continuously to *55 degrees* latitude. The coverage from a 12 h Molniya orbit is also shown in Figure 5-7 - Figure 5-12. Where, Figure 5-7 - Figure 5-9 clearly show that three spacecraft on a single plane of a 12 h Molniya orbit, cannot provide continuous coverage to *55 degrees* latitude. Therefore the Molniya orbit requires three spacecraft on three separate orbit planes to provide continuous coverage to *55 degrees* latitude, as shown in Figure 5-10 - Figure 5-12.

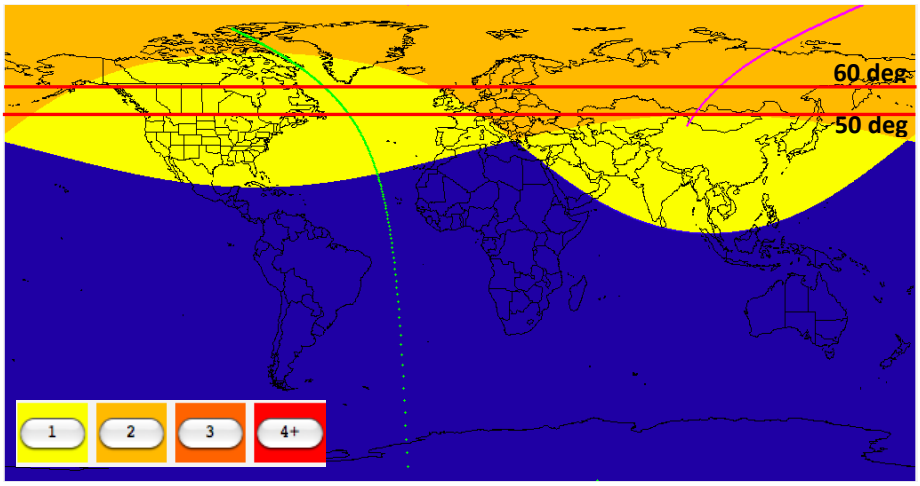

Figure 5-4 - Coverage from two s/c on single plane of 12 h Taranis orbit at 4 hours around orbit (regions showing coverage from one s/c are not necessarily from the same s/c)

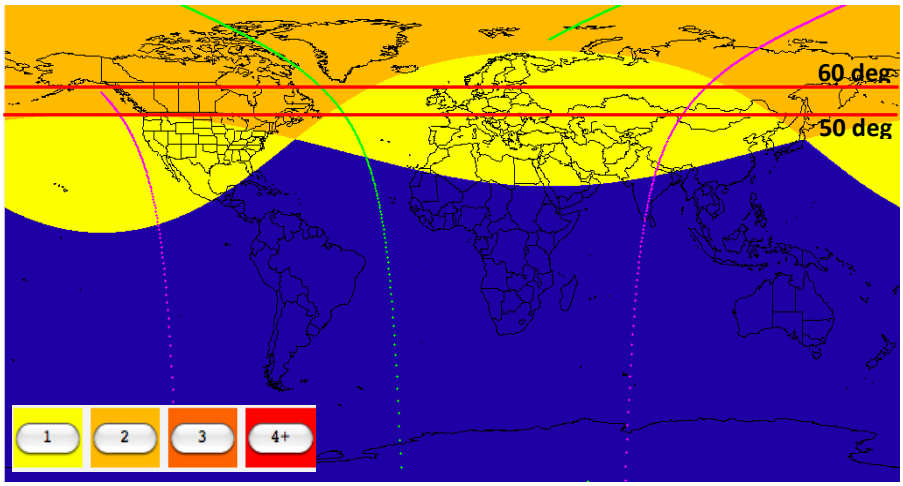

Figure 5-5 - Coverage from two s/c on single plane of 12 h Taranis orbit at 8 hours around orbit (regions showing coverage from one s/c are not necessarily from the same s/c)

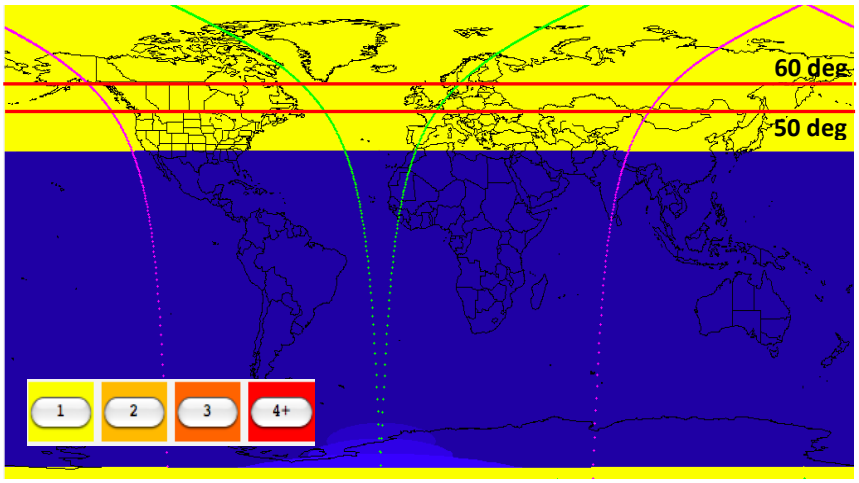

Figure 5-6 - Coverage from two s/c on single plane of 12 h Taranis orbit at 12 hours around orbit (regions showing coverage from one s/c are not necessarily from the same s/c)

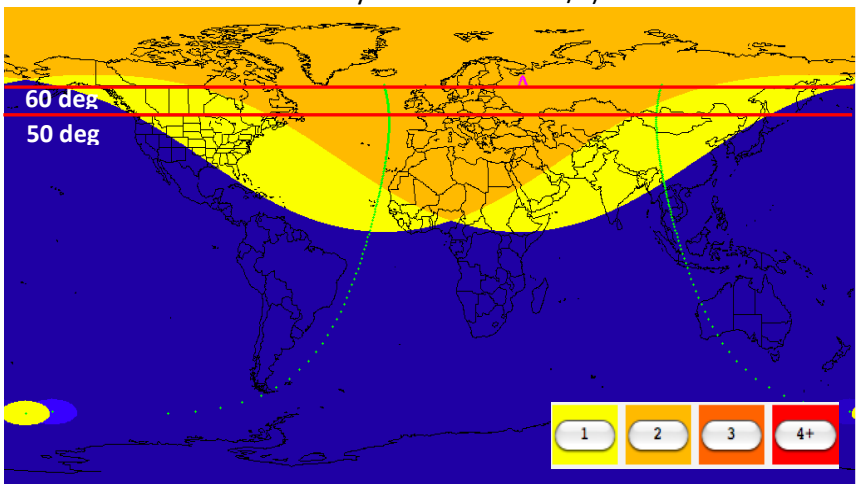

Figure 5-7 - Coverage from three s/c on single plane of 12 h Molniya orbit at 4 hours around orbit (regions showing coverage from one s/c are not necessarily from the same s/c)

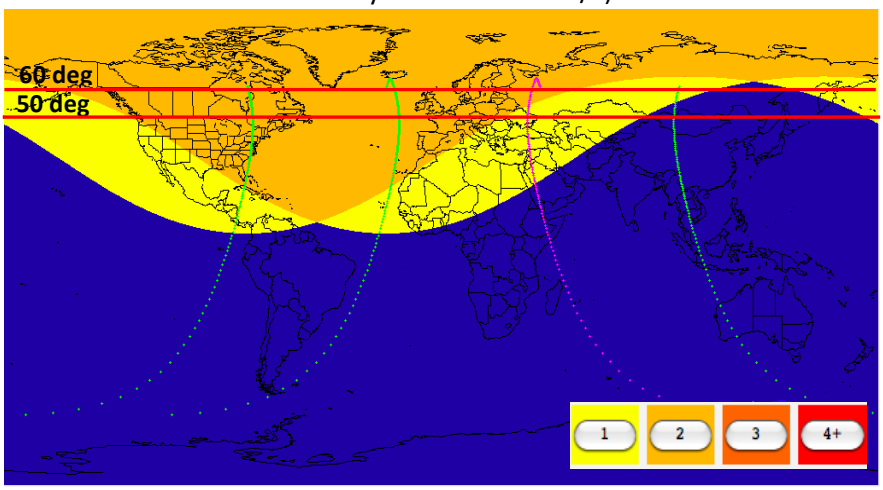

Figure 5-8 - Coverage from three s/c on single plane of 12 h Molniya orbit at 8 hours around orbit (regions showing coverage from one s/c are not necessarily from the same s/c)

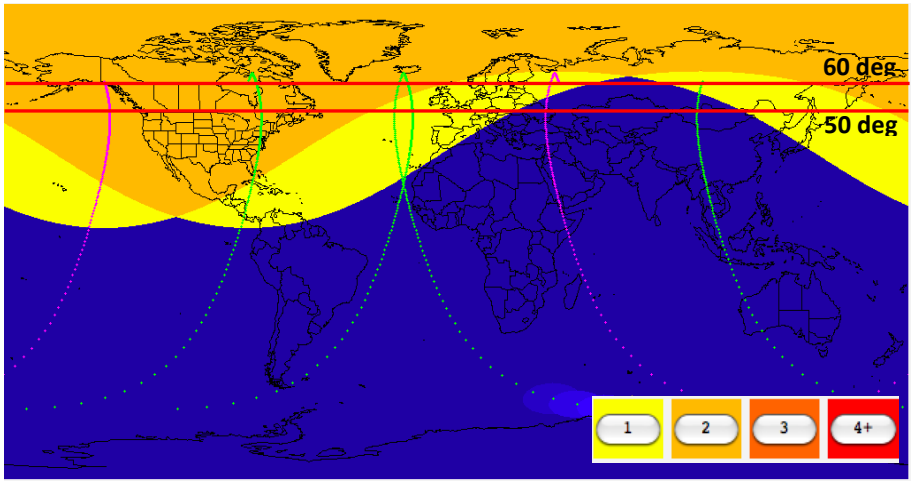

Figure 5-9 - Coverage from three s/c on single plane of 12 h Molniya orbit at 12 hours around orbit (regions showing coverage from one s/c are not necessarily from the same s/c)

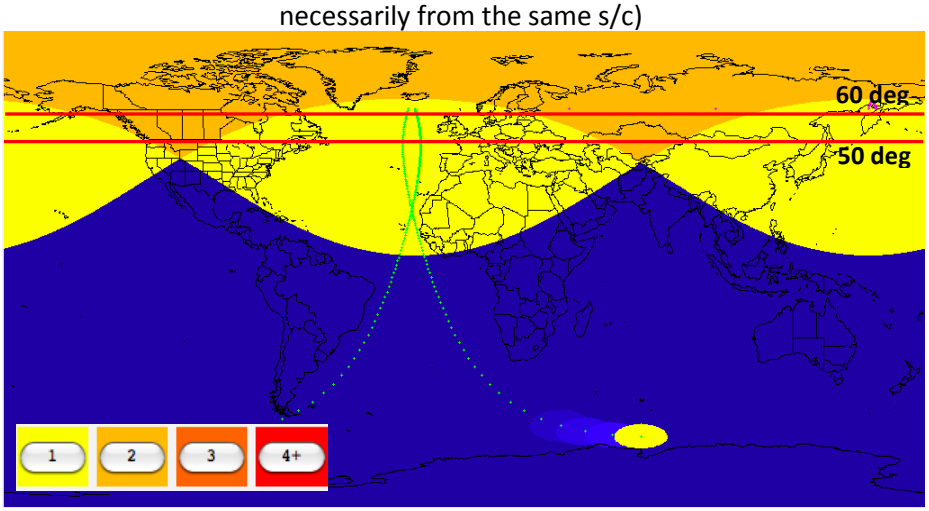

Figure 5-10 - Coverage from three s/c on three orbit planes of 12 h Molniya orbit at 4 hours around orbit (regions showing coverage from one s/c are not necessarily from the same s/c)

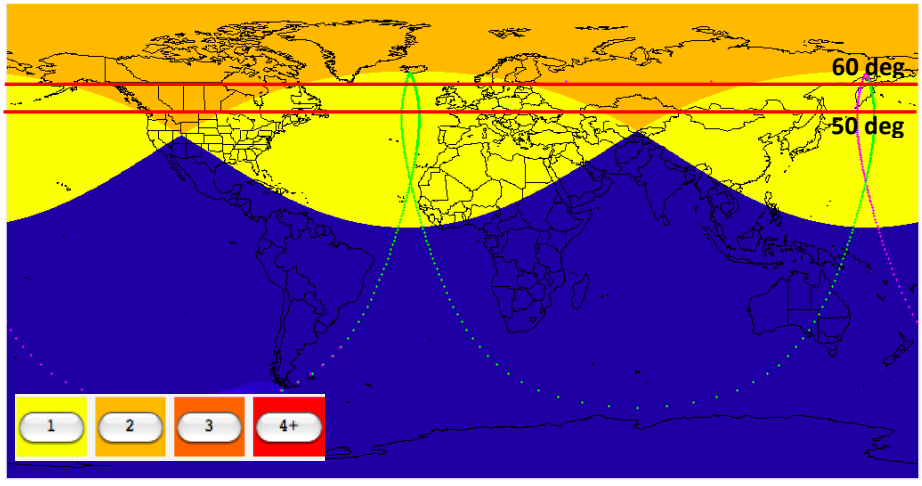

Figure 5-11 - Coverage from three s/c on three orbit planes of 12 h Molniya orbit at 8 hours around orbit (regions showing coverage from one s/c are not necessarily from the same s/c)

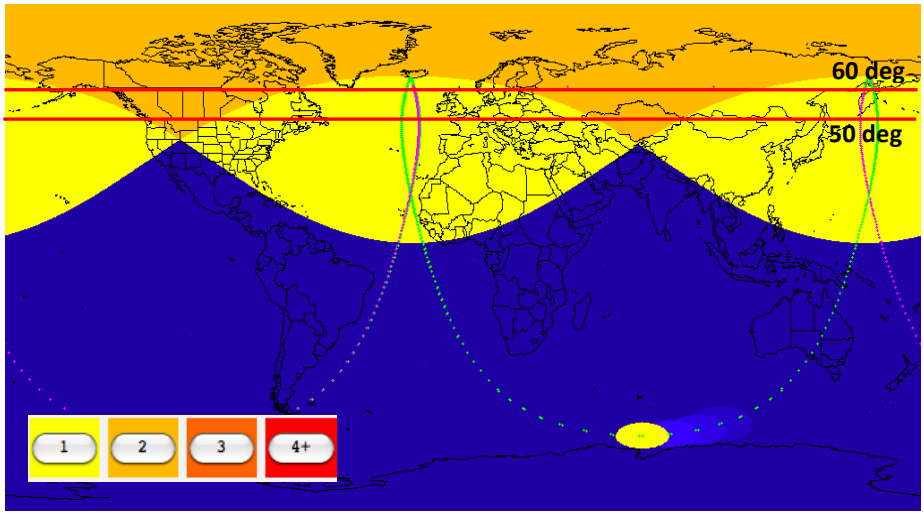

Figure 5-12 - Coverage from three s/c on three orbit planes of 12 h Molniya orbit at 12 hours around orbit (regions showing coverage from one s/c are not necessarily from the same s/c)

Therefore, despite the merits of the Molniya orbit for EO, the problem of viewing frigid and neighbouring temperate regions is not fully resolved as no single platform can provide sufficiently hemispheric observations. This highlights the importance of new high-latitude observation systems such as platforms on *90 degree* inclination Taranis orbits.

5.4.1 Observation to 55 degrees latitude

Within the valid regions shown in Figure 5-3, combinations of perigee and apogee altitudes are possible to give orbits of varying period. Visibility analysis is then conducted to determine the number of spacecraft required to give continuous observation of the region above *55 degrees* latitude using the OZAs, which allow observation to the same quality as that produced by geostationary systems. This is shown in Figure 5-13.

Figure 5-14 illustrates the output from the numerical analysis in MatLab, which is used to determine the number of spacecraft required in a constellation to provide continuous observation, the selected example shows four platforms on a single orbit plane equally spaced around a 16 h, *90 degree* Taranis orbit with perigee altitude of *41,740 km*. Figure

5-14 is created by outputting a value of *1* where the elevation of the spacecraft is above the minimum value specified for all ground stations spaced around *55 degrees* latitude, thus when at least one spacecraft is in view of all ground stations visibility is said to be continuous. Four spacecraft on a 16 h conventional Molniya orbit i.e. *63.43 degree* inclination are shown in Figure 5-15, to further illustrate that no single platform can observe to *55 degrees* latitude with the required OZA.

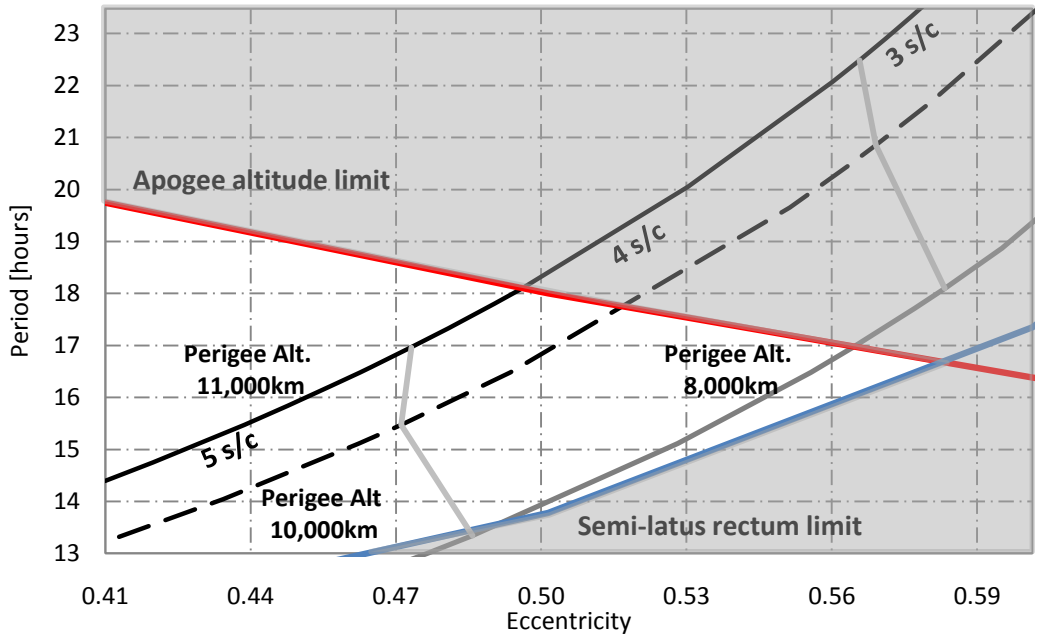

Figure 5-13 Observation to *55 degrees*, showing apogee altitude limit, semi-latus rectum limit and required number of spacecraft (s/c)

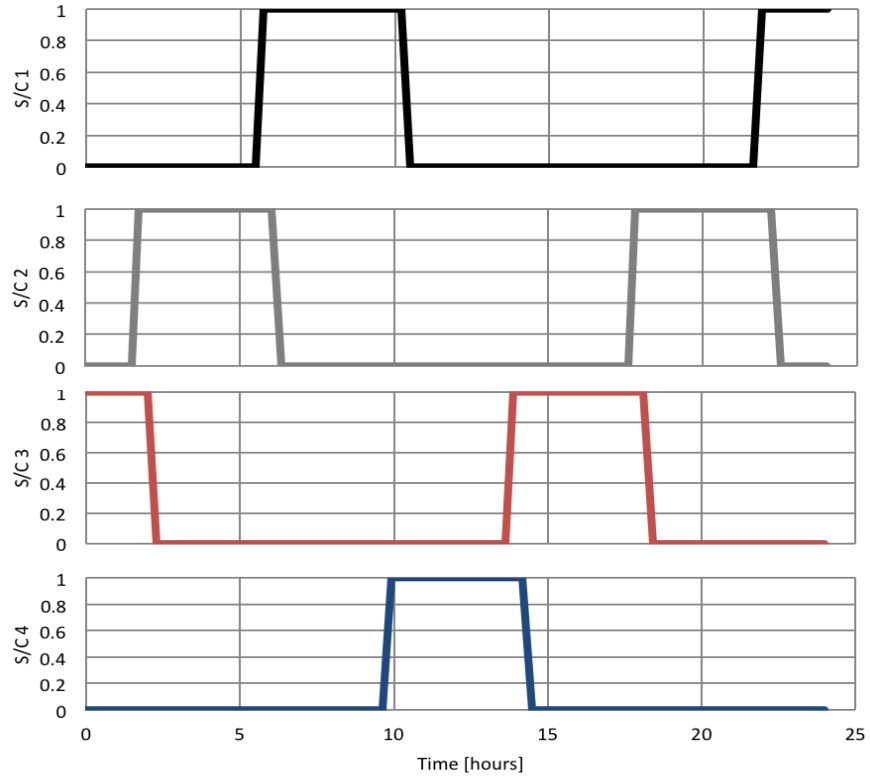

Figure 5-14 – 4 spacecraft Taranis constellation visibility – 16 h orbit

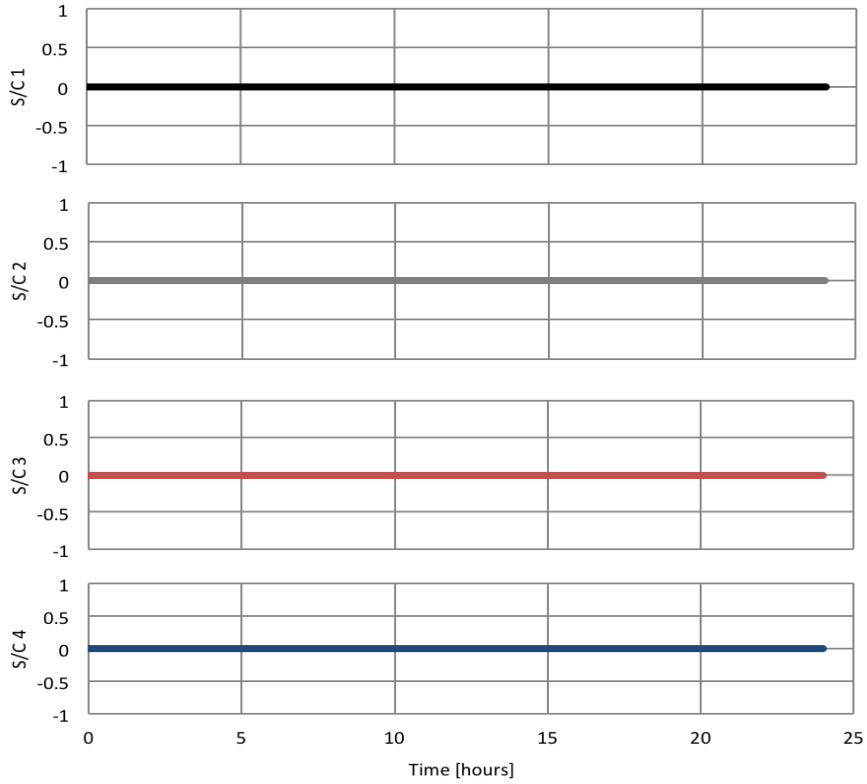

Figure 5-15 - 4 spacecraft Molniya constellation visibility - 16 h orbit

The most beneficial orbit in terms of the number of spacecraft, from Figure 5-13, occurs at the point closest to the intersection of the apogee altitude and semi-latus rectum limit lines. At this point, the orbit period is shown to be around 16.6 hours. However, in order to provide an integer number of revolutions in an integer number of sidereal days such that the ground-track will repeat in a relatively short time, the orbit period is reduced to 16 hours. This gives a repeat ground-track in two days.

The most suitable perigee altitude for the 16 h orbit is then selected to minimise both the number of required spacecraft and the radiation dose from high-energy protons. As the perigee altitude increases, the radiation from high-energy protons decreases. This is illustrated in Figure 5-16, where it is shown that the total proton flux for the 16 h orbit with a perigee altitude of *8,000 km* is almost completely absorbed after approximately *7 mm* of aluminium shielding; this is compared with only *2 mm* for a perigee altitude of *10,000 km.* However, as perigee altitude increases, apogee altitude decreases, thus eccentricity and the time above high-latitude regions decreases, therefore these orbits may require a greater number of spacecraft to provide continuous observation. The orbit parameters for the 16 h Taranis orbits and the required number of spacecraft in the constellation are given in Table 5-1. This table also gives the total magnitude of acceleration required by the EP system to alter the critical inclination to *90 degrees* for the given orbital parameters. The method for determining the total required acceleration has been previously derived in **Chapter 3**.

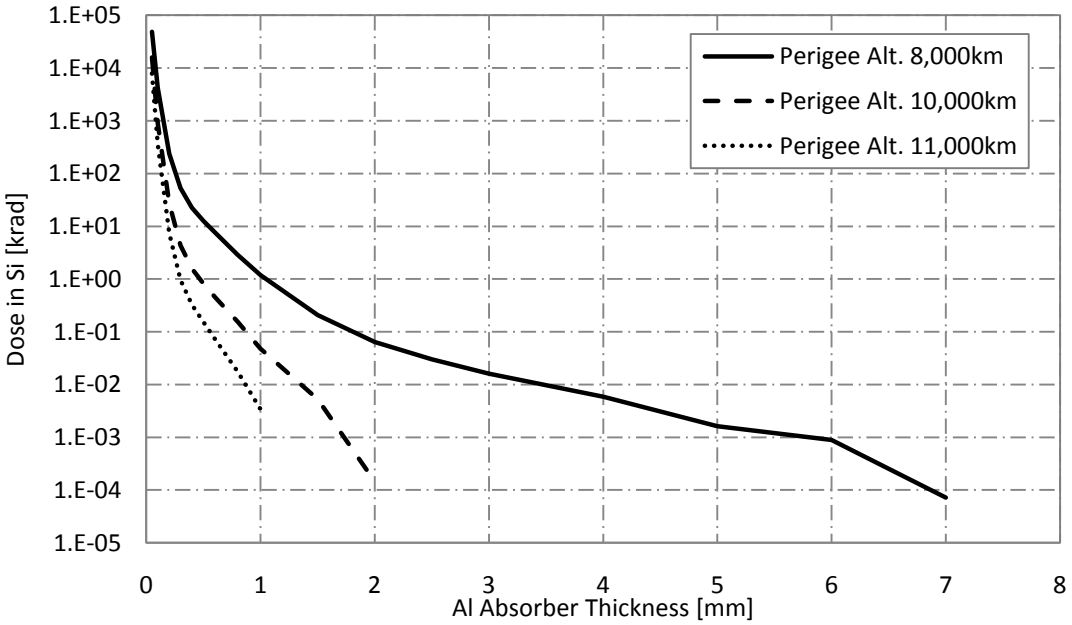

Figure 5-16 Comparison of trapped proton dose for 16 h Taranis orbits of varying perigee altitudes found using SPENVIS

Table 5-1 Comparison of 16 h Taranis orbits of varying perigee altitudes

	Perigee Altitude 8,000 km	**Perigee Altitude 10,000 km**	**Perigee Altitude 11,000 km**
Apogee Altitude	43,740 km	41,740 km	40,740 km
Eccentricity	0.5543	0.4922	0.4612
Required Acceleration	11.3 µm/s^2	8.34 µm/s^2	6.97 µm/s^2
No. Spacecraft	4	4	5

Table 5-1 shows that four spacecraft are required to give continuous observation for perigee altitudes between *8,000* and *10,000 km*. Since the radiation from high-energy protons decreases with increasing perigee altitude, a perigee altitude of *10,000 km* is more beneficial. Although increasing the perigee altitude to *11,000 km* further reduces the radiation dose, the number of spacecraft required in the constellation is seen to increase

from four to five. For this reason, a 16 h Taranis orbit with perigee altitude of *10,000 km* and apogee altitude of *41,740 km* is selected as the most beneficial for high latitude observation when taking into consideration both the radiation dose and apogee altitude constraints.

It is shown in Figure 5-13 that when taking the radiation dose into consideration, a minimum of four spacecraft are necessary to provide continuous observation to *55 degrees* latitude. An investigation is therefore conducted to determine to what extent the perigee altitude needs to be lowered to provide continuous observation to *55 degrees* latitude using only three spacecraft. Although lowering the perigee of the orbit will increase the radiation dose from high-energy protons, it is anticipated that it may be more cost efficient to employ additional radiation shielding if the number of spacecraft can be reduced. Furthermore, launching to a perigee altitude of *10,000 km* is expected to be both difficult and costly.

Visibility analysis is once again conducted to *55 degrees*, simply placing a restriction on the maximum apogee altitude of the orbit to determine the number of spacecraft required in this case. Visibility analysis showing orbits with constant perigee altitudes of *300*, *1,000* and *2,000 km* are shown in Figure 5-17. Disregarding the radiation constraints, it is found that the minimum number of spacecraft required for continuous observation to *55 degrees* can be reduced to three. This holds true for minimum apogee altitudes of *28,000*, *30,000* and *33,000 km* for each of the *300*, *1,000* and *2,000 km* perigee altitudes respectively, below which the number of required spacecraft increases to four. The maximum perigee altitude that can allow continuous observation maintaining the use of three spacecraft is *7,500 km* with an apogee altitude on the *45,000 km* limit. The corresponding figure output from the visibility analysis to determine the number of spacecraft required for continuous

observation is shown in Figure 5-18. This shows three equally spaced platforms on a single orbit plane on a 12 h Taranis orbit orbit with a perigee altitude of *300 km*, it is clear that three spacecraft can provide continuous observation to *55 degrees* latitude. Once again the same analysis is conducted for a Molniya orbit with an inclination of *63.43 degrees*, where it is shown in Figure 5-19 that no single platform can observe to *55 degrees* using the required OZA.

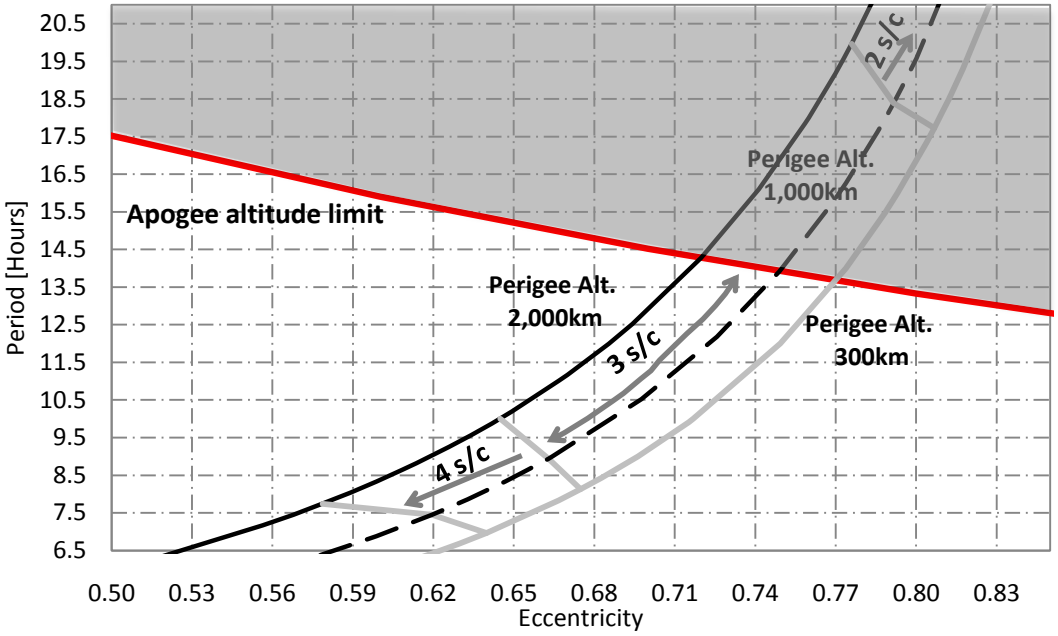

Figure 5-17 Observation to *55 degrees*, showing apogee altitude limit and required number of spacecraft (s/c)

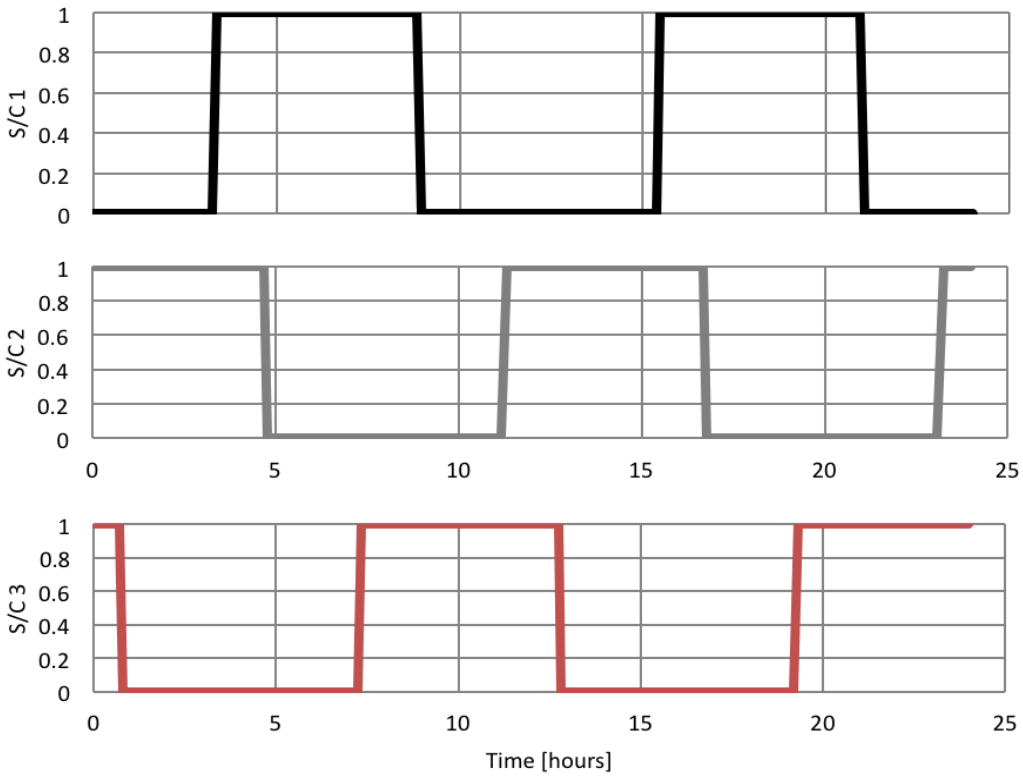

Figure 5-18 - 3 spacecraft Taranis constellation visibility - 12 h orbit

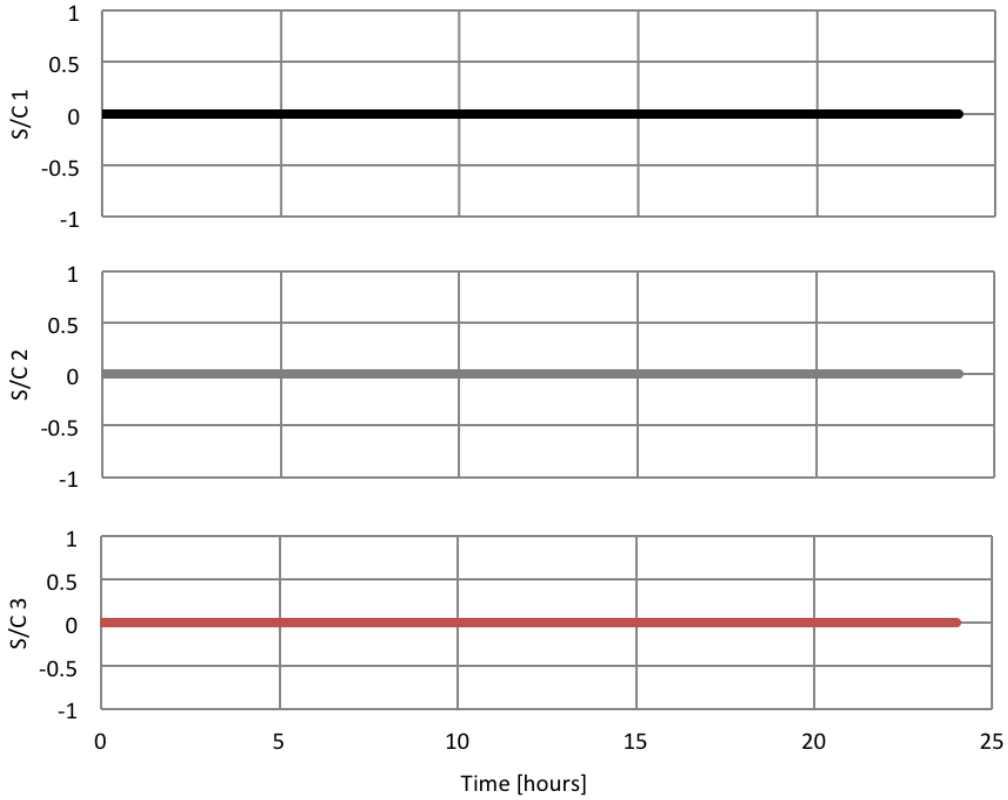

Figure 5-19 – 3 spacecraft Molniya constellation visibility – 12 h orbit

In a similar manner to the 16 h 'low-radiation' orbit, consideration must be given to the selection of orbit period and subsequently the perigee altitude. In the region where three spacecraft are required in Figure 5-17, orbit periods of 12 and 9 hours are of interest as these allow repeat ground-tracks within one and three days respectively, and therefore simplified spacecraft operations.

5.4.1.1 12 hour orbits

In order to comply with debris mitigation guidelines, at EoL the spacecraft can either be re-orbited to an orbit with perigee altitude *> 2,000 km*, or de-orbited to an orbit where perigee altitude is *≤ 300 km* and where it will naturally degrade due to atmospheric drag and re-enter the Earth's atmosphere within 25 years. It is clear that a spacecraft in an initial orbit with perigee altitude below *300 km* or above *2,000 km* will not require a manoeuvre at EoL. If, however, the perigee altitude is within this range, comparison must be made between the amount of propellant required to de-orbit or re-orbit the spacecraft at EoL versus the propellant required to maintain an orbit throughout its life at *300 km* perigee altitude due to the degrading effects of atmospheric drag.

If a perigee altitude of *2,000 km* is selected, such that a re-orbit manoeuvre is avoided, the corresponding apogee altitude, for a 12 h orbit, is *38,500 km*. If at EoL the spacecraft is simply decommissioned in this orbit and all systems are powered down, the orbit will drift as the continuous low-thrust previously preventing this is turned off, and over long periods of time may intersect the GEO ring, thus violating debris mitigation guidelines. This therefore drives the orbit selection towards an orbit with a lower perigee altitude.

Generally, spacecraft on orbits with perigee altitudes below *1,000 km* are susceptible to the degrading effects of atmospheric drag and therefore require propellant to maintain the

orbit throughout its lifetime. However, spacecraft on 12 h orbits with perigee altitudes higher than approximately *300 km* will require an EoL de-orbit manoeuvre to reduce the perigee altitude to this value to allow it to re-enter the Earth's atmosphere within 25 years, this was validated through numerical simulation. An investigation is therefore conducted to compare the propellant required to transfer the perigee altitude from *1,000* to *300 km* versus the propellant necessary to maintain an orbit at *300 km* perigee to mitigate the effects of atmospheric drag. This is achieved by comparing the orbit manoeuvre size from numerical analysis, by considering the Δv required in each case, where Δv is a measure of the amount of propellant used to change from one trajectory to another, with units m/s.

Firstly considering the Δv required to maintain an orbit with perigee altitude at *300 km* and apogee altitude of *40,170 km* (12 h orbit) due to the effects of atmospheric drag. Eq. (5.6) is implemented in the numerical analysis to determine the average acceleration due to atmospheric drag over one year, using a spacecraft mass of *1000 kg*, drag coefficient of *2* and area of $6\ m^2$ which is based on the solar array size for this particular orbit. Eq. (4.21) is then used to determine the Δv to maintain the orbit due to the atmospheric drag effects, which was found to equal *17 m/s* per year.

This value of Δv can then be compared with that required to transfer the spacecraft from a perigee altitude of *1,000* to *300 km*, determined using Eq. (4.21), where the acceleration in this case is specified as $0.076\ mm/s^2$ i.e. the acceleration required to maintain zero change in argument of perigee of the Taranis orbit with a perigee altitude of *1,000 km* and apogee altitude of *39,479 km*. The radius of pericentre locally optimal control law (Eq. (5.9)) derived from the radius of pericentre variational equation, in terms of classical orbital elements, is then used to maximise the instantaneous rate of change of the radius of pericentre, giving the transfer time which results in a Δv of *94 m/s.* It is therefore shown to be more

beneficial in terms of propellant requirements to maintain the orbit with a perigee altitude of *300 km* and apogee altitude of *40,170 km* for mission lifetimes less than 5 and a half years.

$$\frac{dr_p}{d\theta} = \begin{bmatrix} R & T & N \end{bmatrix} \lambda_{r_p} \tag{5.8}$$

where

$$\lambda_{r_p} = \begin{bmatrix} \dfrac{2ae(1-e)\sin(\theta)}{p} - \sin(\theta) \\ \dfrac{2a(1-e)(1+e\cos(\theta))}{p} - (\cos(\theta) + \cos(E)) \\ 0 \end{bmatrix} \tag{5.9}$$

5.4.1.2 9 hour orbits

It is shown from Figure 5-17 that to enable a Taranis constellation using a 9 h orbit while maintaining the use of three spacecraft, the perigee altitude is limited to *1,000 km*. For a 9 h orbit, perigee altitudes below around *200 km* will ensure the spacecraft naturally re-enters the Earth's atmosphere within 25 years, this was again simulated using a numerical simulation implementing the U.S. Standard 1976 atmosphere model, as introduced in **Section 5.3**. Note that the reduction in perigee altitude to allow re-entry within 25 years is due to the shorter time period the spacecraft spends in the region where atmospheric drag has an effect when the orbit period is reduced. Comparison is again made between the propellant requirements to maintain an orbit with a perigee altitude of *200 km* due to the effects of atmospheric drag and to transfer the spacecraft at EoL from a perigee altitude of *1,000* to *200 km*.

The Δv required to maintain a 9 h orbit with perigee and apogee altitudes of *200* and *31,000 km* respectively due to the effects of atmospheric drag is calculated again using the numerical analysis. The spacecraft is assigned a mass of *1000 kg*, drag coefficient of *2* and area of *8* m^2 which is again based on the solar array area, to find the average atmospheric drag acceleration over one year. Eq. (4.21) is once again used to calculate a required Δv of *158 m/s* per year to maintain the perigee altitude at *200 km* for the 9 h orbit.

This is once again compared with the Δv required to transfer from a perigee altitude of *1,000* to *200 km*, to allow the spacecraft to re-enter the atmosphere within 25 years, calculated using Eq. (4.21). For this Taranis orbit an acceleration of *0.1* mm/s^2 is required to maintain the zero change in argument of perigee condition and so this value is therefore used for the pericentre altitude transfer at EoL. The pericentre altitude locally optimal control law in Eq. (5.9) is again used to determine the transfer time producing a Δv of *154 m/s.* The significant amount of propellant required to maintain a 9 h orbit with a perigee altitude of *200 km* due to the significant increase in atmospheric drag effects means it is more cost efficient to perform an EoL manoeuvre to transfer the perigee altitude.

Comparing the propellant requirements with those of the 12 h orbit reveals that considerably more propellant is required to achieve a 9 h Taranis orbit, and so a 12 h orbit with perigee altitude of *300 km* is considered herein.

5.4.1.3 Spacecraft Environment

Comparison between the trapped proton dose for a conventional Molniya orbit, the 16 h 'low-radiation' Taranis orbit with perigee altitude of *10,000 km* and the 12 h 'high-radiation' Taranis orbit with perigee altitude of *300 km* are shown in Figure 5-20.

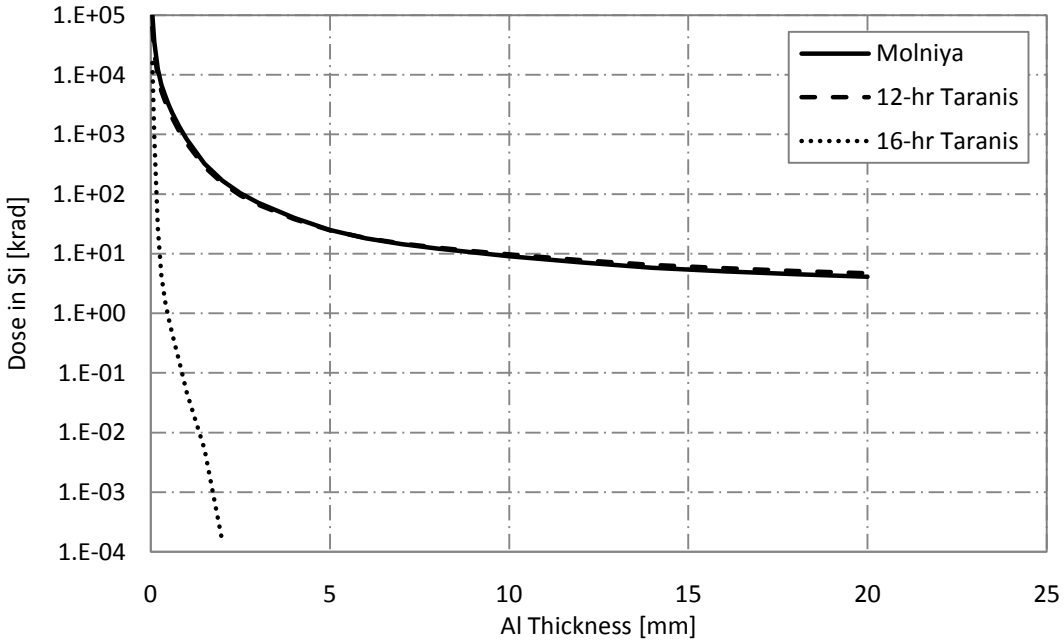

Figure 5-20 Trapped proton dose for Molniya orbit, and 12 h and 16 h Taranis orbits found using SPENVIS

It can be seen that the proton dose from the 16 h Taranis orbit is significantly lower than both the Molniya orbit and the 12 h Taranis orbit. It is shown that the 12 h Taranis orbit receives a radiation dose from high-energy protons comparable to the conventional Molniya orbit. However, a comparison is then made between the total ionising dose for each of these orbits and a GEO in Figure 5-21, where the notional radiation limits for commercial off the shelf (COT), space qualified, and radiation hardened components are also shown. It can be seen that for typical aluminium absorber thicknesses, between *2* and *4 mm* [3], COT components cannot be used for either the 12 or 16 h Taranis orbit platforms. However, the values of radiation are below those requiring radiation hard materials. The radiation environments of spacecraft on each of the Taranis orbits are shown to be similar to that experienced by a spacecraft in GEO, with the exception of a higher trapped proton dose for the low perigee altitude HEOs. The additional cost required to launch to the 16 h,

lower radiation orbit and the extra spacecraft required is expected to be significantly more than employing additional shielding and launching to a substantially lower perigee altitude.

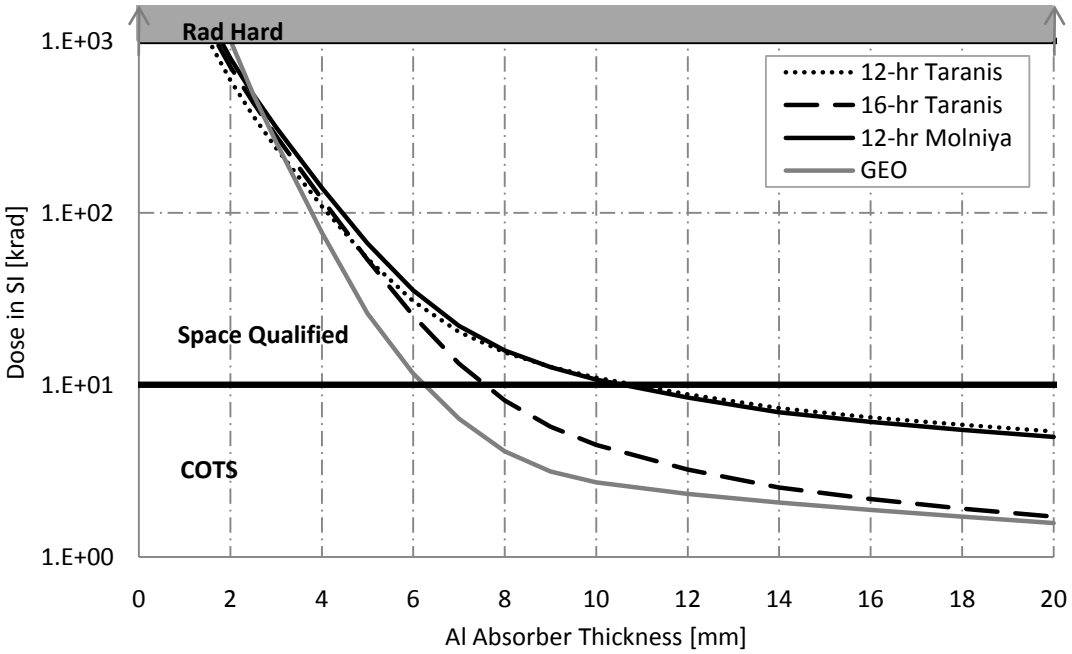

Figure 5-21 Total ionising dose for various orbits with mission durations of 5 years, showing notional radiation limits found using SPENVIS

5.4.2 Observation to 50 degrees latitude

The previous analysis details the minimum requirements to complete the GOS as observations from GEO begin to degrade at around *55 degrees* latitude. However, it may be beneficial to provide a more significant overlap in sensing from GEO. Thus, the analysis is repeated to identify the Taranis constellation capable of providing continuous observation to *50 degrees* latitude and equal quality sensing to that produced by GEO.

Considering radiation and apogee altitude constraints, the number of spacecraft required to give continuous observation is shown in Figure 5-22 for orbits with constant perigee altitudes of *8,000* and *10,000 km*. Figure 5-22 shows that the number of spacecraft increases significantly in this case. For example, a 16 h orbit requires a minimum of seven

spacecraft. Considering the 16 h orbit with a perigee altitude of *10,000 km* previously identified from Figure 5-22 requires eight spacecraft to continuously observe one polar region and thus sixteen spacecraft to complete the GOS.

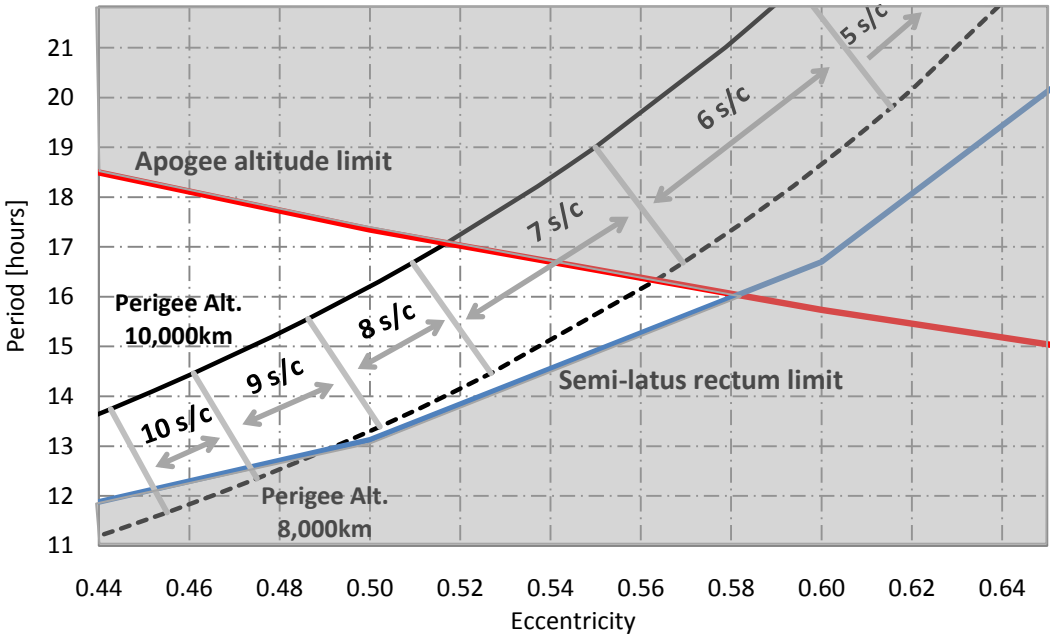

Figure 5-22 Observation to *50 degrees*, showing apogee-altitude limit, semi-latus rectum limit and required number of spacecraft

Once again, the radiation constraint is neglected in order to determine the reduction in the required number of spacecraft. The results of the visibility analysis showing only the maximum apogee altitude limit are given in Figure 5-23. It is shown that a minimum of four spacecraft are required for continuous observation to *50 degrees* using an orbit with 13.5 h period and perigee altitude of *300 km*.

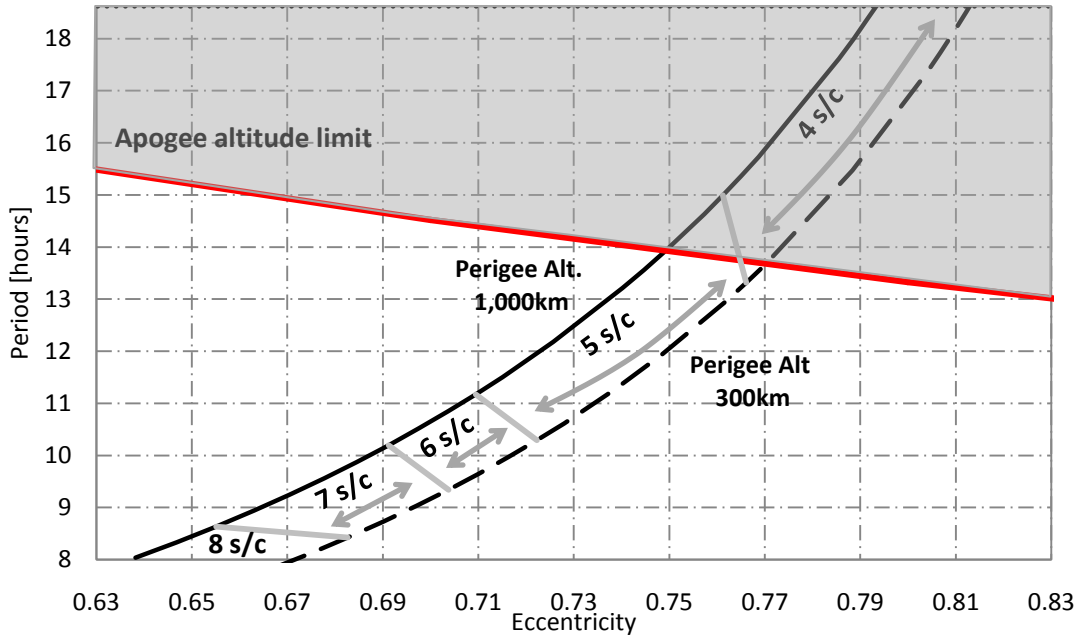

Figure 5-23 Observation to *50 degrees*, showing apogee-altitude limit and required number of spacecraft

In order to allow a repeat ground-track and so simplify spacecraft operations, orbit periods of 9 or 12 hours are desirable. From Figure 5-23 it is clear that to enable a 9 h orbit, seven spacecraft are required to allow continuous remote sensing. This clearly discounts a 9 h orbit for observation to *50 degrees* latitude. A 12 h orbit with a perigee altitude of *300 km* is again expected to be the most beneficial, depending on the mission lifetime, as the propellant requirements to maintain this orbit due to atmospheric drag are less than those required to transfer the perigee altitude to an orbit which will re-enter within 25 years.

A constellation of five spacecraft can therefore provide the desired level of coverage, giving a reduction of three spacecraft if additional radiation shielding is employed on the spacecraft. Once again this is expected to be more cost efficient than launching three additional spacecraft to a considerably higher perigee altitude.

5.5 Orbit Visualisation

In order to illustrate the view as seen by the spacecraft at apogee on a 12 h, *90 degree* inclination Taranis orbit, the images are shown in Figure 5-24 were generated using the Celestia software package.

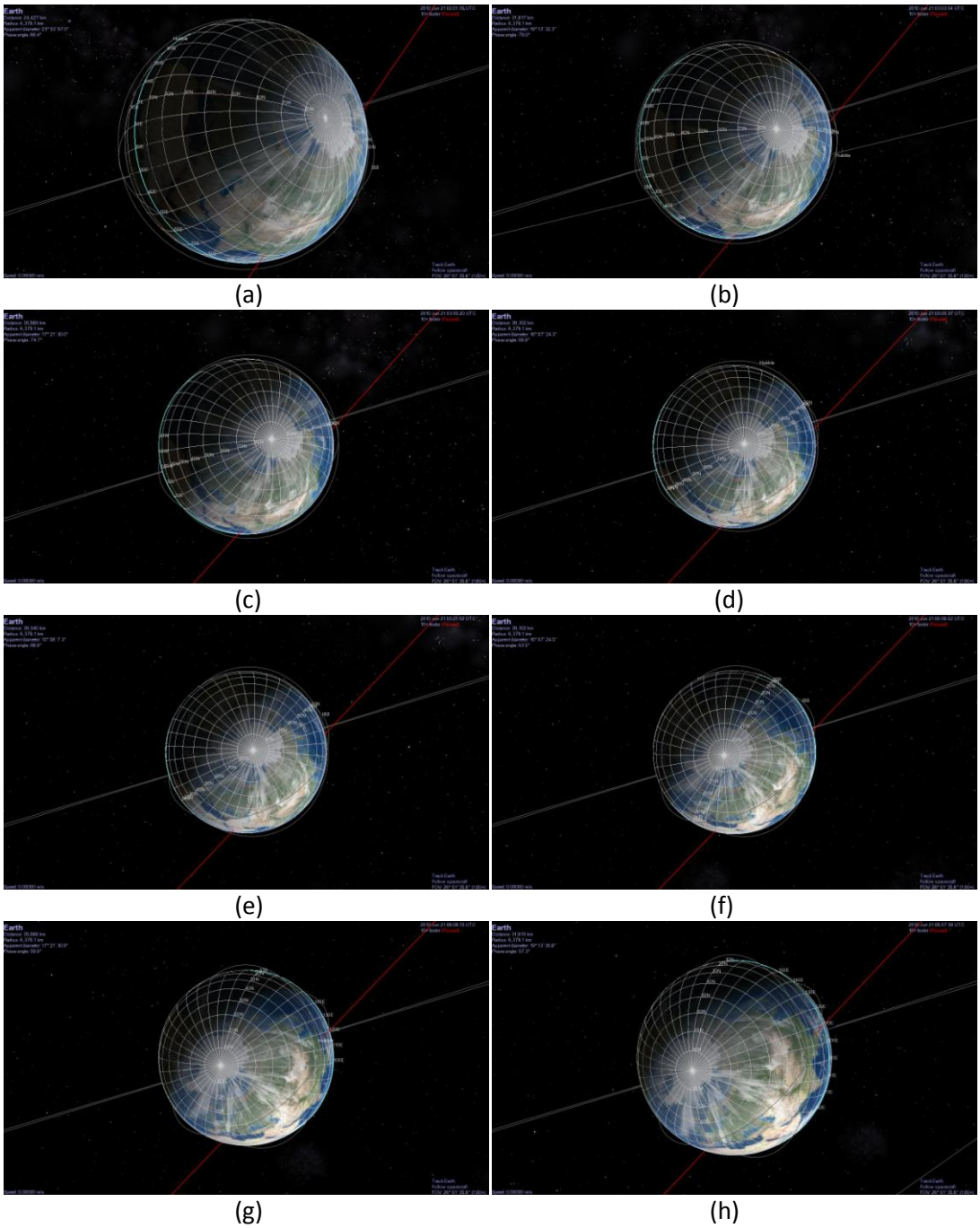

(a) (b)

(c) (d)

(e) (f)

(g) (h)

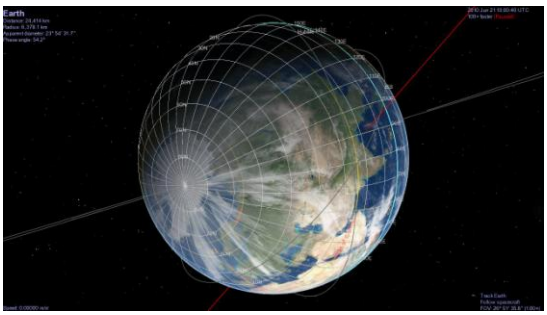

(i)

Figure 5-24 Images of Northern hemisphere as seen from a Taranis spacecraft from (a) Apogee – 4 h (b) Apogee – 3 h (c) Apogee – 2 h (d) Apogee – 1 h (e) Apogee (f) Apogee + 1 h (g) Apogee + 2 h (h) Apogee + 3 h (i) Apogee + 4 h

Figure 5-24 shows the rotation of the Earth below a Taranis spacecraft on a 12 h orbit $\pm$ 4 hours from apogee. It is clear that near apogee very little rotation of the Earth is observed, allowing an almost geostationary view of the high-latitude regions which can offer significant benefits for remote sensing of these regions.

5.6 Validation of Results

As stated in **Section 5.4**, visibility analysis of spacecraft on Taranis orbits is conducted using the same numerical technique described in **Section 5.4** to determine the time spacecraft can view ground stations located at *10 degree* longitude intervals at particular latitudes, using the required maximum OZAs. NOVA Satellite Tracking Software is considered to validate these numerical results.

Nova Satellite Tracking Software is available from Northern Lights Software Associates (NLSA) and is used by industry and the US Air Force[9]. It provides real-time satellite tracking information for all artificial satellites and gives accurate, clear positioning of spacecraft.

[9] http://www.nlsa.com/index.html Accessed on 14th January 2013

5.6.1 NOVA Satellite Tracking Software

An existing spacecraft on a conventional Molniya orbit, Molniya 3-47, with orbital parameters given in Table 5-2, was selected for comparison with the numerical method described earlier in **Chapter 5**.

Table 5-2 Orbital parameters for the Molniya 3-47 spacecraft, from NOVA software

Orbital Element	Value
Semi-Major Axis	2.66×10^4 (km)
Eccentricity	0.7426
Inclination	63.15 (degrees)
Right Ascension of Ascending Node	350 (degrees)
Argument of Perigee	254 (degrees)

The ground station used for communication with the Molniya spacecraft was selected to be Barrow, Alaska with the parameters given in Table 5-3.

Table 5-3 Location parameters for ground station in Barrow, Alaska

Parameter	Value
Latitude	71.33 (degrees)
Longitude	-156 (degrees)
Altitude	13 (m)

NOVA software outputs the time the spacecraft spends above the horizon, in view of a particular ground station. In this case, the Molniya 3-47 spacecraft was in view of the ground station in Barrow, Alaska for 10.1 hours during the first pass of the spacecraft.

5.6.2 Numerical Analysis

The Molniya orbit analysed in **Sections 5.6.1** is considered using the existing numerical model introduced in **Section 5.4**. The orbital parameters are the same as those in Table 5-2 and the spacecraft elevation over time is shown in Figure 5-25.

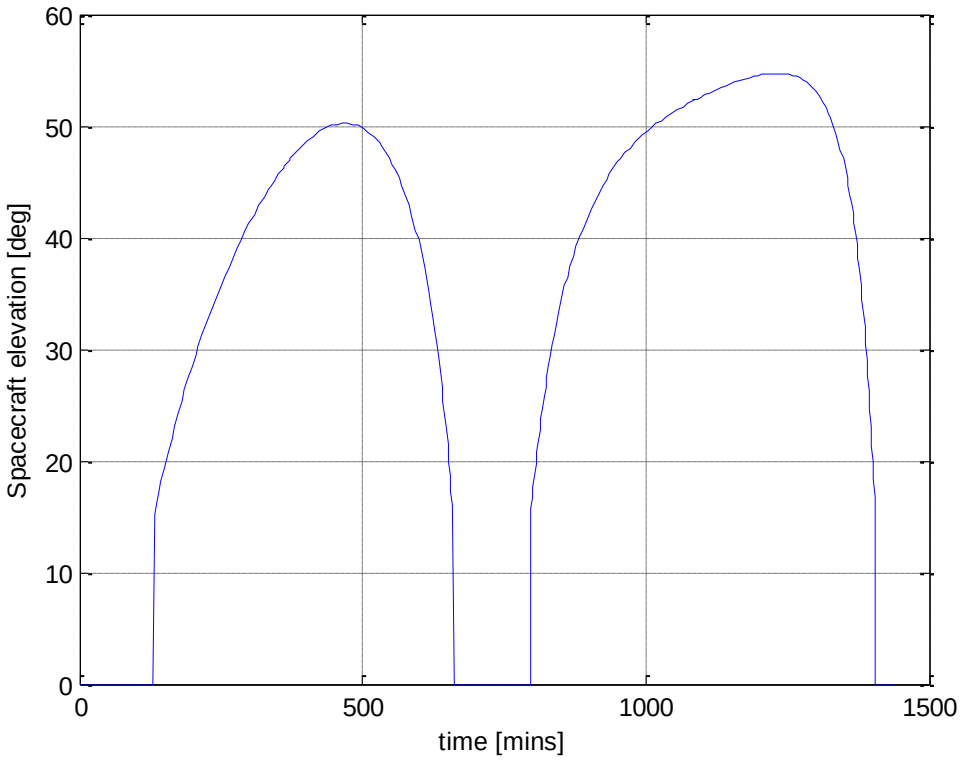

Figure 5-25 Molniya spacecraft elevation over time, from numerical analysis

From Figure 5-25 it is shown that the maximum and minimum time the spacecraft is in view of the ground station at Barrow, Alaska is 10.1 and 8.8 hours respectively. The solution obtained using NOVA satellite tracking software is therefore equal to that of the first pass of the spacecraft shown in Figure 5-25. Thus the numerical analysis used to determine the number of spacecraft required on Taranis orbits to give continuous observation is shown to be valid.

5.7 Summary

This chapter has considered the design of a constellation of spacecraft on highly-elliptical Taranis orbits to provide continuous remote sensing above *55 degrees* latitude as a minimum requirement, due to the degradation of imaging from geostationary systems beyond this point.

Requirements for the constellation have been outlined which include constraints on the maximum apogee altitude of the orbit, the maximum observational zenith angle, the restriction of the use of composite images and the rotation of the argument of perigee of the orbit, in addition to the requirement of the mission to comply with debris mitigation guidelines. Consideration is also given to the radiation environment of the spacecraft, although this is not considered to be a strict requirement.

Following analysis using these requirements the orbit selected for the constellation is a 16 h orbit with a perigee altitude of *10,000 km* and apogee altitude of *41,740 km*, which requires four spacecraft for continuous remote sensing. This is determined by taking into consideration the radiation environment experienced by the spacecraft and so is referred to as the 'low-radiation' orbit. In order to reduce the number of spacecraft, the perigee altitude is lowered and the constraints to minimise the effects from high-energy protons are neglected. In this case, a 12 h orbit with a perigee altitude of *300 km* is selected as the most beneficial; this is known as the 'high-radiation' orbit. Although constraints to minimise the radiation have been neglected in this case, the total ionising dose of both the 16 and 12 h Taranis orbits are found to be comparable to that experienced by geostationary platforms. Launching three spacecraft on the 12 h orbit and employing additional radiation shielding is anticipated to be significantly less costly than launching an additional spacecraft to a considerably higher perigee altitude on a 16 h orbit. Observation to *50 degrees*

latitude is also considered, where constellations require eight spacecraft on a 16 h, 'low-radiation' orbit and five spacecraft neglecting constraints to minimise the radiation on a 12 h orbit.

Validation of the visibility analysis is also conducted using NOVA Satellite Tracking Software. The analysis considered a spacecraft on a conventional Molniya orbit with orbital parameters given from NOVA to determine the time the spacecraft was in view of a ground station located in Barrow, Alaska. Comparison was made between these results and those obtained from a numerical analysis using Matlab, which were shown to be in agreement with those obtained from NOVA. The numerical simulation used to determine the number of spacecraft required in a constellation is therefore shown to be accurate.

Chapter 6

6 Sun-Synchronous Elliptical Orbits

Chapters 3 - 5 have considered the development of novel, highly-elliptical Taranis orbits and the subsequent design of constellations of spacecraft on these orbits to fill the gap in data that occurs at high-latitude regions of the Earth. These newly proposed orbits use continuous acceleration to alter the critical inclination and achieve the zero change in the argument of perigee essential to highly-elliptical orbits. In this chapter similar methods are used to develop novel, highly-elliptical, sun-synchronous orbits. **Section 6.2** presents a general perturbations solution which is then validated using a special perturbations method in **Section 6.3**.

6.1 Introduction

This chapter extends the theory of the highly-elliptical, Taranis orbits introduced in **Chapter 3** to develop sun-synchronous Taranis orbits, using methods detailed in recent research for the extension of sun-synchronous orbits [100]. Within this work, the thrust magnitude required is not defined as a function of the local gravity field but instead by the magnitude of the perturbations within that field, augmenting the Earth oblateness perturbation to modify the sun-synchronous orbit and allow free selection of the orbit inclination and altitude. Previously, in **Chapter 3**, Taranis orbits have been developed using continuous radial and transverse accelerations. Consequently sun-synchronous Taranis orbits are achieved by the addition of a further element of low-thrust, directed out of the orbit plane. This ensures the rate of change of the ascending node of the Taranis orbit matches the

mean rotation of the Sun within an Earth-centred inertial frame. It is likely that sun-synchronous HEOs will offer benefits in terms of simplified instrument design as a result of the predictable thermal environment.

6.2 General Perturbations Solution

To develop sun-synchronous Taranis orbits, two conditions must be satisfied: firstly a sun-synchronous orbit requires that the rate of change of the ascending node matches the motion of the Mean Sun, which at Earth is equal to *2π radians* in *365.25 days*; and secondly, Taranis orbits require that the rate of change of the argument of perigee remain unchanged in order that the position of apogee is not affected by the perturbations caused by the oblate nature of the Earth. The first condition is described by the expression for the rate of change of the ascending node angle given in **Chapter 3** by Eq. (3.37) and the Taranis condition is satisfied using Eq. (3.6). These orbits are again derived using the disturbing force components in the radial, transverse and normal directions with the addition of low-thrust terms, given by Eqs. (3.17) - (3.19).

6.2.1 Ascending Node Angle

A continuous acceleration is firstly added in the out-of-plane direction to ensure that the change in ascending node angle is equal to approximately *1 degree per day* for any orbit under consideration and so maintain the sun-synchronous condition. The expression for the rate of change of ascending node with the application of low-thrust is determined by inserting Eq. (3.19) into Eq. (3.37) to give Eq. (3.38), which is repeated for clarity

$$\frac{d\Omega}{d\theta}=\frac{a^2\left(1-e^2\right)^2\sin\left(\theta+\omega\right)}{\sin\left(i\right)\left(1+e\cos\left(\theta\right)\right)^3}\left(F_n\,\mathrm{sgn}\left[\sin\left(\theta+\omega\right)\right]-\frac{3J_2R_E^2\mu\left(1+e\cos\left(\theta\right)\right)^4\sin\left(2i\right)\sin\left(\theta+\omega\right)}{2a^4\left(1-e^2\right)^4}\right) \tag{3.38}$$

As first noted in **Chapter 3**, the normal low-thrust component switches sign as a function of the argument of latitude; consequently the value assigned to the argument of perigee becomes important. Thus considering the argument of perigee equal to both *0* and *270 degrees* and integrating Eq. (3.38) over one orbital revolution results in two expressions for the change in ascending node angle. These are given by Eq. (3.39) and (3.40) from **Chapter 3**, which are shown again for clarity.

$$\left[\left(\Delta\Omega\right)_0^{2\pi}\right]_{\omega=0} = \frac{4a^2F_n\cos\left(\omega\right)}{\mu\sin\left(i\right)} - \frac{3J_2\pi R_E^2\cos\left(i\right)}{a^2\left(-1+e^2\right)^2} \tag{3.39}$$

$$\begin{aligned}\left[\left(\Delta\Omega\right)_0^{2\pi}\right]_{\omega=\frac{3\pi}{2}} = (&-\frac{a^2F_n}{\sin\left(i\right)\sqrt{-1+e^2}\,\mu}(4\sqrt{-1+e^2}+2e^2\sqrt{-1+e^2}-12e\,\mathrm{Arctanh}\left[\frac{-1+e}{\sqrt{-1+e^2}}\right]\\ &-3e\ln\left[\frac{1-e}{\sqrt{-1+e^2}}\right]+3e\ln\left[\frac{-1+e}{\sqrt{-1+e^2}}\right])\sin\left(\omega\right))+\left(-\frac{3J_2\pi R_E^2\cos\left(i\right)}{a^2\left(-1+e^2\right)^2}\right)\end{aligned} \tag{3.40}$$

Switching the rate of change of ascending node per rotation to per second, Eqs. (3.39) and (3.40) are then given by Eqs. (6.1) and (6.2) respectively

$$\left[\Delta\Omega\right]_{\omega=0} = \frac{1}{2\pi}\sqrt{\frac{\mu}{a^3}}\left(\frac{4a^2F_n\cos\left(\omega\right)}{\mu\sin\left(i\right)} - \frac{3\pi J_2R_E^2\cos\left(i\right)}{a^2\left(-1+e^2\right)^2}\right) \tag{6.1}$$

$$\begin{aligned}\left[\Delta\Omega\right]_{\omega=\frac{3\pi}{2}} = &\frac{1}{2\pi}\sqrt{\frac{\mu}{a^3}}(-\frac{3J_2\pi R_E^2\cos\left(i\right)}{a^2\left(-1+e^2\right)^2}-1/\\ &\left(\sqrt{-1+e^2}\,\mu\right)a^2F_n\csc\left(i\right)(4\sqrt{-1+e^2}+2e^2\sqrt{-1+e^2}-12e\,\mathrm{Arctanh}\left[\frac{-1+e}{\sqrt{-1+e^2}}\right]\\ &-3e\ln\left[\frac{1-e}{\sqrt{-1+e^2}}\right]+3e\ln\left[\frac{-1+e}{\sqrt{-1+e^2}}\right])\sin\left(\omega\right))\end{aligned} \tag{6.2}$$

If no acceleration is applied Eqs. (6.1) and (6.2) simplify to the standard expression for the sun-synchronous orbit

$$i = \cos^{-1}\left[-\frac{2}{3}\frac{\Delta\Omega}{J_2}\frac{a^{7/2}\left(1-e^2\right)^2}{{R_E}^2\sqrt{\mu}} \right] \tag{6.3}$$

6.2.2 Argument of Perigee

These sun-synchronous Taranis orbits are also required to give zero change in the argument of perigee over one orbital revolution. Thus, continuous radial and transverse accelerations are added to maintain this condition and compensate for the applied out-of-plane acceleration. This was first introduced in **Chapter 3**, where Eqs. (3.17) - (3.19) are substituted into Eq. (3.6) to give Eq. (3.20). Again, the change in argument of perigee is found by integrating Eq. (3.20) over one orbital revolution. The total change in argument of perigee is given by Eq. (3.21), shown again for clarity,

$$\left(\Delta\omega\right)_0^{2\pi} = \left(\Delta\omega\right)_{J_2} + \left(\Delta\omega\right)_{F_r} + \left(\Delta\omega\right)_{F_t} + \left(\Delta\omega\right)_{F_n} \tag{3.21}$$

Eq. (3.21) consists of the change in argument of perigee due to J_2 and each of the R, T, and N accelerations previously given by Eqs. (3.22) - (3.25) respectively. Although two solutions exist depending on the value of the argument of perigee, an argument of perigee of *270 degrees* is considered in the remainder of this chapter.

Sun-synchronous Taranis orbits are developed by firstly substituting values of the orbital elements into Eq. (6.2) and solving for the normal acceleration, F_n. This is substituted, along with the orbital element values into Eq. (3.21). This is then solved for the required radial and transverse accelerations required to compensate for the applied out-of-plane acceleration and maintain the zero change in argument of perigee condition. The radial, transverse, normal and corresponding total acceleration magnitude to achieve sun-synchronous Taranis orbits of varying orbital period and inclination are given in Figure 6-1 - Figure 6-4, where the perigee altitude is *813 km*.

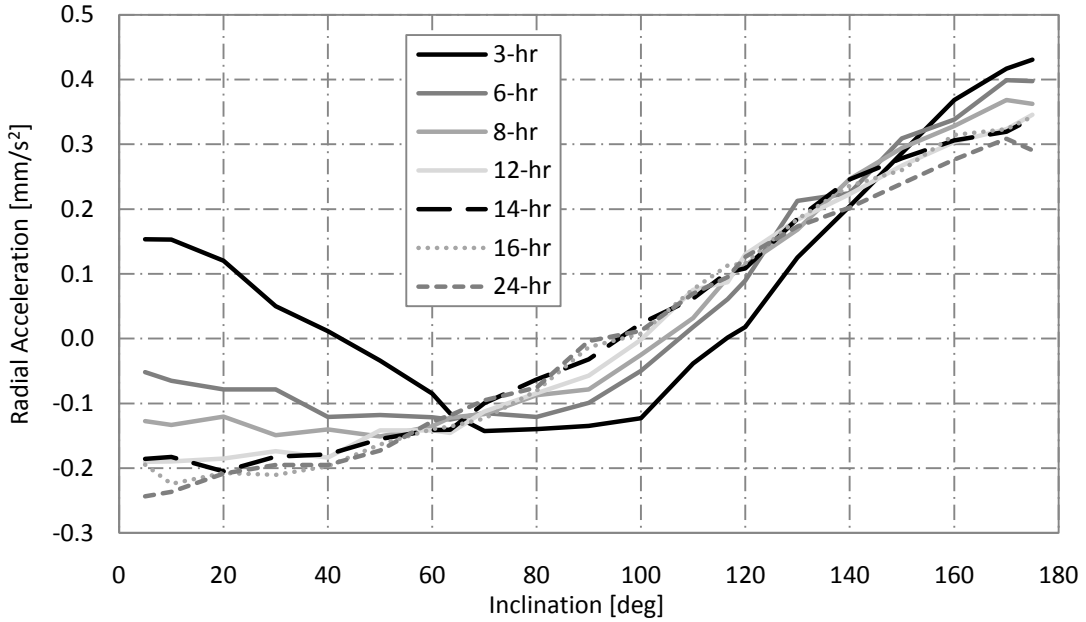

Figure 6-1 Radial acceleration to achieve sun-synchronous Taranis orbits of varying period and inclination

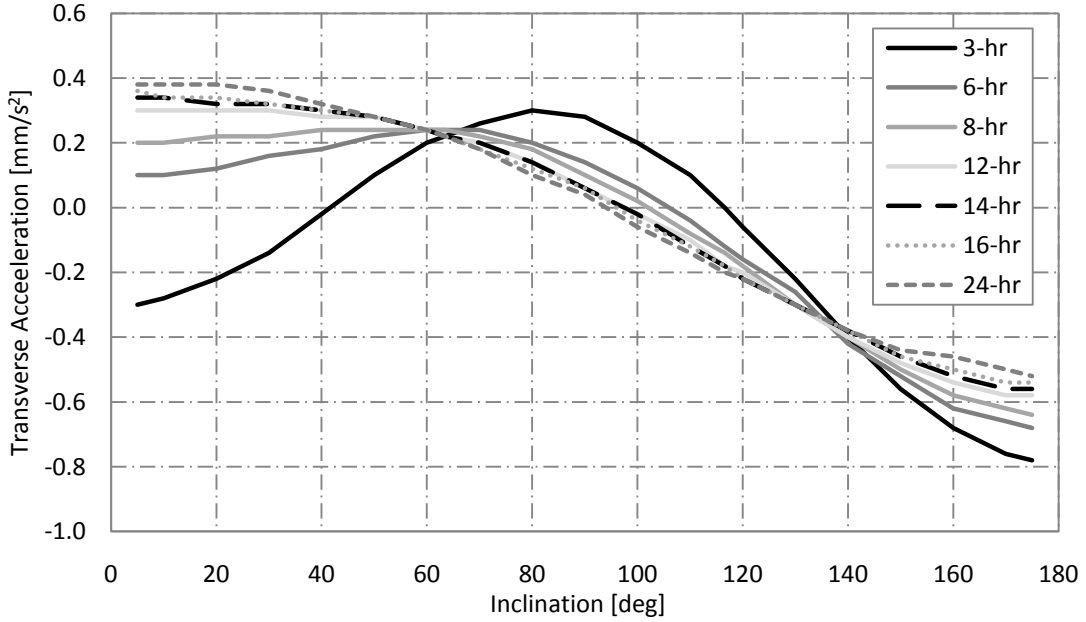

Figure 6-2 Transverse acceleration to achieve sun-synchronous Taranis orbits of varying period and inclination

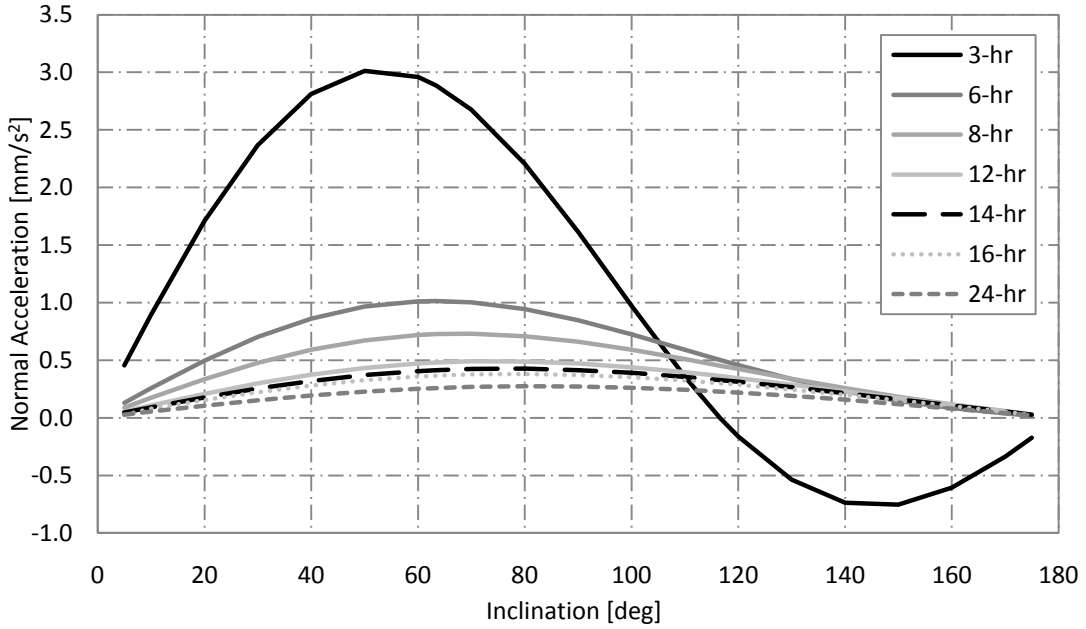

Figure 6-3 Normal acceleration to achieve sun-synchronous Taranis orbits of varying period and inclination

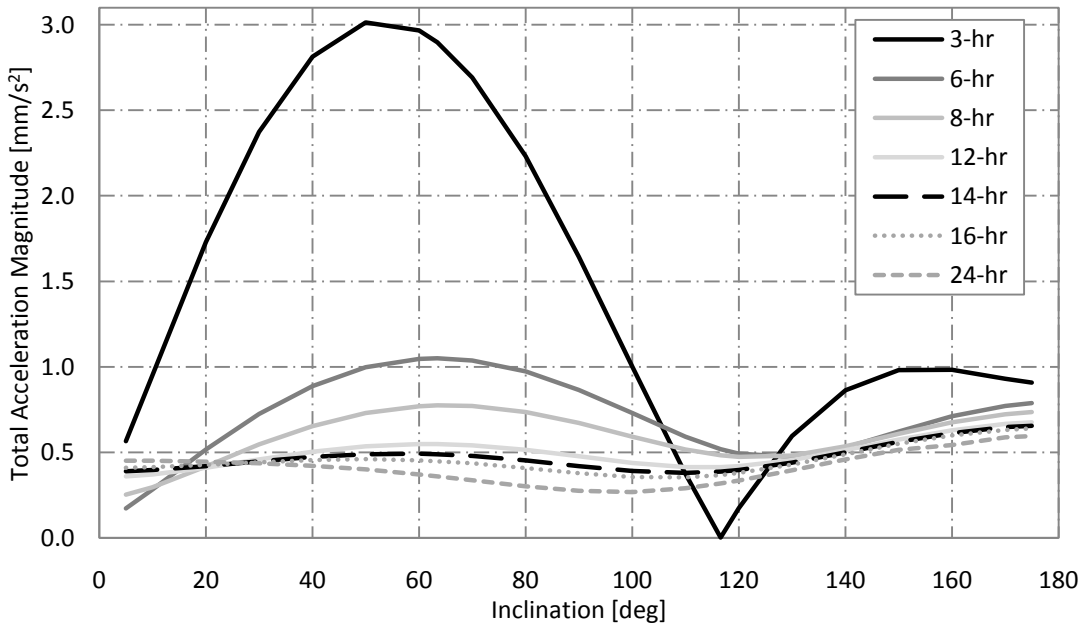

Figure 6-4 Total acceleration magnitude to achieve sun-synchronous Taranis orbits of varying period and inclination

A natural sun-synchronous orbit without the use of any low-thrust propulsion is shown to exist in Figure 6-4. This occurs for a 3 h orbit at the conventional critical inclination of *116.6 degrees*. The other results shown in Figure 6-4 are therefore an extension of this solution, and are only enabled through the use of applied acceleration. As explained in previous chapters, for improved high-latitude observation the most beneficial inclination is *90 degrees*, and the total acceleration magnitude required to enable a 12 h, *90 degree* inclination sun-synchronous Taranis orbit is *0.478 mm/s*^{2}. In this case, the majority of the acceleration is in the normal direction (*0.470 mm/s*^{2}) and for a 1-ton spacecraft a maximum thrust of *478 mN* is required. Although this is higher than the thrust level required to achieve a *90 degree* inclination Taranis orbit without the sun-synchronous condition, shown to require *81 mN* in **Chapter 3**, sun-synchronous Taranis orbit thrust levels are still achievable using current or near-term technology. For example the HiPEP thruster, which as detailed in **Chapter 2** is capable of providing a maximum of *670 mN* [83], whilst the NEXIS can provide a maximum thrust level of *476 mN* [82].

Figure 6-4 also shows that, as with the acceleration magnitude for Taranis orbits in Figure 3-14, as the orbital period increases the acceleration magnitude decreases. To reach an inclination of *90 degrees* a 24 h orbit requires *0.275 mm/s*^{2}, while a 6 h orbit requires *0.865 mm/s*^{2}. Thus, orbits with lower periods are expected to require development in EP technology before they become feasible.

6.2.3 Change in Orbital Elements

As with the previous Taranis orbit solutions, the change in remaining orbital elements is determined to ensure the desired zero secular rate of change of orbital elements is maintained in the presence of continuous low-thrust. This derivation is the same as that presented for the Taranis orbits in **Chapter 3** for the semi-major axis, eccentricity and

inclination in Eqs. (3.28), (3.31) and (3.36) respectively, which show the change in these elements to be zero over the orbit period. Therefore no adverse affect is caused by the application of continuous low-thrust.

6.3 Special Perturbations Solution

To verify the solutions generated using the general perturbations method, a special perturbations solution is generated. This method is the same as that presented in **Section 3.4**, and uses a set of Modified Equinoctial Elements (Eqs. (3.43) - (3.48)) to propagate the position of the spacecraft. The numerical model verifies that the change in semi-major axis, eccentricity, inclination and argument of perigee is negligible over one orbit revolution, and that the change is the ascending node angle is approximately equal to *1 degree per day*. These results are shown in Figure 6-5.

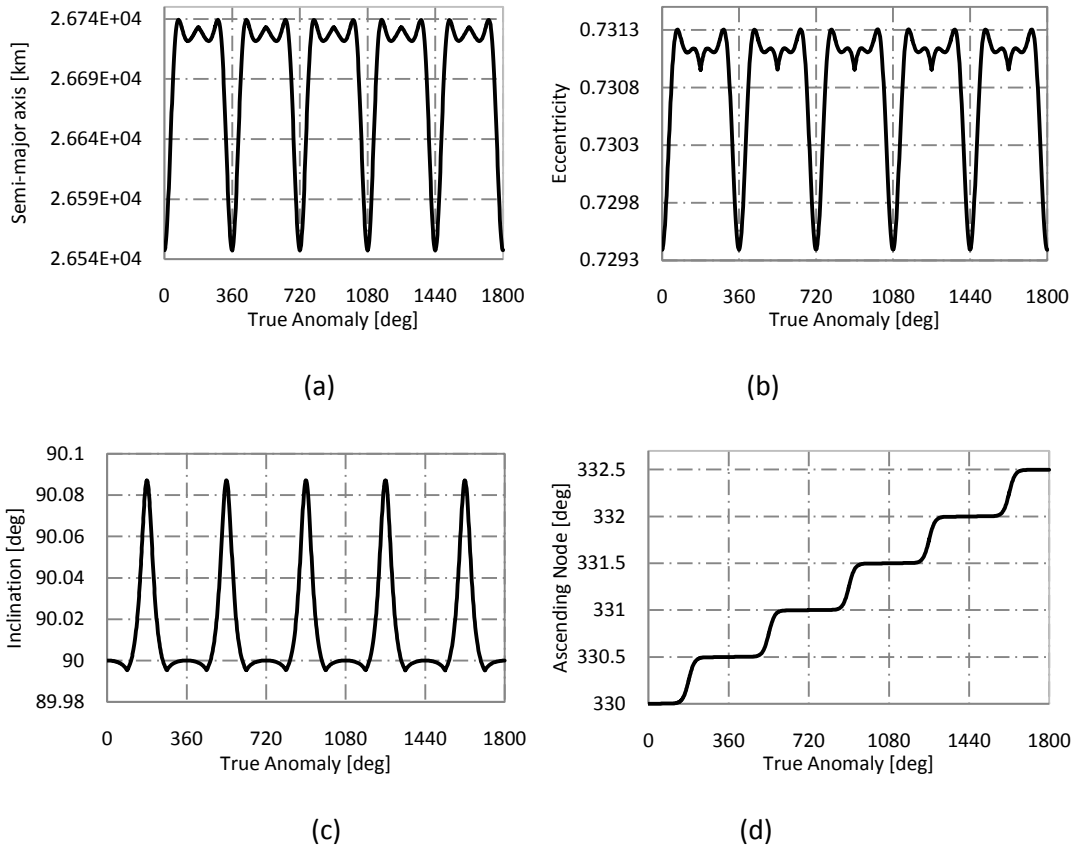

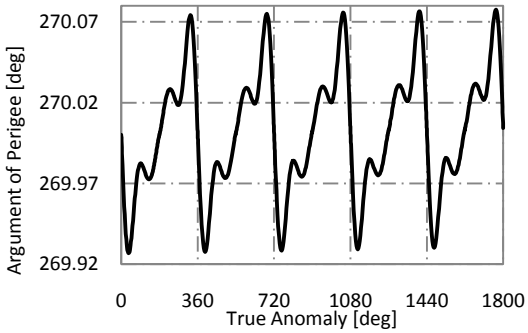

(e)

Figure 6-5 Oscillation of orbital elements over five orbital revolutions of a 12 h, *90 degree* inclination sun-synchronous Taranis orbit (a) Semi-major axis (b) Eccentricity (c) Inclination (d) Ascending node angle (e) Argument of perigee

6.4 Summary

The use of continuous low-thrust propulsion has been shown to enable highly-elliptical sun-synchronous orbits around the Earth, termed sun-synchronous Taranis orbits. These orbits are achieved by using continuous acceleration to alter both the natural critical inclination of highly-elliptical orbits to any inclination, and maintain the sun-synchronous orbit condition. As such, a sun-synchronous Taranis orbit inclined at *90 degrees* can be enabled, allowing both improved high-latitude imaging and simplified instrument design through significant simplification of the thermal environment. To enable a 12 h, *90 degree* inclination orbit a total acceleration of around $0.5\ mm/s^2$ is required. Although this is considerably higher than the acceleration required to enable a *90 degree* Taranis orbit without the sun-synchronous condition ($0.081\ mm/s^2$), it is likely to be achievable using current or near term technology (for example the High Power Electric Propulsion Thruster).

Chapter 7

7 Non – Terrestrial Observation Systems

Chapters 3 - 6 have considered the development of new Earth Observation systems, in particular to fill the gap in data which occurs at the high-latitudes. There has recently however been significant interest in non-terrestrial observation systems, particularly for observation of the Martian environment. This chapter therefore uses the methods introduced in previous chapters to develop novel orbits around Mars, Mercury and Venus, in **Sections 7.2, 7.3** and **7.4** respectively, to significantly enhance the remote sensing opportunities. Each section consists of the extension of highly-elliptical orbits and the development of both circular and elliptical sun-synchronous orbits using general and special perturbations methods.

7.1 Introduction

Planetary observation is vital to gain an insight into the history of the Solar System and in turn the formulation of Earth and can be used to determine whether extra-terrestrial habitable environments exist in the Solar System. Significant benefits can also be gained from the technology innovation as a result of these missions and through development in STEM education.

The Martian environment is of particular interest with recent missions including Mars Odyssey [46], Mars Express [43], MRO [45], and the Curiosity rover [10]. Such missions have allowed a comprehensive view of Mars to be obtained through data of the Martian surface geology, mineral composition, subsurface structure, radiation environment and weather. However additional significance has recently been placed on exploration of Mars with the reformulation of the Mars Exploration Program. This program aims to assess both near-term mission concepts and longer-term foundations of program level architectures for future robotic exploration. As a result missions must be developed which are responsive to the scientific goals of both the National Research Council Planetary Decadal Survey [48] and the ESA Aurora Programme [11]. **Section 7.2** therefore develops novel orbits of Mars to enable new and unique investigations and allow the necessary investigation into the Martian surface, subsurface and atmosphere for future human exploration.

Similarly, the NASA Vision and Voyages Decadal Survey for 2013 – 2022 has identified three themes for the future development of planetary science, within which the importance of investigating the evolution of the inner planets and their atmospheres is highlighted [48]. The importance of examining the chemistry, climates and geology of the inner planets is also highlighted to lead to a better understanding of climate change on Earth [48]. The importance of further exploration of Mercury and Venus is therefore clear.

Previously in **Chapter 1**, it was stated that both sun-synchronous orbits and highly-elliptical orbits inclined at the critical inclination exist at Mars. In contrast, at Mercury and Venus, although highly-elliptical orbits can be derived, the reciprocal of flattening is so low that natural perturbations are of no use for generating sun-synchronous orbits. This chapter therefore uses methods presented in previous chapters to extend existing highly-elliptical

[10] http://www.nasa.gov/mission_pages/msl/index.html Accessed 15 January 2013
[11] http://www.esa.int/esaMI/Aurora/ Accessed 27 August 2012

orbits at these bodies, extend natural sun-synchronous orbits around Mars, and enable sun-synchronous orbits around Mercury and Venus, as such significantly enhancing the opportunities for remote sensing of these bodies.

7.2 Mars

As on Earth the oblateness term, J_2, is the dominating perturbation at Mars. However the other first few harmonic coefficients have a greater effect at Mars as they are around 1 – 2 orders of magnitude lower than J_2 compared to 3 – 4 orders of magnitude lower at Earth. Thus, where **Chapters 3** considered the free selection of the critical inclination at Earth independent of the orbit semi-major axis and eccentricity, the magnitude of the first few harmonic coefficients at Mars means these must be included when determining the critical inclination of Martian orbits. The value of the critical inclination for orbits at Mars is therefore dependent on the semi-major axis and eccentricity. The work presented in this section extends these natural orbits using the methods introduced in **Chapter 3**.

Similarly to the work presented in **Chapter 6**, these solutions can be extended using an element of continuous acceleration directed out of the orbit plane to produce Martian highly-elliptical sun-synchronous orbits.

New Martian orbits may be of use for communication relay for human missions, UAVs or detailed mapping of the Martian surface. The transition from single spacecraft exploration of Mars to fleets of spacecraft both around Mars and on the Martian surface further highlights possible benefits of these novel orbits.

7.2.1 Spacecraft Motion about Mars

At Earth the most dominant perturbation is the oblateness term, J_2, with a value of 1.082627×10^{-3}. As stated in **Chapter 3** the harmonic coefficients J_3 and J_4 are around three

orders of magnitude smaller than the J_2 term, with $J_3 = -2.53266x10^{-6}$, and $J_4 = -1.61962x10^{-6}$, and thus have a negligible effect on the determination of the critical inclination. At Mars, the J_2 perturbation is also dominant, with a value of $1.95545x10^{-3}$. However, zonal harmonics through to J_5 are only around two orders of magnitude lower than the J_2 perturbation, with values of $J_3 = 3.14498x10^{-5}$, $J_4 = -1.53774x10^{-5}$, and $J_5 = 9.0793x10^{-6}$, and so will have an impact on the determination of the critical inclination at Mars. As a result higher order terms must be taken into consideration in this instance.

The gravitational potential of a body is described by Eq. (3.3), where in this case μ is the gravitational parameter of Mars, and R_e in this equation is altered to R_B, the radius of the body under consideration. For Mars, $R_B = R_m$. Including perturbations to the order of J_5 and using spherical triangle laws, Eq. (3.3) becomes

$$\begin{aligned} U(r,\beta) = U_0 + U_p = {} & \frac{\mu}{r} - J_2 \frac{\mu R_B^{\,2}}{2r^3}\left(3\sin^2(i)\sin^2(\theta+\omega)-1\right) \\ & - J_3 \frac{\mu R_B^{\,3}}{2r^4}\left(5\sin^3(i)\sin^3(\theta+\omega)-3\sin(i)\sin(\theta+\omega)\right) \\ & - J_4 \frac{\mu R_B^{\,4}}{8r^5}\left(3-30\sin^2(i)\sin^2(\theta+\omega)+35\sin^4(i)\sin^4(\theta+\omega)\right) \\ & - J_5 \frac{\mu R_B^{\,5}}{8r^6}\left(63\sin^5(i)\sin^5(\theta+\omega)-70\sin^3(i)\sin^3(\theta+\omega)+15\sin(i)\sin(\theta+\omega)\right) \end{aligned} \tag{7.1}$$

This results in the expressions for the perturbing accelerations in the R, T and N directions of

$$\begin{aligned} R_J = {} & \frac{\mu R_B^2}{8r^7}(-12J_2r^3 + 15J_4rR_B^2 + \sin(i)\sin(\theta+\omega)(-48J_3r^2R_B + 90J_5R_B^3 \\ & + \sin(i)\sin(\theta+\omega)(6r(6J_2r^2 - 25J_4R_B^2) + R_B\sin(i)\sin(\theta+\omega) \\ & (80J_3r^2 - 420J_5R_B^2 + 7R_B\sin(i)\sin(\theta+\omega)(25J_4r + 54J_5R_B\sin(i)\sin(\theta+\omega)))))) \end{aligned} \tag{7.2}$$

$$\begin{aligned} T_J = {} & -\frac{R_B^2\mu\cos(\theta+\omega)\sin(i)}{8r^7}(-12J_2r^2R_B + 15J_5rR_B^3 + \sin(i)\sin(\theta+\omega) \\ & (24J_2r^2 - 60J_4rR_B^2 + 5R_B\sin(i)\sin(\theta+\omega)(6(2J_3r^2 - 7J_5R_B^2) \\ & + 7R_B\sin(i)\sin(\theta+\omega)(4J_4r + 9J_5R_B + 7R_B\sin(i)\sin(\theta+\omega))))) \end{aligned} \tag{7.3}$$

$$N_J = -\frac{R_B^2 \mu \cos(i)}{8r^7}(-12J_3 r^2 R_B + 15J_5 R_B^3 + \sin(i)\sin(\theta+\omega)$$
$$(24J_2 r^3 - 60J_4 r R_B^2 + 5R_B \sin(i)\sin(\theta+\omega)(6(2J_3 r^2 - 7J_5 R_B^2)$$
$$+7R_B \sin(i)\sin(\theta+\omega)(4J_4 r + 9J_5 R_B \sin(i)\sin(\theta+\omega))))) \quad (7.4)$$

7.2.2 Highly-Elliptical Orbits

7.2.2.1 General Perturbations Solution

In order to determine the critical inclination of highly-elliptical orbits at Mars Eqs. (7.2) - (7.4) are substituted into Eq. (3.6) and integrated over one orbital revolution. Inserting orbital element values into the resulting formula, and setting this equal to zero, gives the value of the critical inclination. For example, a 12 h orbit with a pericentre altitude of *800 km* and apogee altitude of *17,724 km* including perturbations to the order of J_4 results in critical inclinations of *63.29* and *116.71 degrees*. Increasing the perturbations to include J_5 alters the critical inclination values to *63.24* and *116.76 degrees.* Thus including the J_5 perturbation results in a difference of less than *0.1 %* from the J_4 results, and can therefore be neglected in order to significantly reduce the complexity of the solutions.

Eqs. (7.2) - (7.4) are simplified and low-thrust terms are added to allow the extension of the solutions. As in **Chapter 3** low-thrust terms are added using locally optimal control laws [64].

$$R_{J+F_r} = \frac{\mu R_B^2}{8r^7}(-12J_2 r^3 + 15J_4 r R_B^2 + \sin(i)\sin(\theta+\omega)$$
$$(-48J_3 r R_B + \sin(i)\sin(\theta+\omega)(6(6J_2 r^2 - 25J_4 R_B^2)$$
$$+5R_B \sin(i)\sin(\theta+\omega)(16J_3 r + 35J_4 R_B \sin(i)\sin(\theta+\omega))))) + F_r \operatorname{sgn}\left[\cos(\theta)\right] \quad (7.5)$$

$$T_{J+F_t} = \frac{R_B^2 \mu \cos(\theta+\omega)\sin(i)}{2r^6}(3J_3 r R_B - \sin(i)\sin(\theta+\omega)$$
$$(6J_2 r^2 - 15J_4 R_B^2 + 5R_B \sin(i)\sin(\theta+\omega)$$
$$(3J_3 r + 7J_4 R_B \sin(i)\sin(\theta+\omega)))) + F_t \operatorname{sgn}\left[\sin(\theta)\right] \quad (7.6)$$

$$
\begin{aligned}
N_{J+F_n} = \frac{R_B^2 \mu \cos(i)}{2r^6} (3J_3 r R_B - \sin(i)\sin(\theta+\omega) \\
(6J_2 r^2 - 15J_4 R_B^2 + 5R_B \sin(i)\sin(\theta+\omega) \\
(3J_4 r + 7J_4 R_B \sin(i)\sin(\theta+\omega)))) + F_n \operatorname{sgn}\left[\sin(\theta+\omega)\right]
\end{aligned}
\tag{7.7}
$$

Eqs. (7.5) - (7.7) are again substituted into Eq. (3.3) and integrated over the orbit. The resulting equation for the change in argument of pericentre is given by Eq. (3.21). **Chapter 3** also states the benefit of including normal acceleration is negligible when altering the critical inclination of highly-elliptical orbits. Thus this equation includes contributions from gravity perturbations to the order of J_4 (Eq. (7.8)), and radial and transverse acceleration terms given previously by Eqs. (3.22) and (3.23) respectively.

$$
\begin{aligned}
(\Delta\omega)_J = \frac{3\pi R_B^2}{512 a^4 e\left(-1+e^2\right)^4} (e(384a^2\left(-1+e^2\right)^2 J_2 - 135\left(4+5e^2\right) J_4 R_B^2 \\
+20(32a^2\left(-1+e^2\right)^2 J_2 - \left(52+63e^2\right) J_4 R_B^2)\cos(2i) \\
-35\left(28+27e^2\right) J_4 R_B^2 \cos(4i)) + 10eJ_4 R_B^2 (-6+5e^2 \\
+4\left(-2+7e^2\right)\cos(2i) + 7\left(2+9e^2\right)\cos(4i))\cos(2\omega) + 16a\left(-1+e^2\right) \\
J_3 R_B (-1-3e^2 - 4\cos(2i) + 5\left(1+7e^2\right)\cos(4i))\csc(i)\sin(\omega)))
\end{aligned}
\tag{7.8}
$$

Eq. (3.21) is set equal to zero and solved for the radial and transverse acceleration required to achieve any value of critical inclination for any given orbit, where the magnitude of acceleration in each direction is not assumed to be equal. The resulting acceleration magnitudes are shown, for a variety of orbit periods between 6 and 24 hours to achieve inclinations between *5* and *175 degrees* for a constant periapsis altitude of *800 km*, to compensate for the drift in argument of pericentre caused by perturbations to the order of J_4. The radial, transverse and total magnitude of acceleration required are shown in Figure 7-1 - Figure 7-3 respectively for an argument of pericentre value of *270 degrees*, and in Figure 7-4 - Figure 7-6 for and argument of pericentre equal to *0 degrees*. Comparison of

Figure 7-1 - Figure 7-6 reveals very little difference between the acceleration magnitudes required for each value of argument of pericentre considered.

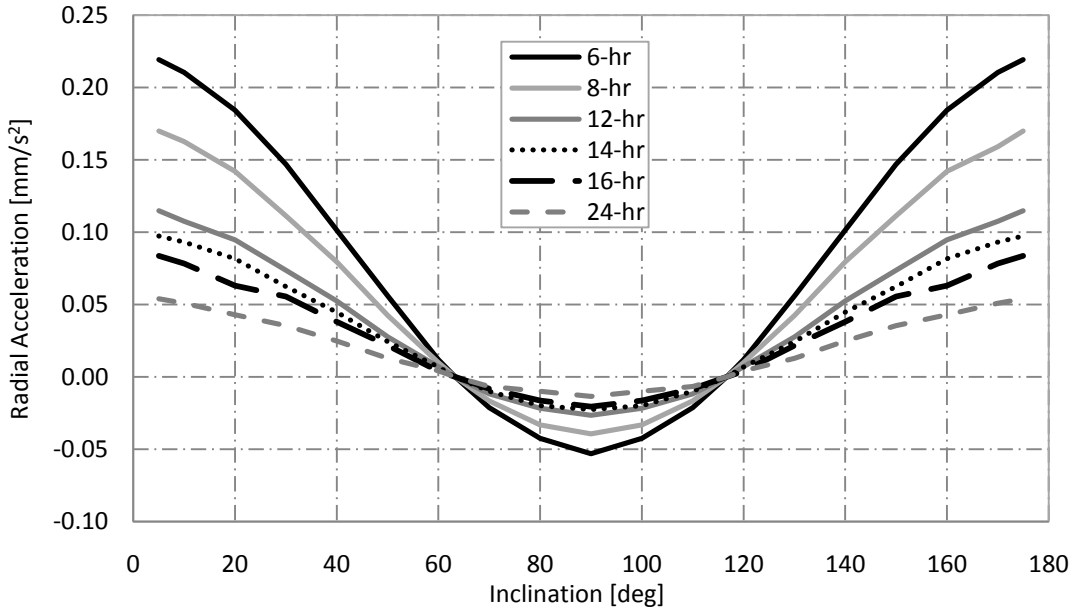

Figure 7-1 Required radial acceleration for the extension of highly-elliptical orbits at Mars - *270 degree* argument of pericentre

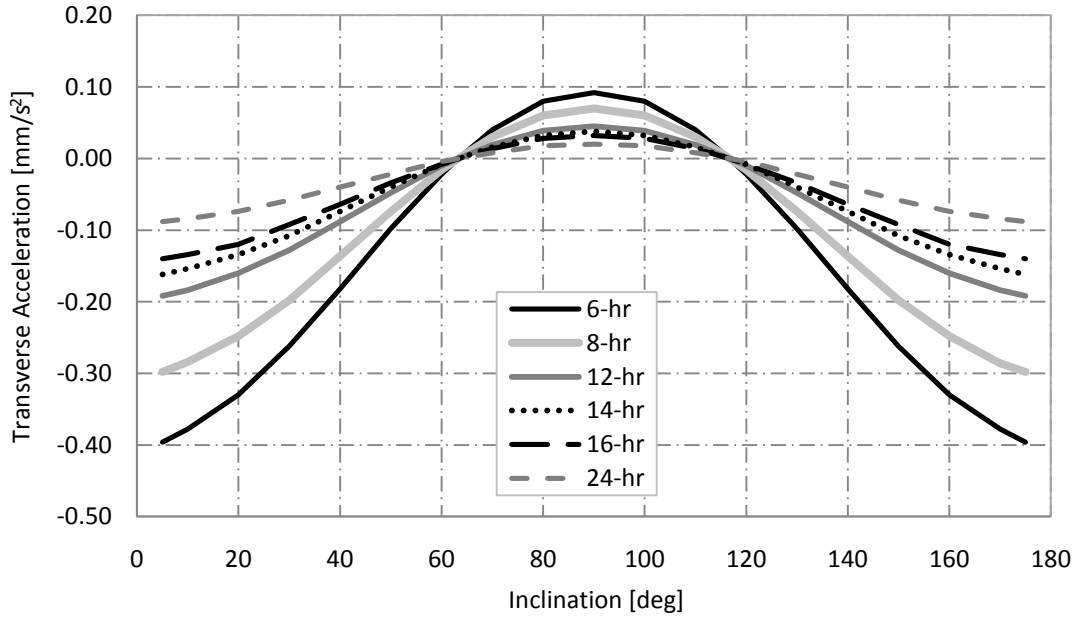

Figure 7-2 Required transverse acceleration for the extension of highly-elliptical orbits at Mars – *270 degree* argument of pericentre

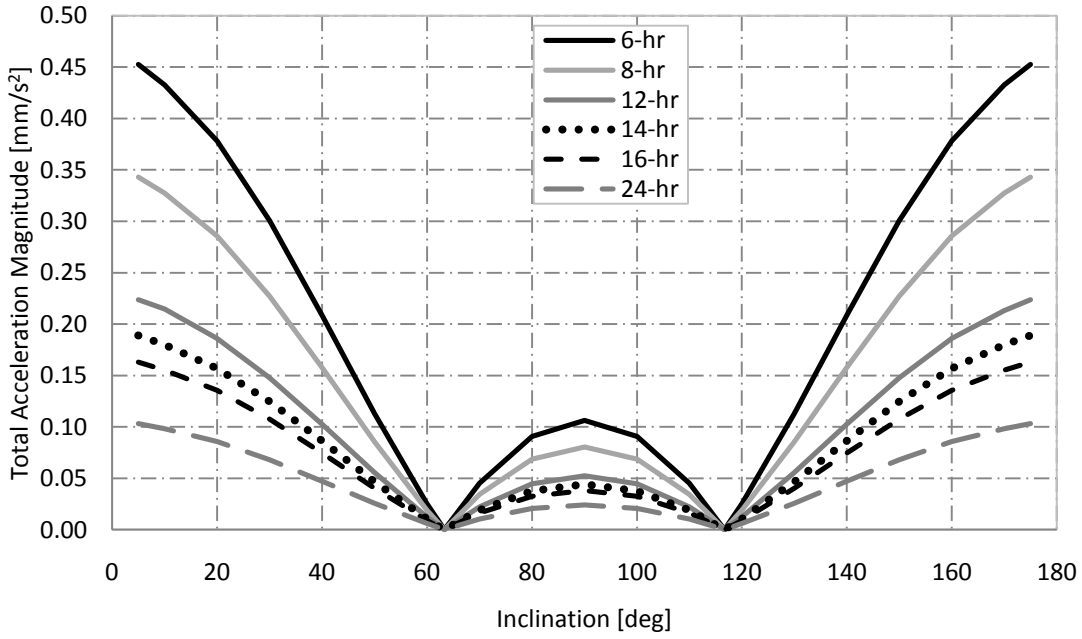

Figure 7-3 Total acceleration magnitude for the extension of highly-elliptical orbits at Mars – *270 degree* argument of pericentre

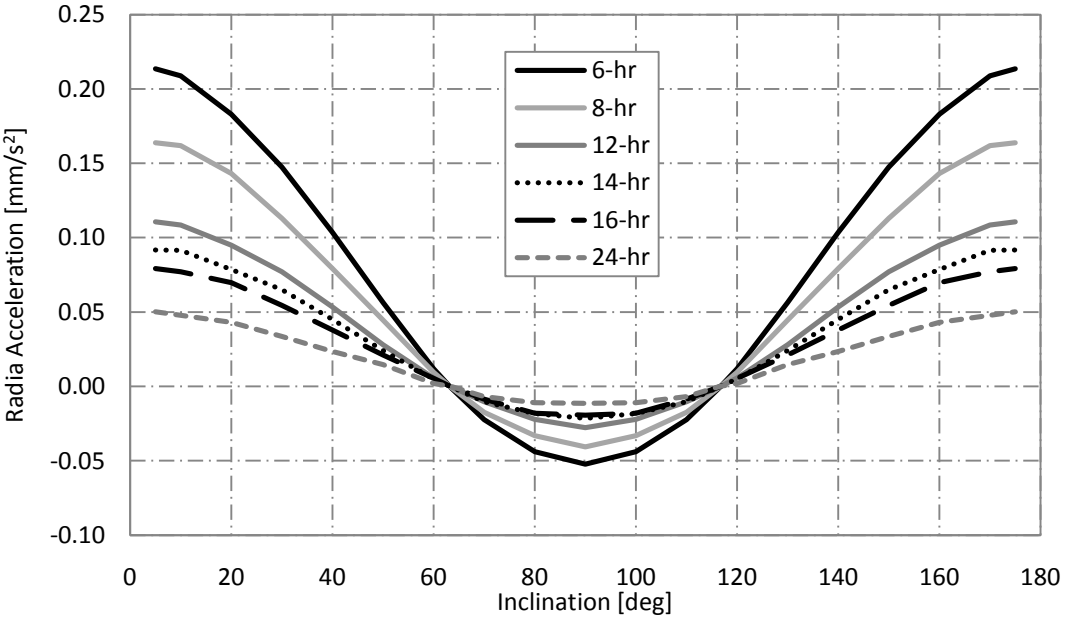

Figure 7-4 Required radial acceleration for the extension of highly-elliptical orbits at Mars - *0 degree* argument of pericentre

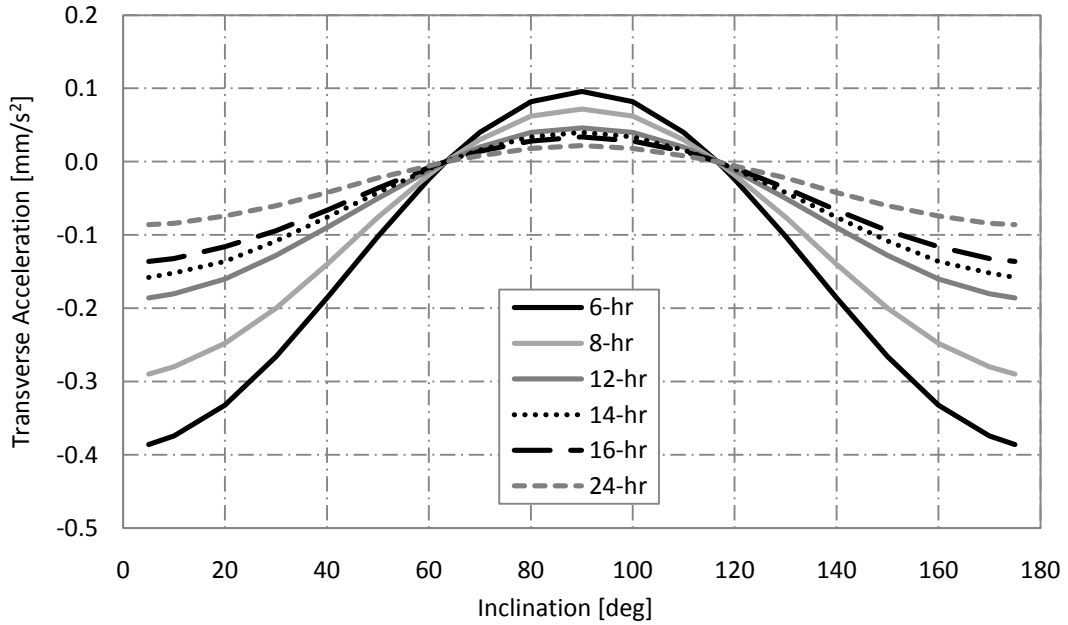

Figure 7-5 Required transverse acceleration for the extension of highly-elliptical orbits at Mars – *0 degree* argument of pericentre

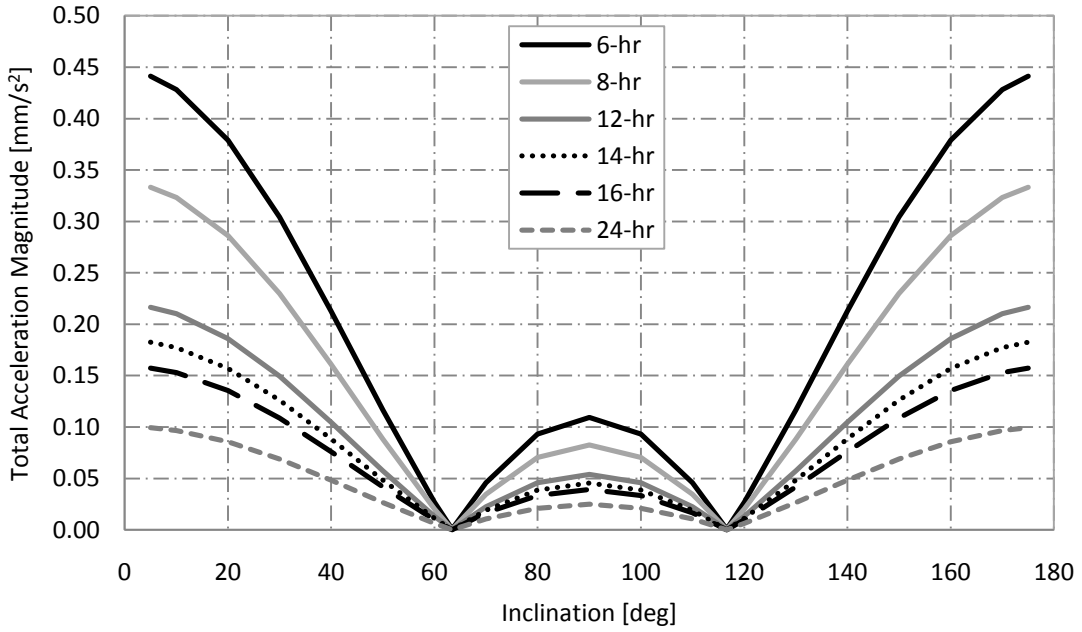

Figure 7-6 Total acceleration magnitude for the extension of highly-elliptical orbits at Mars – *0 degree* argument of pericentre

Considering the case where the argument of pericentre is equal to *270 degrees*, a 12 h orbit with an inclination of *90 degrees* requires a total acceleration magnitude of *0.05 mm/s²*. For a 1-ton spacecraft this corresponds to an initial thrust level of *50 mN*, which is within the capabilities of current thruster technology. Such as the NSTAR thruster (thrust range *20 – 94 mN*) [76] and the QinitiQ T6 thruster (thrust range *30 – 210 mN*) [86]. Thus, both thrusters are capable of providing the required level of thrust for this particular case.

7.2.2.2 Special Perturbations Solution

Analytical solutions are again verified using a special perturbations solution, maintaining the same tolerances as stated in **Chapter 3**. The results are shown for the orbital elements for five revolutions of a 12 h orbit with *90 degree* inclination and *270 degree* argument of periapsis in Figure 7-7 and argument of periapsis of *0 degrees* in Figure 7-8. These results show that although the semi-major axis, eccentricity and argument of pericentre oscillate

over each orbital revolution, these elements return to the original value after each orbit. It is also shown that there are no changes experienced by inclination and ascending node angle.

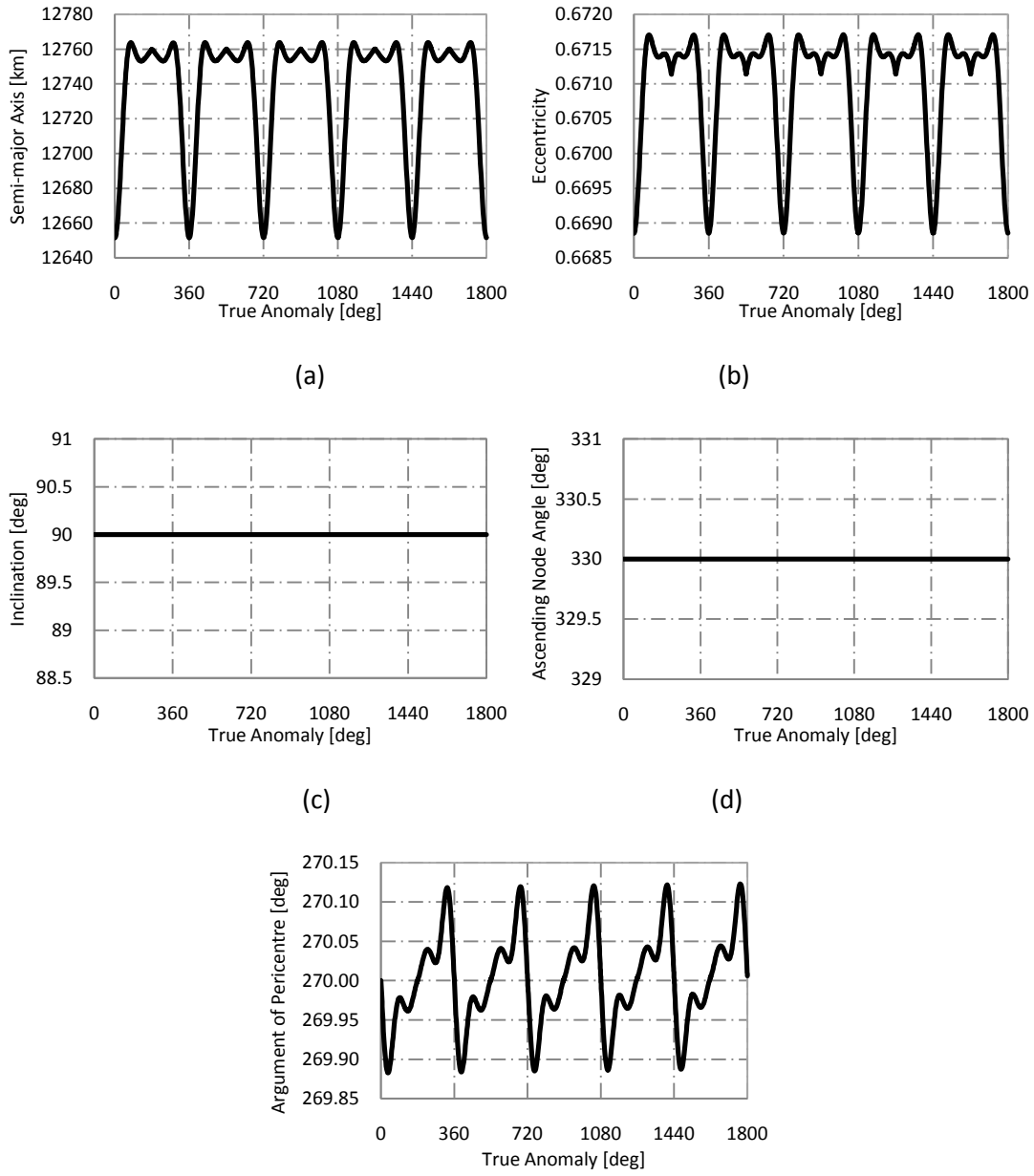

Figure 7-7 Oscillation of orbital elements over five orbital revolutions of a 12 h, *90 degree* inclination orbit at Mars (*270 degree* argument of periapsis) (a) Semi-major axis (b) Eccentricity (c) Inclination (d) Ascending node angle (e) Argument of pericentre

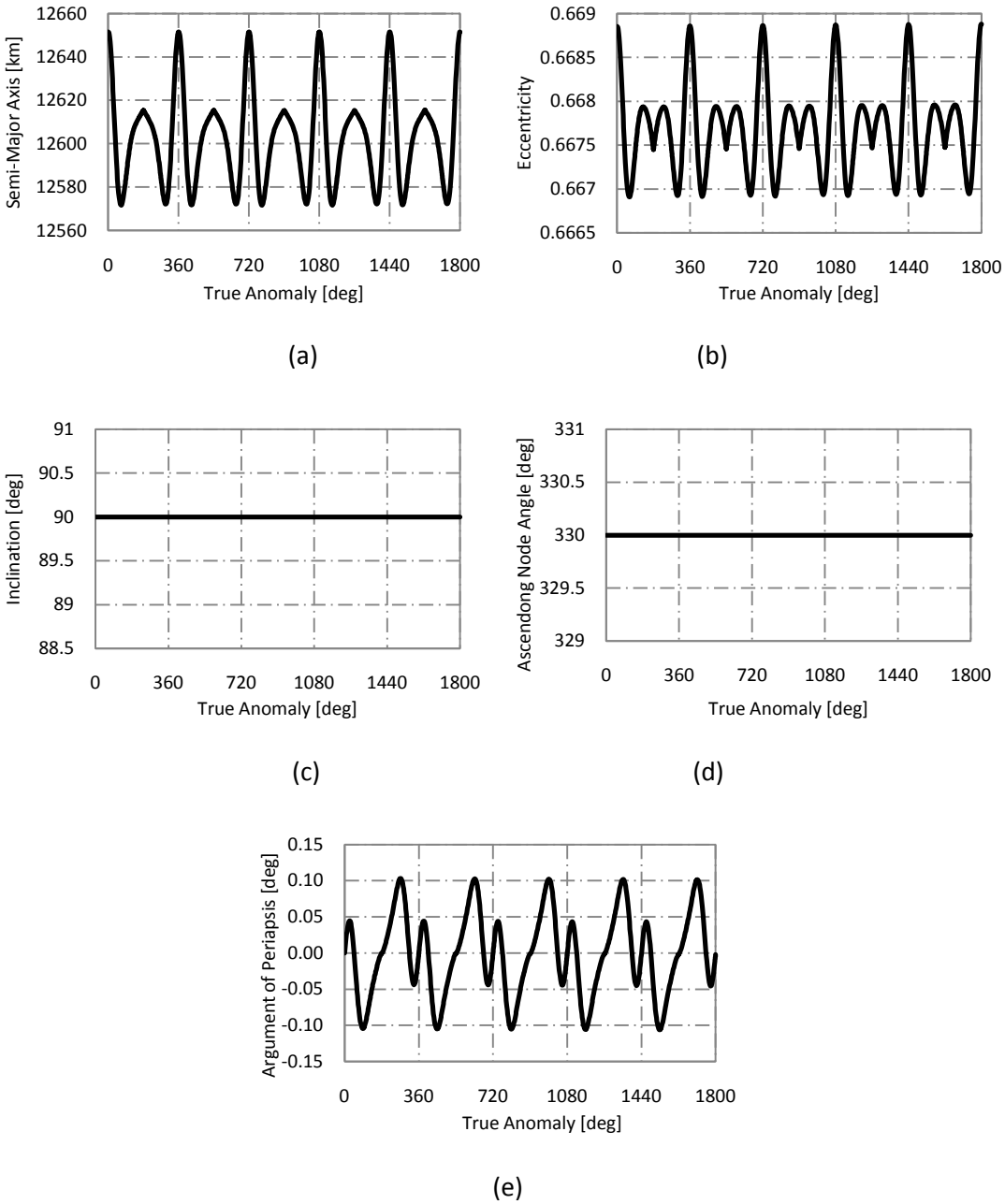

Figure 7-8 Oscillation of orbital elements over five orbital revolutions of a 12 h, *90 degree* inclination orbit at Mars (*0 degree* argument of periapsis) (a) Semi-major axis (b) Eccentricity (c) Inclination (d) Ascending node angle (e) Argument of pericentre

7.2.3 Sun-Synchronous Orbits

As with Earth, continuous low-thrust propulsion can also be used to extend existing sun-synchronous orbits to allow free selection of the orbit inclination and altitude. At Mars,

sun-synchronous orbits require the rotation in the ascending node to equal 2π *radians* in *686.429 days*. As first outlined in **Chapter 6**, the extension of sun-synchronous orbits is achieved by substituting the expression for the normal perturbation including a gravity term, to the order of J_4, and an additional continuous acceleration term (Eq. (7.7)) into the equation for the rate of change of ascending node (Eq. (3.37)) and integrating over the orbit. As an out-of-plane acceleration is applied which is dependent on the argument of latitude, two solutions are again given for the change in ascending node angle, for argument of pericentre values of *0* and *270 degrees* respectively. The change in ascending node is given by

$$\left(\Delta\Omega\right)_0^{2\pi} = \left(\Delta\Omega\right)_J + \left(\Delta\Omega\right)_{F_n} \tag{7.9}$$

where

$$\begin{aligned}\left(\Delta\Omega\right)_J = \frac{3\pi R_B^2}{32a^4\left(-1+e^2\right)^4}(&\cos\left(i\right)(-32a^2\left(-1+e^2\right)^2 J_2 + 5\left(2+3e^2\right)J_4 R_B^2 \\ &+35\left(2+3e^2\right)J_4 R_B^2\cos\left(2i\right)) - 5e^2 J_4 R_B^2(5\cos\left(i\right)+7\cos\left(3i\right)) \\ &\cos\left(2\omega\right) - 2ae\left(-1+e^2\right)J_3 R_B(\cos\left(i\right)+15\cos\left(3i\right))\csc\left(i\right)\sin\left(\omega\right))\end{aligned} \tag{7.10}$$

$$\left(\Delta\Omega\right)_{F_n,\omega=0} = -\frac{4a^2 F_n\cos\left(\omega\right)\cot\left(i\right)}{\mu} \tag{7.11}$$

$$\begin{aligned}\left(\Delta\Omega\right)_{F_n,\omega=270} = -\frac{a^2 F_n\csc\left(i\right)}{\sqrt{-1+e^2}\,\mu}(&4\sqrt{-1+e^2}+2e^2\sqrt{-1+e^2} \\ &-12e\,\text{ArcTanh}\left[\frac{-1+e}{\sqrt{-1+e^2}}\right]-3e\ln\left[\frac{1-e}{\sqrt{-1+e^2}}\right]+3e\ln\left[\frac{-1+e}{\sqrt{-1+e^2}}\right]\sin\left(\omega\right))\end{aligned} \tag{7.12}$$

Switching the rate of change of the ascending node angle per rotation to per second and re-arranging, the two solutions for the change in ascending node per second for argument of periapsis equal to *0* and *270 degrees* respectively, are

$$
\begin{aligned}
(\Delta\Omega)_{\omega=0} = \frac{\sqrt{\mu}}{2\sqrt{a^3}\pi}\Big(&\frac{4a^2F_n\cos(\omega)\csc(i)}{\mu} + \frac{1}{(32a^4(-1+e^2)^4)}3\pi R_B^2(\cos(i)\\
&(-32a^2(-1+e^2)^2 J_2 + 5(2+3e^2)J_4R_B^2 + 35(2+3e^2)J_4R_B^2\cos(2i)) \\
&-5e^2J_4R_B^2(5\cos(i)+7\cos(3i))\cos(2\omega) - 2ae(-1+e^2)J_3R_B(\cos(i)\\
&+15\cos(3i))\csc(i)\sin(\omega)))
\end{aligned}
\tag{7.13}
$$

$$
\begin{aligned}
(\Delta\Omega)_{\omega=270} = \frac{\sqrt{\mu}}{2\sqrt{a^3}\pi}\Big(&\frac{-1}{(\sqrt{-1+e^2}\mu)}a^2F_n\csc(i)(4\sqrt{-1+e^2}+2e^2\sqrt{-1+e^2}\\
&-12e\,\mathrm{ArcTanh}\left[\frac{-1+e}{\sqrt{-1+e^2}}\right] - 3e\ln\left[\frac{1-e}{\sqrt{-1+e^2}}\right] + 3e\ln\left[\frac{-1+e}{\sqrt{-1+e^2}}\right])\sin(\omega)\\
&+\Big(\frac{1}{(32a^4(-1+e^2)^4)}\Big)3\pi R_B^2(\cos(i)(-32a^2(-1+e^2)^2J_2 + 5(2+3e^2)^2J_2\\
&+5(2+3e^2)J_4R_B^2 + 35(2+3e^2)J_4R_B^2\cos(2i)) - 2ae(-1+e^2)J_3R_B\\
&(\cos(i)+15\cos(3i))\csc(i)\sin(\omega)))
\end{aligned}
\tag{7.14}
$$

7.2.3.1 Circular Sun-Synchronous Orbits

Firstly, considering the extension of circular orbits, the acceleration magnitude directed out of the orbit plane to achieve free-selection of the inclination for a range of orbit altitudes is given in Figure 7-9.

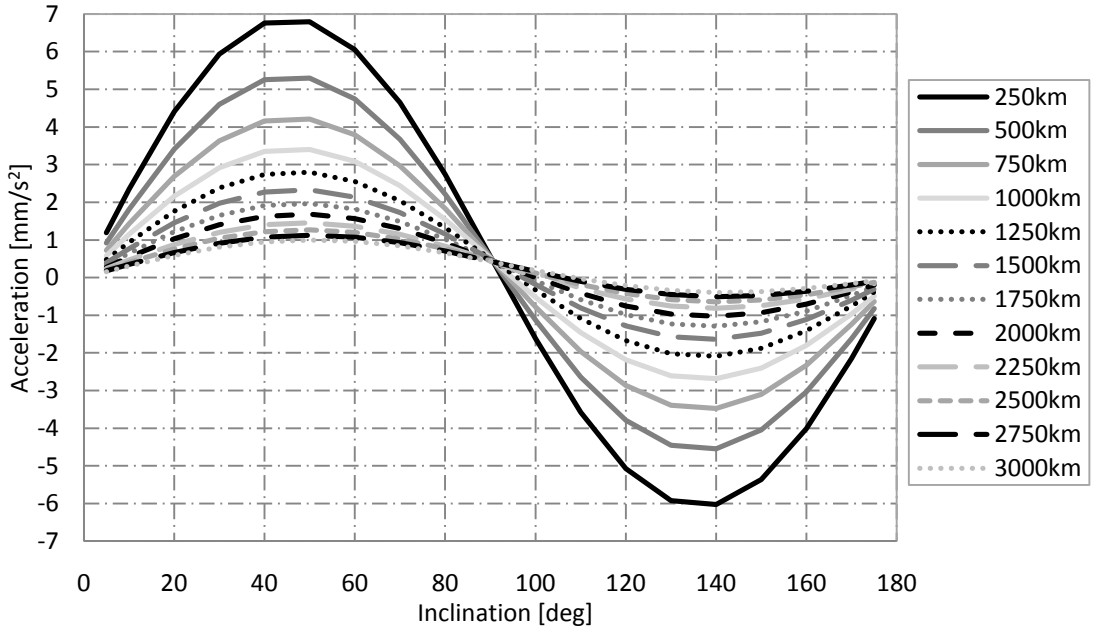

Figure 7-9 Required normal acceleration for the extension of circular sun-synchronous orbits at Mars

Figure 7-9 shows that circular sun-synchronous orbits with free selection of the inclination can be enabled using continuous out-of-plane acceleration. It is shown that orbits around *90 degrees* require feasible acceleration, and the further the inclination drifts from this region, the level of acceleration required becomes infeasible using existing thruster technology.

7.2.3.2 Highly-Elliptical Sun-Synchronous Orbits

7.2.3.2.1 General Perturbations Solution

As described in **Chapter 6**, to enable elliptical sun-synchronous orbits, two conditions must be combined to ensure the desired rate of change of the ascending node (from Eq. (7.13) or Eq. (7.14)) is obtained and that the zero change in the argument of periapsis (from Eq. (3.21)) is maintained using continuous accelerations in each of the *R*, *T* and *N* directions. The radial, transverse, normal and total acceleration magnitude to achieve elliptical sun-

synchronous orbits of varying orbital period and inclination are given in Figure 7-10 - Figure 7-13 for an argument of pericentre equal to *270 degrees* and in Figure 7-14 - Figure 7-17 for an argument of pericentre of *0 degrees.* In both cases the results are shown for a constant pericentre altitude of *800 km.* Comparison of the results presented show that the value of argument of pericentre does not significantly affect the level of acceleration required to achieve elliptical sun-synchronous orbits at Mars and the acceleration magnitudes in both cases are of the same order of magnitude.

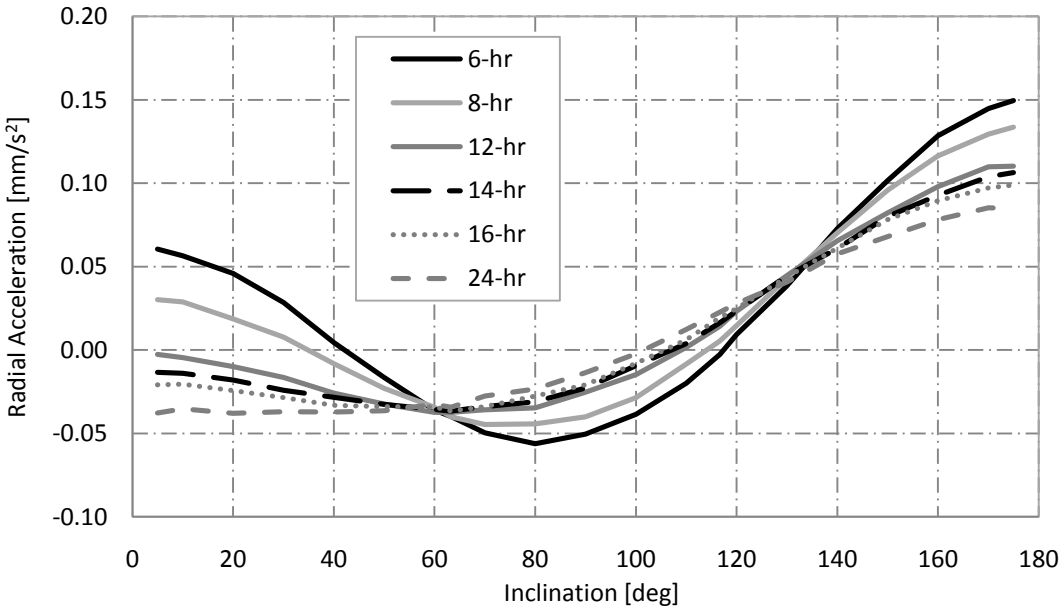

Figure 7-10 Required radial acceleration for the extension of elliptical sun-synchronous orbits at Mars - *270 degree* argument of pericentre

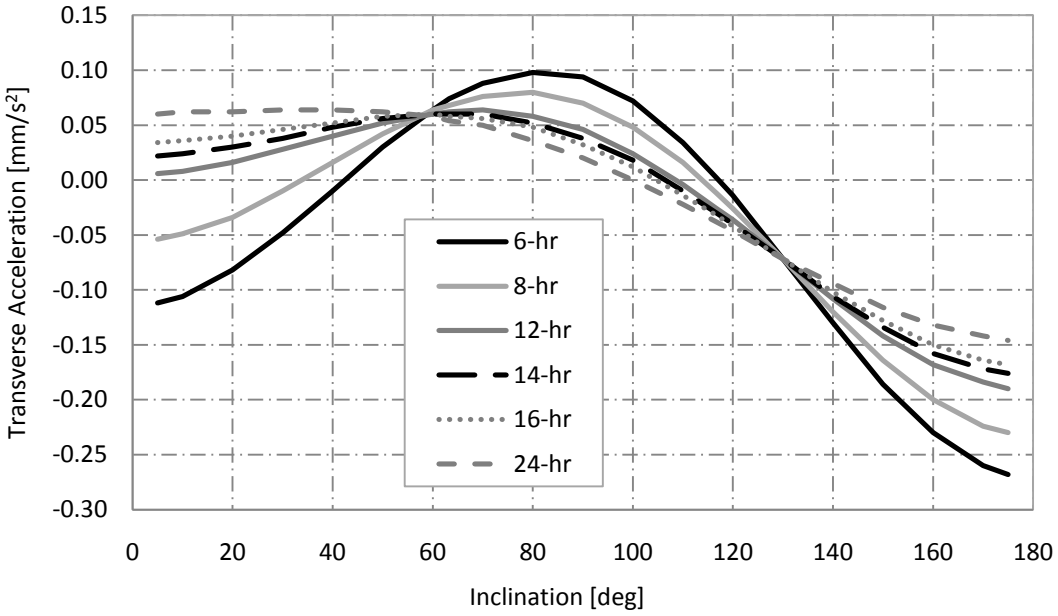

Figure 7-11 Transverse radial acceleration for the extension of elliptical sun-synchronous orbits at Mars - *270 degree* argument of pericentre

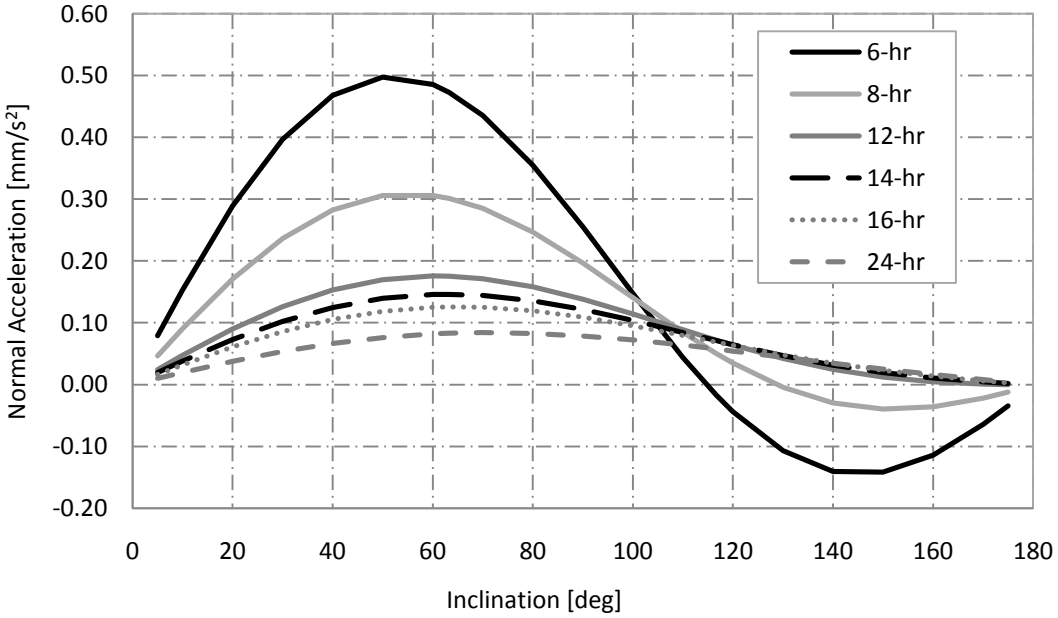

Figure 7-12 Normal radial acceleration for the extension of elliptical sun-synchronous orbits at Mars - *270 degree* argument of pericentre

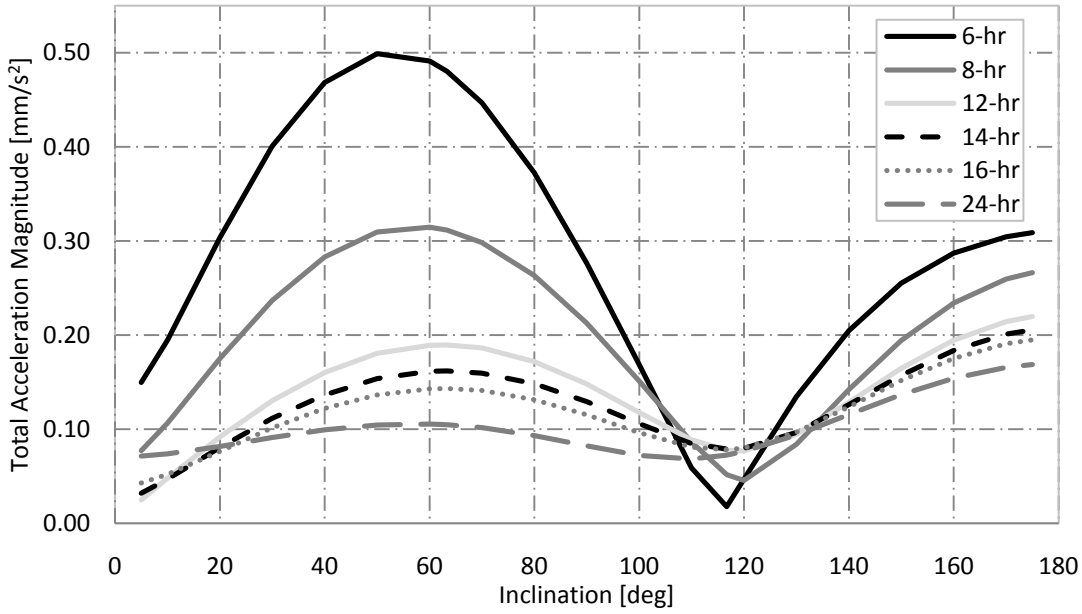

Figure 7-13 Total acceleration required for the extension of elliptical sun-synchronous orbits at Mars - *270 degree* argument of pericentre

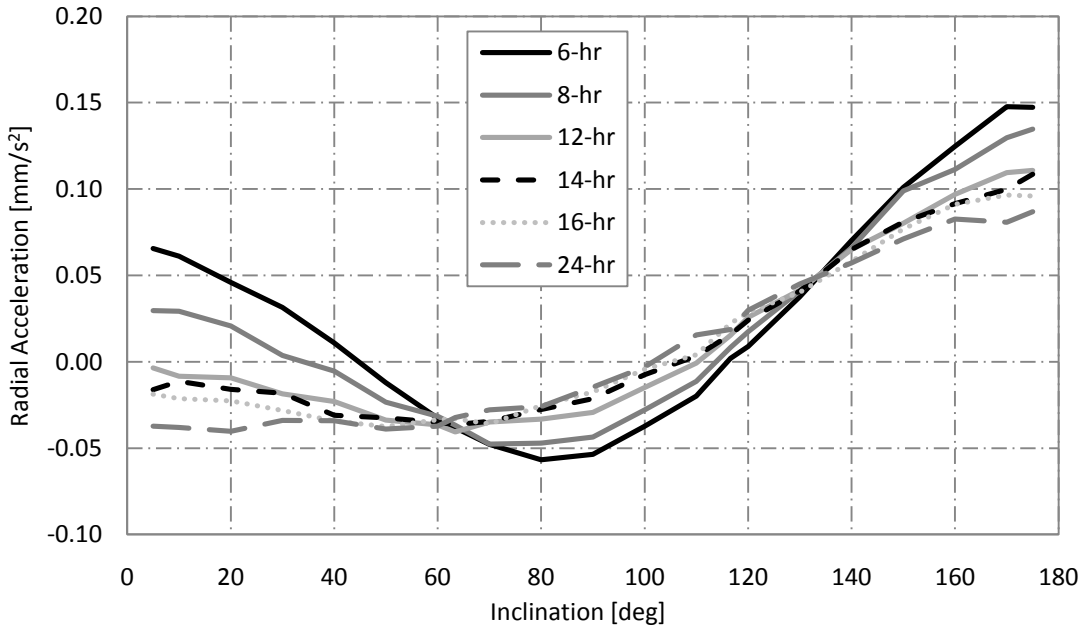

Figure 7-14 Required radial acceleration for the extension of elliptical sun-synchronous orbits at Mars - *0 degree* argument of pericentre

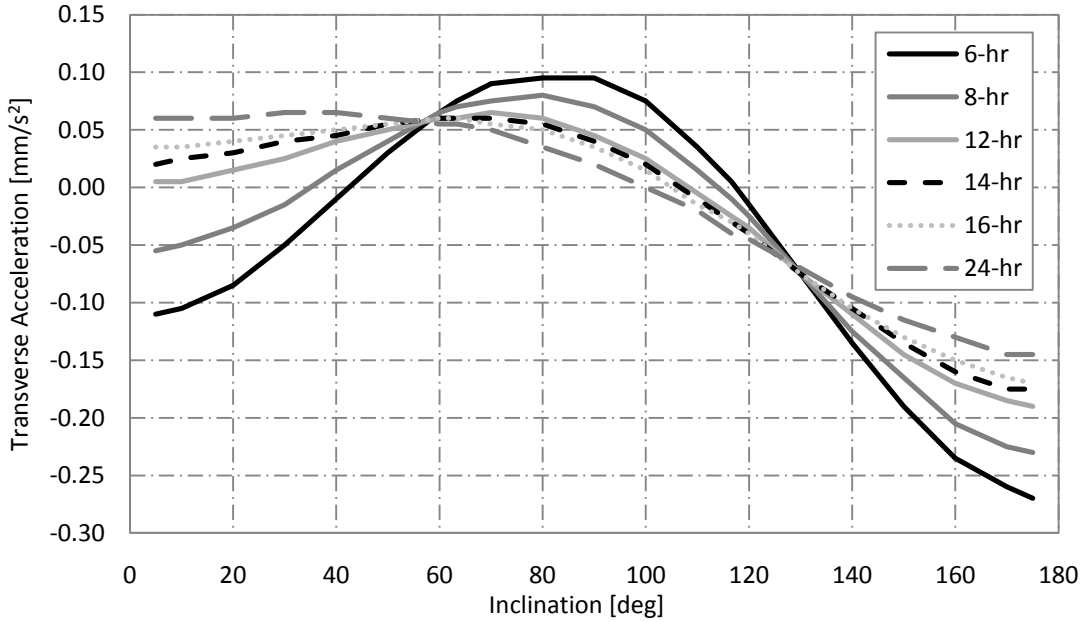

Figure 7-15 Required transverse acceleration for the extension of elliptical sun-synchronous orbits at Mars - *0 degree* argument of pericentre

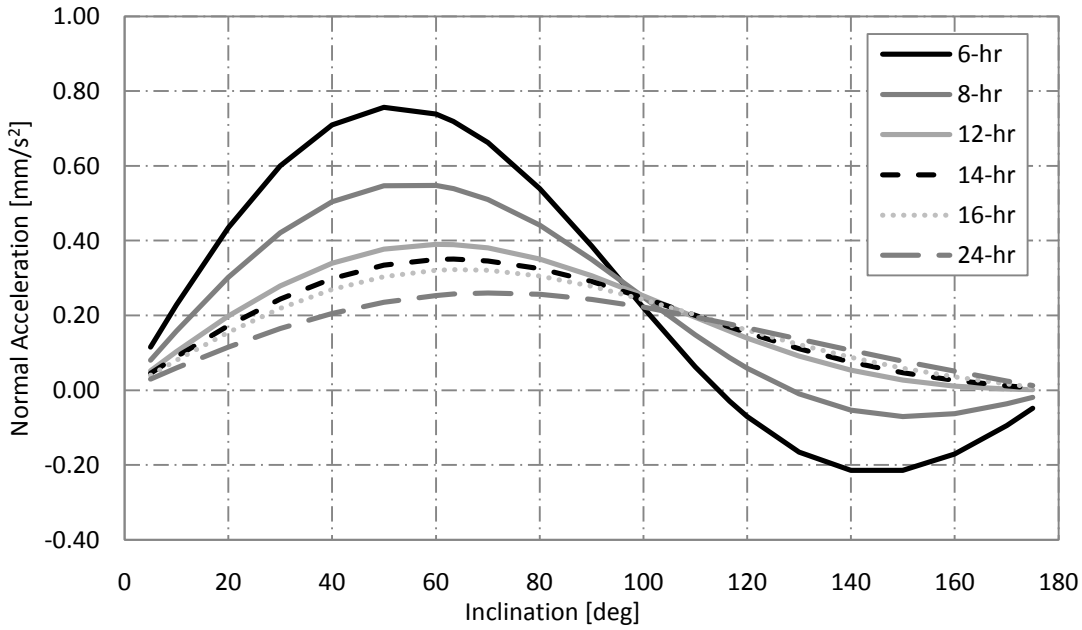

Figure 7-16 Required normal acceleration for the extension of elliptical sun-synchronous orbits at Mars - *0 degree* argument of pericentre

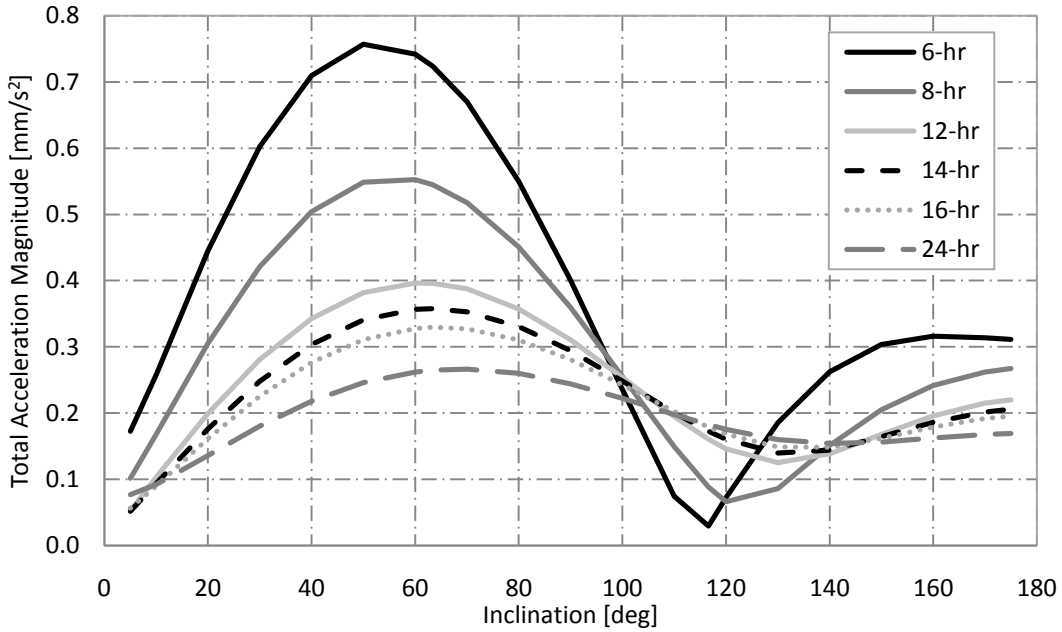

Figure 7-17 Total acceleration required for the extension of elliptical sun-synchronous orbits at Mars - *0 degree* argument of pericentre

From Figure 7-13 and Figure 7-17 a 12 h orbit with an inclination of *90 degrees* requires a total acceleration magnitude of *0.15 mm/s²* and *0.31 mm/s²* for argument of pericentre values of *270* and *0 degrees* respectively, corresponding to initial thrust levels of *150* and *310 mN* for a 1-ton spacecraft. Although these thrust levels are higher than that required for the orbits excluding the sun-synchronous condition, these levels are still within capabilities of emerging thrusters. For example, the HiPEP thruster (maximum thrust *670 mN*) [83] or NEXIS (maximum thrust *476 mN*) [82].

7.2.3.2.2 Special Perturbations Solution

The solutions presented in **Section 7.2.3.2.1** are validated using a special perturbations technique. The oscillation of orbital elements for an orbit with an argument of pericentre of *270 degrees* are shown in Figure 7-18 and in Figure 7-19 for an argument of pericentre of *0 degrees*.

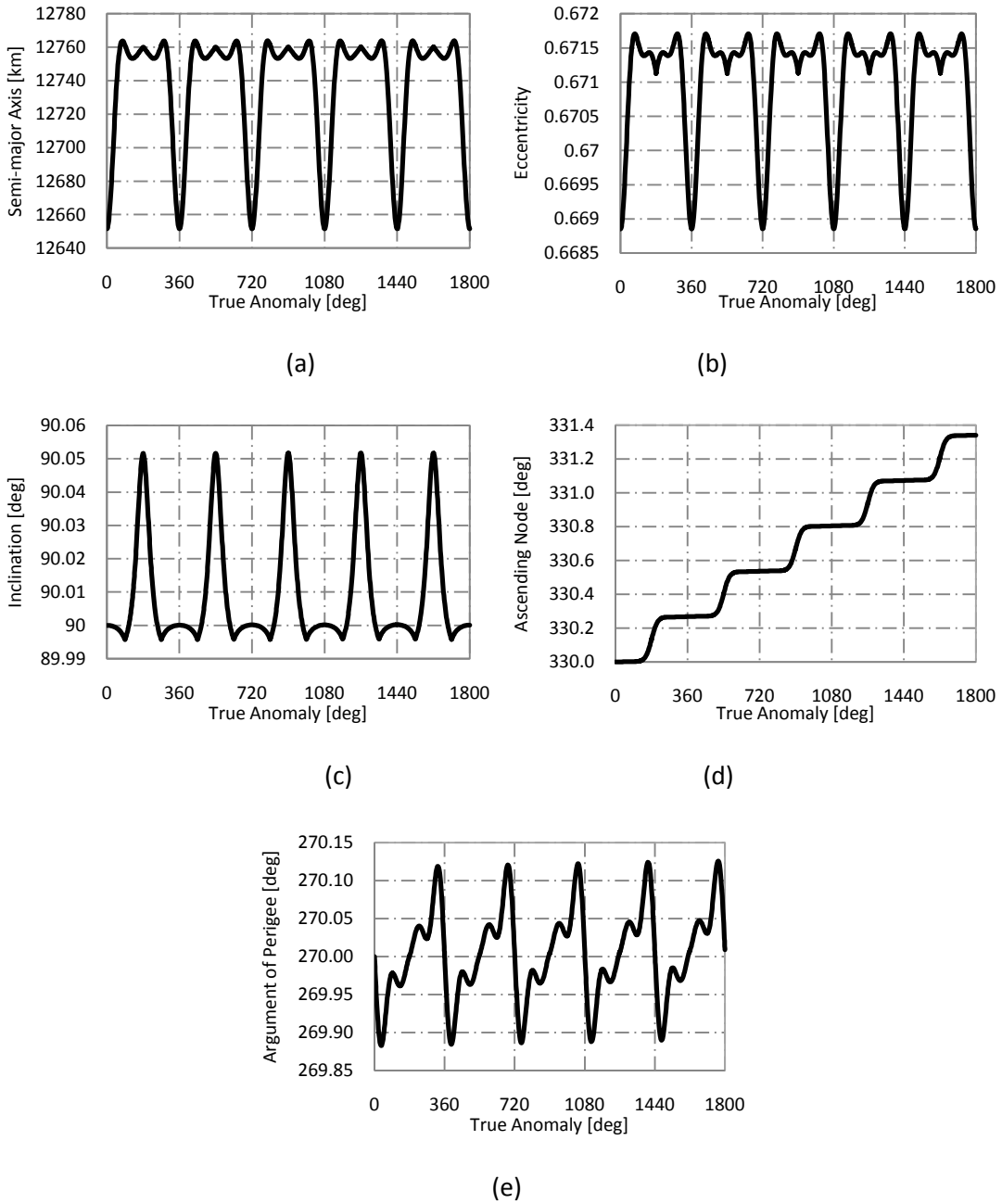

Figure 7-18 Oscillation of orbital elements over five orbital revolutions of a 12 h, *90 degree* inclination, sun-synchronous orbit at Mars (*270 degree* argument of periapsis) (a) Semi-major axis (b) Eccentricity (c) Inclination (d) Ascending node angle (e) Argument of pericentre

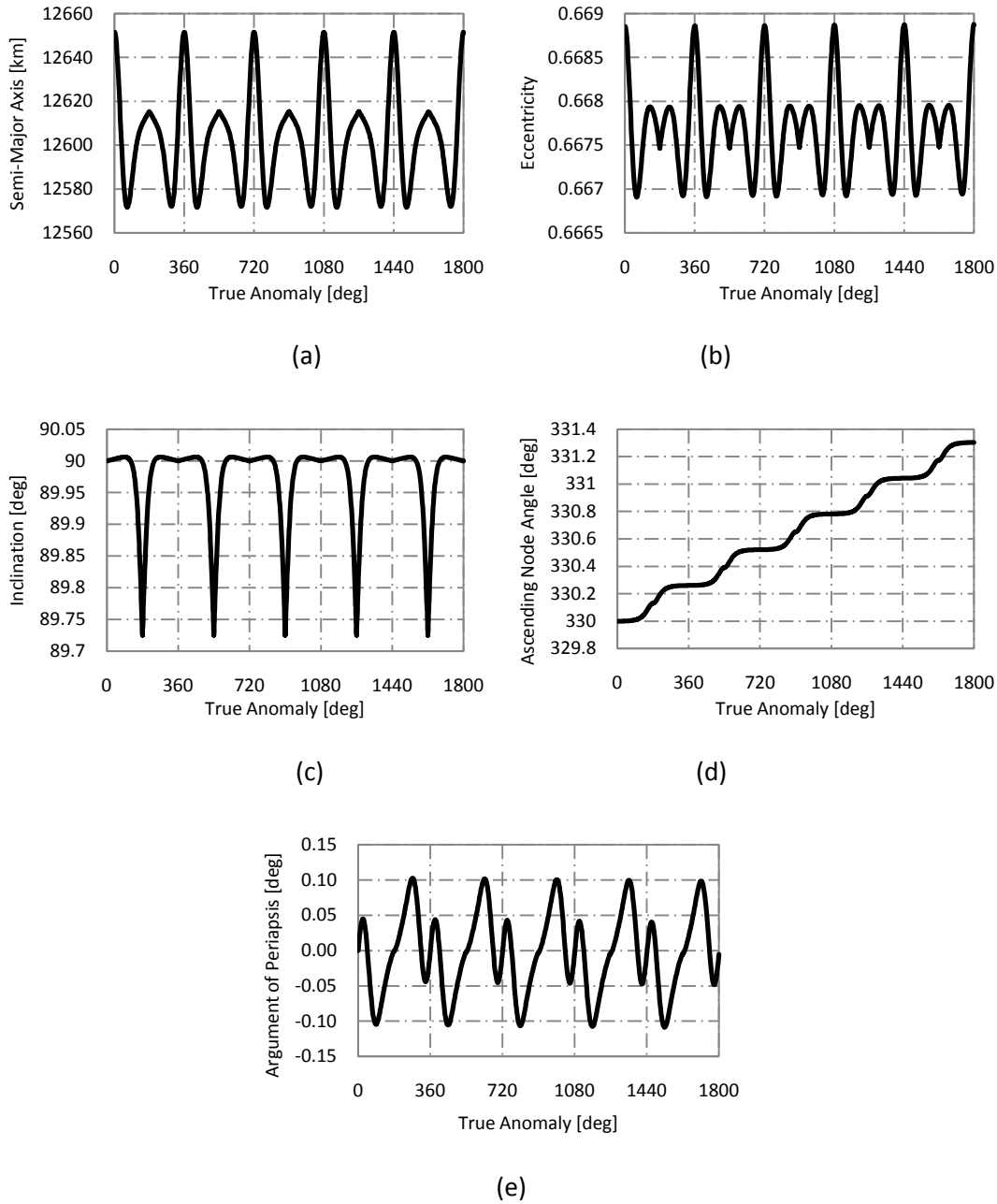

Figure 7-19 Oscillation of orbital elements over five orbital revolutions of a 12 h, *90 degree* inclination, sun-synchronous orbit at Mars (*0 degree* argument of periapsis) (a) Semi-major axis (b) Eccentricity (c) Inclination (d) Ascending node angle (e) Argument of pericentre

7.3 Venus

As stated in **Section 7.1**, like Earth and Mars, orbits at the critical inclination exist at Venus, which can offer benefits for remote sensing. Therefore as with Earth and Mars, low-thrust

propulsion can also be used for the extension of these orbits which is presented in **Section 7.3.1**.

Sun-synchronous orbits on the other hand do not naturally occur at Venus due to the low reciprocal of flattening. Continuous acceleration is therefore considered to enable these orbits where they are otherwise not possible, highlighting the important difference in this work from that of previous chapters. Enabling sun-synchronous orbits could considerably enhance the opportunities for remote sensing at Venus and allow significant simplification of the spacecraft thermal environment.

7.3.1 Highly-Elliptical Orbits

7.3.1.1 General Perturbations Solution

As the gravitational terms of Venus to the order of J_4 are of the same order of magnitude, development of orbits, like at Mars, must therefore include these higher order terms. The extension of the critical inclination at Venus is therefore performed by inserting Eqs. (7.5) - (7.7) into Eq. (3.6), integrating over one orbital revolution, setting the resulting expression equal to zero and solving for the radial and transverse accelerations required to alter the inclination. In these equations J_2, J_3 and J_4 are equal to $4.458x10^{-6}$, $-2.1082x10^{-6}$ and $-2.1471x10^{-6}$ respectively. As higher order gravity terms are significant in the case of Venus, the values of the critical inclination of orbits are dependent on the semi-major axis and eccentricity of the orbit. For example, a 12 h orbit with a pericentre altitude of *800 km* and apocentre altitude of *36,810 km* has critical inclinations of *85.3* and *94.7 degrees,* significantly differing from the natural critical inclination values derived for both Earth and Mars for the same orbital parameters. The radial, transverse and total acceleration magnitude required to alter these values of critical inclination to any inclination, for orbits of varying period and with a constant pericentre altitude of *800 km* are presented in Figure

7-20 - Figure 7-22 for an argument of pericentre of *270 degrees* and in Figure 7-23 - Figure 7-25 for an argument of pericentre of *0 degrees*.

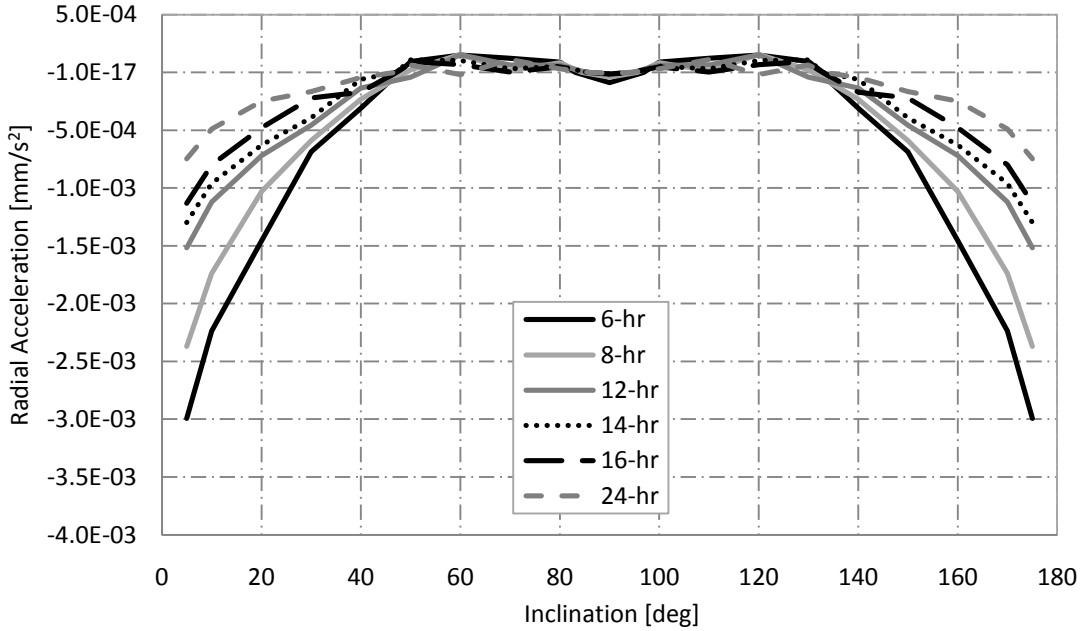

Figure 7-20 Required radial acceleration for the extension of highly-elliptical orbits at Venus - *270 degree* argument of pericentre

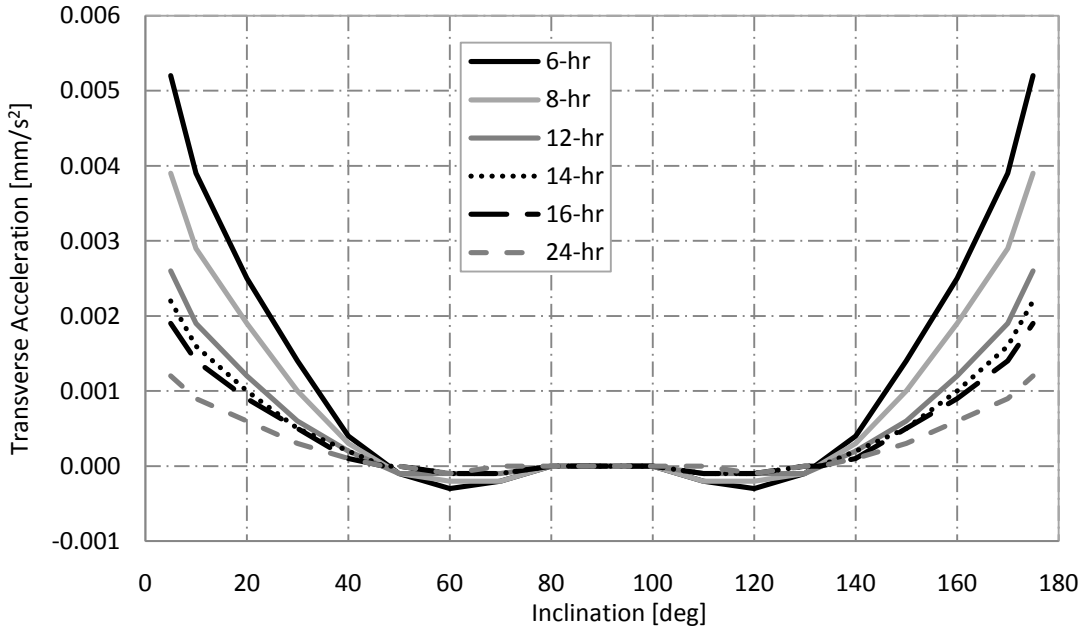

Figure 7-21 Required transverse acceleration for the extension of highly-elliptical orbits at Venus - *270 degree* argument of pericentre

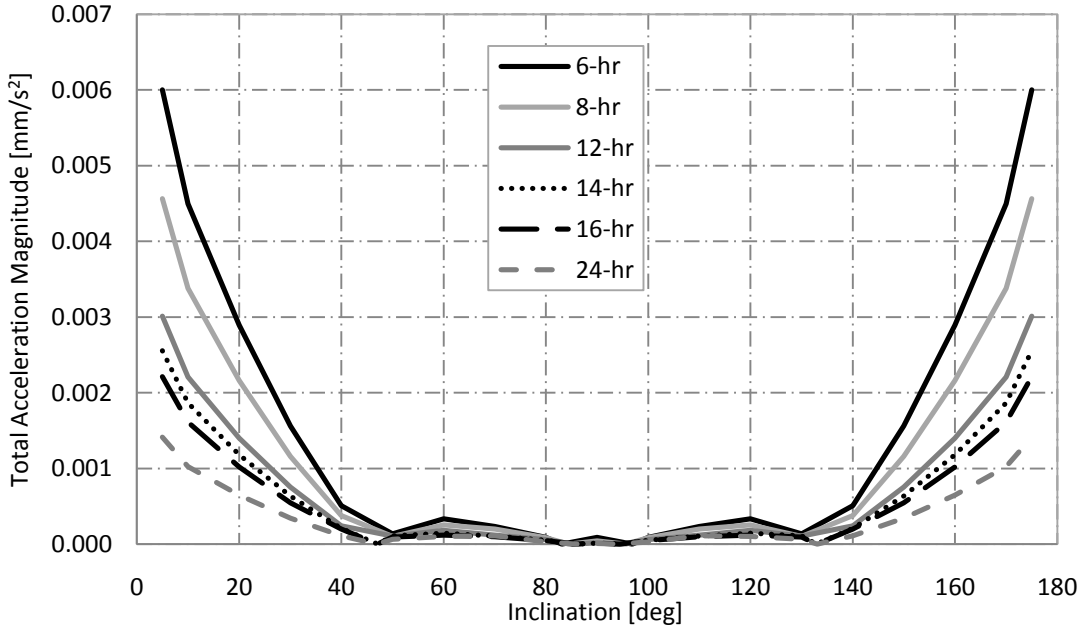

Figure 7-22 Total acceleration magnitude for the extension of highly-elliptical orbits at Venus - *270 degree* argument of pericentre

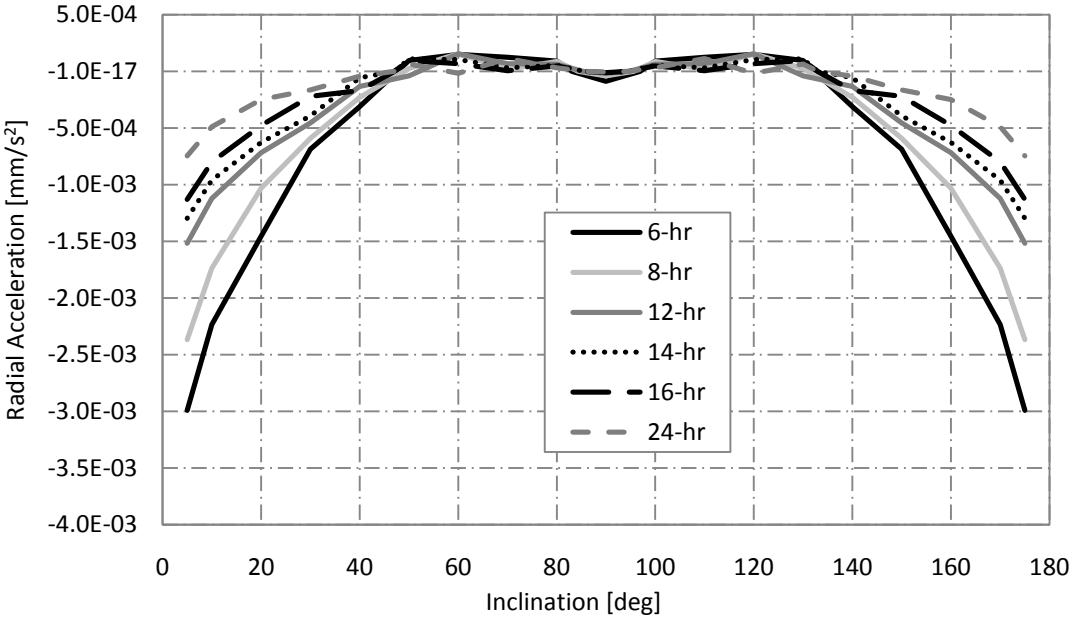

Figure 7-23 Required radial acceleration for the extension of highly-elliptical orbits at Venus - *0 degree* argument of pericentre

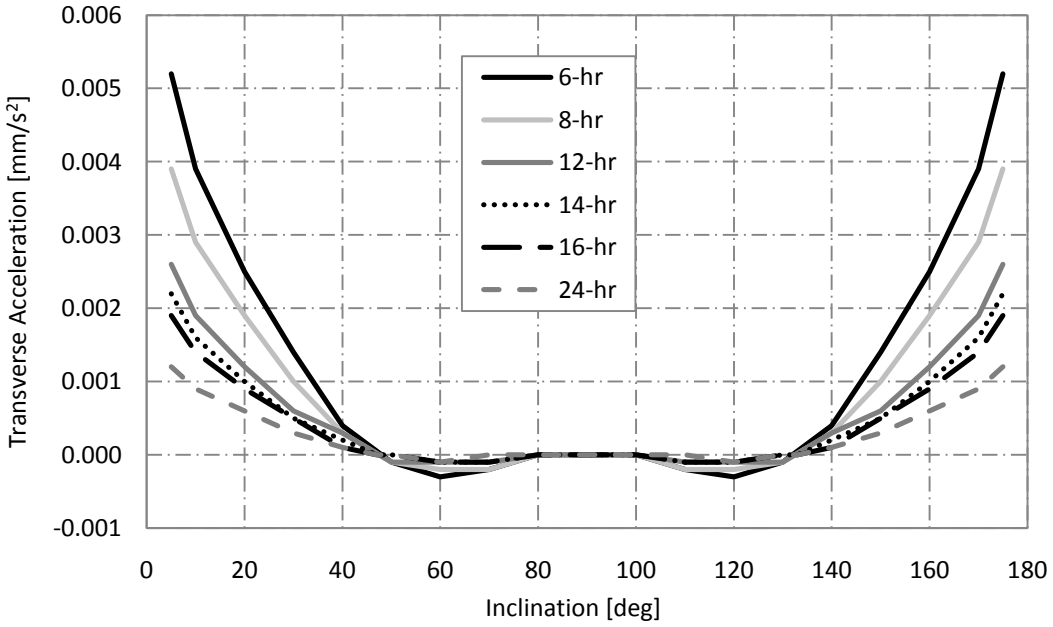

Figure 7-24 Required transverse acceleration for the extension of highly-elliptical orbits at Venus - *0 degree* argument of pericentre

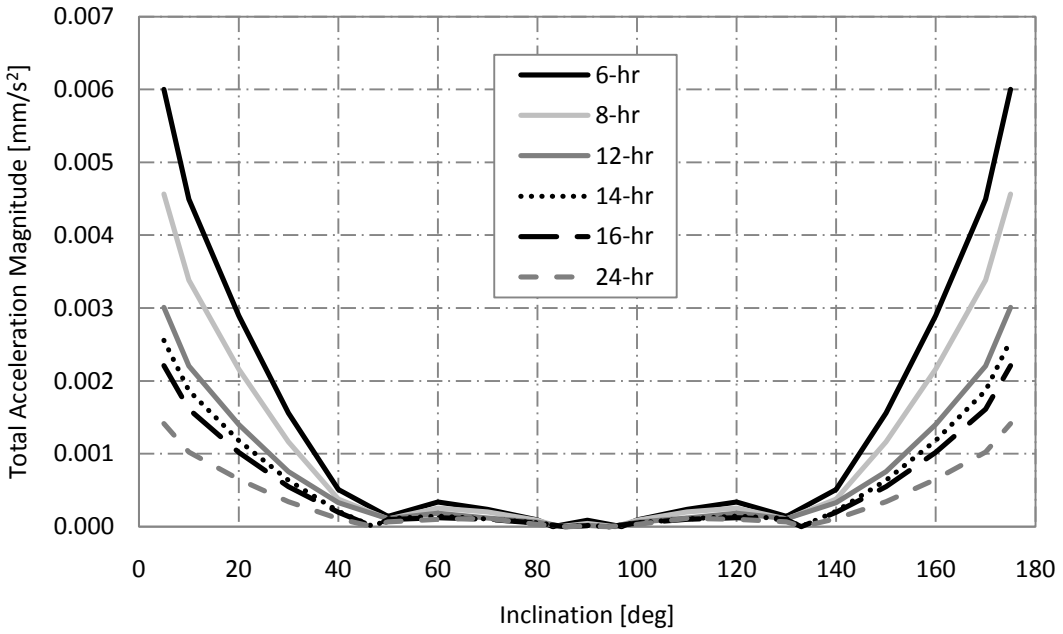

Figure 7-25 Total acceleration magnitude for the extension of highly-elliptical orbits at Venus - *0 degree* argument of pericentre

Comparison of Figure 7-20 - Figure 7-22 with Figure 7-23 - Figure 7-25 for each value of the argument of periapsis shows negligible difference between the magnitude of acceleration required to alter the inclination for each case. Considering an argument of periapsis value of *270 degrees*, to enable a 12 h, *90 degree* inclination orbit requires a total acceleration magnitude of $1.8x10^{-5}$ mm/s^2. For a *1000 kg* spacecraft this corresponds to a considerably low thrust level of *0.0185 mN*.

7.3.1.2 Special Perturbations Solution

The general perturbations solutions are once again validated using a numerical model. A 12 h orbit is selected to demonstrate the special perturbations solution, results of which are given in Figure 7-26 and Figure 7-27 for argument of periapsis values of *270* and *0 degrees* respectively. Once again, the semi-major axis and eccentricity show oscillations over the orbit, but values return to the original value after each revolution of the spacecraft, and both the inclination and ascending node angle show no drift over the orbit. The argument of periapsis in both cases is shown to experience a small drift over the spacecraft orbit,

however, this is only around $-6.3x10^{-4}$ and $-3.5x10^{-4}$ *degrees* per orbit for argument of periapsis values of *270* and *0 degrees* respectively which is thought to be an acceptable cost.

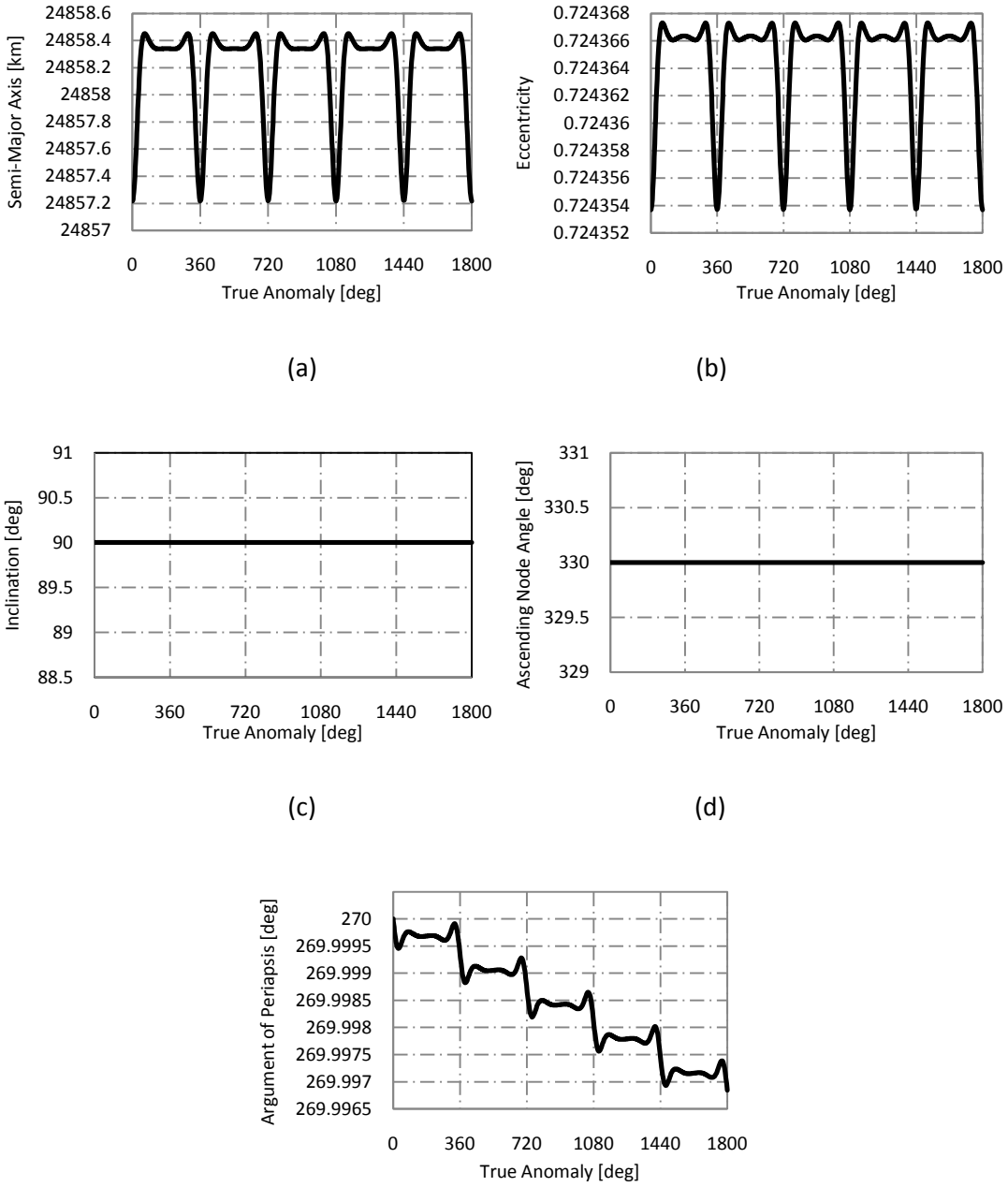

Figure 7-26 Oscillation of orbital elements over five orbital revolutions of a 12 h, *90 degree* inclination orbit at Venus (*270 degree* argument of periapsis) (a) Semi-major axis (b) Eccentricity (c) Inclination (d) Ascending node angle (e) Argument of pericentre

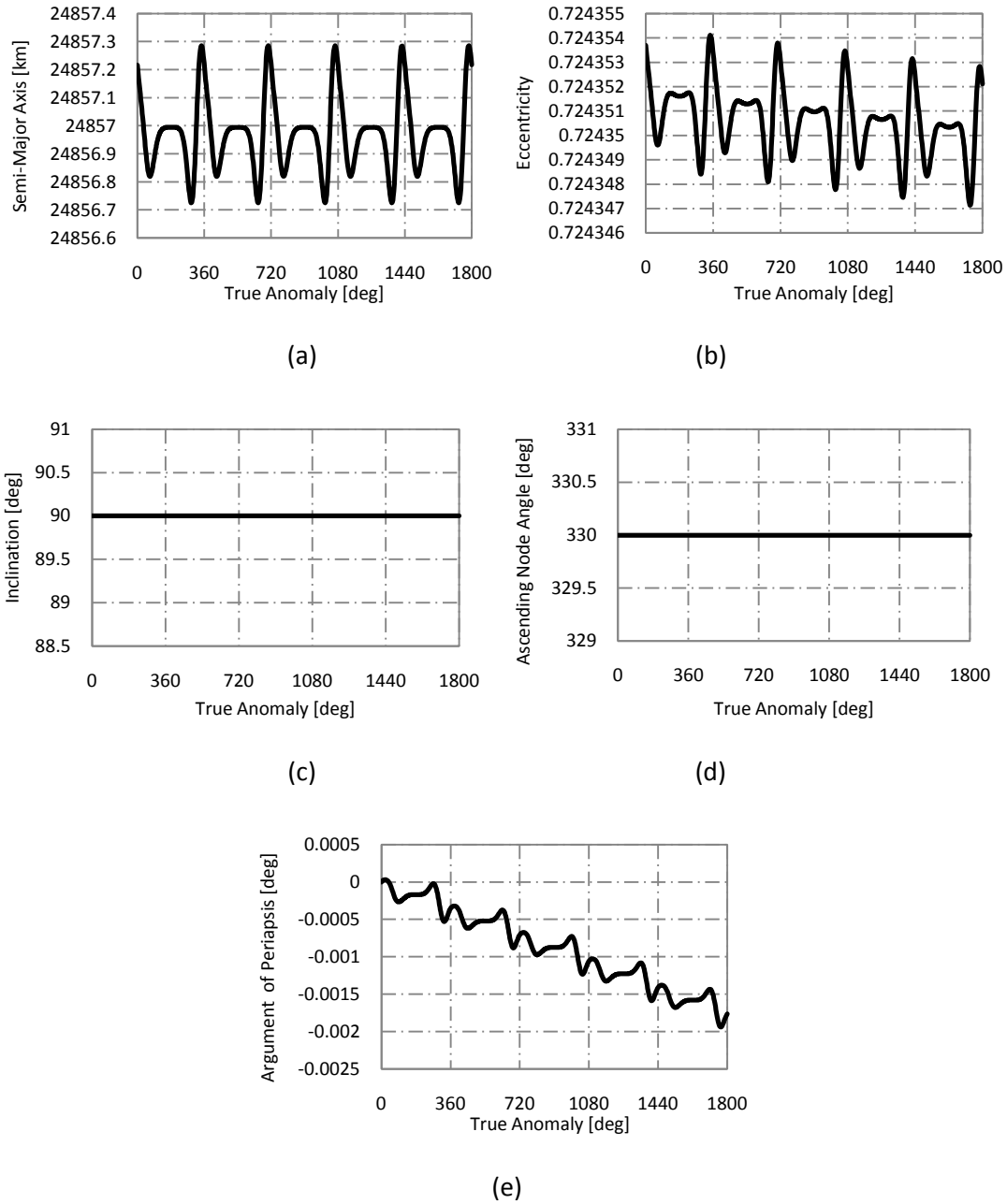

Figure 7-27 Oscillation of orbital elements over five orbital revolutions of a 12 h, *90 degree* inclination orbit at Venus (*0 degree* argument of periapsis) (a) Semi-major axis (b) Eccentricity (c) Inclination (d) Ascending node angle (e) Argument of pericentre

7.3.2 Sun-Synchronous Orbits

As stated previously, natural sun-synchronous orbits do not occur at Venus. **Sections 7.3.2.1** and **7.3.2.2** therefore present the use of continuous acceleration to enable circular

and elliptical sun-synchronous orbits respectively, using low-thrust to achieve a rotation of the ascending node angle of 2π *radians* in *225 days*.

7.3.2.1 Circular Sun-Synchronous Orbits

Eq. (7.13) is once again solved for the normal acceleration required to enable various circular sun-synchronous orbits around Venus and the results subsequently shown in Figure 7-28.

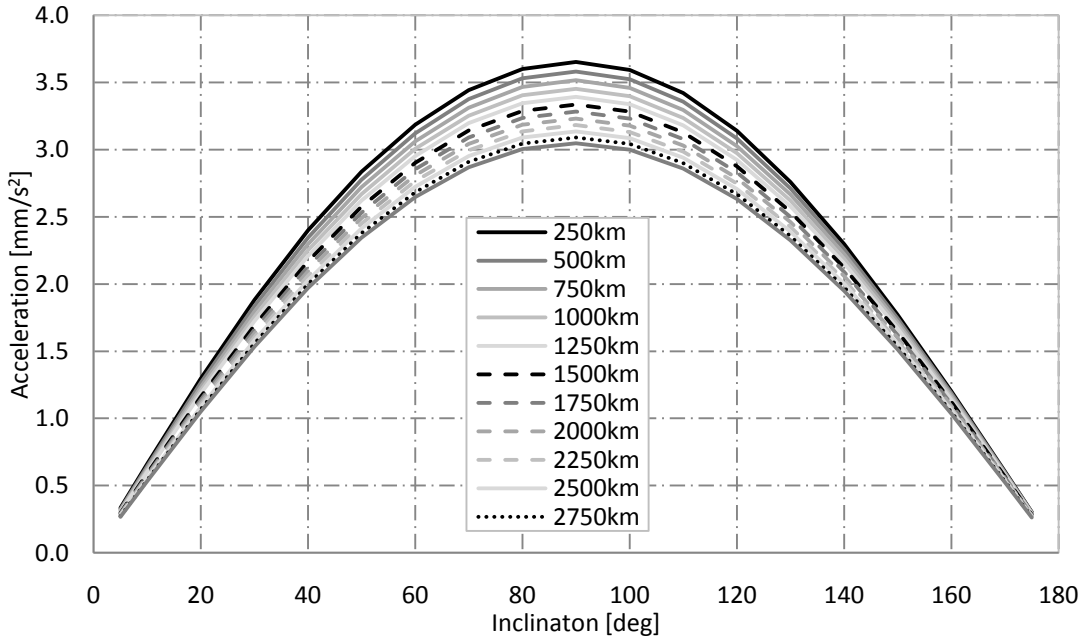

Figure 7-28 Normal acceleration required for the extension of circular sun-synchronous orbits at Venus

In order to enable circular sun-synchronous orbits a significant increase in acceleration magnitude is shown in Figure 7-28 from the extension of the critical inclination solutions. For example, a *1000 km* altitude orbit with an inclination of *90 degrees* requires a significant acceleration of *3.45 mm/s*^{2}.

7.3.2.2 Highly-Elliptical Sun-Synchronous Orbits

7.3.2.2.1 General Perturbations Solution

Once again, two conditions are combined to develop elliptical sun-synchronous orbits around Venus. Eqs. (7.13) and (7.14) are used to determine the normal acceleration necessary to force the required rotation in the ascending node angle, and Eq. (3.21) is used to determine the radial and transverse acceleration necessary to ensure zero change in the argument of periapsis over the orbit. The required radial, transverse, normal and total accelerations are given in Figure 7-29 - Figure 7-32 for an argument of periapsis value of *270 degrees* and in Figure 7-33 - Figure 7-36 for an argument of periapsis value of *0 degrees*.

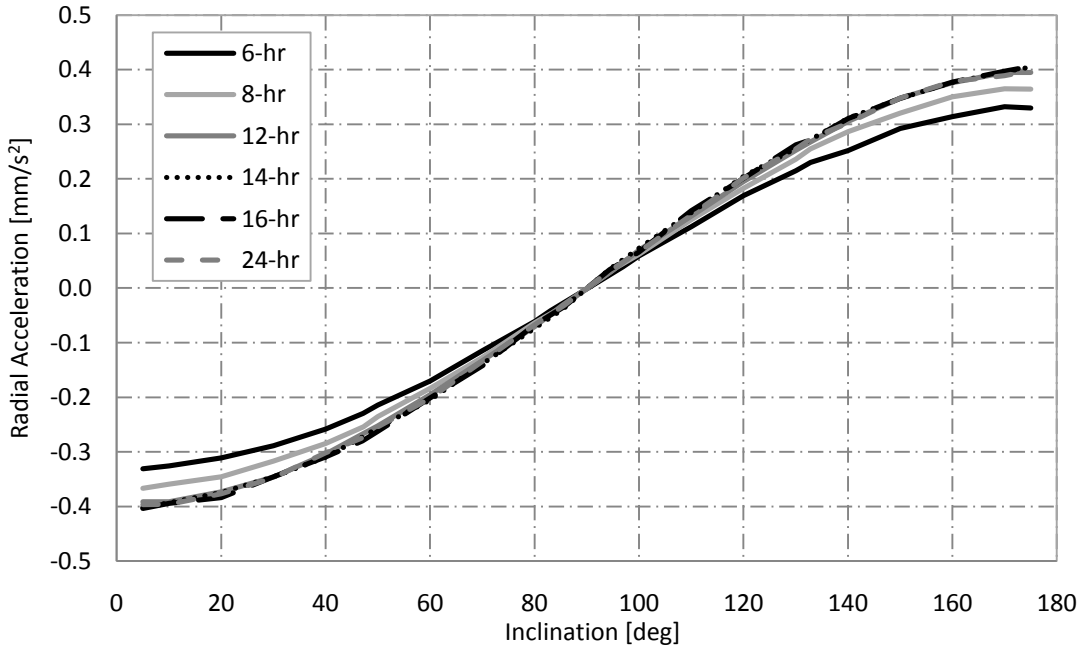

Figure 7-29 Required radial acceleration for the extension of elliptical sun-synchronous orbits at Venus - *270 degree* argument of pericentre

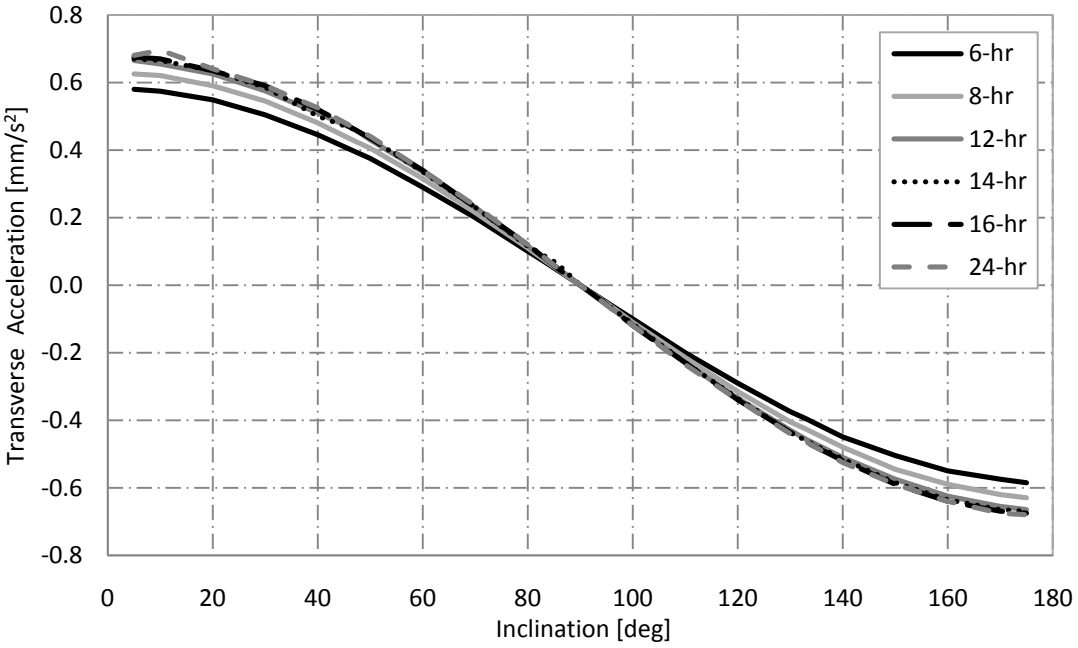

Figure 7-30 Required transverse acceleration for the extension of elliptical sun-synchronous orbits at Venus - *270 degree* argument of pericentre

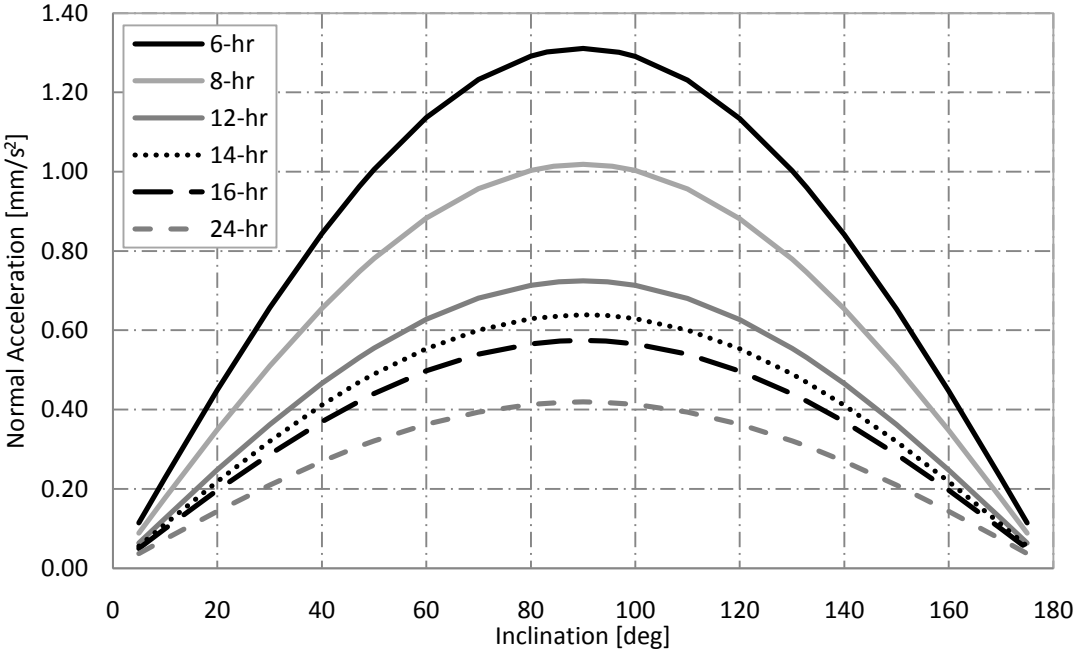

Figure 7-31 Required normal acceleration for the extension of elliptical sun-synchronous orbits at Venus - *270 degree* argument of pericentre

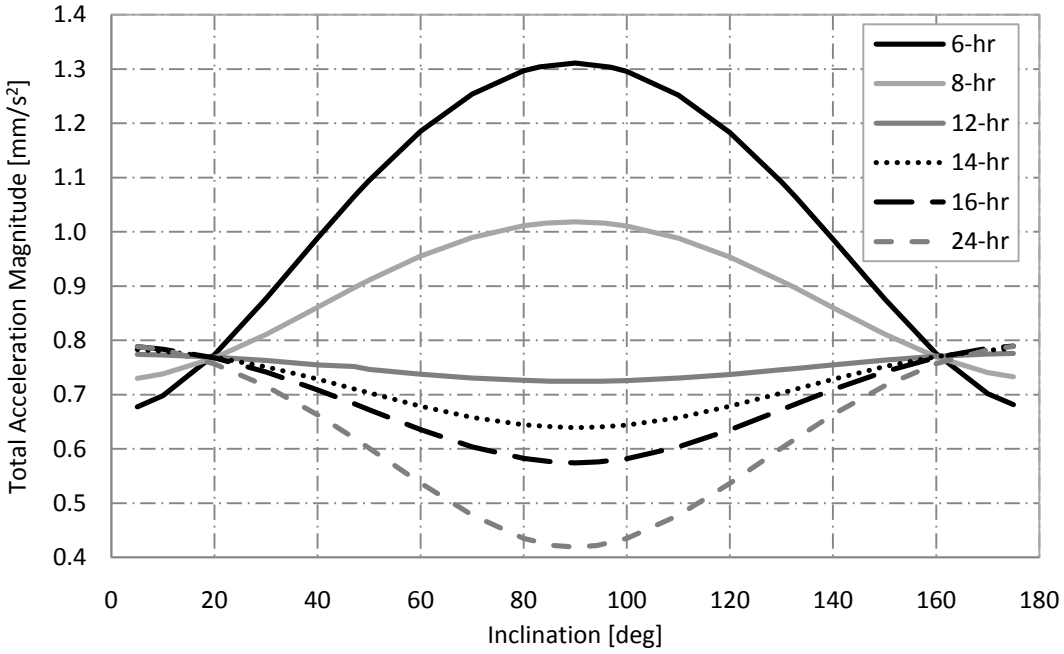

Figure 7-32 Total acceleration required for the extension of elliptical sun-synchronous orbits at Venus - *270 degree* argument of pericentre

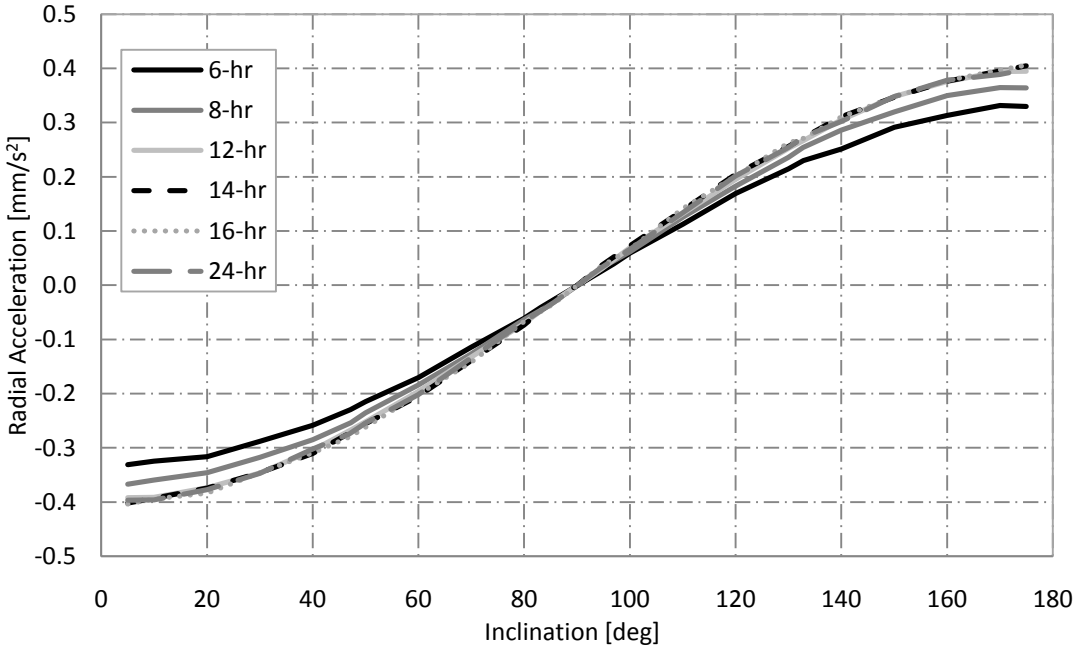

Figure 7-33 Required radial acceleration for the extension of elliptical sun-synchronous orbits at Venus - *0 degree* argument of pericentre

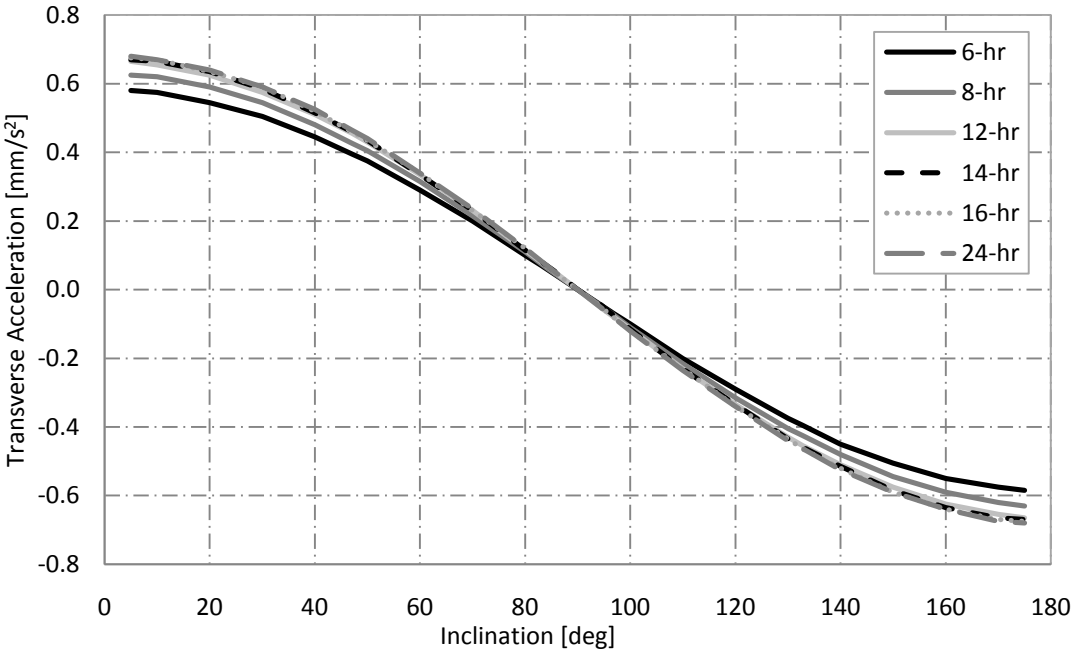

Figure 7-34 Required transverse acceleration for the extension of elliptical sun-synchronous orbits at Venus - *0 degree* argument of pericentre

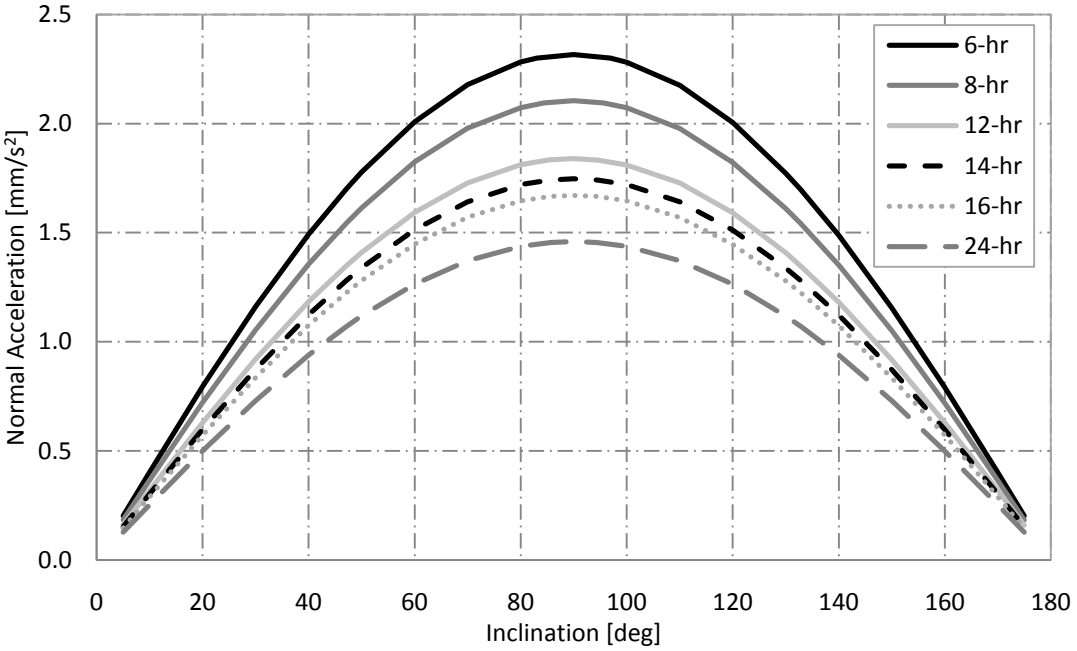

Figure 7-35 Required normal acceleration for the extension of elliptical sun-synchronous orbits at Venus - *0 degree* argument of pericentre

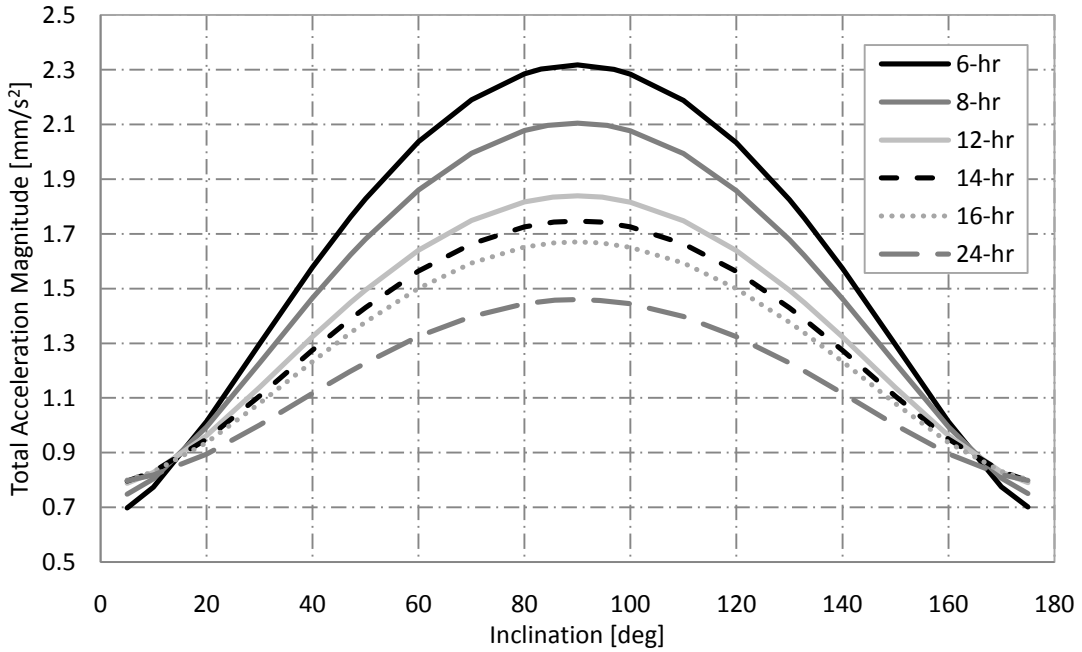

Figure 7-36 Total acceleration required for the extension of elliptical sun-synchronous orbits at Venus - *0 degree* argument of pericentre

Examination of Figure 7-32 and Figure 7-36 illustrates the increase in acceleration magnitude required to enable elliptical sun-synchronous orbits over simply an extension of the critical inclination for each argument of periapsis value shown in Figure 7-22 and Figure 7-25. Considering a 12 h orbit with an argument of periapsis of *270 degrees* and *90 degree* inclination requires an acceleration magnitude of *0.724 mm/s²*, corresponding to *724 mN* of thrust for a *1000 kg* spacecraft, which is currently beyond the capabilities of existing low-thrust propulsion systems. Development in EP thruster capabilities is therefore required before these orbits can become feasible.

7.3.2.2.2 Special Perturbations Solution

Figure 7-37 and Figure 7-38 give the variation of orbital elements for 12 h elliptical sun-synchronous orbits at Venus, with argument of periapsis values of *270* and *0 degrees* respectively as a result of numerical simulations. The required change in ascending node

angle of *0.8 degrees* per orbit is shown to be achieved, with negligible changes in semi-major axis, eccentricity and inclination over each orbital revolution. As was the case with the extension of the critical inclination at Venus (Figure 7-26 and Figure 7-27), a small drift in the argument of periapsis is found when enabling elliptical sun-synchronous orbits. A drift in ω of $1.12x10^{-3}$ and $-3.21x10^{-3}$ *degrees* per orbit is detected for argument of periapsis values of *270* and *0 degrees* respectively, which equates to around *0.5* and *1.5 degrees* per Venusian year. This is once again expected to be an acceptable cost. The slight increase in the drift of the argument of periapsis exhibited for elliptical sun-synchronous orbits at Venus is caused by the oscillation of the semi-major axis, eccentricity and inclination in this case, which has an impact on the argument of periapsis. The analytical solution makes the assumption that the changes in all elements are zero; the numerical simulation however indicates that in this case this assumption begins to break down.

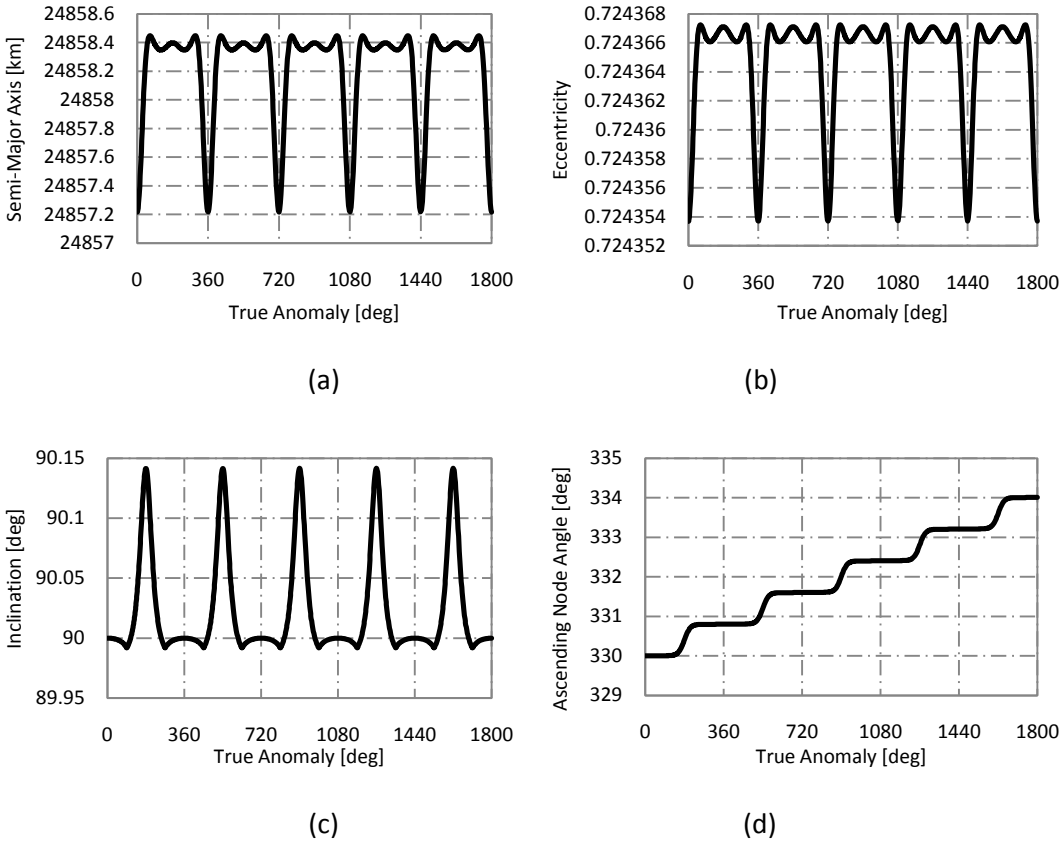

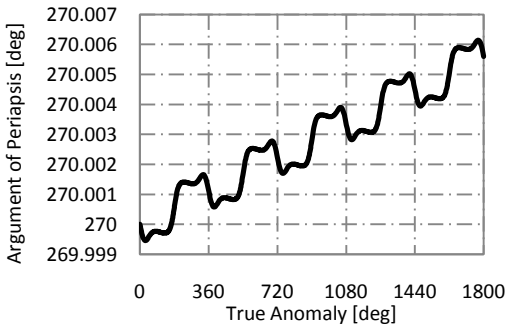

(e)

Figure 7-37 Oscillation of orbital elements over five orbital revolutions of a 12 h, *90 degree* inclination, sun-synchronous orbit at Venus (*270 degree* argument of periapsis) (a) Semi-major axis (b) Eccentricity (c) Inclination (d) Ascending node angle (e) Argument of pericentre

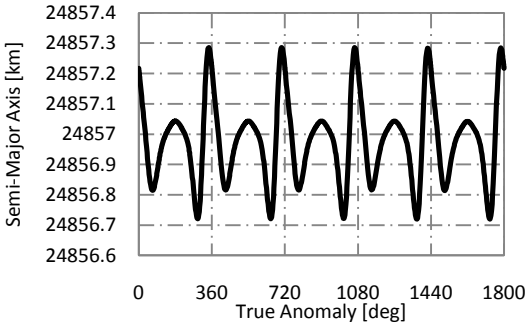

(a)

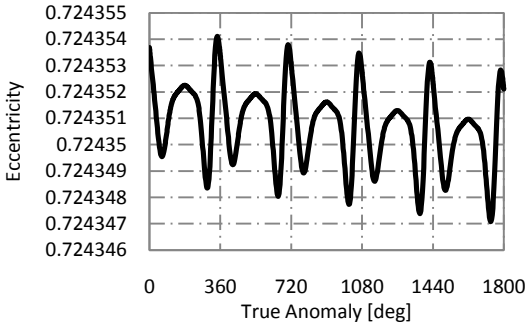

(b)

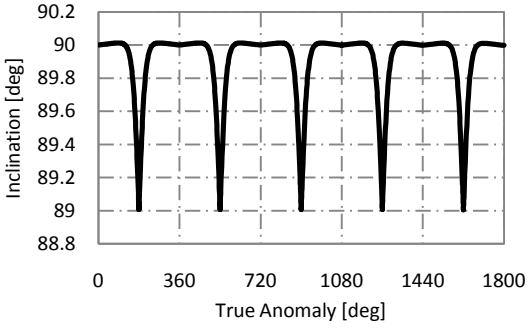

(c)

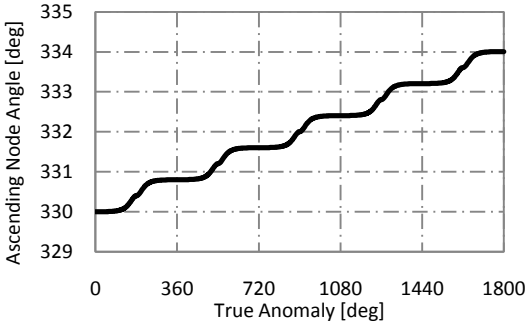

(d)

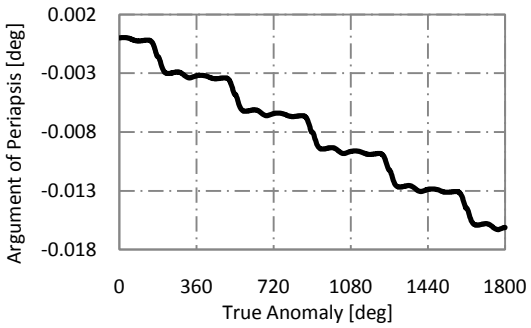

(e)

Figure 7-38 Oscillation of orbital elements over five orbital revolutions of a 12 h, *90 degree* inclination, sun-synchronous orbit at Venus (*0 degree* argument of periapsis) (a) Semi-major axis (b) Eccentricity (c) Inclination (d) Ascending node angle (e) Argument of pericentre

7.4 Mercury

Mercury is the final planet under consideration. In a similar way to the analysis presented for Venus the extension of orbits at the critical inclination is presented in **Section 7.4.1**, and the use of low-thrust to enable circular and elliptical sun-synchronous orbits which do not naturally exist at Mercury is presented in **Sections 7.4.2.1** and **7.4.2.2** respectively. These newly developed orbits can once again increase the opportunities for remote sensing, and sun-synchronous orbits can offer simplification of the spacecraft operations in terms of the thermal environment. It is noted that previous work has considered the use of solar sails to generate sun-synchronous orbits at Mercury with the MESSAGE mission proposed in 1996 [63].

7.4.1 Highly-Elliptical Orbits

As Mercury is the least explored planet of the inner Solar System, detailed gravity field information is not yet available. This section therefore considers spacecraft motion about Mercury using gravity perturbations to the order of J_2 only, where J_2 is equal to $6x10^{-5}$ [160].

It is therefore expected that the accuracy of this work could be significantly enhanced by the inclusion of higher order gravity terms when these become available. This issue addressed in the future work section of this thesis in **Chapter 8**. As perturbations only include J_2 terms, the derivation of the natural critical inclination of orbits at Mercury is the same as that at Earth (from Eq. (3.14)) and therefore the critical inclination values are *63.43* and *116.6 degrees* irrespective of the orbit semi-major axis and eccentricity. It is expected that these values will change significantly when higher order gravity terms are included.

7.4.1.1.1 General Perturbations Solution

The extension of the critical inclination at Mercury is conducted using Eq. (3.21) where the gravity perturbation is given in Eq. (3.14) and radial and transverse acceleration components are given by Eqs. (3.22) and (3.23) respectively. The radial, transverse and total accelerations required to extend the inclination to a range of values, for various orbit periods with a constant periapsis altitude of *800 km* are given in Figure 7-39 - Figure 7-41 respectively.

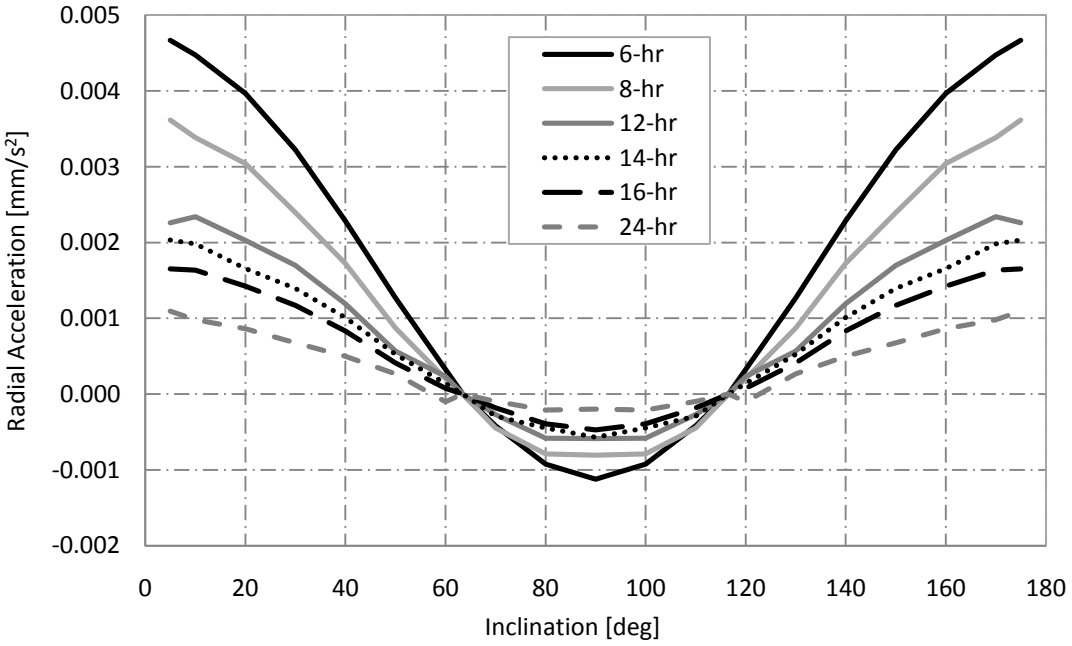

Figure 7-39 Required radial acceleration for the extension of highly-elliptical orbits at Mercury

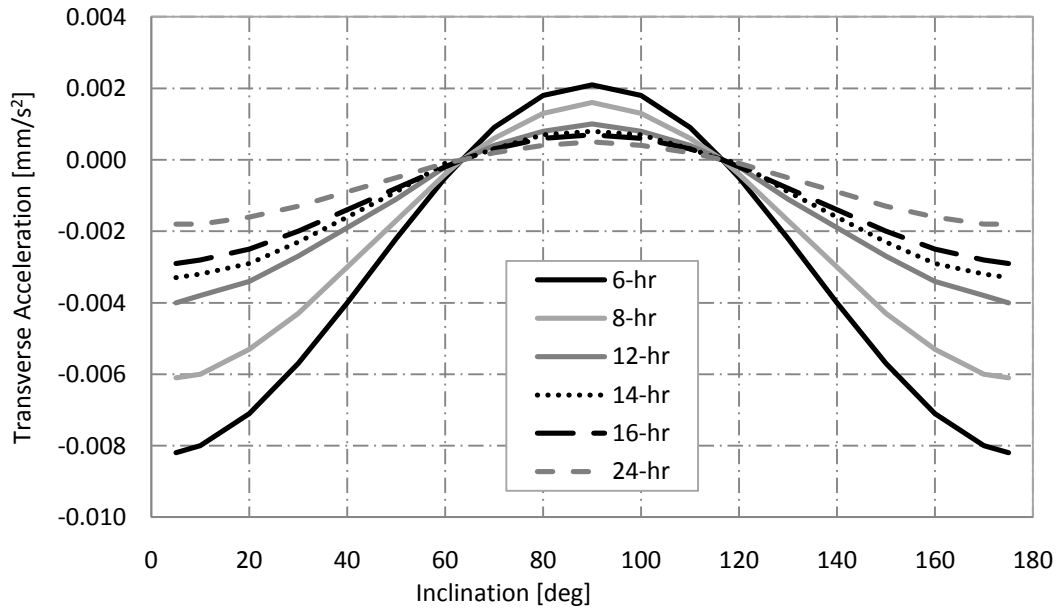

Figure 7-40 Required transverse acceleration for the extension of highly-elliptical orbits at Mercury

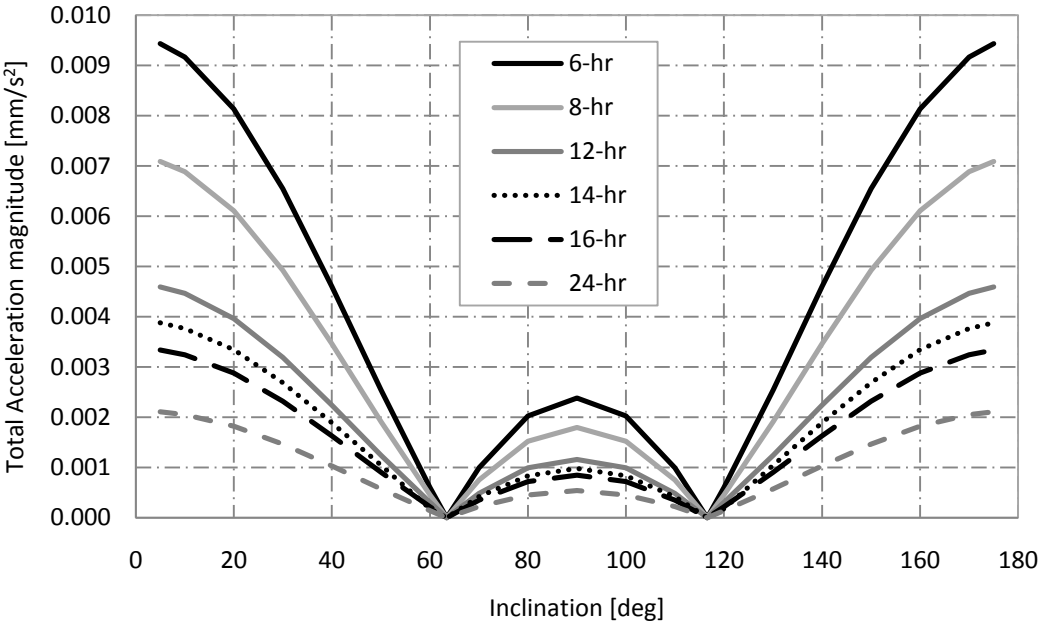

Figure 7-41 Total acceleration magnitude for the extension of highly-elliptical orbits at Mercury

Figure 7-41 shows curves of minimum total acceleration consisting of unequal radial and transverse components (from Figure 7-39 and Figure 7-40) to alter the critical inclination of the orbits to a wide range of values. It is shown that to enable all of the considered orbits, very small acceleration magnitudes are required. For example, considering a 12 h orbit with an inclination of *90 degrees* requires a total acceleration magnitude of *0.0012 mm/s²*. This equates to *1.2 mN* of thrust for a 1-ton spacecraft, which can be provided by the QinetiQ T5 thruster which is capable of providing thrust levels between *1* and *20 mN* [84].

7.4.1.1.2 Special Perturbations Solution

The general perturbations solution is validated using the same numerical model used throughout the thesis. The results are shown for five revolutions of a spacecraft on a 12 h orbit with an inclination of *90 degrees* in Figure 7-42. No variation in the inclination and ascending node angle is illustrated for the extension of the critical inclination at Mercury.

Oscillations in the semi-major axis, eccentricity and argument of periapsis are also displayed and show no variation over each orbit revolution.

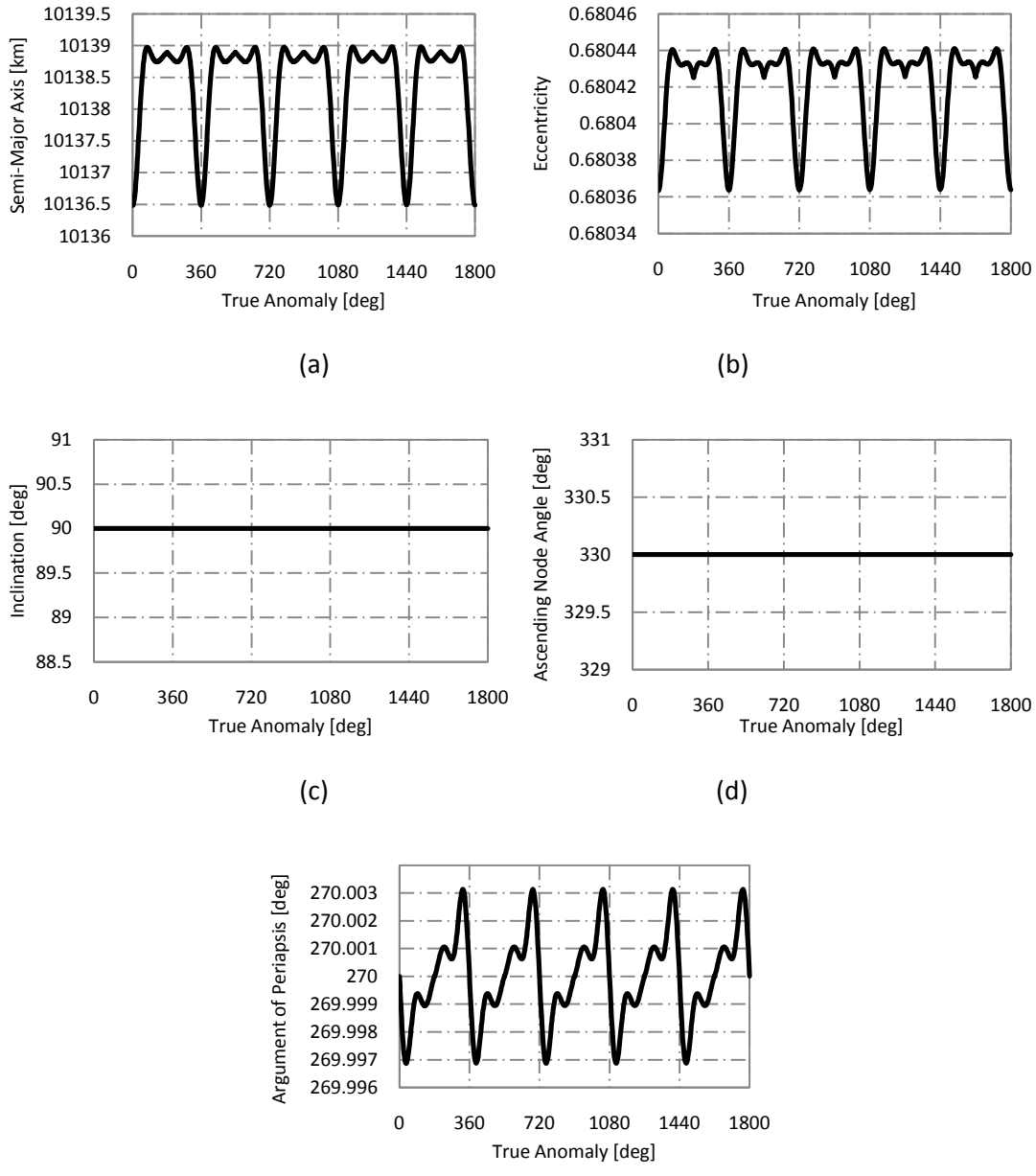

Figure 7-42 Oscillation of orbital elements over five orbital revolutions of a 12 h, *90 degree* inclination elliptical orbit at Mercury (a) Semi-major axis (b) Eccentricity (c) Inclination (d) Ascending node angle (e) Argument of pericentre

7.4.2 Sun-Synchronous Orbits

7.4.2.1 Circular Sun-Synchronous Orbits

The development of circular sun-synchronous orbits at Mercury is achieved via the addition of out-of-plane acceleration to the equation for the rate of change of ascending node angle (Eq. (7.13)). Perturbations only to the order of J_2 are included and the ascending node angle in this instance is required to rotate 2π *radians* in *88 days,* the required acceleration is shown in Figure 7-43 for various orbit altitudes.

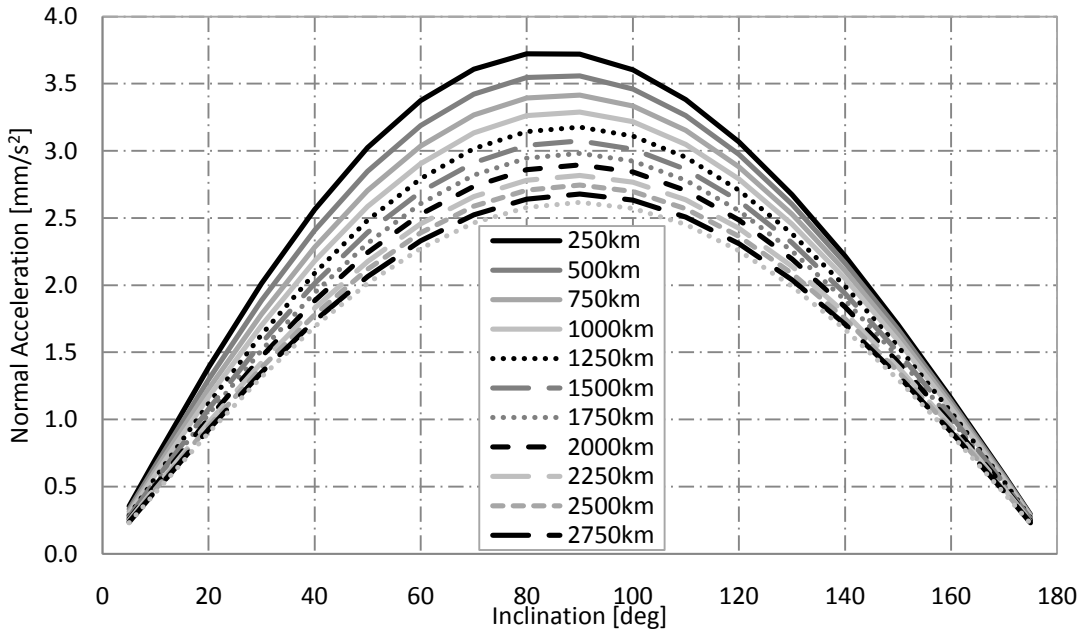

Figure 7-43 Normal acceleration required for the extension of circular sun-synchronous orbits at Mercury

It is clear from Figure 7-43 that low-thrust propulsion could potentially be used to enable circular sun-synchronous orbits at Mercury where they otherwise do not naturally occur. This being said, the acceleration required to enable these orbits is significantly higher than is required to alter the critical inclination, and is shown to be comparable to that required

to enable circular sun-synchronous orbits at Venus, from Figure 7-28. For example, a *1000 km* altitude orbit inclined at *90 degrees* requires *3.29 mm/s*^{2} of acceleration.

7.4.2.2 Highly-Elliptical Sun-Synchronous Orbits

7.4.2.2.1 General Perturbations Solution

As the development of orbits at Mercury only includes gravity terms to the order of J_2, Eqs. (3.39) and (3.40) used for the extension of sun-synchronous orbits at Earth give the change in ascending node angle for argument of periapsis values of *0* and *270 degrees* respectively. Eq. (3.21) is then used to ensure zero rate of change of argument of periapsis over the orbit, where the normal acceleration components for argument of pericentre values of *0* and *270 degrees* and given by Eqs. (3.24) and (3.25) respectively. The required accelerations in each axis and the corresponding total acceleration magnitude are presented for orbits with a constant pericentre altitude of *800 km* in Figure 7-44 - Figure 7-47 where an argument of periapsis value of *270 degrees,* is considered and in Figure 7-48 - Figure 7-51 for an argument of periapsis value of *0 degrees*.

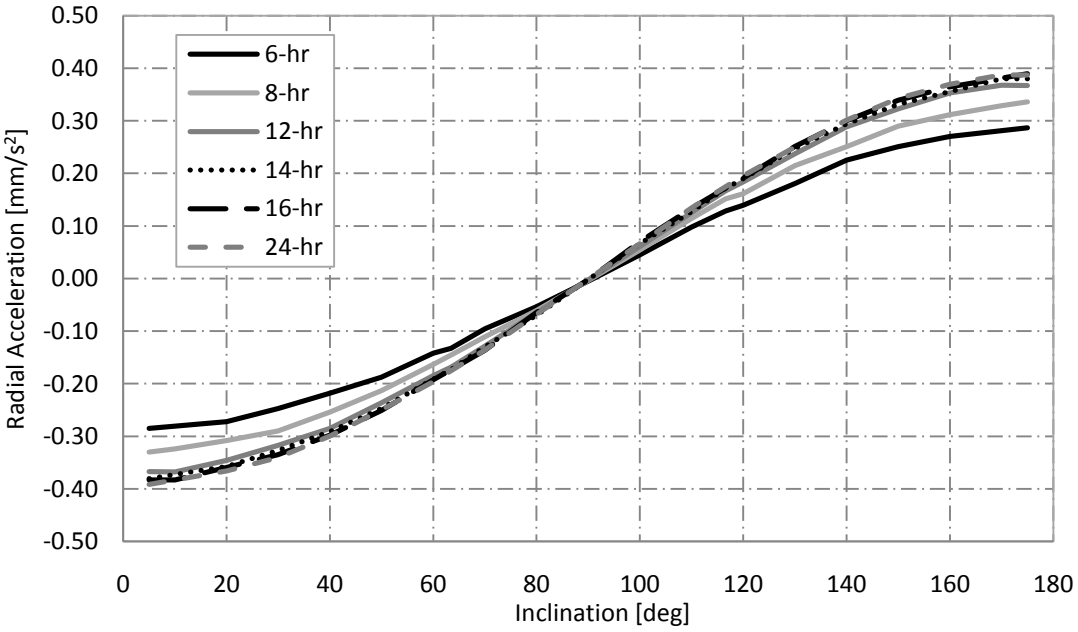

Figure 7-44 Required radial acceleration for the extension of elliptical sun-synchronous orbits at Mercury - *270 degree* argument of pericentre

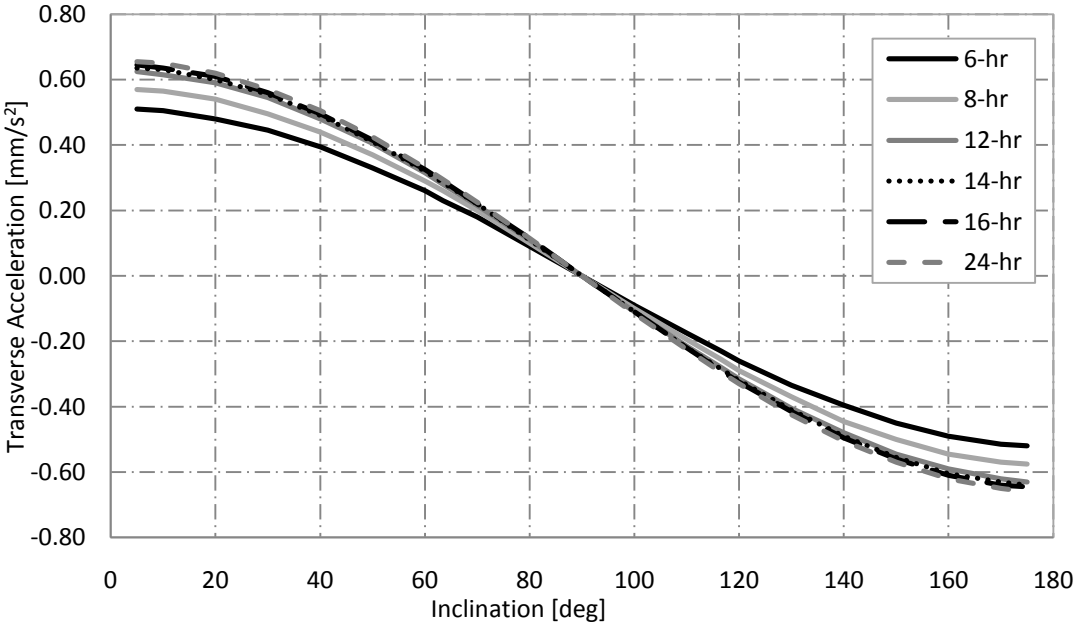

Figure 7-45 Required transverse acceleration for the extension of elliptical sun-synchronous orbits at Mercury - *270 degree* argument of pericentre

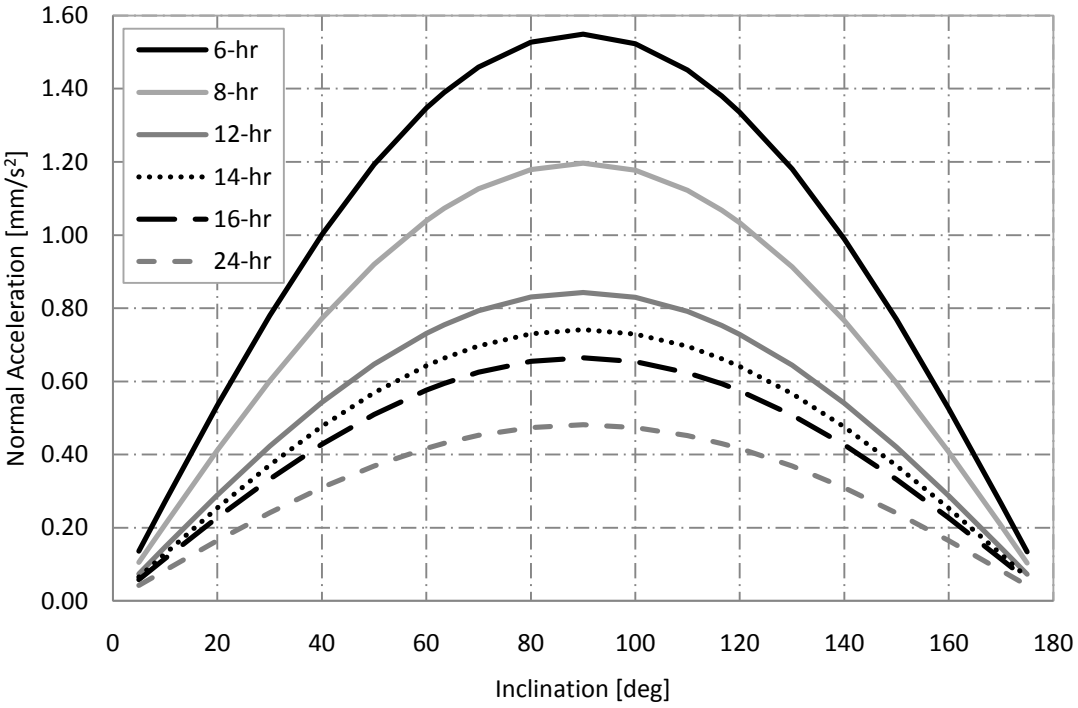

Figure 7-46 Required normal acceleration for the extension of elliptical sun-synchronous orbits at Mercury - *270 degree* argument of pericentre

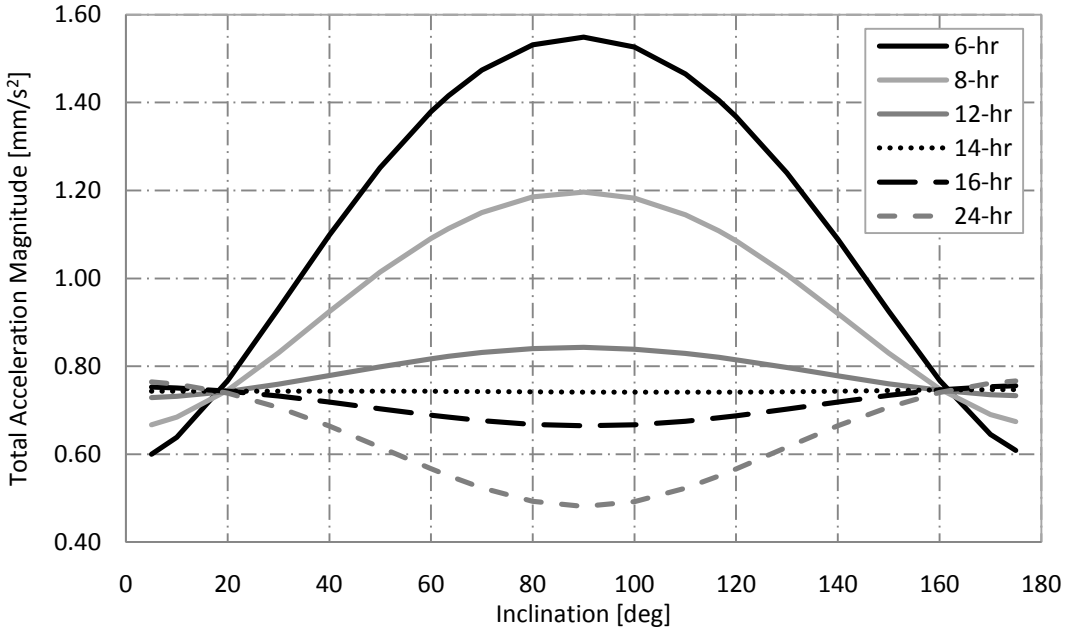

Figure 7-47 Total acceleration required for the extension of elliptical sun-synchronous orbits at Mercury - *270 degree* argument of pericentre

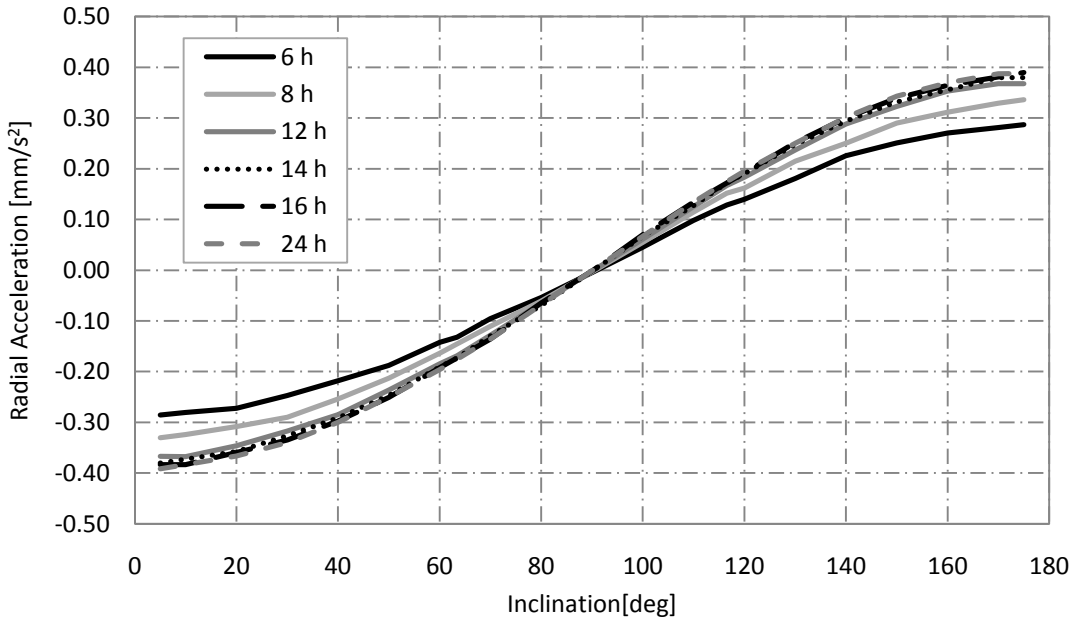

Figure 7-48 Required radial acceleration for the extension of elliptical sun-synchronous orbits at Mercury - *0 degree* argument of pericentre

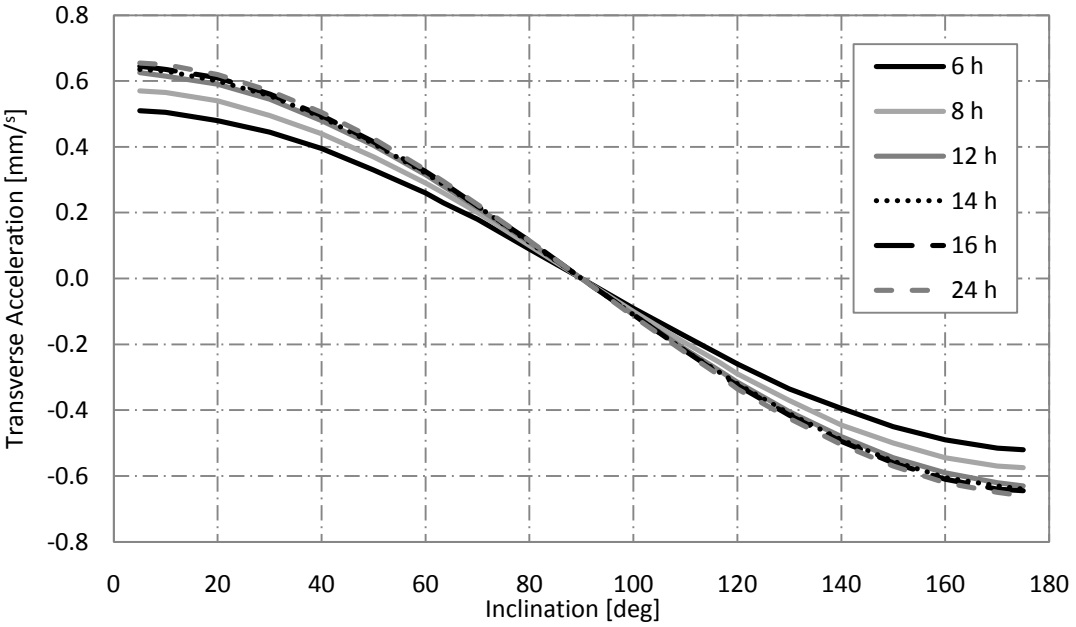

Figure 7-49 Required transverse acceleration for the extension of elliptical sun-synchronous orbits at Mercury - *0 degree* argument of pericentre

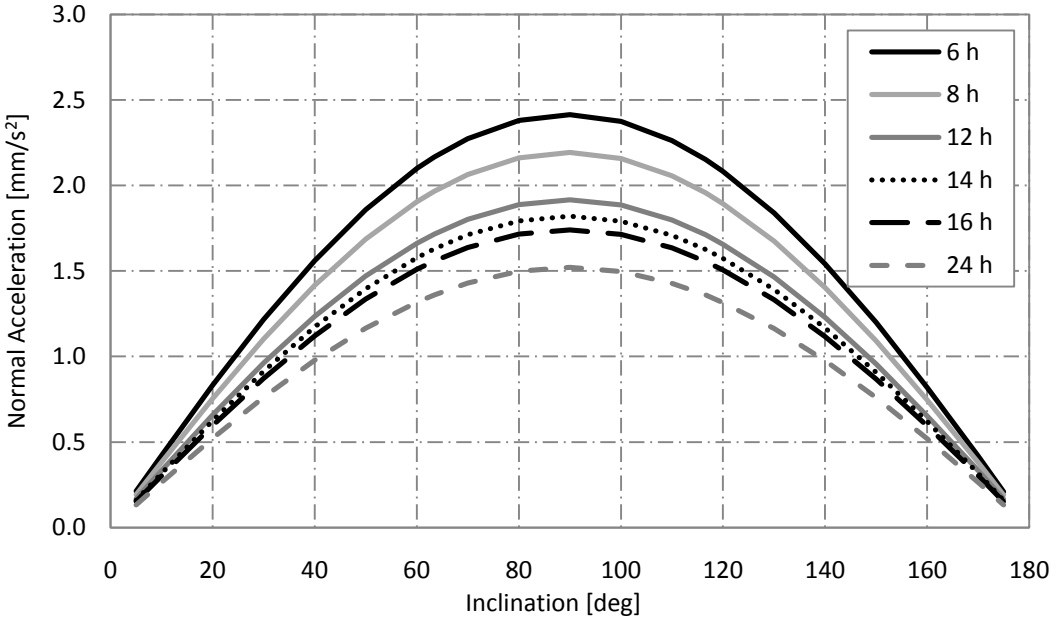

Figure 7-50 Required normal acceleration for the extension of elliptical sun-synchronous orbits at Mercury - *0 degree* argument of pericentre

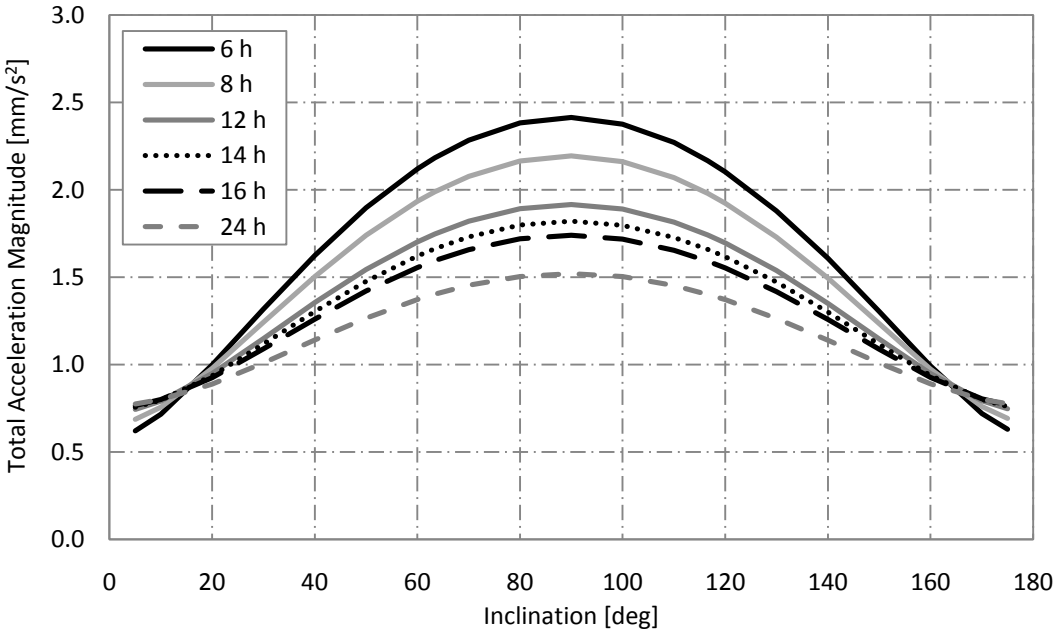

Figure 7-51 Total acceleration required for the extension of elliptical sun-synchronous orbits at Mercury - *0 degree* argument of pericentre

From Figure 7-44 - Figure 7-51 it is shown that the acceleration magnitudes required to enable elliptical sun-synchronous orbits at Mercury are comparable to those required at Venus. The required magnitudes are, however, shown to be out with the capabilities of current electric propulsion systems. Considering an argument of periapsis value of *270 degrees,* a 12 h elliptical sun-synchronous orbit inclined at *90 degrees* to the equator requires an acceleration magnitude of *0.84 mm/s*^{2} or *840 mN* of thrust for a *1000 kg* spacecraft.

7.4.2.2.2 Special Perturbations Solution

Numerical simulations are again run for comparison with the general perturbations solution. The evolution of the orbital elements over five revolutions are shown in Figure 7-52 and Figure 7-53 for argument of periapsis values of *270* and *0 degrees* respectively. The results presented show negligible change in the semi-major axis, eccentricity and inclination in each case, with the rotation of the ascending node shown to agree with the analytical solutions with a rotation of around *2 degrees* per orbit. However, as was the case with Venus, a small drift in the argument of periapsis is exhibited, with a drift of around *0.01 degrees* per orbit for an argument of periapsis of *270 degrees* and *-0.017 degrees per orbit* for an argument of periapsis of *0 degrees*. Although a drift is shown in each case, these amount to less than *2 degrees* and less than *3 degrees* per Mercury year respectively, which is expected to be an acceptable cost. This drift is again caused by the oscillation in semi-major axis, eccentricity and inclination in the numerical solution, which is assumed to be negligable in the analytical solution. The numerical simulation therefore highlights that this assumption begins to breakdown in this case.

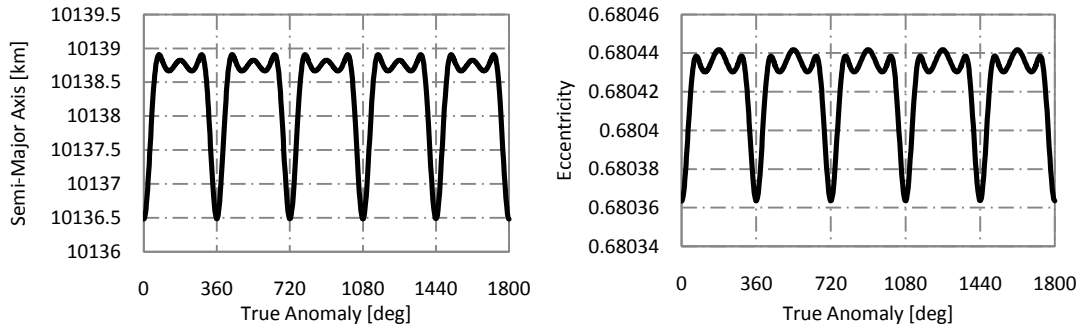

(a)

(b)

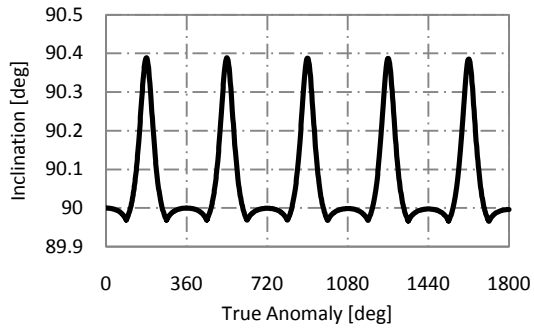

(c)

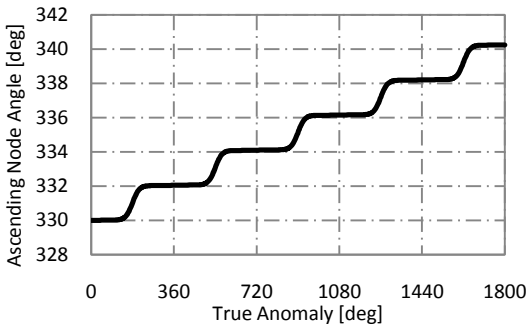

(d)

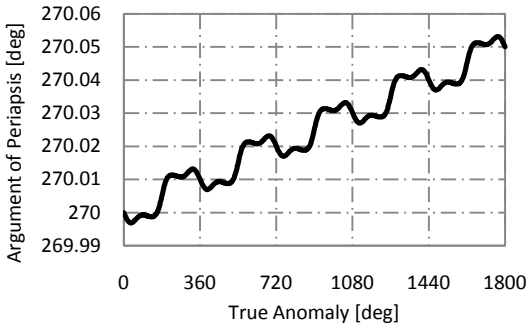

(e)

Figure 7-52 Oscillation of orbital elements over five orbital revolutions of a 12 h, *90 degree* inclination, sun-synchronous orbit at Mercury (*270 degree* argument of periapsis) (a) Semi-major axis (b) Eccentricity (c) Inclination (d) Ascending node angle (e) Argument of pericentre

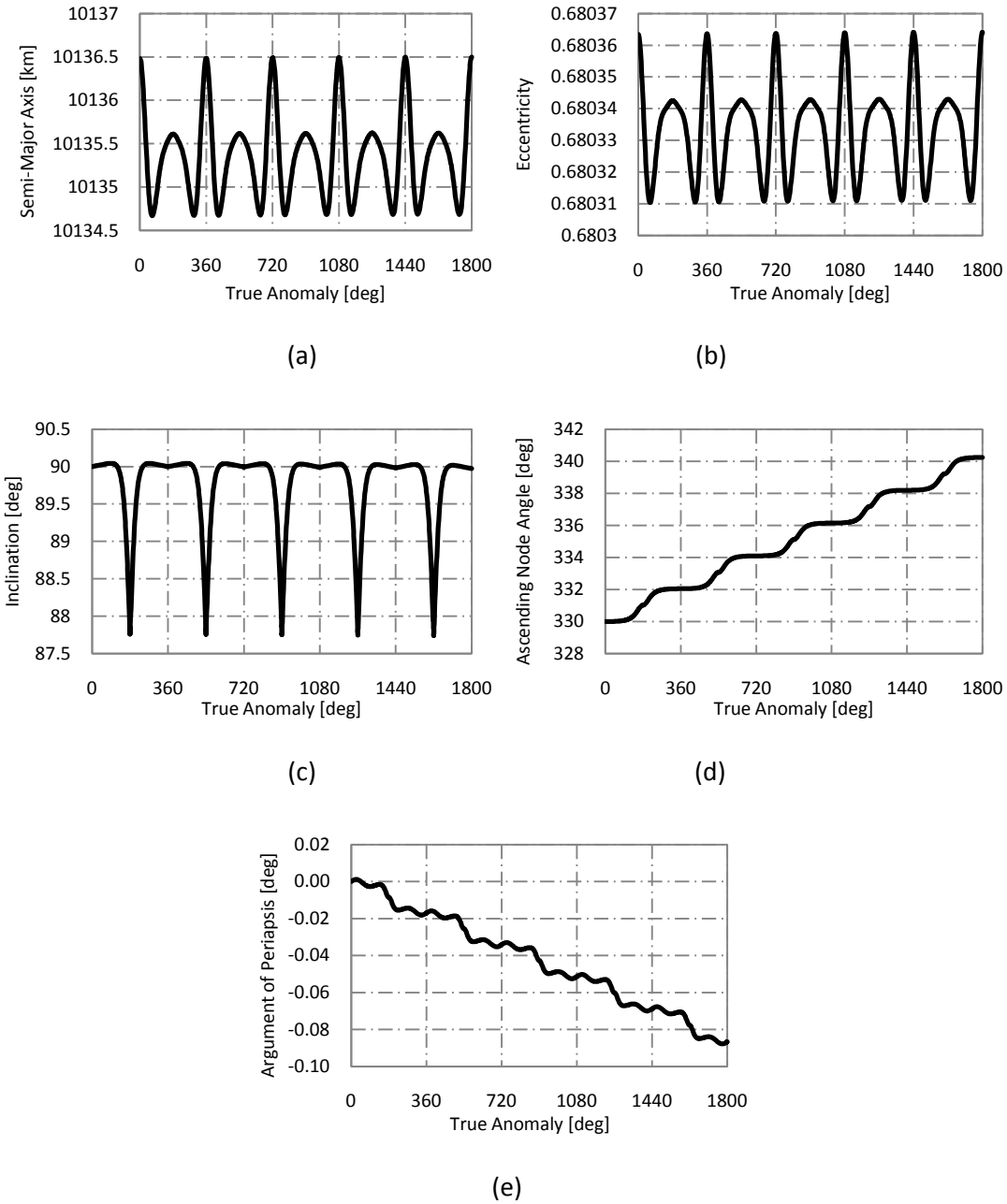

Figure 7-53 Oscillation of orbital elements over five orbital revolutions of a 12 h, *90 degree* inclination, sun-synchronous orbit at Mercury (*0 degree* argument of periapsis) (a) Semi-major axis (b) Eccentricity (c) Inclination (d) Ascending node angle (e) Argument of pericentre

7.5 Summary

The importance of exploration of the inner planets of the Solar System to aid the understanding of the formulation of Earth and other planetary bodies, to determine whether extra-terrestrial habitable environments exist in the Solar System, and for technology innovation has been highlighted in this chapter.

Continuous low-thrust propulsion has therefore been shown to extend highly-elliptical orbits at the critical inclination at Mars, Mercury and Venus; extend sun-synchronous orbits at Mars; and to enable circular and elliptical sun-synchronous orbits at Mercury and Venus, which otherwise do not naturally occur. This chapter uses methods introduced in **Chapters** 3 and 6 to significantly enhance the opportunities for remote sensing of the inner planets of the Solar System.

The extension of the critical inclination at each planet is performed using continuous, unequal components of radial and transverse acceleration. Considering 12 h highly-elliptical orbits at each planet and extending the inclination to *90 degrees* requires *0.05*, *0.0012* and 1.8×10^{-5} *mm/s*^{2} of acceleration for Mars, Mercury and Venus respectively, which for Mercury and Mars can be provided by existing electric propulsion systems.

An additional component of acceleration directed out of the orbit plane to force a rotation in the ascending node angle of 2π *radians* in *686.429 days* allows the extension of existing sun-synchronous orbits at Mars. This enhances the observation opportunities and simplifies the spacecraft operations through simplification of the thermal environment. Although these orbits require higher acceleration than simply extending the critical inclination the acceleration, values are still within the limits of current thruster technology.

At Mercury and Venus, natural perturbations do not allow sun-synchronous orbits to exist; this chapter therefore presents the use of continuous acceleration to enable circular and elliptical Sun-synchronous orbits which otherwise are not possible, again offering simplification of the spacecraft thermal environment. At Venus the ascending node angle is required to rotate 2π *radians* in *225 days* and at Mercury by 2π *radians* in *88 days*. The acceleration magnitudes required for these orbits are, however, significantly higher than that required for the extension of the inclination and it is expected that considerable development in electric propulsion systems is required before these orbits become feasible.

Chapter 8

8 Summary, Conclusions and Future Work

8.1 Summary

This thesis has addressed the following areas of work:

1. Development of new orbit solutions to provide possible resolutions to the critical data deficit at the high-latitude regions of the Earth, through consideration of advanced orbital dynamics.
2. Examination of the use of electric, chemical and hybrid solar sail / electric propulsion systems to enable new Earth Observation missions.
3. Trade space analysis of possible mission concepts, and mission analysis to characterise the mission lifetimes and mass budgets.
4. Development of highly-elliptical sun-synchronous orbits around Earth, through consideration of advanced orbital dynamics.
5. Development of novel orbits around other bodies in the Solar System to enhance the opportunities for remote sensing.

Firstly, **Chapter 1** provided an introduction to Earth and planetary observation systems highlighted the limitations of current Earth Observation systems for remote sensing of high-latitude regions of the Earth. The necessity for new mission architectures to overcome this

data deficit was also identified. Additionally, the importance of new systems to enable enhanced observation of the inner planets of the Solar System was discussed in this chapter. The objectives of the thesis were outlined, and stated the necessity of the use of low-thrust propulsion systems to develop new orbits around Earth and the inner planets to significantly enhance the opportunities for remote sensing.

Chapter 2 therefore provided an overview of various low-thrust propulsion systems and their possible applications and uses to date; this included electric propulsion, solar sailing and hybrid solar sail and electric propulsion systems.

The main contribution to knowledge was presented in **Chapter 3**, where novel highly-elliptical orbits, termed Taranis orbits, were derived using continuous low-thrust propulsion to allow free selection of the critical inclination to best satisfy the mission objectives. These orbits were firstly derived using a general perturbations solution applying the acceleration using locally optimal control laws. Analytical solutions considered combinations of acceleration in each of the radial, transverse and normal directions, which revealed the most effective application of acceleration combining radial and transverse accelerations. A special perturbations solution was also used to verify the general perturbations technique and optimisation of the solution conducted using pseudospectral optimisation to produce fuel optimal solutions. Although Taranis orbits allow free selection of the inclination, the most significant benefit was identified as an orbit with an inclination of *90 degrees* to provide a potential solution to the data deficit at high-latitude regions of the Earth and therefore address Aim 1. This particular example was therefore considered in subsequent chapters.

To address Aim 2, **Chapter 4** examined the use of hybrid solar sail and electric propulsion systems and conventional chemical propulsion systems and compared these with a pure

electric propulsion system by performing mission analysis to determine the available useful payload masses and possible mission lifetimes. Hybrid solar sail and electric propulsion systems, in theory, lower the demand on the electric propulsion system by reducing the propellant consumption, thus increasing the possible lifetime of the mission or the capacity for useful payload. Two constraining parameters were considered in this chapter to determine if this was in fact true for Taranis orbits, firstly the case where the launch mass of the spacecraft is fixed, and secondly where the maximum thrust of the electric propulsion thruster constrains the system. When the launch mass of the spacecraft is fixed, the increase in the mission lifetime from the pure electric propulsion system was shown to be negligible and as such there was found to be no tangible benefit from the addition of a solar sail. The solar sails required to achieve these increases in lifetime are extremely large, light sails, and thus considerable developments in solar sail technology are necessary to make these missions feasible. In the case of the fixed maximum thrust, the increase in mission lifetime was greater than that achieved using a fixed launch mass. In addition to this, the physical size of the solar sails required are of the same order of magnitude as the fixed launch mass sails, however, these are much heavier sails making them more feasible solutions. It has therefore been shown that the benefit of adding a solar sail to the system is very little to enable the 12 h, *90 degree* inclination Taranis orbit, unless the initial mass is increased significantly. The use of chemical propulsion to enable the orbits was also shown to be impractical for longer duration missions and electric propulsion was therefore shown to be the most viable means of propulsion to enable a 12 h, *90 degree* inclination Taranis orbit for high-latitude observation. It is also important to note that such an orbit can be enabled using existing electric propulsion systems.

Chapter 5 considered the design of a constellation of spacecraft on highly elliptical Taranis orbits to provide continuous remote sensing above *55 degrees* latitude as a minimum

requirement, due to the degradation of imaging from geostationary systems beyond this point. Requirements of the constellation were defined which included constraints on the maximum apogee altitude of the orbit, the maximum observational zenith angle, the restriction of the use of composite images and the rotation of the argument of perigee of the orbit in addition to the requirement of the mission to comply with debris mitigation guidelines. Consideration was also given to the radiation environment of the spacecraft, although this was not considered to be a strict requirement. Analysis revealed a constellation of four spacecraft on 16 h orbit orbits with perigee altitudes of *10,000 km* and apogee altitude of *41,740 km*. Such an orbit takes the radiation constraint into consideration and was therefore referred to as the 'low-radiation' orbit. A 'high-radiation' 12 h orbit with perigee altitude of *300 km* orbit was also identified to reduce the number of spacecraft. In this case, the constellation consists of three spacecraft. Although this would require additional radiation shielding it was expected to be significantly less costly than launching an additional spacecraft to a considerably higher perigee altitude on a 16 h orbit. Observation to *50 degrees* latitude was also considered, where constellations require eight spacecraft on a 16 h, 'low-radiation' orbit and five spacecraft neglecting constraints to minimise the radiation on a 12 h orbit. This chapter also presented validation of the visibility analysis and thus the number of spacecraft in each constellation using NOVA satellite tracking software. The results presented proved the numerical simulation used to determine the number of spacecraft to be accurate**.**

The addition of a further element of acceleration to force a rotation in the ascending node angle of highly elliptical Taranis orbits to develop sun-synchronous Taranis orbits was presented in **Chapter 6** to address Aim 4**.** These orbits were achieved by using continuous acceleration to alter both the natural critical inclination of highly-elliptical orbits to any inclination, and to maintain the sun-synchronous orbit condition. As such, a sun-

synchronous Taranis orbit inclined at *90 degrees* can be enabled, allowing both improved high-latitude imaging and simplified instrument design through significant simplification of the thermal environment. Although the required acceleration to enable such an orbit is significantly higher than that required to enable a *90 degree* Taranis orbit without the sun-synchronous condition, it is likely to be achievable using current or near term technology.

Finally, the use of continuous low-thrust propulsion to derive novel orbits at Mars, Mercury and Venus was presented in **Chapter 7** to address Aim 5. This work consisted of: the extension of the critical inclination of highly elliptical orbits at Mars, Mercury and Venus; the extension of sun-synchronous orbits at Mars; and development of circular and elliptical sun-synchronous orbits at Mercury and Venus, which otherwise do not naturally occur. This chapter used methods introduced in **Chapters 3** and **6** to significantly enhance the opportunities for remote sensing of the inner planets of the Solar System and revealed that current electric propulsion systems could provide the required acceleration to achieve an inclination of *90 degrees* for 12 h orbits at Mars and Mercury. Although the extension of sun-synchronous orbits at Mars requires higher acceleration magnitude than simply extending the critical inclination, the acceleration values are still within the limits of current thruster technology. At Mercury and Venus, natural perturbations do not allow sun-synchronous orbits to exist; this chapter therefore presented the use of continuous acceleration to enable circular and elliptical sun-synchronous orbits which otherwise are not possible, again offering simplification of the spacecraft thermal environment. However, the acceleration magnitudes required for these orbits was shown to be significantly higher than that required for the extension of the inclination and it is expected that considerable development in electric propulsion systems would be required before these orbits become feasible.

8.2 Limitations

Some note should be made of the limitations of this work, and possible improvements that could be made. The majority of the thesis focuses on a *90 degree* inclination Taranis orbit enabled using continuous acceleration, however in the future, attention should be given to other inclinations to minimise the propellant consumption while still achieving the specified requirements. Similarly, the assumption that the acceleration is continuous relies on the platform collecting science data while the thrusters are in operation, clearly it would be of significant benefit to introduce coast arcs to allow science instruments to operate without contamination from the propulsion system.

8.3 Technology Development

Several developments in technology are required to allow the Taranis mission concept to become feasible these are as follows:

- Imaging from the Taranis orbit would require changes to be made over LEO or GEO missions due to the variation in altitude caused by the elliptical nature of the Taranis orbit. These changes could include different algorithms for data acquisition, different mirror scanning techniques, a variety of on-board processing electronics, on-board software processing or only operating the instrument around apogee.
- Design life of the thruster will also be a significant factor as the mission requires long duration thrusting. Initial research into including coast arcs into the orbit, has shown for a nominal 5 year mission, a thruster design life of around 16,000 hours is required.

- Although the radiation environment of HEO may be seen as problematic, a number of HEO mission have successfully survived a varying radiation and thermal environment, including NASA/NRO operated TWINS mission, which has an operational payload after several years of operation [161].

Although some technology developments are required to enable the Taranis mission concept, none of the identified obstacles are expected to be critical to prevent such a mission operating successfully.

8.4 Conclusions

Following summary of the research presented in **Section 8.1**, distinct conclusions can be drawn in relation to the objectives first stated in **Chapter 1**:

1. Novel highly-elliptical orbits, termed Taranis orbits, have been developed successfully using low-thrust propulsion to alter the inclination to *90 degrees* to allow the critical high-latitude data deficit to be filled using fewer spacecraft and to higher resolution than any other proposed system.
2. Electric Propulsion was shown to be the most effective means of enabling the Taranis mission concepts. Notably these orbits can be enabled using existing thruster technology.
3. Trade space analysis revealed high and low – radiation orbit constellations for imaging to *55* and *50 degrees* latitude. Continuous coverage to *55 degrees*: four spacecraft on 16 h low-radiation orbit with perigee altitude of *10,000 km*, three spacecraft on 12 h high-radiation orbit with perigee altitude of *300 km*. Continuous coverage to *50 degrees*: eight spacecraft on low-radiation orbit, five spacecraft on high-radiation orbit.

4. Highly-elliptical sun-synchronous Earth orbits were developed, to allow both high-latitude observation and significant simplification of the spacecraft thermal environment.
5. Extension of existing Martian orbits has been performed using continuous low-thrust to generate new highly-elliptical and sun-synchronous orbits. Similarly, low-thrust propulsion has been shown to extend highly-elliptical orbits and enable sun-synchronous orbits at Mercury and Venus where they otherwise do not naturally occur.

8.5 Future Work

This thesis has introduced a system to improve high-latitude observation of the Earth, however, there is scope to expand the Taranis orbit concept further and improve the research in the following ways;

- Preliminary work has been conducted, but is not included within this dissertation, to investigate the introduction of coast arcs into the Taranis orbit to reduce the thrusting time. Consideration has been given to thrusting only when no science data is being collected by the on board instrumentation and coasting while the spacecraft is in shadow, however further research could be conducted in this area
- Although a *90 degree* inclination orbit has been extensively studied in this thesis, future work should include investigation into the most beneficial inclination to minimise the propellant consumption while still meeting the specified requirements
- Detailed investigation into possible instrumentation for a Taranis platform.
- Development of a suitable platform configuration for both a baseline and ideal mission using Computer Aided Design and Finite Element Analysis

- Research into the effect of the electric propulsion system on the local spacecraft environment
- Investigation into the operation of the spacecraft and instrument in a high-radiation environment
- Investigation into possible launcher configurations for single and multiple spacecraft options
- Communication link budget analysis and design of the ground segment.
- Analysis of orbits at Mercury using higher order gravity data when this becomes available
- Analysis of the effect of other perturbations, such as solar radiation pressure, on orbits at Mars Mercury and Venus.
- Development of novel frozen orbits using low-thrust propulsion, for EO and planetary exploration

9 References

1. "Global Monitoring of Essential Climate Variables," *ESA/PB-EO(2009)32*. Esa-Earth Observation Programme Board, February 2009.
2. "EO Handbook - The Important Role of Earth Observations: Observations of Climate by Earth Orbiting Satellites." Committee on Earth Observation Satellites, Accessed Online October 3rd 2012.
3. Macdonald, M., and Badescu, V. *The International Handbook and Space Technology*. 2013.
4. Boain, R. J. "A-B-Cs of Sun-Synchronous Orbit Mission Design", *14th AAS/AIAA Space Flight Mechanics Conference*, 2004. AIAA, AIAA, Reston, VA, February 2004
5. ESA. "CryoSat Mission and Data Description." Vol. 3, ESTEC, Noordwijk, The Netherlands, 2007, CS-RP-ESA-SY-0059.
6. ESA. "Mission Objectoves and Scientific Requirements of the Soil Moisture and Ocean Salinity (SMOS) Mission." Vol. 5, 2002.
7. Drinkwater, M. R., Haagmans, R., Muzi, D., Popescu, A., Floberghagen, R., Kern, M., and Fehringer, M. "The GOCE Gravity Mission: ESA's First Core Earth Explorer," *3rd International GOCE User Workshop*. Vol. SP-627, ESA Special Publication, Frascati, Italy, 2006, pp. 1-8.
8. Vallado, D. A. *Fundamentals of Astrodynamics and Applications*. 3rd ed ed., Springer, New York, 2007. p. 1055.
9. ESA. "Meteosat Second Generation - The Satellite Development." ESA Publications Division, ESTEC, Noordwijk, The Netherlands, 1999.
10. Riishojgaard, L. P. "Report on Molniya Orbits", *World Meteorological Organization Commission for Basic Systems, OPAG on Integrated Observing Systems Expert Team on Observational Data Requirements and Redesign of the Global Observing System, CBS/OPAGIOS/ODRRGOS-7/Doc.7.5, Seventh Session*. Geneva Switzerland, 12-16 July 2004
11. Lazzara, M. A., Dworak, R., Santek, D. A., Velden, C. S., and Key, J. R. "High Latitude Atmospheric Motion Vectors: Application of Antarctic and Arctic Composite Satellite Imagery", *10th International Winds Workshop*, 2010. Tokyo, Japan, 22-26 February 2010

12. Lazzara, M. A., Stearns, C. R., Staude, J. A., and Knuth, S. L. "10 Years of Antarctic Composite Images," *7th Conference on Polar Meteorology and Oceanography and Joint Symposium on High-Latitude Climate Variations*. Proceedings. Boston, Ma, American Meteorological Society, Hyannis, MA, 2003, 12-16 May 2003.
13. WMO. "WMO vision for the GOS in 2025." Port of Spain, Trinidad and Tobago, January 2009.
14. Holland, M. M., and Bitz, C. M. "Polar amplification of climate change in couples models", *Climate Dynamics* Vol. 21, 2003, pp. 221-232.
15. "Towards an Integrated Arctic Observing Network." The National Academies, 2006.
16. Serreze, M. C., and Francis, J. A. "The Arctic Amplification Debate", *Climate Change* Vol. 76, 2006, pp. 241-264.
17. Hakegard, E. J. "ArctiCOM," *ARTES 1 FInal Presentation days*. ESTEC, 2011, 12-13 December 2011.
18. "Arctic Marine Shipping Assessment 2009 Report." Arctic Council, 2009.
19. Kvamstad, B., Fjortoft, K., and Bekkadal, F. "Future Needs and Visions for Maritime Safety Management in the High North", *MarSafe North - Maritime Safety Management in the High North*, 2012.
20. Zhang, J. "Warming of the Arctic Ice-Ocean System is Faster than the Global Average Since the 1960s", *Geophysical Research Letters* Vol. 32, No. 19, 2005, doi: 10.1029/2005GL024216.
21. Curry, J. A., Schramm, J. L., and Ebert, E. E. "Sea Ice-Albedo Climate Feedback Mechanism", *Journal of Climate* Vol. 8, No. 2, 1995, pp. 240-247, doi: http://dx.doi.org/10.1175/1520-0442(1995)008%3C0240:SIACFM%3E2.0.CO;2.
22. Comiso, J. C., Parkinson, C. L., Gersten, R., and Stock, L. "Accelerated Decline in the Arctic Sea Ice Cover", *Geophysical Research Letters* Vol. 35, No. 1, 2008, doi: 10.1029/2007GL031972.
23. Kidder, S. Q., and Vonder Haar, T. H. "Notes and Correspondence - On the Use of Molniya Orbits for Meteorological Observation of Middle and High Latitudes", *Journal of Atmospheric and Oceanic Technology* Vol. 7, 1990, pp. 517-522.
24. Larson, W. J., and Wertz, J. R. *Space Mission Analysis and Design*. 3rd ed., Microcosm Press and Kluwer Academic Publishers, Dordrecht, The Netherlands, California, 1999.

25. Draim, J. E., Cefola, P. J., and Castiel, D. "Elliptical Orbit Constellations - A New Paradigm for Higher Efficiency in Space Systems?," *Aerospace Conference Proceedings*. Vol. 7, IEEE, 2000, pp. 27-35.

26. Draim, J. E. "Three- and Four- Satellite Continuous - Coverage Constellations", *Journal of Guidance, Control and Dynamics* Vol. 8, No. 9, 1985, pp. 725-730.

27. Trishchenko, A. P., and Garand, L. "Spatial and Temporal Sampling of Polar Regions from Two-Satellite System on Molniya Orbit", *Journal of Atmospheric and Oceanic Technology* Vol. 28, 2011, pp. 977-992.

28. Trishchenko, A., and Garand, L. "Three Apogee 16-h Highly Elliptical Orbit As Optimal Choice For Continuous Meteorological Imaging Of Polar Regions", *Journal of Atmospheric and Oceanic Technology* Vol. 28, No. 11, 2011, pp. 1407-1422.

29. "Space and the Arctic. Developing a European Union Policy towards the Arctic Region: Progress Since 2008 and Next Steps." European Commission, Brussels, 2012.

30. Asmus, V. V., Krovotyntsev, V. A., and Pyatkin, V. P. "Satellite Monitoring of Ice Conditions in Polar Regions", *Pattern Recognition and Image Analysis* Vol. 22, No. 1, 2012, pp. 1-9, doi: 10.1134/S1054661812010075.

31. Driver, J. M. "Analysis of an Arctic Polesitter", *Journal of Spacecraft and Rockets* Vol. 17, No. 3, 1980, pp. 263-269.

32. Ceriotti, M., and McInnes, C. R. "An Earth Pole-Sitter using Hybrid Propulsion", *AIAA/AAS Astrodynamics Specialist Conference,* AIAA-2010-7830. 2010. American Astronomical Society / American Institute of Aeronautics and Astronautics, Toronto, Canada, 2nd August - 5th August 2010

33. Ceriotti, M., and McInnes, C. R. "Systems Design of a Hybrid Sail Pole-Sitter", *Advances in Space Research* Vol. 48, No. 11, 2011, pp. 1754-1762, 0273-1177, doi: 10.1016/j.asr.2011.02.010.

34. Ceriotti, M., and McInnes, C. R. "Natural and Sail-Displaced Doubly-Symmetric Lagrange Point Orbits for Polar Coverage", *Celestial Mechanics and Dynamical Astronomy* Vol. 114, No. 1-2, 2012, pp. 151-180.

35. Sonett, C. P. "A Summary Review of the Scientific Findings of the Mariner Venus Mission", *Space Science Reviews* Vol. 2, No. 6, 1963, pp. 751-777, doi: 10.1007/BF00208814.

36. Steinbacher, R. H., Kliore, A., Lorell, J., Hipsher, H., Barth, C. A., Masursky, H., Munch, G., Pearl, J., and Smith, B. "Mariner 9 Science Experiments: Preliminary Results", *Science 21* Vol. 175, No. 4019, 1972, pp. 293-294, doi: DOI: 10.1126/science.175.4019.293

37. Soffen, G. A. "Scientific Results of the Viking Mission", *Science 17* Vol. 194, No. 4271, 1976, pp. 1274-1276, doi: DOI: 10.1126/science.194.4271.1274

38. Perminov, V. G. *The Difficult Road to Mars - A Brief History of Mars Explorationin the Soviet Union*. Chichester, England, 1999. pp 1.

39. Lyons, D. T., Beerer, J. G., Esposito, P., and Johnston, D. M. "Mars Global Surveyor: Aerobraking Mission Overview", *Journal of Spacecraft and Rockets* Vol. 36, No. 3, 1999, pp. 307-313.

40. Albee, A. L., Arvidson, R. E., Palluconi, F., and Thorpe, T. "Overview of the Mars Global Surveyor Mission", *Journal of Geophysical Research* Vol. 106, No. E10, 2001, doi: 10.1029/2000JE001306

41. Bibring, J. P., Langevin, Y., Poulet, F., Gendrin, A., Gondet, B., Berthe, M., Soufflot, A., Drossart, P., Combes, M., Bellucci, G., Moroz, V., Mangold, N., and Schmitt, B. "Perennial Water Ice Identified in the South Polar Cap of Mars", *Nature* Vol. 428, 2004, pp. 627-630, doi: 10.1038/nature02461.

42. Saunders, R. S., Arvidson, R. E., Badhwar, G. D., Boynton, W. V., Christensen, P. R., Cucinotta, F. A., Feldman, W. C., Gibbs, R. G., Kloss, C., Landano, M. R., Mase, R. A., McSmith, G. W., Meyer, M. A., Mitrofanov, I. G., Pace, G. D., Plaut, J. J., Sidney, W. P., Spencer, D. A., Thompson, T. W., and Zeitlin, C. J. "2001 Mars Odyssey Mission Summary", *Space Science Reviews* Vol. 110, No. 1-2, 2003, pp. 1-36, doi: 10.1023/B:SPAC.0000021006.84299.18.

43. Chicarro, A., Martin, P., and Trautner, R. "The Mars Express Mission: An Overview." ESA, ESTEC, SP-1240. Noordwijk, The Netherlands, 2004.

44. Titus, T., Kieffer, H. H., and Christensen, P. R. "Exposed Water Ice Discovered near the South Pole of Mars", *Science* Vol. 299, No. 5609, 2003, pp. 1048-1051, doi: 10.1126/science.1080497

45. Zurek, R. W., and Smrekar, S. E. "An overview of the Mars Reconnaissance Orbiter (MRO) science mission", *Journal of Geophysical Research* Vol. 112, No. E05S01, 2006, doi: 10.1029/2006JE002701

46. Smith, J. C., and Bell, J. M. "2001 Mars Odyssey Aerobraking", *Journal of Spacecraft and Rockets* Vol. 42, No. 3, 2005, pp. 406-415.

47. Jai, B., Wenkert, D., Hammer, B., Carlton, M., Johnston, D., and Halbrook, T. "An Overview of Mars Reconnaissance Orbiter Mission and Operations Challenges", *AIAA Space 2007 Conference & Exposition*, 2007. Long Beach, California,

48. Squyres, S. "Vision and Voyages For Planetary Science in the Decade 2013-2022." 2011.

49. Macdonald, M., McKay, R., Vasile, M., Bosquillon de Frescheville, F., Biggs, J., and McInnes, C. R. "Low-Thrust Enabled Highly Non-Keplerian Orbits in Support of Future Mars Exploration", *Journal of Guidance, Control and Dynamics* Vol. 34, No. 5, 2011, pp. 1396-1940, 0731-5090, doi: 10.2514/1.52602.

50. Strom, R. G., and Sprague, A. L. *Exploring Mercury The Iron Planet*. Chichester, Uk. New York Springer, 2003. pp 16.

51. Solomon, S. C., McNutt, R. L., Gold, R., Acuna, M. H., Baker, D. N., Boynton, W. V., Champan, C. R., Cheng, A. F., Gloeckler, G., Head, J. W., Krimigis, S. M., McClintock, W. E., Murchie, S. L., Peale, S. J., Phillips, R. J., Robinson, M. S., Slavin, J. A., Smith, D. E., Strom, R. G., Trombka, J. I., and Zuber, M. T. "The MESSENGER Mission to Mercury: Scientific Objectives and Implementation", *Planetary and Space Science* Vol. 49, No. 14-15, 2001, pp. 1445-1465, doi: 10.1016/S0032-0633(01)00085-X.

52. Benkhoff, J., Casteren, J. V., Hayakawa, H., Fujimoto, M., Laakso, H., Novara, M., Ferri, P., Middleton, H. R., and Ziethe, R. "BepiColombo - Comprehensive Exploration of Mercury: Mission Overview and Science Goals", *Planetary and Space Science* Vol. 58, No. 1-2, 2010, pp. 2-20, doi: 10.1016/j.pss.2009.09.020.

53. Stewart, R. W. "Interpretation of Mariner 5 and Venera 4 Data on the Upper Atmosphere of Venus", *Journal of the Atmospheric Sciences* Vol. 25, 1968, pp. 578-582, doi: 10.1175/1520-0469.

54. Mazets, E. P., Golenetskii, S. V., Il'inskii, V. N., Panov, V. N., Aptekar, R. L., Gur'yan, Y. A., Sokolov, I. A., and Kharitonova, T. V. "Venera 11 and 12 Observations of Gamma-Ray Bursts - The Cone Experiment", *Soviet Astronomy Letters* Vol. 5, 1979, pp. 87-90, doi: 0360-0327/79/02 0087-04.

55. Surkov, Y. A., Bersukov, V. L., Moskalyeva, L. P., and Kharyukova, V. P. "New Data on the Composition, Structure, and Properties of Venus Rock Obtained by Venera 13

and Venera 14", *Journal of Geophysical Research* Vol. 89, 1984, pp. 393-402, 0148-0227, doi: 10.1029/JB089iS02p0B393.

56. Surkov, Y. A. "Geochemical Studies of Venus by Venera 9 and 10 Automatic Interplanetary Stations," *8th Lunar Science Conference*. Vol. 3, Pergamon Press, Houston, Texas, 1977, March 14 - 18 1977.

57. Niemann, H. B., Hartle, R. E., Kasprzak, W. T., Spencer, N. W., Hunten, D. M., and Carignan, G. R. "Venus Upper Atmosphere Neutral Composition: Preliminary Results from the Pioneer Venus Orbiter", *Science* Vol. 203, 1979, pp. 770-772.

58. Barsukov, V. L., Basilevsky, A. T., Burba, G. A., Bobinna, N. N., Kryuchkov, V. P., Kuzmin, R. O., Nikolaeva, O. V., Pronin, A. A., Ronca, L. B., Chernaya, I. M., Shashkina, V. P., Garanin, A. V., Kushky, E. R., Markov, M. S., Sukhanov, A. L., Kotelnikov, V. A., Rzhiga, O. N., Petrov, G. M., Alexandrov, Y. N., Sidorenko, A. I., Bogomolov, A. F., Skrypnik, G. I., Bergman, M. Y., Kudrin, L. V., Bokshtein, I. M., Kronrod, M. A., Chochia, P. A., Tyuflin, Y. S., Kadnichansky, S. A., and Akim, E. L. "The Geology and Geomorphology of the Venus Surface as Revealed by the Radar Images Obtained by Veneras 15 and 16", *Journal of Geophysical Research* Vol. 91, 1986, pp. 378-398, doi: 10.1029/JB091iB04p0D378.

59. Konopliv, A. S., Banerdt, W. B., and Sjogren, W. L. "Venus Gravity: 180th Degree and Order Model", *Icarus* Vol. 139, No. 1, 1999, pp. 3-18.

60. Svedhem, H., Titov, D. V., McCoy, D., Lebreton, J. P., Barabash, S., Bertaux, J. L., Drossart, P., Formisano, V., Hausler, B., Korablev, O., Markiewicz, W. J., Nevejans, D., Patzold, M., Piccioni, G., Zhang, T. L., Taylor, F. W., Lellouch, E., Koschny, D., Witasse, O., Eggel, H., Warhaut, M., Accomazzo, A., Rodriguez-Canabal, J., Febrega, J., Schirmann, T., Clochet, A., and Coradini, M. "Venus Express - The First European Mission to Venus", *Planetary and Space Science* Vol. 55, No. 12, 2007, pp. 1636-1652.

61. Mori, O., Sawada, H., Funase, R., Endo, T., Morimoto, M., Yamamoto, T., Tsuda, Y., Kawakatsu, Y., and Kawaguchi, J. "Development of First Solar Power Sail Demonstrator - IKAROS," *Proceedings of 21st International Symposium on Space Flight Dynamics, ISSFD 2009*. Toulouse, France, 2009.

62. Leipold, M., Borg, E., Linger, S., Pabsch, A., Sachs, R., and Seboldt, W. "Mercury Orbiter with a Solar Sail Spacecraft", *Acta Astronautica* Vol. 35, No. 1, 1995, pp. 635-644.

63. Leipold, M., Seboldt, W., Lingner, S., and Borg, E. "Mercury Sun-Synchronous Polar Orbiter with a Solar Sail", *Acta Astronautica* Vol. 39, No. 1-4, 1996, pp. 143-151.

64. Macdonald, M., and McInnes, C. R. "Analytical Control Laws for Planet-Centered Solar Sailing", *Journal of Guidance, Control and Dynamics* Vol. 28, No. 5, 2005, pp. 1038-1048.

65. Choueiri, E. Y. "A Critical History of Electric Propulsion: The First 50 Years (1906-1956)", *Journal of Propulsion and Power* Vol. 20, No. 2, 2004, pp. 193-203.

66. Goebel, D. M., and Katz, I. *Fundamentals of Electric Propulsion: Ion and Hall Thrusters*. John Wiley & Sons, Inc, Hoboken, New Jersey, 2008.

67. Macdonald, M., and McInnes, C. R. "Solar Sail Science Mission Applications and Advancement: Solar Sailing: Concepts, Technology, Missions", *Advances in Space Research* Vol. 48, No. 11, 2011, pp. 1702-1716, 0273-1177.

68. Macdonald, M. "Solar Sailing: Applications and Technology Advancement," *Advances in Spacecraft Technologies*. InTech, Published Online, 2011, pp. 35-60.

69. Jahn, R. G., and Choueiri, E. Y. "Electric Propulsion", *Encyclopedia of Physical Science and Technology* Vol. 5, 2002, pp. 125-141.

70. Fortescue, P., Stark, J., and Swinerd, G. *Spacecraft Systems Engineering*. 3rd ed., Wiley, New York, 2003.

71. Dankanich, J. W. *Low-Thrust Propulsion Technologies, Mission Design, and Application*. INTECH, 2010.

72. Molina-Cabrera, P., Herdrich, G., Lau, M., and Fausolas, S. "Pulsed Plasma Thrusters: A Worldwide Review and Long Yearned Classification," *32nd International Electric Propulsion Conference*. Wiesbaden, Germany, 2011, September 11 -15 2011.

73. Braga-Illa, A. A. "Automatic Orbit Control of the Lincoln Experimental Satellite LES-6." Vol. 469, 1969, July 10 1969.

74. Zakrzwski, C., Benson, S., Sanneman, P., and Hoskins, A. "On-Orbit Testing of the EO-1 Pulsed Plasma Thruster," *38th AIAA/ASME/SAE/ASEE Joint Propulsion Conference and Exhibit*. Indianapolis, IN, 2002, 7 - 10 July 2002.

75. Chien, K., Hart, S. L., Tighe, W. G., De Pano, M. K., Bond, T. A., and Spears, R. "L-3 Communications ETI Electric Propulsion Overview," *29th International Electric Propulsion Conference* Princeton University, 2005, October 31 - November 4 2005.

76. Brophy, J. R., Kakuda, R. Y., Polk, J. E., Anderson, J. R., Marcucci, M. G., Brinza, D., Henry, M. D., Fujii, K. K., Mantha, K. R., Stocky, J. F., Sovey, J., Patterson, M., Rawlin, V. K., Hamley, J., Bond, T., Christensen, J., Cardwell, H., Benson, G., Gallagher, J., Matranga, M., and Bushway, D. "Ion Propulsion System (NSTAR) DS1 Technology Validation Report," *JPL Publication 00-10*. NASA, 2000.

77. Polk, J. E., Brinza, D., Kakuda, R. Y., Brophy, J. R., Katz, I., Anderson, J. R., Rawlin, V. K., Patterson, M. J., Sovey, J., and Hamley, J. "Demonstration of the NSTAR Ion Propulsion System on the Deep Space One Mission", *27th International Electric Propulsion Conference*, 2001. Pasadena, CA, 15-19 October 2001

78. Brophy, J. R. "NASA's Deep Space 1 Ion Engine", *Review of Scientific Instruments* Vol. 73, No. 2, 2002, pp. 1071-1078.

79. Brophy, J. R., Marcucci, M. G., Ganapathi, G. B., and Garner, C. E. "The Ion Propulsion System for Dawn " *39th Joint Propulsion Conference*. Huntsville, Alabama, 2003, July 20 - 23.

80. Kuninaka, H., Nishiyama, K., Funakai, I., Tetsuya, and Shimizu, Y. "Asteroid Rendezvous of HAYABUSA Explorer Using Microwave Discharge Ion Engines," *29th International Electric Propulsion Conference*. Princeton University, 2005, October 31 - November 4 2005.

81. Patterson, M. J., and Benson, S. W. "NEXT Ion Propulsion System Development Status and Performance," *43rd AIAA/ASME/SAE/ASEE Joint Propulsion Conference and Exhibit*. 2007, July 8 - 11 2007.

82. Randolph, T. M., and Polk, J. E. "An overview of the Nuclear Electric Xenon Ion System (NEXIS) Activity", *40th AIAA/ASME/SAE/ASEE Joint Propulsion Conference,* AIAA-2003-4713. 2004. Fort Lauderdale, Florida, July 2004

83. Foster, J. E., Haag, T., Patterson, M., Williams, G. J., Sovey, J. S., Carpenter, C., Kamhawi, H., Malone, S., and Elliot, F. "The High Power Electric Propulsion (HiPEP) Ion Thruster", 2004.

84. Edwards, C. H., Wallace, N. C., Tato, C., and Put, C. V. "The T5 Ion Propulsion Assembly for Drag Compensation on GOCE," *Second International GOCE User Workshop "GOCE, The Geoid and Oceanography"*. Frascati, Italy, 2004, 8-10 March 2004.

85. ESA. "ESA Bulletin." Vol. 152, 2012, November 2012.

86. Wallace, N. C. "Testing of The QinetiQ T6 Thruster in Support of the ESA BepiColombo Mercury Mission," *4th International Spacecraft Propulsion Conference (ESA SP-55)*. Cagliari, Sardinia, Italy, 2004, 2-4 June 2004.

87. Kim, V., Popov, G., Arkhipov, B., Murashko, V., Gorshkov, O., Koroteyev, A., Garkusha, V., Semekin, A., and Tverdokhlebov, S. "Electric Propulsion Activity in Russia," *27th International Electric Propulsion Conference*. Pasadena, CA, 2001, 15 - 19 October 2001.

88. Koppel, C. R., and Estublier, D. "The SMART-1 Hall Effect Thruster Around the Moon: In Flight Experience," *29th International Electric Propulsion Conference*. Princeton University, 2005, October 31 - November 4 2005.

89. Marchandise, F., Cornu, N., Darnon, F., and Estublier, D. "PPS 1350-G Qualification Status 10500h," *The 30th International Electric Propulsion Conference*. Florence, Italy, 2007, September 17 - 20 2007.

90. Mathers, A., Grys, K. D., and Paisley, J. "Performance Variation in BPT-4000 Hall Thrusters," *31st International Electric Propulsion Conference*. University of Michigan, Ann Arbor, Michigan, 2009, 20 - 24 September 2009.

91. Fisher, J., Wilson, A., King, D., Meyer, S., Engelbrecht, C., Grys, K. D., and Werthman, L. "The Development and Qualification of a 4.5kW Hall Thruster Propulsion System for GEO Satellite Applications," *27th International Electric Propulsion Conference*. Pasadena, CA, 2001, 15 - 19 October 2001.

92. Pencil, E. J., Peterson, T. T., Anderson, D. J., and Dankanich, J. "Overview of NASA's Electric Propulsion Development Activities for Robotic Science Missions," *32nd International Electric Propulsion Conference*. Wiesbaden, Germany, 2011, September 11 - 15 2011.

93. Brophy, J. "Advanced Propulsion for Small Body Missions Part 2," *Small Body Assessment Group meeting*. NASA, Washington DC, United States, 2011, January 24 2011.

94. Rayman, M. D., and Patel, K. C. "The Dawn Project Transition To Mission Operations: On Its Way to Rendezvous With Vesta and Ceres," *59th International Astronautical Congress*. Glasgow, Scotland, 2008, 29 September - 3 October 2008.

95. McElrath, T. P., Strange, N. J., and Lang, J. J. "Phobos and Deimos Sample Return to Earth-Moon L2 using Small SEP Spacecraft in 2018-2023," *Concepts and Approaches for Mars Exploration*. Houston, Texas, 2012, June 12-14 2012.

96. Gilland, J. H., LaPointe, M. R., Oleson, S., Mercer, C., Pencil, E., and Maosn, L. "MW-Class Electric Propulsion System Designs for Mars Cargo Transport," *AIAA SPACE 2011 Conference and Exposition*. Long Beach, CA, United States, 2011, September 27 2011.

97. Sankaran, K., Cassady, L., Kodys, A. D., and Choueiri, E. Y. "A Survey of Propulsion Options for Cargo and Piloted Missions to Mars", *Annals of the New York Academy of Sciences* Vol. 1017, No. 1, 2004, pp. 450-467, doi: 10.1196/annals.1311.027.

98. McKay, R., Macdonald, M., Biggs, J., and McInnes, C. R. "Survey of Highly Non-Keplerian Orbits With Low-Thrust Propulsion", *Journal of Guidance, Control and Dynamics* Vol. 34, No. 3, 2011, pp. 645-666, doi: 10.2514/1.52133.

99. Ceriotti, M., Diedrich, B., and McInnes, C. R. "Novel Mission Concepts for Polar Coverage: An Overview of Recent Developments and Possible Future Applications", *Acta Astronautica* Vol. 80, 2012, pp. 89-104, doi: 10.1016/j.actaastro.2012.04.043.

100. Macdonald, M., McKay, R., Vasile, M., and Frescheville, F. B. d. "Extension of the Sun-Synchronous Orbit", *Journal Guidance Control and Dynamics* Vol. 33, No. 6, 2010, pp. 1935-1940.

101. Tsiolkovsky, K. E. "Extension of Man into Outer Space", 1921.

102. Tsander, K. "From a Scientific Heritage", *NASA Technical Translation TTF-541*, 1967.

103. Kawaguchi, J. I., Mimasu, Y., Mori, O., Funase, R., Yamamoto, T., and Tsuda, Y. "IKAROS - Ready for lift-off as the world's first solar sail demonstration in interplanetary space," *60th International Astronautical Congress (IAC 2009)*. Daejeon, Korea, 2009.

104. Newton, K. "NASA's First Solar Sail Nano Sail-D Deploys in Low-Earth Orbit."http://www.nasa.gov/centers/marshall/news/news/releases/2011/11-010.html, cited 24 October 2012

105. Wiley, C., [pseudonym Sanders, R] "Clipper Ships of Space," *Astounding Science Fiction*, p. 135, May 1951

106. Garwin, R. L. "Solar Sailing - A Practical Method of propulsion Within the Solar System", *Jet Propulsion* Vol. 28, 1958, pp. 188-190.

107. Dunne, J. A., and Burgess, E. *The Voyage of Mariner 10 Mission to Venus and Mercury*. NASA History Office, 1978. pp 30.

108. McInnes, C. R. *Solar Sailing Technology, Dynamics and Mission Applications*. Praxis Publishing, Chichester, UK, 1999.

109. Freeland, R. E., Bilyeu, G. D., Veal, G. R., Steiner, M. D., and Carson, D. E. "Large Inflatable Deployable Antenna Flight Experiment Results," *48th International Astronautical Congress*. Torino, Italy, 1997, October 1997.

110. Leipold, M., Eiden, M., Garner, C. E., Herbeck, L., Kassing, D., Niederstadt, T., Kruger, T., Pagel, G., Rezazad, M., Rozemeijer, H., Sebolt, W., Schoppinger, C., Sickinger, C., and Unckenbold, W. "Solar Sail Technology Development and Demonstration", *Acta Astronautica* Vol. 52, No. 2-6, 2003, pp. 317-326, doi: 10.1016/S0094-5765(02)00171-6,.

111. Lichodziejewski, D., Derbes, B., West, J., Reinert, R., Belvin, K., and Pappa, R. "Bringing an Effective Solar Sail Design Towards TRL 6," *39th AIAA Joint Propulsion Conference*. Hunstville, 2003, July 2003.

112. Mann, T., Behun, V., Lichodziejewski, D., Derbes, B., and Sleight, D. "Ground Testing a 20-Meter Inflation Deployed Solar Sail," *47th AIAA/ASME/ASCE/AHS/ASC Structures, Structural Dynamics, and Materials Conference*. Newport, RI, 2006, May 2006.

113. Tsuda, Y., Mori, O., Funase, R., Sawada, H., Yamamoto, T., Saiki, T., Endo, T., Yonekura, K., Hoshino, H., and Kawaguchi, J. "Achievement of IKAROS - Japanese Deep Space Solar Sail Demonstartion Mission", *Acta Astronautica* Vol. 82, No. 2, 2013, pp. 183-188, doi: 10.1016/j.actaastro.2012.03.032,.

114. Johnson, L., Whorton, M., Heaton, A., Pinson, R., Laue, G., and Adams, C. "NanoSail-D: A Solar Sail Demonstration Mission", *Acta Astronautica* Vol. 68, 2011, pp. 571-575, doi: 10.1016/j.actaastro.2010.02.008,.

115. Lappas, V., Adeli, N., Visagie, L., Fernandez, J., Theodorou, T., Steyn, W., and Perren, M. "CubeSail: A Low Cost CubeSat Based Solar Sail Demonstration Mission", *Acta Astronautica* Vol. 48, No. 11, 2011, pp. 1890-1901, doi: 10.1016/j.asr.2011.05.033,.

116. Biddy, C., and Svitek, T. "LightSail-1 Solar Sail Design and Qualification," *41st Aerospace Mechanism Symposium*. Pasadena, CA, 2012, May 16 - 18 2012.

117. ASTM. "E490-00a Solar Constant and Zero Air Mass Solar Spectral Irradiance Tables," *Solar Constant*. 2006.

118. McInnes, C. R., Macdonald, M., and Hughes, G. "Technology Roadmap, Technical Note 13(a), Technical Assistance in the Study of Science Payloads Transported Through Solar Sailing." 2004, December 2004.

119. Forward, R. L. "Light Levitated Geostationary Cylindrical Orbits", *Journal of the Astronautical Sciences* Vol. 29, No. 1, 1981, pp. 73-80.

120. Forward, R. L. "Light Levitated Geostationary Cylindrical Orbits Using Perforated Light Sails", *Journal of the Astronautical Sciences* Vol. 32, No. 2, 1984, pp. 221-226.

121. Baig, S., and McInnes, C. R. "Light Levitated Geostationary Cylindrical Orbits are Feasible", *Journal of Guidance, Control and Dynamics* Vol. 33, No. 3, 2010, pp. 782-793, 0731-5090.

122. Jehn, R., Rossi, A., Flohrer, T., and Navarro-Reyes, D. "Reorbiting of Satellites in High Altitudes," *5th European Conference on Space Debris*. Darmstadt, Germany, 2009, 30 March - 2 April 2009.

123. Forward, R. L. "Statite: A spacecraft that does not orbit", *Journal of Spacecraft and Rockets* Vol. 28, No. 5, 1991, pp. 606-611.

124. McInnes, C. R. "Artificial Lagrange Points for a Partially Reflecting Flat Solar Sail", *Journal of Guidance, Control and Dynamics* Vol. 22, No. 1, 1999, pp. 185-187.

125. West, J. L. "The GeoStorm Warning Mission: Enhanced Opportunities Based on New Technology," *14th AAS/AIAA Space Flight Mechanics Conference*. AAS Publications Office, Maui, Hawaii, 2004, February 8-12 2004.

126. Macdonald, M., and McInnes, C. R. "GeoSail: An Enhanced Magnetosphere Mission, using a Small Low Cost Solar Sail," *51st International Astronautical Congress*. Rio de Janeiro, Brazil, 2000, 2-6 October 2000.

127. Macdonald, M., Hughes, G. W., McInnes, C. R., Lyngvi, A., Falkner, P., and Atzei, A. "GeoSail: An Elegant Solar Sail Demonstration Mission", *Journal of Spacecraft and Rockets* Vol. 44, No. 4, 2007, pp. 784-796, 0022-4650, doi: 10.2514/1.22867

128. Folta, D., Young, C., and Ross, A. "Unique Non-Keplerian Orbit Vantage Locations for Sun-Earth Connection and Earth Science Vision Roadmaps," *2001 Flight Mechanics Symposium*. Greenbelt, Maryland, 2001, June 19-21 2001, pp. 41-51.

129. Leipold, M., and Gotz, M. "Hybrid Photonic/Electric Propulsion," *GMBH, Rept, SOL4-TR-KTH-001*. Munich, Germany, January 2002.

130. Baig, S., and McInnes, C. R. "Artificial Three-Body Equilibria for Hybrid Low-Thrust Propulsion", *Journal of Guidance, Control and Dynamics* Vol. 31, No. 6, 2008, pp. 1644-1655, doi: 10.2514/1.36125.

131. Heiligers, J., Ceriotti, M., McInnes, C. R., and Biggs, J. "Displaced Geostationary Orbit Design using Hybrid Sail Propulsion", *Journal of Guidance, Control and Dynamics* Vol. 34, No. 6, 2011, pp. 1852-1866, 0731-5090, doi: 10.2514/1.53807

132. Heiligers, J., McInnes, C. R., Biggs, J., and Ceriotti, M. "Displaced Geostationary Orbits using Hybrid Low-Thrust Propulsion", *Acta Astronautica* Vol. 71, 2012, pp. 51-67, 0094-5765, doi: 10.1016/j.actaastro.2011.08.012.

133. Bate, R. R., Mueller, D. D., and White, J. E. *Fundamentals of Astrodynamics*. Dover New York, 1971. p. 455.

134. Walker, M. J. H., Ireland, B., and Owens, J. "A set of Modified Equinoctial Orbital Elements", *Celestial Mechanics* Vol. 36, No. 4, 1985, doi: 10.1007/BF01227493.

135. Dormand, J. R., and Prince, P. J. "A family of embedded Runge-Kutta formulae", *Journal of Computational and Applied Mathematics and Statistics* Vol. 6, No. 1, 1980, pp. 19-26, doi: 10.1016/0771-050X(80)90013-3

136. Becerra, V. M. "PSOPT Optimal Control Solver User Manual." University of Reading, Reading, UK, 2010.

137. Macdonald, M. "Analytical Methodologies for Solar Sail Trajectory Design", *Department of Aerospace Engineering* Ph.D., Thesis, Univeristy of Glasgow, Glasgow. 2005.

138. Macdonald, M. "Analytical Methodologies for Solar Sail Trajectory Design", *Department of Aerospace Engineering* Doctor of Philosophy, University of Glasgow, Glasgow. 2005.

139. Green, A. J. "Optimal Escape Trajectories from a High Earth Orbit by use of Solar Radiation Pressure", *Department of Aeronautics and Astronautics* M.S Thesis, No. T-652, Massachusetts Institude of Technology, Cambridge, MA. 1977.

140. Gonzalez, J., and Saccoccia, G. "ESA Electric Propulsion Activities", *32nd International Electric Propulsion Conference*, 2011. Wiesbaden, Germany, September 11-15

141. Macdonald, M., Hughes, G. W., McInnes, C. R., Lyngvi, A., Falkner, P., and Atzei, A. "Solar Polar Orbiter: A solar sail Technology Reference Study", *Journal of Spacecraft and Rockets* Vol. 43, 2006, pp. 960-972.

142. Ceriotti, M., and McInnes, C. R. "A Near Term Pole-Sitter using Hybrid Solar Sail Propulsion," *2nd International Symposium on Solar Sailing*. New York City College of Technology, New York, USA, 2010, July 20-22 2010.

143. Gershman, R., and Seybold, C. "Propulsion Trades for Space Science Missions", *Acta Astronautica* Vol. 45, No. 4-9, 1999, pp. 541-548.

144. Brophy, J. R. "Advanced Ion Propulsion Systems for Affordable Deep-Space Missions", *Acta Astronautica* Vol. 52, No. 2 - 6, 2003, pp. 309-316.

145. Kitamura, S., Ohkawa, Y., Hayakawa, Y., Yoshida, H., and Miyazaki, K. "Overview and research status of the JAXA 150-mN ion engine", *Acta Astronautica* Vol. 61, No. 1-6, 2007, pp. 360-366.

146. McKay, R., Macdonald, M., Vasile, M., and Frescheville, F. B. "A Novel Interplanetary Communications Relay", *AIAA/AAS Astrodynamics Specialist Conference*, 2010,doi: 10.2514/6.2010-7964. Toronto Ontario Canada, 2-5 August 2010

147. D'Accolti, G., Beltrame, G., Ferrendo, E., Brambilla, L., Contini, R., Vallini, L., Mugnuolo, R., Signorini, C., Caon, A., and Fiebrich, H. "The Solar Array Photovoltaic Assembly for the Rosetta Orbiter and Lander Spacecrafts," *Sixth European Conference*. Porto, Portugal, 2002, 6-10 May 2002.

148. Racca, G. D., Marini, A., Stagnaro, L., Van Dooren, J., Di Napoli, L., Foing, B. H., Lumb, R., Volp, J., Brinkmann, J., Grunagel, R., Estublier, D., Anflo, K., Berge, S., Bodin, P., Edfors, A., Hussain, A., Kugelberg, J., Larsson, N., Ljung, B., Meijer, L., Mortsell, A., Nordeback, T., Persson, S., and Sjoberg, F. "SMART-1 Mission Description and Development Status", *Planetary and Space Science* Vol. 50, No. 14-15, 2002, pp. 1323-1337.

149. McInnes, C. R., and Macdonald, M. "GEOSAIL: Exploring the Geomagnetic Tail Using a Small Solar Sail", *Journal of Spacecraft and Rockets* Vol. 38, No. 4, 2001, pp. 622-629, doi: 10.2514/2.3727.

150. "Space Engineering - System engineering general requirements," *European Cooperation for Space Standardization*. ESA-ESTEC, Noordwijk, The Netherlands, 2009.

151. "Position Paper on Space Debris Mitigation Implementing Zero Debris Creation Zones," *International Academy of Astronautics (IAA)*. 2005.

152. Wertz, J. R., ed. *Spacecraft Attitude Determination and Control*: D. Reidel Publishing Company, 1978.

153. LaBel, K. A., and Barth, J. L. "An Insider's Guide to Designing Spacecraft Systems and Instruments for Operation in the Natural Space Radiation Environment," *Goddard Space Flight Centre Systems Engineering Seminar*. 2001, April 5th 2001.

154. Wittmann, K., ed. *Handbook of Space Technology*. Chichester, UK: John Wiley and Sons, 2009.

155. Dyer, C. "Radiation Effects on Spacecraft & Aircraft," *Proceedings of the Second Solar Cycle and Space Weather Euroconference*. ESA Publications Division, Vico Equense, Italy, 2002.

156. Blake, J. B. "The Energetic Radiation Environment in a Highly Elliptical (Molniya) Orbit." El Segundo, California, 1992.

157. Sawyer, D. M., and Vette, J. I. "Ap-8 trapped proton environment for solar maximum and solar minimum," *NSSDC WDC-A-R&S Report 76-06 NASA-GSFC*. 1976, p. 173.

158. Vette, J. I. "The AE-8 trapped electron model environment," *NSSDC/WDC-A-R&S Report 91-24, NASA-GSFC*. 1991, p. 138.

159. Standardization, E. C. f. S. "Space Engineering - Space Environment," *9.2 Requirements for energetiv particle radiation environments*. ESA Requirements and Standards Division, ESTEC, The Netherlands, 2008, p. 62.

160. Anderson, D. J., Colombo, G., Esposito, P. B., Lau, E. L., and Trager, G. B. "The Mass, Gravity Field and Ephemeris of Mercury", *Icarus* Vol. 71, No. 3, 1987, pp. 337 - 349, doi: 10.1016/0019-1035(87)90033-9.

161. Bailey, J., and Gruntman, M. "Experimental Study of Exospheric Hydrogen Atom Distribution by Lyman-Alpha Detectors on the TWINS mission", *Journal of Geophysical Research* Vol. 116, No. A9, 2011, doi: 10.1029/2011JA016531.